The role of DNA methylation in lower urinary tract development and prostate homeostasis

By

Diya Binoy Joseph

A dissertation submitted in partial fulfillment of the requirements for the degree of

Doctor of Philosophy
(Cellular and Molecular Biology)

at the
UNIVERSITY OF WISCONSIN-MADISON
2018

Date of final oral examination: 12/06/2018
The dissertation is approved by the following members of the Final Oral Committee:
Dale E. Bjorling, Professor, Surgical Sciences
Robert J. Lipinski, Assistant Professor, Comparative Biosciences
John P. Svaren, Professor, Comparative Biosciences
Jyoti J. Watters, Professor, Comparative Biosciences
Chad M. Vezina, Associate Professor, Comparative Biosciences

Dedicated to:

My parents, grandparents and sister for their love and support

Acknowledgements

At the outset, I thank and praise the Almighty for guidance and blessings throughout my research work.

I am extremely grateful to my mentor Dr. Chad Vezina for allowing me to work in his laboratory. In addition to being a skilled and resourceful scientist, Dr. Vezina is an excellent mentor who strives to bring out the best in all his students. I thank him for allowing me to think independently while being a source of constant support and encouragement. I am also very grateful for the future opportunities that working in his laboratory has provided me, which have come to me because of the good will and respect he has earned among his colleagues.

I thank all the members of the Vezina lab for helpful discussions and moral support. I would like to specially thank Lisa Abler and Kyle Wegner for their help and guidance when I was new to the lab. I also thank my fellow graduate students Mark Cadena, Anne Turco and Hannah Ruetten and undergraduates Anoop Chandrashekar and Simran Sandhu for their support.

I am grateful for the facilities and infrastructure provided by the University of Wisconsin-Madison for pursuing my graduate education. I would like to acknowledge the School of Veterinary Medicine and the members of the Developmental Endocrinology Group for their valuable support. I am indebted to my committee members Dr. Robert Lipinski, Dr. Jyoti Watters, Dr. Dale Bjorling and Dr. John Svaren for their insight and guidance.

I would like to thank the Cellular and Molecular Biology graduate program and specifically director Dr. David Wassarman and coordinators Lauren Weitkamp and Sarah Bierke for ensuring a great graduate experience.

I would also like to extend my thanks to Dr. Aseem Ansari, Dr. Linda Schuler, Dr. Peiqing Wang, Linda Gauer, Dr. Caroline Alexander, Dr. Christopher Bradfield and Dr. Wei Xu for help along the way. I would like to thank my collaborators Dr. Li-Fang Chu (James Thomson lab, UW-Madison), Caden Ulschmid (Robert Lipinski lab, UW-Madison), Dr. Xin Sun (UCSD), Cathy Mendelsohn (Columbia University) and Dr. Douglas Strand (UT Southwestern) for their valuable contributions to this work.

I would like to thank all my teachers from Toc-H Public School, Vytilla and the National Institute of Technology, Calicut for a wonderful education and for instilling in me a love for learning.

I am thankful to my mother who has been a great source of support and inspiration for me and to my father for working hard to provide opportunities for me to further my career goals. I would like to thank my sister for always being on my side. I would like to thank my grandparents for always encouraging me in my academic career and for being wonderful examples for the value of education, hard work and integrity. Lastly, I would like to acknowledge the contribution of the animals, without which this work would not have been possible.

DIYA BINOY JOSEPH

Table of Contents

LIST OF FIGURES AND TABLES

ABSTRACT

The male lower urinary tract consisting of the urethra, prostate and bladder develops during the fetal stage in eutherian mammals from the endoderm-derived urogenital sinus. The establishment of specialized epithelium and specification of epithelial progenitors are crucial steps that occur during lower urinary tract development. Classical signaling pathways in lower urinary tract development have been well studied but the role of epigenetic mechanisms including DNA methylation is not fully known. Further, endocrine disrupting chemicals modify lower urinary tract development with accompanying DNA methylation changes, but the role of DNA methylation in normal prostate development is not well understood. I used a genetic model of epithelial specific deletion of the key DNA methylating enzyme, DNA methyltransferase-1 (*Dnmt1*), which revealed the requirement for DNA methylation in prostate bud formation by regulating cell cycle progression and survival of early prostate progenitors. *Dnmt1* deletion also induced hypomethylation, DNA damage, p53-activation and apoptosis of bladder progenitor cells and thinning of the fetal bladder epithelium. I made the unexpected discovery that apoptosis associated with *Dnmt1* deletion resulted in the breakdown of the Wolffian duct-urethra junction, which allowed mesodermal Wolffian duct cells to repopulate the depleted bladder epithelium. The ability of Wolffian duct cells to repopulate the bladder and acquire bladder characteristics reveals a hitherto unappreciated plasticity of the embryonic Wolffian duct epithelium with implications for bladder regenerative therapies. To investigate the role of DNA methylation in the adult prostate, I tested the impact of a diet enriched with the methyl donor folic acid on prostate homeostasis and response to castration induced

androgen deprivation. After castration, folic acid fed mice had larger prostates and increased secretory activity compared to castrated mice fed a control diet. Considering the widespread consumption of folic acid and the use of androgen deprivation as a treatment for prostate cancer, these results warrant further investigation into the interaction between folic acid and androgen deprivation. Together, my research has resulted in several insights and opened future lines of investigation into the role of DNA methylation in lower urinary tract development and prostate homeostasis.

CHAPTER 1. INTRODUCTION

Adapted from **Diya B Joseph** and Chad M Vezina. (2018).

Male Reproductive Tract: Development Overview. In M. K. Skinner (Ed.),

Encyclopedia of Reproduction. vol. 1, pp. 248–255. Academic Press: Elsevier.

http://dx.doi.org/10.1016/B978-0-12-801238-3.64366-0

ISBN: 9780128118993

And

Diya B Joseph, Douglas W Strand and Chad M Vezina (2018).

DNA methylation in development and disease: an overview for prostate researchers (American Journal of Clinical and Experimental Urology, under review)

1.1. Perceived contributions of thesis

Through my dissertation research, I have endeavored to extend our understanding of the role of DNA methylation in the developing urogenital tract and its adult derivatives. Developmental exposures (environmental toxins, nutrient deprivation, maternal stress and diet) can impact methylation patterns with far-reaching consequences on adult disease. The role of DNA methylation in transcriptional control has been studied extensively at the cellular level. In recent years, there has been a growing interest in understanding the role of epigenetic factors, including DNA methylation in growth and morphogenesis at the tissue and organ level.

There is an emerging role for DNA methyltransferase 1 (*Dnmt1*) in the maintenance of embryonic tissue progenitors. In Chapter 2, I present the consequences of conditional *Dnmt1* ablation in the mouse lower urinary tract epithelium. *Dnmt1* ablation depleted bladder progenitors which resulted in the recruitment of cells from the Wolffian duct into the bladder. The recruitment of Wolffian duct cells into the bladder is made possible through breakdown of the Wolffian duct-urethra junction, a unique structure that forms when epithelial tissues from two germ layers fuse. This is a paradigm shifting finding that demonstrates the ability of the damaged bladder to recruit stem cells from a non-bladder source to repair itself.

Epigenetic factors are being increasingly recognized as key regulators in morphogenesis. The importance of this process on prostate formation has been highlighted by the effects of pharmacological DNA methylation inhibition on prostate budding. In Chapter 3, I present the results of specific genetic inactivation of *Dnmt1* in the epithelium of the developing prostate. *Dnmt1* deletion causes cell cycle defects and depletes prostate

progenitors through apoptosis. By comparing recruitment of normal DNMT1 expressing cells versus replication impeded DNMT1 null cells to prostate buds, I obtained a unique insight into prostate bud formation. There is differential requirement for DNMT1 in the margins of prostate buds versus the core of prostate buds. I have employed DNMT1 deletion as a tool to render select cell populations replication incompetent and utilize this technique to obtain insights into prostate budding.

Given the dramatic role of DNMT1 in the developing lower urinary tract and prostate, I asked whether enhancing DNA methylation through a methyl-donor enriched diet could influence adult prostate homeostasis. I present in Chapter 4 that a folic acid enriched diet changes global transcription in the adult prostate and attenuates the response to androgen deprivation.

To increase rigor, reproducibility and transparency, raw image files and other data described in this dissertation were deposited into the GUDMAP consortium database and can be accessed through www.gudmap.org and directly at https://doi.org/10.25548/W-QXXC .

The following sections provide a survey of the current state of knowledge of male urogenital tract development and DNA methylation.

1.2. Male reproductive tract: Developmental Overview

Understanding the normal development of the Wolffian duct-urethra junction and the male urogenital system is crucial to understanding the recruitment of Wolffian duct cells to injured bladders (described in Chapter 2). A developmental overview of the male reproductive tract is provided in this section.

The male reproductive tract functions in the storage, maintenance and transportation of male reproductive cells. The human male reproductive tract structures develop during early fetal life and require contributions from all three germ layers. This section provides an overview of the embryological origins, morphogenesis and differentiation of structures comprising the developing male reproductive tract and their adult derivatives. Additionally, a summary of key developmental and hormonal signaling pathways involved in male reproductive tract development is provided along with a brief description of congenital anomalies affecting the male reproductive tract.

The male reproductive tract consists of organs involved in the storage, maintenance and transportation of male reproductive cells. The major structures of the male reproductive tract originate from the endoderm-derived cloaca and the mesoderm-derived Wolffian ducts. Male reproductive tract and urinary system development are closely linked and together their structures comprise the urogenital system. All human developmental ages mentioned in this chapter are counted from the day of fertilization.

1.2.1. Developmental origins of the male reproductive tract

Gastrulation gives rise to three germ layers: the endoderm, ectoderm and mesoderm. Male reproductive tract development begins early in gestation and involves cells from all three germ layers (Figure 1.1). The cloaca is a transient pouch-like structure at the terminal portion of the endoderm-derived hindgut in the early embryo. The cloaca (Latin for ‘sewer’) differentiates into the urogenital sinus, bladder, urethra and prostate in males. Paired epithelial Wolffian ducts derive from the mesoderm and insert into the cloaca. Testicular factors including testosterone masculinize male reproductive structures and drive cellular differentiation within them. The Wolffian duct gives rise to the epididymis,

vas deferens and seminal vesicle. In the mature adult, sperm are transported through the epididymis and vas deferens to the urethra. At the urethra, the seminal vesicle and prostate contribute secretions to the ejaculate that promote sperm health. The urethra is the conduit for deposition of sperm during reproduction (Moore and Persaud, 2003).

- ***Urethra, Urogenital sinus and Prostate***

Growth and re-positioning of mesenchymal tissue divides the cloaca into the urogenital sinus ventrally and the anorectal sinus dorsally by week 7 of gestation.

Urogenital Sinus

The ventral portion of the cloaca gives rise to the urogenital sinus (UGS). The UGS is a transient structure comprised of a simple epithelial tube featuring a balloon-shaped central cavity (Figure 1.1). Paired Wolffian ducts insert into the UGS around week 4 of gestation. The UGS is divided into three parts:

- The cranial or upper part of the UGS differentiates into the urinary bladder
- The middle or pelvic portion develops into the pelvic urethra and prostate
- The caudal or lower part develops into the phallic urethra

Urethra

The urethra develops from the middle and caudal regions of the UGS. The pelvic urethra extends from the bladder to the body wall. The phallic urethra extends from the body wall to the tip of the external genitalia. Urethral glands (Littre's glands) and bulbourethral glands (Cowper's glands) emerge as urethral outgrowths around week 12 of gestation.

Lineage tracing studies following the fate of endodermal cells within the developing lower urinary tract show that the entire urethral epithelium derives from endoderm (Seifert et

al., 2008). The developing urethra forms a stratified epithelium comprised of basal, intermediate and superficial layers. Epithelial-mesenchymal interactions are crucial for urethral morphogenesis. Sonic hedgehog (SHH) peptide is secreted from epithelium and activates GLI transcription factors in nearby mesenchyme. GLI transcription factors drive bone morphogenetic protein 4 (BMP4) transcription and mesenchymal differentiation. Molecular mapping studies in the mouse embryo reveal a multilayered pelvic urethral mesenchyme consisting of lamina propria, muscularis mucosa, submucosa and muscularis propria (Abler et al., 2011). Male urethral morphogenesis is guided by androgens, principally by androgen-induced signals from the male urethral mesenchyme that drive urethral epithelium differentiation and remodeling.

Prostate

The prostate is a male accessory sex gland positioned at the base of the bladder and surrounding the pelvic urethra. Prostate secretions contribute to the ejaculate and promote sperm health. Prostate ductal development initiates *in utero* as solid epithelial buds deriving from the UGS epithelium. The epithelial buds elongate, branch, and canalize to form a complex ductal system draining into the urethral lumen. Most studies on early prostate development have been carried out in rodents. The early development program of prostate budding is remarkably conserved between rodents and humans, even though their prostates differ anatomically at sexual maturity.

In the human fetus, prostate development occurs in response to testosterone production by testicular Leydig cells around week 7 of gestation. Testosterone acts on androgen receptor (AR)-expressing UGS mesenchymal cells. AR activation increases the abundance of UGS mesenchymal steroid 5 alpha reductase type 2 (SRD5A2). SRD5A2

converts testosterone to the more potent dihydrotestosterone (DHT). DHT binding to AR amplifies androgen signaling in UGS mesenchyme, which evokes paracrine signaling mechanisms to instruct UGS epithelium to form prostatic buds. Prostate bud outgrowth begins around week 10 of gestation and continues until week 24.

Studies in mice have shown that prostatic bud number and location are precisely controlled. The Nk-3 transcription factor locus-1 (NKX3-1) is the earliest marker of prostate specified UGS epithelial cells. Although prostatic bud formation cannot occur in the absence testosterone, several other factors including SHH, SOX9, HOXB13 and WNT5A are also required for prostatic bud formation and subsequent prostate ductal development.

Prostate formation is dependent on complex epithelial-mesenchymal interactions. Tissue recombination experiments have shown that androgen signaling deriving from UGS mesenchyme not UGS epithelium directs prostate bud formation. However, epithelial AR is required for prostate epithelial cell differentiation and secretory protein production. UGS mesenchyme is organized into distinct zones, and some zones serve as signaling centers to guide prostate morphogenesis. UGS mesenchymal condensations (mesenchymal pads) lie on the UGS periphery, are characterized by *FGF10* mRNA expression, and guide directional outgrowth of prostatic buds (Thomson and Cunha, 1999). Epigenetic mechanisms including DNA methylation and histone acetylation regulate expression of key genes involved in prostate development. DNA methylation controls E-cadherin (CDH1) and AR abundance, which in turn control prostate bud elongation and timing of bud formation, respectively (Keil et al., 2014a; Keil et al., 2014b). Histone acetylation controls BMP2 expression to regulate prostatic ductal branching (Keil et al., 2015b).

In later stages, the prostate undergoes branching, canalization and differentiation to form a pseudo-stratified epithelium consisting of basal cells, secretory luminal cells and rare neuroendocrine cells. The prostate increases in size following an upsurge in testosterone production during puberty. The study of early prostate development is receiving renewed interest as the reawakening of embryonic processes has been implicated in the pathogenesis of prostate cancer and benign prostatic hyperplasia.

- ***Rete Testis, Epididymis, Vas Deferens, Seminal Vesicle***

The intermediate mesoderm lies between paraxial and lateral plate mesoderm of the fetus and gives rise to ductal structures of the urogenital system. Crests of intermediate mesoderm called urogenital ridges form near the midline and along the cranio-caudal body axis. Early in week 4 of gestation, a non-functional, transient excretory organ called the pronephros develops within the urogenital ridge at the position of the thorax. The rudimentary tubular structures of the pronephros feed into the pronephric duct, which joins the cloaca at approximately week 4 of gestation. The pronephric duct is formed by mesenchymal to epithelial transition of intermediate mesoderm. The pronephros undergoes degeneration through an apoptotic program. The mesonephros forms caudal to the degenerating pronephros late in week 4 of gestation. The mesonephros contains glomeruli and mesonephric tubules that function as temporary kidneys until week 10 of gestation, when the metanephros permanently assumes kidney function. The mesonephric tubules open into mesonephric ducts (also known as Wolffian ducts) which drain into the cloaca. The mesonephros degenerates in the cranial to caudal direction around week 8, leaving a few residual tubules that will give rise to efferent ductules of the testis (Rao and Burnett, 2013).

The Wolffian ducts are precursors for ductal structures in the male reproductive and urinary tracts. The Wolffian ducts elongate along the anteroposterior axis, turn towards the midline and fuse with the cloacal epithelium (precursor of UGS and bladder epithelia). Disruption of Ret (Chia et al., 2011), EphA4/EphA7 (Weiss et al., 2014) or FGF signaling (Attia et al., 2015) results in inappropriate migration and fusion of the Wolffian duct with the cloaca, providing key insights into the molecular mechanisms that regulate Wolffian duct-UGS junction formation. However, mechanisms involved in junction maintenance during the complex morphogenetic changes that occur during urogenital tract development were not previously characterized. In Chapter 2, I demonstrate the role of DNMT1 expression in the maintenance of the Wolffian duct-UGS junction.

The ureteric bud emerges as a Wolffian duct outgrowth near its insertion into the cloaca (Figure 1.1). The ureteric bud undergoes branching and differentiation within a specialized mesenchyme called the metanephric blastema to form the metanephros or permanent kidneys. The ureteric bud is also the precursor for the ureters, which connect the kidneys to the bladder. The caudal portion of the Wolffian duct between the ureteric bud and the insertion site into the UGS is called the common nephric duct. Common nephric duct apoptosis positions the ureters at their final insertion site within the bladder, spatially separating the ureteral and Wolffian duct openings to the lower urinary tract. Ureter separation from the Wolffian duct is completed by week 7 of gestation. The timing of junction formation is critical for urogenital tract development and proper positioning of ureters into the bladder. Paired box 2 (PAX2) expression marks the intermediate mesoderm early after gastrulation. Lineage tracing studies show that the PAX2

expressing intermediate mesoderm gives rise to Wolffian ducts, the ureteric bud and the metanephric blastema (Bouchard et al., 2002).

During the ambisexual stage, two sets of paired genital ducts are present in male and female embryos. The paramesonephric or Müllerian ducts extend in the craniocaudal direction and lie lateral to the Wolffian ducts. Müllerian duct formation occurs between week 6 and 7 of gestation. Lineage tracing studies in chick and mouse models demonstrate that Müllerian ducts develop from the coelomic epithelial layer, which derives from lateral plate mesoderm. Although Wolffian ducts lie in close apposition to and stimulate Müllerian duct formation, the Wolffian ducts do not contribute epithelial cells to the Müllerian ducts (Guioli et al., 2007; Orvis and Behringer, 2007).

Sexual differentiation of the male reproductive tract begins around week 7 of gestation. Müllerian inhibiting substance (MIS) produced by Sertoli cells and testosterone produced by the interstitial Leydig cells of the fetal testis act on the reproductive tract to induce male differentiation. MIS is a glycoprotein of the TGF-β family of growth factors which causes irreversible regression of the Müllerian ducts in males. Testicular MIS production commences by week 8 of gestation and Müllerian duct regression occurs between weeks 8 and 10. The prostatic utricle near the UGS and the appendix testis near the male gonads are Müllerian duct remnants in males. Female reproductive structures including the uterus, vagina and oviducts form in the absence of MIS. Testosterone-mediated AR activation supports Wolffian duct survival in males. Reproductive tract structures derived from the Wolffian ducts are formed between week 9 and 13 of gestation. Regional expression of homeobox (HOX) genes drives segmental differentiation of the Wolffian

duct into the epididymis, vas deferens and seminal vesicle. The Wolffian duct regresses in females due to insufficient testosterone to support its survival (Rao and Burnett, 2013).

Rete testis

After the mesonephros undergoes regression, the remaining mesonephric tubules form the efferent ductules. The seminiferous tubules, which contain sperm cells, are connected to the efferent ductules by a maze-like network of interconnecting tubes called the rete testis. The ciliated cells lining the rete testis guide sperm into the efferent ductules.

Epididymis

The efferent ductules, which receive sperm from the testis, drain into the epididymis. The epididymis is a convoluted series of tubules that derives from a portion of the Wolffian duct adjacent to the testis. The epididymis stores and transports sperm.

Vas Deferens

The medial Wolffian duct segment forms the vas deferens. Androgens drive Wolffian duct differentiation into the vas deferens around week 12 of gestation. Smooth muscle surrounding the vas deferens contracts during ejaculation to propel sperm from the epididymis to the urethra.

Seminal Vesicle

The seminal vesicles develop as lateral outgrowths from the caudal Wolffian duct segment. The seminal vesicles form around week 10 of gestation, after the onset of testosterone synthesis by the fetal testis. Seminal vesicles contribute secretions to the ejaculate. The most caudal Wolffian duct portion, positioned between the seminal vesicle and the urethra, is called the ejaculatory duct. Ejaculatory ducts drain the contents of the seminal vesicle and vas deferens into the urethra.

- ***External Genitalia***

Internal fertilization requires specialized male and female external reproductive organs. Lateral plate mesoderm, endoderm and surface ectoderm cells contribute to the external genitalia. The initial phase of external genitalia development is essentially the same in males and females. In the later phase, androgens drive the masculinization of the external genitalia in males (Blaschko et al., 2012; Yamada et al., 2003).

Early phase: Formation of ambisexual external genitalia

The early phase of external genitalia development, which occurs between 4-7 weeks of gestation, is the same in males and females. This phase occurs independently of androgen action as it happens before the onset of testicular testosterone production. The cloacal membrane, formed by direct contact of the endoderm and surface ectoderm, is intact at 4 weeks of gestation. Proliferating lateral plate mesenchymal cells form paired lateral swellings above the cloacal membrane. These swellings fuse at the midline to form the genital tubercle. The genital tubercle is a bi-potential structure which is the precursor of the penis in males and clitoris in females. Paired mesenchymal swellings called urogenital folds and labio-scrotal swellings form on either side of the cloacal membrane. After cloacal septation around week 7, the cloacal membrane becomes the urogenital membrane ventrally and the anal membrane dorsally. The cloacal membrane ruptures at two sites to form the urethral orifice and the anal opening. The urogenital membrane is bounded by urogenital folds and lies within a temporary indentation on the ventral genital tubercle surface called the urethral groove. The urethral groove is lined by a solid cord of endodermal cells comprising the urethral plate epithelium. The urethral plate epithelium is the region of the phallic urethra distal to the UGS.

Studies in mice have shown that early patterning of the genital tubercle does not depend on androgens but does require Sonic hedgehog (SHH) signaling. Mice harboring inactivating mutations in the SHH gene fail to form external genitalia. SHH signaling from the urethral plate epithelium coordinates cell movements during external genitalia development (Perriton et al., 2002).

Later phase: Sexual differentiation of the external genitalia

Male testicular androgens induce genital tubercle differentiation into the penis. In females, the genital tubercle fails to elongate and forms the clitoris in the absence of androgens. Testosterone synthesis begins by week 7 of gestation and maximal concentrations in the fetus are achieved between weeks 10 and 15 of gestation. Early signs of signs of sexual differentiation in the external genitalia can be detected by week 9 and complete differentiation is achieved by weeks 12-13.

The steroid hormone dihydrotestosterone (DHT) masculinizes the external genitalia. Testosterone is converted to DHT by the action of steroid metabolizing enzymes like SRD5A2 which are expressed in genital tubercle mesenchymal cells. DHT initiates androgen signaling in androgen receptor expressing mesenchymal cells. Interactions between androgen activated mesenchyme and urethral plate epithelium initiate male external genitalia differentiation.

Androgen exposure elongates the genital tubercle into the penis. Early in sexual differentiation, the proximal phallic urethra is a closed hollow tube but the distal portion comprising the urethral plate epithelium remains a solid mass of cells. The urogenital folds lining the penile ventral surface guide midline fusion of the urethral plate, forming a hollow urethral tube that extends the whole length of the penis. The fusion of urogenital

folds occurs in a proximal to distal direction, positioning the urethral orifice at the tip of the penis. Hypospadias, a common birth defect, occur from defective fusion of urogenital folds. Specialized mesenchyme induces the differentiation of the distal urethra into a stratified squamous epithelium. The labio-scrotal swellings fuse in the midline to form the scrotum. The skin covering the developing penis is derived from surface ectoderm. Specialized structures of the penis, the corpus cavernosa and the corpus spongiosum, derive from the proliferation and differentiation of mesoderm derived cells.

The Genitourinary Development Molecular Anatomy Project (GUDMAP) website provides curated information on reproductive tract anatomy, histology, mRNA and protein expression over developmental time (www.gudmap.org).

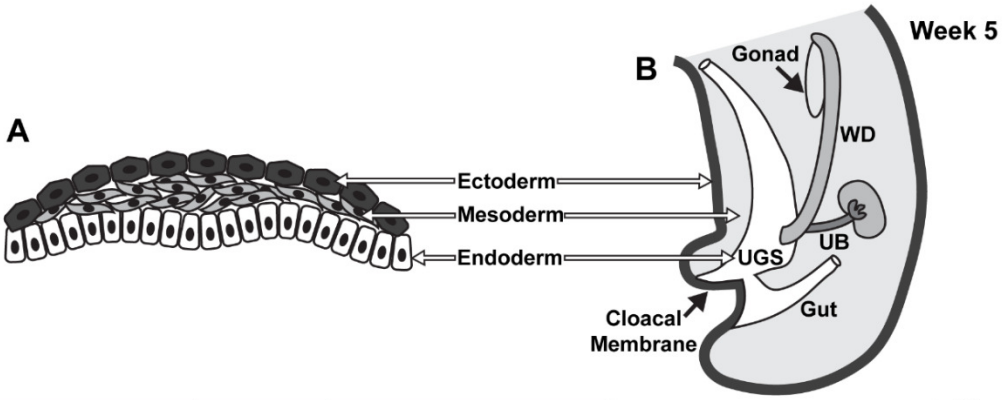

Organ	Origin	Male derivatives
UGS: Urogenital sinus	Endoderm	Urethra, Prostate
UR: Urethra	Endoderm	
PR: Prostate	Endoderm	
WD: Wolffian duct	Mesoderm	Vas deferens, Seminal Vesicle, Ejaculatory duct
VD: Vas deferens	Mesoderm	
SV: Seminal Vesicle	Mesoderm	
ED: Ejaculatory duct	Mesoderm	
UB: Ureteric Bud	Mesoderm	Ureters, Kidney
MD: Mullerian duct	Mesoderm	Prostatic utricle, Appendix testis

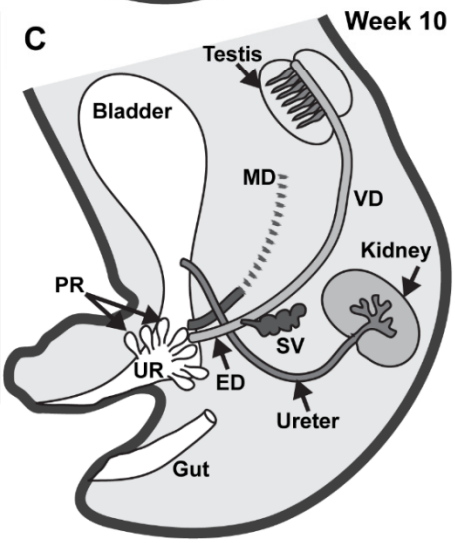

Figure 1.1 Germ cell layer of origin of male reproductive tract structures

(A) Cross sectional view of a gastrulation stage embryo showing the three germ layers: endoderm (white), mesoderm (light grey) and ectoderm (dark grey). (B) Sagittal view of the male reproductive tract in a week 5 embryo during the bi-potential stage. (C) Sagittal view of the male reproductive tract in a week 10 embryo after the onset of sexual differentiation. Structures of the reproductive tract are colored according to germ layer of origin.

Table 1.1 Chronology of male reproductive tract development in human and mouse

Human	Internal Reproductive Tract	External Genitalia	Mouse
Week 3	Gastrulation; Cloacal Membrane forms		E6-E6.5
Week 4	Nephrogenic cord forms		E8.5
	Pronephros forms		E9
	Cloaca develops from hindgut		E9.5
	Mesonephros forms		E9.5-E11.5
	Wolffian duct fuses with cloaca (Day 26)		E9.5
		Genital tubercle forms	E11-E11.5
Week 5	Ureteric bud forms (Day 28)		E10.5-E11.5
	Cloacal septation begins		E10.5
	Common nephric duct apoptosis		E11-E12
Week 6	Müllerian duct forms		E12-E13
		Urogenital and labio-scrotal folds form	E14
Week 7	Cloacal septation complete	Cloacal membrane rupture	E13-E13.5
	Ureters join bladder		E13-E14
	Onset of testosterone synthesis		E13-E13.5
Week 8	Müllerian ducts reach UGS		E13.5
	ONSET OF SEXUAL DIMORPHISM		
Week 9	Müllerian duct degeneration		E16.5
	Wolffian duct differentiation		E16.5-P1
Week 10	Müllerian duct degeneration complete		E16.5
	Seminal vesicle forms		E16.5
	Prostate forms		E16.5-E18.5
	Wolffian duct differentiation		E16.5-P1
Week 11	Wolffian duct differentiation		E16.5-P1
Week 12	Wolffian duct differentiation		E16.5-P1
Week 13		Urethral tube closure	E16.5
2nd Trimester		Growth of external genitalia	E15.5 to P1
		Inguinal descent (Week 23)	E15.5-E17.5
3rd Trimester		Growth of external genitalia	E15.5-P1
		Scrotal descent (Week 24-34)	E17.5-P20

1.2.2. Signaling pathways in male reproductive tract development

Studies in rodents have greatly advanced our knowledge of signaling pathways involved in male reproductive tract development. Table 1.1 provides a parallel chronology of the major events in male reproductive tract development in human and mouse.

- ***Sonic Hedgehog signaling***

Sonic hedgehog (SHH) peptide is a developmental morphogen secreted by epithelial cells of the bladder, urethra and prostate. The secreted SHH peptide relieves the repression of smoothened (SMO) by binding to its inhibitor patched (PTCH1). SMO activation initiates transcription of GLI transcription factors which are involved in several developmental and morphogenetic processes. SHH is expressed in hindgut-derived structures including the cloacal epithelium, where it patterns the surrounding mesenchyme. SHH induces mesenchymal GLI2, which regulates epithelial and mesenchymal proliferation and apoptosis during cloacal development. SHH regulates cloacal septation by promoting proliferation of mesenchymal cells in the urorectal septum (Seifert et al., 2009). SHH signaling is required for prostate formation and external genitalia development. Treatment with SHH inhibitors impairs prostate ductal growth and morphogenesis (Podlasek et al., 1999). SHH knockout mice show a complete absence of external genitalia (Haraguchi et al., 2001).

- ***WNT-beta catenin signaling***

WNT ligand binding to cell surface Frizzled receptors stabilizes and activates the transcription factor beta-catenin. WNT signaling is involved in several aspects of urogenital development including the septation of the cloaca into the urogenital and anorectal sinuses. Disruption of WNT signaling results in rectourethral fistulas (abnormal

connection between the urethra and rectum). Epithelial beta-catenin is also required for prostate development and growth (Mehta et al., 2013). The WNT-beta catenin pathway acts downstream of SHH signaling to regulate external genitalia development (Miyagawa et al., 2009).

- ***Bone morphogenetic proteins***

Bone morphogenetic proteins (BMPs) are growth factors belonging to the TGF-beta superfamily. BMPs bind to serine threonine kinase receptors and initiate intracellular signaling through SMAD proteins. BMP7 expression in the urorectal septum is required for cloacal septation. In addition, BMP7 expression maintains proliferation and cell survival in the cloacal epithelium (Xu et al., 2012). Expression of BMP7 in the UGS mesenchyme restricts prostate ductal budding and prevents excessive branching of elongating ducts (Grishina et al., 2005).

- ***Fibroblast growth factors***

Fibroblast growth factors are a family of secreted growth factors that signal through tyrosine kinase fibroblast growth factor receptors to regulate proliferation, differentiation and morphogenesis during embryonic development. FGF signaling is required for cell survival during the early stages of genital tubercle outgrowth. FGF signaling in the ectoderm is required for urethral tube formation. Deletion of FGF10 or its receptor FGFR2 results in severe hypospadias (Harada et al., 2015). FGFR2, a critical regulator of prostate development, is required for branching and growth of prostate buds. FGF10 is a paracrine mediator of epithelial to mesenchymal signaling during prostate bud formation. FGF10 knockout mice fail to form prostate, seminal vesicle, bulbourethral glands and caudal vas deferens (Thomson and Cunha, 1999).

- ***PAX genes***

Paired box (PAX) genes are tissue specific transcriptions factors that determine lineage specification in the early embryo. PAX2 and PAX8 are required for Wolffian duct formation from the intermediate mesoderm. In PAX2 and PAX8 double mutant mice, the intermediate mesoderm fails to undergo the mesenchymal to epithelial transition required for Wolffian duct formation (Bouchard et al., 2002). GATA3, a downstream effector of PAX2, regulates Wolffian duct growth and caudal extension which is required for fusion with the cloaca and formation of definitive kidneys (Grote et al., 2006).

- ***EPH receptors/Ephrins***

EPH receptors are a family of receptor tyrosine kinases with plasma membrane bound ligands called ephrins. EPH receptor/ephrins are involved in the maintenance of cell-cell adhesion and communication between similar or different cell types during developmental processes. The ephrin receptors EPHA4 and EPHA7 are expressed in the mesenchyme surrounding the cloaca and Wolffian duct where they mediate Wolffian duct fusion with the cloaca (Weiss et al., 2014). Signaling from EPHA4 and EPHB2 is required for apoptosis of the common nephric duct for proper separation of ureters from Wolffian ducts (Peuckert et al., 2016). EphrinB1 expressed by prostatic mesenchyme regulates prostate growth and branching (Ashley et al., 2010).

- ***Vitamin A/Retinoic acid signaling***

Retinoic acid, a derivative of Vitamin A (retinol), binds to nuclear retinoic acid receptors to activate transcriptional programs for differentiation and organogenesis. The spatial expression of retinaldehyde dehydrogenases, which convert retinaldehyde to retinol, is tightly regulated in a tissue specific manner. Apoptosis induced by retinoic acid signaling

is required for ureter separation from the Wolffian duct and proper positioning in the bladder (Batourina et al., 2005). Retinoic acid is a powerful inducer of prostate budding (Vezina et al., 2008a). Retinoic acid signaling regulates external genitalia formation by maintaining SHH and BMP4 expression in the genital tubercle (Liu et al., 2012).

- ***Müllerian inhibiting substance***

Müllerian inhibiting substance (MIS) or anti-Müllerian hormone (AMH) is a gonadal hormone secreted by Sertoli cells of the developing testis. The secreted glycoprotein MIS belongs to the TGF-beta family of transcription factors. MIS acts through AMH Type II receptors expressed by Müllerian duct mesenchyme to initiate apoptosis and degeneration of the Müllerian duct (Abler et al., 2011; Behringer, 1995).

- ***Androgens, INSL3***

Testosterone synthesis initiates from fetal Leydig cells during Week 7 of gestation. Testosterone is converted to the more potent dihydrotestosterone (DHT) by the enzyme SRD5A2. DHT acts on AR expressing cells to initiate androgen-dependent transcriptional programs. DHT regulates prostate and seminal vesicle formation, external genitalia masculinization and formation of the vas deferens and epididymis. The Leydig cell specific insulin-like peptide INSL3 binds to relaxin/insulin like family peptide receptor 2 (RXFP2) to promote testicular descent into the scrotum (Barsoum and Yao, 2006).

- ***Endocrine disruptors***

Environmental toxins with the capability of interfering with endocrine signaling are known as endocrine disruptors (Prusinski et al., 2016). *In utero* exposure to endocrine disruptors adversely affects hormone-dependent development and increases risk of adulthood disease. The prostate is susceptible to endocrine disruptors like Bisphenol A and Dioxin

that have DNA hypomethylating activity. Understanding the role of DNA methylation in the development of the prostate will help us study how fetal exposures to environmental toxins leads to epigenetic changes and susceptibility to prostate disease in adults. Maternal exposure to low doses of Bisphenol A, an estrogenic compound found in plastics, has been shown to increase prostate size in rodent models (Dolinoy et al., 2007a; Gupta, 2000). Early exposure to Bisphenol A can also increase the risk of prostate cancer in rodent models of estrogen-induced carcinogenesis by inducing long-term changes to the DNA methylome (Cheong et al., 2016). The anti-androgenic endocrine disruptor vinclozolin found in fungicides, can induce hypospadias in mice (Buckley et al., 2006). *In utero* exposure to persistent environmental pollutants called 2,3,7,8 tetrachlorodibenzo-*p*-dioxin or dioxins, impairs reproductive function of male and female rodents (Bjerke and Peterson, 1994; Gray and Ostby, 1995). *In utero* dioxin exposure disrupts mouse prostate formation (Vezina et al., 2008b) and sensitizes mice to hormone-mediated urinary dysfunction (Ricke et al., 2016a).

1.2.3. Congenital anomalies of the male reproductive tract

Congenital anomalies of the male reproductive tract can reduce fertility. Hypospadias are the most common congenital anomaly of the male reproductive tract, with an occurrence of 1 in 250 live male births. Hypospadias occur when the urethral opening is not at the tip of the penis, but instead on the ventral surface or scrotal region. Defects in urethral tube closure result in hypospadias (Baskin and Ebbers, 2006). Genetic, endocrine and environmental factors have been implicated in hypospadias. Epispadias, which occur when the urethral opening is on the dorsal surface of the penis, is a much rarer condition (affecting 1 in 117,000 males) (J.P. Gearhart, 1992). Unlike hypospadias, epispadias

result from defects in the cloacal membrane (Suzuki et al., 2017). Another congenital anomaly called chordee is associated with increased curvature of the penis. A congenital condition called posterior urethral valves is associated with the occurrence of flaps of urethral tissue that obstruct urine flow and impair reproductive function (Agarwal, 1999).

Persistent Müllerian duct syndrome is a rare anomaly of the reproductive tract in which Müllerian duct derivatives (uterus and oviduct) persist in males. The persistence of Müllerian duct derivatives can be due to insufficient production of Müllerian inhibiting substance (MIS) or insensitivity of the Müllerian duct to MIS (Elias-Assad et al., 2016).

Congenital anomalies of Wolffian duct derivatives include ectopic insertion of the ureter into the urethra, seminal vesicle, ejaculatory duct or vas deferens. Ectopic ureters are a result of abnormal ureteric bud formation and abnormal separation from the Wolffian duct during kidney development. Ectopic ureter insertion into the seminal vesicle results in the development of congenital seminal vesicle cysts. Seminal vesicle anomalies on their own do not contribute to male infertility. However, these defects are often observed with other Wolffian duct defects that affect fertility (Kroovand and Perlmutter, 1981).

Defects in vas deferens development are a major cause of male infertility. Congenital bilateral absence of the vas deferens results in male infertility from obstructive azoospermia (lack of sperm in semen). This condition is highly prevalent in males who have abnormal mucus production from mutations in the Cystic fibrosis transmembrane conductance regulator (CFTR) gene. Abnormal mucus production in affected individuals results in obstruction and destruction of the vas deferens, leading to infertility in later life (Stuhrmann and Dork, 2000). Other congenital anomalies of Wolffian duct derivatives

include agenesis of the epididymis, epididymal cysts with loss of continuity, agenesis of the seminal vesicle and agenesis of the ejaculatory duct.

1.3. Mesenchyme instructs differentiation of the multi-potent epithelial cells of the urogenital tract

The epithelial structures of the urogenital tract derive from two germ layers namely the intermediate mesoderm and the endoderm. The urogenital sinus (UGS) and bladder epithelium derive from the endoderm layer. The ureters and kidney collecting ducts derive from the intermediate mesoderm layer. The Wolffian duct (precursor of the seminal vesicle, vas deferens, epididymis) and the Mullerian duct (precursor of the vagina, uterus and oviducts) also derive from the intermediate mesoderm. Epithelial structures of the urogenital tract have unique protein expression profiles and specialized characteristics that aid in their function. For example, the epithelium of the bladder forms specialized Uroplakin plaques to protect against urine exposure. Prostate and seminal vesicle epithelium differentiate in response to androgens, but they have distinct secretory gene profiles. The specialized characteristics of these epithelial structures are determined by epithelial-mesenchymal interactions with their unique mesenchyme. Embryonic mesenchyme possesses an inductive capacity to remodel epithelium. Our understanding of this inductive capacity and the role of epithelial-mesenchymal interactions in urogenital tract development have been greatly advanced by tissue recombination studies.

A typical tissue recombination experiment involves isolation of epithelial compartments and mixing with isolated mesenchyme from the same source (homotypic) or a different source (heterotypic). The recombined tissues are cultured *in vitro* or in renal grafts to assess epithelial growth and differentiation. Tissue recombination studies have identified

the capacity of embryonic mesenchyme to induce epithelial differentiation in its corresponding epithelium and reprogram epithelia from other organs. In addition, these studies have identified that the epithelial reprogramming is limited by germ layer of origin of the epithelium (Boutin et al., 1991, 1992; Cunha and Baskin, 2016). UGS mesenchyme, which normally directs prostate formation, induces prostate differentiation when recombined with endodermal bladder epithelium (Donjacour and Cunha, 1993; Neubauer et al., 1983). When UGS mesenchyme is recombined with Wolffian duct epithelium, it induces seminal vesicle differentiation not prostate differentiation (Cunha and Baskin, 2016). Similarly, seminal vesicle mesenchyme induces prostatic differentiation in bladder epithelium (Donjacour and Cunha, 1995). Thus, the reprogramming capacity of inductive mesenchyme appears to be restricted by the germ layer of origin of the epithelium in the urogenital tract. These tissue recombination studies have also demonstrated that inductive embryonic mesenchyme can change the developmental fate of embryonic, neonatal and adult epithelia. This demonstrates that adult epithelial stem cells retain the capacity to de-differentiate and acquire new characteristics under mesenchymal induction.

Although germ layer plasticity in reprogramming has not been demonstrated in the urogenital tract, exceptions to this exist in recombination studies involving multiple organ systems. Studies have shown that prostatic mesenchyme can induce mammary epithelia (ectoderm-derived) to express both prostatic and mammary characteristics simultaneously. Endoderm-derived bladder epithelium trans-differentiates to acquire ectoderm like characteristics while retaining endodermal characteristics when recombined with ectoderm associated mesenchyme (Taylor et al., 2009). In another

study, adult rat stem Leydig cells transdifferentiate to acquire characteristics of endodermal and ectodermal epithelium when recombined with corresponding mesenchyme (Nanjappa et al., 2017). Together, these studies demonstrate the remarkable inductive capacities of embryonic mesenchyme and the ability of adult tissue stem cells to transdifferentiate across lineages in response to mesenchymal cues.

Epithelial-mesenchymal interactions are crucial for bladder development. The bladder develops from the anterior urogenital sinus. Epithelium-mesenchymal interactions pattern the mesenchyme surrounding the bladder to form the lamina propria and muscularis propria layer (Baskin et al., 2001). The lamina propria is a loose matrix of cells and connective tissue, devoid of smooth muscle, that allows the bladder to expand during filling. The muscularis propria is composed of organized smooth muscle bundles required for bladder emptying (Georgas et al., 2015). Embryonic bladder mesenchyme is unable to differentiate into smooth muscle without *Shh* secreted by the bladder epithelium (Cao et al., 2010). Patterning of bladder mesenchyme, resulting in a smooth muscle free lamina propria and smooth muscle expressing muscularis propria, is also dependent on *Shh* signaling mediated by *Gli* transcription factors and *Bmp4* (Tasian et al., 2010).

Bladder mesenchyme supports the survival, growth and differentiation of the urothelium. Isolated bladder urothelium recombined with bladder mesenchyme forms differentiated bladder tissue under renal grafts while bladder urothelium alone fails to survive (Oottamasathien et al., 2006). Embryonic bladder mesenchyme can direct embryonic stem cells and bone marrow derived stem cells to form differentiated bladder urothelium characterized by Uroplakin expression (Anumanthan et al., 2008; Oottamasathien et al., 2007). The question then arises whether other urogenital tract epithelia can be trans-

differentiated into urothelium. However, no previous tissue recombination studies had reported the results of recombining bladder mesenchyme with embryonic Wolffian duct or urogenital sinus epithelium (Cunha and Baskin, 2016). Wolffian duct epithelial cell movement into the inductive bladder mesenchyme niche, described in Chapter 2, provides a unique opportunity to study Wolffian duct reprogramming by bladder mesenchyme. We observed that ectopic Wolffian duct epithelial cells in the bladder gradually acquire bladder markers (FOXA1, KRT5, P63 and Uroplakins) and transform from a columnar to cuboidal morphology. This is a unique demonstration of cross-germ layer plasticity in the urogenital tract. We also demonstrate using tissue recombination studies that the embryonic bladder mesenchyme has the capacity to reprogram normal Wolffian duct epithelium. In the next section, I have discussed how the inductive capacity of the bladder can be leveraged for bladder regenerative therapies.

1.4. Leveraging developmental knowledge to advance bladder replacement strategies

The ability of bladder mesenchyme to direct urothelial differentiation has important implications for bladder replacement strategies. Neurogenic bladder, exstrophy or vesicoureteral reflex can impair bladder emptying and damage the entire urinary tract. There are a few examples of conditions that necessitate removal and replacement of the bladder to restore normal urinary outflow. Conditions like bladder carcinoma require the removal of large portions of the bladder to prevent dissemination of the cancer. Bladder augmentation uses bowel segments (ileum, colon or stomach) to form a pouch that serves as a urine reservoir. However, the disparate characteristics of the bladder urothelium and bowel segments leads to several side effects. Use of ileal segments has an increased risk of perforation and can lead to excess mucus production. The transplanted bowel

segments are also at risk for developing cancer (Subramaniam, 2017). Clinical studies have described the use of ureters for bladder augmentation, but this is used only in rare cases when patients present with a unilateral non-functioning kidney and megaureter. In addition, the small size of the ureter limits the size of the urinary reservoir (Özdemir and Arıkan, 2013). Bladder tissue engineering strategies involve seeding urothelial cells in acellular matrices to mimic the 3D environment in which bladder differentiation occurs. Seeded urothelial cells can proliferate to regenerate the damaged bladder and the scaffold provides support for new cell growth. Most of these strategies are being tested in animal models and are not yet in clinical practice due to the inherent challenges in culturing urothelial cells derived from the host (Akbal et al., 2006; Bolland et al., 2007). A recent study describes the use of tissue-engineered autologous bladders, grown from patient derived urothelial and muscle cells seeded on a biodegradable collagen scaffold (Atala et al., 2006). Use of autologous bladder urothelium for re-growing functional urothelium is precluded in patients with carcinoma.

Based on our observations (described in Chapter 2), Wolffian duct epithelium or its derivatives (ureters, seminal vesicle, vas deferens) could serve as alternative sources of bladder regenerating cells. Under the influence of bladder mesenchyme, the embryonic Wolffian duct epithelium differentiates to form bladder urothelium in a step wise manner that mimics normal bladder differentiation. This is despite the disparate embryonic origins of the bladder and Wolffian duct epithelium.

1.5. Nephrogenic Adenoma: Clinical evidence for mesodermal replacement of bladder urothelium

Though the bladder is quiescent under normal conditions, it has the remarkable capacity to regenerate itself when injured. The stem cells for bladder regeneration were thought to reside solely in the basal and intermediate layers of the urothelium. But what happens when there is irreversible damage to these stem cell populations? The model described in Chapter 2 provides the first experimental demonstration of bladder epithelial regeneration by an extra-bladder source, mesodermal cells.

I searched the literature for observations of mesodermal cells in bladder epithelium of human patients. Nephrogenic adenoma, a rare benign condition of the bladder, is characterized by the appearance of PAX2 and PAX8 positive mesodermal cells in the urothelium and surrounding mesenchyme. Nephrogenic adenoma lesions can occur throughout the urinary tract (renal pelvis, ureters, bladder, urethra) but are most commonly observed in the bladder. The first description of benign focal growth in the bladder was reported in 1949 (Davis, 1949) and the term ‘nephrogenic adenoma’ was coined in 1950 to describe this condition (Friedman and Kuhlenbeck, 1950). The lesions were called nephrogenic adenoma for their similarity to renal structures. Nephrogenic adenoma can occur in patients of all ages and in both males and females. In a retrospective study of 70 cases of nephrogenic adenoma, most patients had a history of urethral or bladder surgery with lesions often localized to the site of surgery (Ford et al., 1985). Nephrogenic adenoma is almost always associated with a pre-disposing risk factor including congenital bladder anomalies, bladder inflammation, trauma, surgery or renal transplant (Pycha et al., 1998).

Nephrogenic adenoma lesions have been identified within the urothelium and bladder mucosa (Pina-Oviedo et al., 2013). The lesions are thought to occur by seeding of nephric-lineage cells from the kidney in injured regions of the bladder. This has been demonstrated in renal transplant patients, where nephrogenic adenoma tissues have sex chromosomes matching the renal transplant donor not the recipient (Mazal et al., 2002). This suggests that sloughed off renal cells in the urine could be seeding injured regions of the bladder damaged by surgery or inflammation (Mazal et al., 2002). The nephric lineage markers PAX2 and PAX8 are used as diagnostic markers of nephrogenic adenoma distinguishing it from adenocarcinoma (Tong et al., 2006; Tong et al., 2008).

Nephrogenic adenoma closely parallels the phenotype described in Chapter 2, but there are some key differences. In both cases, bladder injury precedes the advent of mesodermal cells in the bladder. In my model, *Dnmt1* loss induces bladder damage allowing mesodermal Wolffian duct epithelial cells to repopulate the bladder while sloughed off mesodermal kidney tubule cells have been shown to give rise to nephrogenic adenoma. In contrast to ectopic Wolffian duct cells in *Dnmt1* mutants, mesodermal cells in nephrogenic adenoma do not acquire markers like p63 (Kao et al., 2013). Despite differences, these two instances demonstrate the ability of mesodermal cells to seed damaged bladders and proliferate.

1.6. Overview of DNA methylation

1.6.1. Epigenetics: Historical perspective

Developmental biologists in the early-twentieth century grappled with the question of how cells containing the same genetic code could behave so differently during development and develop specialized functions. The term epigenetics, meaning above the genome,

was coined by Waddington in 1942 to explain how non-coding changes to the genetic material could direct cell specialization during development (Waddington, 2012). In recent times, definitions of epigenetics have moved beyond developmental biology to encompass other fields including cancer biology and toxicology. One widely accepted definition states that epigenetics is “the study of changes in gene function that are mitotically and/or meiotically heritable and that do not entail change in DNA sequence” (Holliday, 1994; Wu and Morris, 2001). The modern definition of epigenetics includes DNA methylation changes, histone modifications and non-coding RNAs which act together to finely regulate gene expression.

1.6.2. Introduction to DNA methylation

DNA methylation refers to the addition of methyl groups to the 5’ position of cytosine bases in DNA, preferentially at CpG dinucleotides sites (Doskočil and Šorm, 1962). 60% of CpG dinucleotides in the mammalian genome are methylated (Bestor et al., 1984). CpG dinucleotides often reside in clusters called CpG islands which are generally unmethylated and associated with gene promoters. Based on bacterial methylases, DNA methylases that would act on hemi-methylated sites were proposed in mammals (Holliday and Pugh, 1975; Riggs, 1975). Studies using restriction enzymes to probe methylated sites (methylated sites resist restriction enzyme cleavage) identified that the methylation status of CpG dinucleotide pairs was the same on both strands (either unmethylated or fully methylated) (Bird, 1978). This study supported the existence of a DNA methylase that would act preferentially at hemi-methylated sites to complete DNA methylation (Bird, 1978). This ensures the maintenance of methylation patterns through replication for stable inheritance of epigenetic information. Unique methylation patterns develop in

differentiated cells which correlate with gene expression. Usually active promoter regions are hypomethylated, which suggests that DNA methylation controls access to tissue specific transcription factors.

DNA methylation patterns are laid down by DNA methyltransferases that add methyl groups to cytosines or adenines. Cytosine methylation is more widespread in mammals and most research in DNA methylation has concentrated on this modification and not adenine methylation. The identification of bacterial methylases spurred researchers to identify DNA methyltransferases in mammals. An enzyme with DNA methyltransferase activity and preference for hemi-methylated DNA was purified from murine cells (Bestor et al., 1984; Bestor and Ingram, 1983). This was followed by cloning of murine (Bestor et al., 1988) and human DNA methyltransferase cDNA (Yen et al., 1992). This enzyme would later come to be known as DNA methyltransferase-1 (DNMT1) following the discovery of other DNA methyltransferases. Targeted mutation of the DNA methyltransferase gene did not affect cultured murine embryonic stem (ES) cells but resulted in embryonic lethality in mutant mice with a 3-fold decrease in 5mC levels (Li et al., 1992). *De novo* methylation or the addition of methyl groups to unmodified DNA is crucial for laying down methylation patterns in the early embryo and during gametogenesis. It was still unclear whether there was only a single mammalian DNA methyltransferase responsible for both maintenance and *de novo* methylation. ES cells null for the DNA methyltransferase (*Dnmt1*) gene retained *de novo* methylation activity, indicating that other DNA methyltransferases capable of *de novo* methylation were present in mammals (Lei et al., 1996). These enzymes were found to be encoded by *Dnmt3a* and *Dnmt3b* (Okano et al., 1998). DNMT3A and DNMT3B have *de novo*

methylating activity and are required for mammalian development (Okano et al., 1999). Another DNMT3 family member, DNMT3L is catalytically inactive, but cooperates with DNMT3A and DNMT3B (Chédin et al., 2002; Hata et al., 2002).

Studying the protein structures of DNMTs has provided key insights into their function. The transfer of methyl groups to cytosines in DNA is a highly conserved process. Methyltransferases bind to DNA, 'flip' out cytosine from the DNA helix and attach the methyl group from S-adenosyl methionine to the 5' position of cytosine. DNMTS have N-terminal regulatory domains and C-terminal catalytic domains. The N-terminal regulatory domain contains motifs for protein-DNA interactions, protein-protein interactions and nuclear localization. The C-terminal region contains the conserved motifs that define the active site of the enzyme. The N-terminal region of DNMT3L shares similarities with that of *DNMT3A* and *DNMT3B* but it lacks the catalytic active site in its C-terminal domain.

Broadly, the division of labor between DNMTs is clear. DNMT3A and DNMT3B *de novo* methylate the genome during early development and gametogenesis. DNMT1, with its preference for hemi-methylated DNA, propagates methylation patterns during tissue growth. I will briefly summarize the cellular localization, binding partners and major functions of each of the four DNMTs below:

- ***DNMT1***

DNMT1 is a large protein comprised of ~1620 amino acids. DNMT1 localizes to sites of replication during S-phase and shows a distinct punctate staining in the nuclei. During other stages of the cell cycle, DNMT1 staining is diffuse in the nucleus. The N-terminal region of DNMT1 contains an RFTS (Replication foci targeting sequence) that targets it to sites of replication (Leonhardt et al., 1992). Autoinhibition of MTase domain of DNMT1

by interaction with the RFTS domain determines substrate specificity. Conformational changes in the N-terminal region inhibit catalytic activity when DNMT1 is bound to unmethylated CpG substrates. This inhibition is released when DNMT1 is bound to hemi-methylated CpG substrates (Zhang et al., 2015b). Preferential localization to replication foci and substrate specificity for hemi-methylated DNA allows DNMT1 to stably propagate tissue specific methylation patterns. DNMT1 is highly expressed in a cell cycle dependent manner (peaking in S-phase) in replicating cells but present only at low levels in non-replicating cells (Szyf et al., 1985). During fetal prostate development, *Dnmt1* is initially expressed in the urethral mesenchyme but shifts to the developing prostate bud epithelium at later stages (Keil et al., 2013).

DNMT1 can also participate in *de novo* methylation in coordination with DNMT3A (Fatemi et al., 2002). Evidence of methylation independent functions of DNMT1 have also emerged. A catalytically inactive form of DNMT1 was shown to regulate E-cadherin expression through interaction with its transcriptional repressor SNAIL1 and no appreciable changes in E-cadherin promoter methylation (Espada et al., 2011).

DNMT1 localization and function is regulated by its binding partners. The PCNA binding domain (PBD) in the N-terminal region of DNMT1 mediates interaction with the Proliferating Cell Nuclear Antigen (PCNA). PCNA acts as clamp around DNA during replication and recruits various proteins to replication sites to increase processivity. DNMT1 recruitment to replication forks by PCNA is not strictly required for post-replicative DNA methylation, but it increases efficiency (Schermelleh et al., 2007). UHRF1 (ubiquitin-like, containing PHD and RING finger domains 1) is another direct binding partner of DNMT1. UHRF1 binds to hemi-methylated DNA through its methyl-binding domain and

recruits DNMT1 to these sites (Bostick et al., 2007). UHRF1 ubiquitinates histone H3 to which DNMT1 binds using its RFTS. In addition, DNMT1 can also directly interact with the Ubiquitin-like domain of UHRF1 (Li et al., 2018). UHRF1 colocalizes with DNMT1 during S-phase and recruits it to replication foci. In zebrafish, *uhrf1* mutants phenocopy *DNMT1* mutants highlighting the importance of the *uhrf1-dnmt1* interaction (Jacob et al., 2015).

Knockout, mutation and inhibition studies have provided key insights into the role of DNMT1 in maintaining global methylation. Targeted mutation of *Dnmt1* in mouse ES cells results in a 3-fold reduction in 5mC levels with no loss of cell viability. Mouse embryos carrying the same targeted mutation have a similar 3-fold reduction in 5mC levels but are not viable (Li et al., 1992). In contrast to mouse ES cells, *DNMT1* knockout in human ES cells leads to apoptosis (Liao et al., 2015). Conditional deletion of *Dnmt1* in mouse fibroblasts leads to severe hypomethylation, p53-dependent apoptosis and aberrant gene expression (Jackson-Grusby et al., 2001). This study suggests that widespread DNA demethylation could be perceived as DNA damage by the cell resulting in P53 upregulation. Loss of DNMT1 results in elevated mutation rates, genomic instability (Chen et al., 1998), microsatellite instability (Loughery et al., 2011), DNA damage (Palii et al., 2008) and cell cycle arrest (Chen et al., 2007; Unterberger et al., 2006). DNMT1 activity and expression is upregulated in prostate cancer, where it serves to methylate and suppress key tumor suppressor genes (Patra et al., 2002)

Mutations in the RFTS domain of *DNMT1* have been linked to two neurodegenerative syndromes: Autosomal dominant cerebellar ataxia-deafness and narcolepsy (ADCA-DN) and Hereditary sensory neuropathy with dementia and hearing loss (HSN1E) (Baets et

al., 2015; Klein et al., 2011; Maresca et al., 2015; Winkelmann et al., 2012). These mutations prevent DNMT1 from binding to heterochromatin, leading to aberrant methylation patterns and DNMT1 protein aggregation in the cytosol (Klein et al., 2011). There is increasing evidence for the association of single nucleotide polymorphisms of DNA methyltransferases with incidence of different tumor types, including prostate cancer (He et al., 2014; Li et al., 2016; Tao et al., 2015).

- ***DNMT3 family***

The DNMT3 family of methyltransferases is comprised of DNMT3A, DNMT3B and DNMT3L. The DNMT3 enzymes have a regulatory N-terminal region and a catalytic C-terminal region. Except for conserved motifs in the C-terminal catalytic region, the DNMT3 enzymes do not share much sequence similarity with DNMT1 (Okano et al., 1998). Their N-terminal domains are considerably shorter than that of DNMT1. DNMT3 enzymes lack the N-terminal regulatory elements that confer specificity towards hemi-methylated DNA. As a result, DNMT3A and DNMT3B show no preference for hemi-methylated DNA over unmethylated DNA and are called *de novo* methyltransferases (Gowher and Jeltsch, 2001; Lei et al., 1996). DNMT3L is catalytically inactive but functions as a co-regulator with DNMT3A and DNMT3B. DNMT3A localizes to pericentromeric heterochromatin while DNMT3B is diffusely localized in the nucleus (Bachman et al., 2001). Nuclear localization of DNMT3L to chromatin foci is dependent on physical interaction with the DNMT3A2 isoform (Nimura et al., 2006). DNMT3A and DNMT3B are highly expressed in early embryonic tissues, with overlapping expression in the embryonic ectoderm (Okano et al., 1999). In the developing prostate, *Dnmt3a* and *Dnmt3b* are predominantly expressed in the urethral mesenchyme during fetal stages but localizes to prostate bud tips postnatally

(Keil et al., 2013). DNMT3A and DNMT3B are highly expressed in undifferentiated embryonic cells but are barely detectable in differentiated and adult tissues (Okano et al., 1998). DNMT3A2 is a variant of DNMT3A which is regulated by an alternative promoter. DNMT3A2 is highly expressed in embryonic stem cells, testis, ovary, thymus and spleen. In contrast to DNMT3A which localizes to heterochromatin, DNMT3A2 localizes to euchromatin and has high *de novo* methyltransferase activity (Chen et al., 2002). Several DNMT3B isoforms have also been identified in cancer cell lines (Ostler et al., 2007; Shah et al., 2010). DNMT3L is highly expressed during gametogenesis (Bourc'his et al., 2001).

Targeting DNMT3A and DNMT3B to specific genomic regions is essential for their specialized function. The N-terminal regions of DNMT3A and DNMT3B have two conserved domains: the PWWP domain and the PHD domain. The PWWP domains target DNMT3A and DNMT3B to pericentromeric heterochromatin for methylation of major satellite repeats (Chen et al., 2004). DNMT3A and DNMT3B have an N-terminal PHD (plant homeodomain) domain that is not shared by DNMT1. This domain is involved in transcriptional repression by DNMT3A and DNMT3B in a methylation independent manner (Bachman et al., 2001).

DNMT3A and DNMT3B are essential for *de novo* methylation, transcriptional repression and early embryonic development. Inactivation of *Dnmt3a* and *Dnmt3b* simultaneously but not individually blocks *de novo* methylation, suggesting that these enzymes have overlapping functions. DNMT3B is essential for early embryonic development as *Dnmt3b* knockout mice are embryonic lethal. In contrast, *Dnmt3a* knockout mice live up to 4 weeks of age. *Dnmt3a* and *Dnmt3b* double knockout embryos die during mid-gestation. De novo methylation is blocked in these embryos during early development, but maintenance

methylation was not affected. The different phenotypes of *Dnmt3a* and *Dnmt3b* knockout embryos suggest that these enzymes have some non-overlapping functions. DNMT3B, but not DNMT3A, is required for methylation of centromeric minor satellite repeats (Okano et al., 1999). DNMT3A and DNMT3B participate in transcriptional repression in association with histone deacetylases (Bachman et al., 2001). DNMT3L, although lacking in catalytic activity, stimulates *de novo* methylation by DNMT3A (Chédin et al., 2002).

DNMT3A mutations have been observed in acute myeloid leukemia where they are associated with reduced survival (Hou et al., 2012; Ley et al., 2010). DNMT3B mutations are observed in patients with ICF (Immunodeficiency, Centromere instability and facial anomalies) syndrome. Loss of DNMT3B function in ICF syndrome is associated with changes in promoter methylation, altered histone marks and aberrant gene expression (Jin et al., 2008).

- ***Removing methylation marks***

DNA methylation is a reversible modification. When DNMT1 is inhibited, cells can passively lose methyl marks through multiple rounds of replication. The Ten-eleven translocation (TET) family of methylcytosine dioxygenases catalyze the active removal of methyl marks from DNA independent of replication. During early prostate development, *Tet1* and *Tet2* are expressed predominantly in the urethral mesenchyme while *Tet3* is expressed in the urethral epithelium (Keil et al., 2013). TET1, TET2 and TET3 catalyze the conversion of 5mC to 5-hydroxymethylcytosine (5hmC) and subsequently into 5-formylcytosine (5fC) and 5-carboxylcytosine (5caC) (Tahiliani et al., 2009; Tan and Manley, 2009). 5caC is recognized and excised by thymine DNA glycosylase (TDG) (He et al., 2011).

There is increasing evidence that the 5hmC participates in transcriptional regulation (Pfeifer et al., 2013). 5hmC is highly enriched in brain tissue where it is required for neuronal differentiation (Hahn et al., 2013), learning and memory (Qin et al., 2015). 5hmC marks are abundant in ES cells, where they are enriched at enhancers and gene bodies (Stroud et al., 2011). A recent study has shown that 5hmC localizes to sites of DNA damage and promotes genome stability (Kafer et al., 2016). 5hmC levels are dramatically reduced in human cancers, correlating with impaired TET activity (Pfeifer et al., 2014). 5hmC is significantly reduced in prostate cancer and has been proposed as a biomarker for prostate cancer detection. In contrast, 5fC and 5caC are increased in prostate cancer (Storebjerg et al., 2018; Yang et al., 2013).

Active DNA demethylation can also be catalyzed by 5-methylcytosine deaminases like Activation-induced cytidine deaminase (Aid) and Apolipoprotein B mRNA editing enzyme catalytic subunit 1 (APOBEC1) (Morgan et al., 2004). Deamination of 5mC yields thymine which is immediately replaced with unmethylated cytosine by DNA glycosylases like TDG (Fritz and Papavasiliou, 2010).

- ***Methyl CpG binding domain (MBD) proteins***

The MBD proteins are readers of 5mC marks. The mammalian MBD family is comprised of MeCP2, MBD1, MBD2, MBD3 and MBD4 which possess a common Methyl CpG binding domain (MBD). MBD proteins bind to sites of DNA methylation and recruit enzymes for transcriptional repression (Fatemi and Wade, 2006). MECP2, the first identified MBD protein, participates in gene silencing by recruiting histone deacetylase machinery to methylated DNA (Nan et al., 1998). MeCP2 also recruits histone methyltransferase complexes to methylated DNA to maintain repressed chromatin states

(Fuks et al., 2003b). Thus, MECP2 acts as a bridge between DNA methylation and histone modifications. Rett syndrome, a progressive neurodegenerative disease, is caused by MeCP2 mutations and associated epigenetic dysregulation (Amir et al., 1999). MBD1 directly interacts with the histone methylase SUV39H1 and indirectly with histone deacetylases for gene silencing (Fujita et al., 2003). MBD2 is a component of the MECP1 histone deacetylase complex and recruits the histone deacetylase complex NuRD (Nucleosome Remodeling and Histone Deacetylation) to methylated DNA for transcriptional silencing (Feng and Zhang, 2001; Ng et al., 1999). MBD3 is a core component of the NuRD repressor complex and is required for early embryonic development (Kaji et al., 2007). 5mC deamination produces thymidine resulting in a T-G mismatch. MBD4 is a DNA glycosylase that preferentially binds to sites of 5mC deamination and replaces thymines with cytosines (Hendrich et al., 1999).

- ***DNA methylation and histone modifications***

DNA methylation is associated with gene silencing. There are two major paradigms of gene silencing by DNA methylation. One, DNA methylation of CpGs in regulatory regions can prevent binding of transcription factor complexes required for active gene expression. Second, Methyl CpG binding domain (MBD) containing proteins recruit chromatin modifiers to sites of DNA methylation to establish or maintain repressed chromatin states. Conversely, DNA methylation activity can be recruited to repressed chromatin to methylate adjacent DNA and reinforce gene silencing.

Chromatin modifiers add post-translational modifications to histones which relax or compact chromatin. Active transcription occurs from relaxed or euchromatin regions while transcription is repressed in compacted heterochromatin regions. Histone acetylation and

methylation are the most well studied histone modifications. Histone acetyltransferases acetylate lysines on histones, which loosens the interaction between DNA and histones, resulting in an accessible, open chromatin configuration. This is reversed by Histone deacetylases (HDACs) resulting in gene silencing. Histone methyltransferases add methyl groups to lysines and arginines of Histone H3 and H4. H3K9 and H3K27 di- and tri- methylation and H4K20 tri-methylation repress transcriptional activity by blocking transcriptional factors from accessing DNA.

MBD proteins (MECP2, MBD1, MBD2, MBD3, MBD4) bridge the gap between DNA methylation and histone modifications. MECP2 and MBD2 binds to methylated DNA and recruit HDAC activity to silence genes (Nan et al., 1998; Ng et al., 1999). MBD proteins can also recruit histone methyltransferases to sites of DNA methylation. MBD1 recruits the SUV39H1-HP1 heterochromatin complex, which has histone methyltransferase activity, to sites of DNA methylation for transcriptional repression (Fujita et al., 2003). MECP2 binding to methylated DNA increases the appearance of the repressive H3K9 methylation mark (Fuks et al., 2003b). DNMT1 itself has been shown to interact with chromatin modifiers during DNA replication. DNMT1 forms a repressive complex by direct interaction with the transcriptional repressors HDAC2 and DMAP1 (DNMT1 associated protein). Through this complex, DNMT1 targets the transcriptional repressors to replication foci to maintain heterochromatin regions after DNA replication (Rountree et al., 2000). The histone methyltransferase G9a adds H3K9 methyl marks to newly synthesized DNA. DNMT1 and G9a form a complex with PCNA which cooperatively adds methyl marks to DNA and histones after DNA replication (Esteve et al., 2006).

Histone modifications target DNA methylation to specific genomic regions. The DNMT enzymes themselves do not have any sequence specificity apart from a preference for CpG dinucleotides. How is DNA methylation targeted to imprinted regions, centromeres and repetitive sequences? DNA methylation targeting is achieved by the association of DNMTs with transcription factors and chromatin modifiers with greater sequence specificity. DNMT1 forms a complex with Retinoblastoma gene product (Rb), the transcription factor E2F1 and HDAC1 to repress promoters containing E2F1 binding sites. Thus, DNA methylation is actively targeted to E2F1 bound cell cycle genes to suppress abnormal cell proliferation (Robertson et al., 2000). The SUV39 histone methyltransferases add H3K9 methyl marks and target DNMT3B methylation to pericentromeric heterochromatin (Lehnertz et al., 2003). DNMT3A also associates with H3K9 methyltransferase activity by direct interaction with the histone methyltransferase SUV39H1 (Fuks et al., 2003a). The histone methyltransferase G9a recruits DNMT3A and DNMT3B to *de novo* methylate and repress pluripotency genes (Epsztejn-Litman et al., 2008). Thus, DNA methylation and histone modifications function coordinately in transcriptional repression.

1.6.3. DNA methylation in development

In this section, I will summarize the dynamic changes in DNA methylation that occur during embryonic development and the consequences of these changes on embryo growth and morphogenesis.

- ***DNA methylation dynamics during gametogenesis***

Epigenetic cues including DNA methylation gradually commit cells to specialized gene expression programs during development. For sexual reproduction, DNA methylation

marks need to be erased and reset in early germ cells. Primordial germ cells (PGCs) are derived from proliferating somatic precursors in the primitive streak. To restore totipotency, DNA methylation marks are erased in PGCs. Downregulation of methyltransferases allows the proliferating PGCs to be passively demethylated (Kagiwada et al., 2013). Following erasure, sperm or oocyte specific methylation patterns are re-established. Imprinted genes, which are expressed from either the maternal or paternal allele, are methylated during gametogenesis. DNMT3A and DNMT3L are required for the establishment of sex-specific methylation patterns in gametes (Bourc'his et al., 2001; Hata et al., 2002; Kaneda et al., 2004).

- ***DNA methylation dynamics in the early embryo***

At the time of fertilization, the sperm and oocyte have sex-specific methylation patterns. These patterns need to be erased and reset in the zygote. The newly fertilized zygote undergoes global demethylation until the blastocyst stage. The paternal genome is actively demethylated while the maternal genome undergoes passive demethylation (Howlett and Reik, 1991). Methylation at imprinted regions and retrotransposon sequences like intracisternal A-type particle (IAP) is maintained while the majority of the genome is demethylated (Gaudet et al., 2004; Messerschmidt et al., 2014). *Dnmt1o*, a variant of *Dnmt1* translated from oocyte mRNA, maintains methylation at imprinted regions and IAP elements in the preimplantation embryo. *Dnmt1o* lacks 118 amino acid residues at the N-terminus of *Dnmt1* that is used for interaction with DMAP1. In addition, *Dnmt1o* is more stable than *Dnmt1* which could explain why this form is used as a maternal effect protein (Ding and Chaillet, 2002). Embryos from homozygous *Dnmt1o* mutant females, which lack maternal stores of *Dnmt1o* mRNA, are not viable. Although

these embryos do not exhibit global demethylation, loss of methylation at imprinted regions results in death (Howell et al., 2001). The full length DNMT1 protein was thought to be absent in the pre-implantation embryo (Doherty et al., 2002; Howell et al., 2001; Ratnam et al., 2002). Zygotic *Dnmt1* expression has since been demonstrated in the pre-implantation embryo, but at much lower levels than *Dnmt1o*. *Dnmt1* and *Dnmt1o* expression are required for maintenance of methylation at imprinted regions (Hirasawa et al., 2008). It is still not fully understood how methylation is maintained at imprinted regions in the pre-implantation embryo while the rest of the genome is being demethylated. Different chromatin configurations at imprinted regions and maternal effect proteins like Stella are thought to contribute to this asymmetry (Nakamura et al., 2007; Saitou et al., 2012). *De novo* methylation is carried out by DNMT3A and DNMT3B in the post-implantation embryo. Cells continue to gain DNA methylation as they progress towards differentiation. Inheritable methyl marks are maintained by DNMT1 during cell replication.

- ***Genomic imprinting***

In mammals, there are over 100 genes that are expressed solely from the maternal or paternal allele. The expression of genes in a parent-of-origin specific manner is regulated by a process called genomic imprinting (Bartolomei and Ferguson-Smith, 2011). Genomic imprinting is thought to control dosage of key genes involved in growth and metabolism (Smith et al., 2006). Early studies of reconstituted eggs showed that zygotes with two female pronuclei or two male pronuclei develop poorly after implantation. These studies demonstrate that the presence of both maternal and paternal genomes is required for embryogenesis (McGrath and Solter, 1984; Surani et al., 1984). Imprints are laid down

during gametogenesis, a process which differs greatly between males and females. Imprint marks need to be inheritable and reversible. In addition, these marks should be able to communicate with the cellular machinery to regulate transcription.

DNA methylation is now considered the primary mechanism for genomic imprinting. Methyl marks are erased during gametogenesis and reset to indicate maternal (oocyte) or paternal (sperm) origin. This results in the generation of differentially methylated regions (DMRs) between the maternal and paternal genomes. Post-fertilization, methyl marks on imprinted genes are retained during demethylation in the pre-implantation embryo. The preference of DNMT1 for hemi-methylated DNA ensures the faithful transmission of methylation patterns within imprinted genes. Maintenance of methylation at imprinted regions is disrupted in heterozygous embryos obtained from homozygous *Dnmt1o* mutant females. Maternal stores of *Dnmt1o* are responsible for maintaining methylation at imprinted regions in oocytes and preimplantation embryos, which do not express *Dnmt1* (Howell et al., 2001). Paternally methylated regions are located between genes while maternally methylated regions can be found at gene promoters. The role of DNA methylation in genomic imprinting is best illustrated by the well-studied *IGF2/H19* gene locus, a paternal DMR. *IGF2* expressed from the paternal allele and *H19* expressed from the maternal allele are located close to each other. The transcriptional repressor CTCF binds to the unmethylated maternal chromosome while its binding it blocked on the methylated paternal chromosome. CTCF binding blocks *IGF2* expression while driving *H19* expression from the maternal allele. The absence of CTCF binding allows *IGF2* expression from the paternal allele while blocking *H19* expression (Hark et al., 2000). Viable parthenogenetic mice (from two maternal genomes) were generated after

normalizing expression of the maternally expressed *H19* gene and inducing *Igf2* expression (Kono et al., 2004). Expression of the imprinted genes *H19*, *Igf2* and *Igf2r* were altered in *Dnmt1* mutants, which display severe loss of 5mC. Normally silent alleles were activated while normally active alleles were repressed in *Dnmt1* mutant embryos (Li et al., 1993).

Loss of imprinting at the *IGF2* locus (expression from both alleles instead of one) occurs during aging and tumorigenesis in the prostate (Jarrard et al., 1995). In mouse models, increased expression of the critical paracrine growth factor IGF2 by loss of imprinting drives prostatic neoplastic growth (Damaschke et al., 2017). Reduction of CTCF expression and binding activity as a function of age triggers *Igf2* loss of imprinting in the prostate (Fu et al., 2008; Fu et al., 2004). Genomic imprinting is essential for normal development. Prader-Willi syndrome and Angelman syndrome occur from imprinting errors.

- ***X-inactivation***

Male mammals have one X chromosome while females have two. To compensate for gene dosage differences, one X chromosome is inactivated in females in a process called X-inactivation. Much before the isolation and characterization of mammalian DNA methyltransferases, a model of X inactivation by DNA methylation was proposed (Riggs, 1975). Re-activation of X-linked genes by pharmacological inhibition of DNA methylation provided the first evidence for X inactivation by DNA methylation (Mohandas et al., 1981). The initiation and maintenance of X inactivation is regulated by the long non-coding RNA *XIST*. *XIST* is expressed only from the inactivated X-chromosome where it acts in cis to coat the inactive X-chromosome and repress transcription. The 5’ region of the *XIST* gene

is methylated on the active X-chromosome and unmethylated on the inactive X-chromosome, suggesting that DNA methylation could regulate *XIST* expression (Norris et al., 1994). The methylation status of the *XIST* promoter corresponds to expression levels. The *XIST* gene is demethylated and its expression upregulated in *DNMT1* male mutant embryos (Beard et al., 1995). *XIST* expression is aberrantly upregulated in *DNMT1* mutant ES cells where it leads to the inactivation of X-linked genes (Panning and Jaenisch, 1996). In the early embryo, *Xist* is expressed solely from the inactivated paternal X-chromosome. Paternal imprints for *Xist* are removed during demethylation in the pre-implantation embryo. Following this, methylation of *Xist* is random and it can be expressed from either the maternal or paternal X-chromosome (Kay et al., 1993).

- ***Silencing of transposable elements***

Transposable elements or transposons are genes that can change location and copy number within the genome. Approximately 46% of the human genome and 37.5% of the mouse genome are derived from transposable elements (Waterston et al., 2002). In addition to being a source of genetic variability, transposons can cause genomic rearrangements and change the activity of genes near their insertion site (Kuff and Lueders, 1988; Qin et al., 2010). Multiple epigenetic mechanisms, including DNA methylation, are involved in transposon silencing. If unchecked, transposon expression can lead to mutations and genomic rearrangements. Methylation suppresses the expression of transposons. The mouse genome contains ~1000 Intracisternal A particle (IAP) retroviruses. IAPs have Long Terminal Regions (LTRs) that are comprised of multiple repeating DNA sequences. Methylation of LTRs causes transcriptional silencing of IAPs in somatic cells. IAP transcripts are upregulated 50-100-fold in *DNMT1* mutant

mouse embryos (Walsh et al., 1998). Demethylation and activation of IAP genes are observed after treatment with DNA methylation inhibitors (Davis et al., 1989).

IAP sequences are *de novo* methylated during gametogenesis. DNMT3A and DNMT3B are required for the methylation of interspersed repeat sequences during male germ cell development (Kato et al., 2007). DNMT3L expression in the early germ cells within the testis is required for methylation of long-terminal-repeat (LTR) and non-LTR retrotransposons (Bourc'his and Bestor, 2004). Methylation at LTRs of IAPs is retained during the demethylation wave in preimplantation embryos. High levels of DNMT1o expression maintain IAP methylation during the cleavage stage of early embryos. Somatic DNMT1 maintains IAP methylation at post-implantation stages (Gaudet et al., 2004). DNMT3A and DNMT3B can cooperate with DNMT1 to efficiently maintain methylation at murine LINE-1 elements in embryonic stem cells (Liang et al., 2002). Changes in DNA methylation and expression of retrotransposon elements are observed in prostate cancer (Goering et al., 2011). Hypomethylation and re-expression of LINE-1 retrotransposons occur in BPH tissues (Madigan et al., 2012).

- ***Transcriptional control of differentiation***

As a cell progresses from an undifferentiated to a differentiated state, its DNA methylation landscape changes dramatically. Embryonic stem (ES) cells are a powerful model to study transcriptional control of differentiation. Given the right conditions, these cells can be induced to differentiate into multiple different cell types. DNMTs play a central role in the transcriptional control of differentiation. DNMTs suppresses the expression of differentiation genes to maintain cells in an undifferentiated state. Regulation of *DNMT1*

expression by the pluripotency factors OCT4 and NANOG maintains the undifferentiated state of mesenchymal stem cells (Tsai et al., 2012).

Dnmt1 mutant mouse ES cells are viable but aberrantly express X-linked genes and undergo apoptosis when induced to differentiate (Panning and Jaenisch, 1996). *Dnmt3a/Dnmt3b* null ES cells are viable in an undifferentiated state but gradually lose methylation after several passages in culture. This suggests that the fidelity of maintenance methylation by DNMT1 is augmented by DNMT3A and DNMT3B. The ability to differentiate is retained in early passage DNMT3A/3B null ES cells (moderately hypomethylated) and lost in late passage cells (severely hypomethylated) (Jackson et al., 2004). Genome wide methylation studies indicate that the magnitude of methylation reduction at a gene locus is determined by CpG density. Genes with low CpG density are more likely to be de-repressed in *Dnmt* knockout ES cells (Li et al., 2015). Recently, knockout human ES cell lines with targeted deletion in the *DNMT* genes were generated using CRISPR/Cas9 genome editing. Unlike *Dnmt1* knockout mouse ES cells, *DNMT1* knockout human ES cells are not viable. Similar to mouse ES cells, *DNMT3A/3B* null ES cells were initially viable and retained differentiation ability but gradually lost methylation over multiple passages (Liao et al., 2015). During differentiation, DNMTs methylate pluripotency factors like *OCT4* and *NANOG* to prevent the cell from reverting to an undifferentiated state. Global DNA hypomethylation in *DNMT1*(-/-) ES cells does not prevent initiation of differentiation programs. However, unlike wildtype cells, *DNMT1*(-/-) ES are not fully committed to their differentiation programs and can revert to the ES cell state (Schmidt et al., 2012).

Cytidine nucleoside analogs like 5-azacytidine have been used to elucidate the role of DNA methylation in transcriptional control. 5-azacytidine and its 2’-deoxy derivative 5-aza-2'-deoxycytidine can be incorporated into DNA where it inhibits DNA methyltransferase activity and methylation of newly synthesized DNA. When DNMT1 encounters 5-azacytidine, it is locked into an inactive covalent complex which is targeted for degradation. This process results in DNMT1 depletion and gradual hypomethylation of the treated cells. At higher doses, more complete hypomethylation takes place which is lethal for the cell. 5-azacytidine can be incorporated into both RNA and DNA while 5-aza-2'-deoxycytidine is a deoxyribonucleoside which can only be incorporated into DNA.

Non-myoblast mouse embryo cells change their phenotype drastically to form functional striated muscle cells after 5-azacytidine treatment (Constantinides et al., 1977; Constantinides et al., 1978). Swiss3T3 cells treated with 5-azacytidine or 5-aza-2'-deoxycytidine display new mesenchymal phenotypes of contractile muscle, differentiated adipocytes and chondrocytes (Taylor and Jones, 1979, 1982). These results suggest that 5-azacytidine treatment reverts cells to a less differentiated state from which new phenotypes can develop. It was later discovered that 5-azacytidine treated cells were hypomethylated and this was driving the phenotypic alteration in these cells (Jones and Taylor, 1980). Together, these results provide evidence for the role of DNA methylation in maintaining and directing cellular differentiation.

5-aza-2’-deoxycytidine (5AzadC) has been used to study the role of DNA methylation in prostate development and differentiation. In eutherian mammals, the prostate forms during fetal development as solid epithelial buds arising from the urogenital sinus (UGS) epithelium which grow into the surrounding mesenchyme. Epithelial cells of the

developing prostate bud downregulate expression of the epithelial adhesion molecule E-cadherin (*Cdh1*) to achieve invasive growth into the mesenchyme. Treatment of *in vitro* UGS explants with 5AzadC decreased prostate bud elongation and outgrowth without affecting cell viability. 5AzadC treatment decreased *Cdh1* promoter methylation and upregulated *Cdh1* mRNA expression in prostate epithelial cells. Increased expression of *Cdh1* constrained prostate bud elongation and invasive growth into the mesenchyme. Thus, methylation of *Cdh1* promoter downregulates *Cdh1* expression for normal prostate growth and differentiation (Keil et al., 2014b).

Mesenchymal Androgen receptor expression is required for prostate bud initiation. The onset of mesenchymal *Ar* expression corresponds to a reduction in DNMT1 expression and decrease in *Ar* promoter methylation. Treatment of *in vitro* UGS explants with 5AzadC reduces *Ar* promoter methylation and accelerates the onset of *Ar* expression, thereby increasing the number of prostate buds specified (Keil et al., 2014a).

- ***Tissue growth and organogenesis***

The mid-gestational lethality of *Dnmt1* knockout embryos prevents the study of organ system development. To overcome this, context dependent roles of DNMT1 have been studied in several organ systems by employing tissue specific Cre-lox approaches. This involves the use of tissue specific Cre drivers to drive *Dnmt1* deletion is specific tissues during development. Deletion of *Dnmt1* in the developing pancreas resulted in global hypomethylation, growth arrest and tissue atrophy through p53-dependent apoptosis of pancreatic progenitors (Georgia et al., 2013). Intestine specific ablation was used to show that *Dnmt1* was required for proliferation and crypt formation in the perinatal period. Loss of *Dnmt1* in the intestinal epithelium led to increased DNA damage and apoptosis (Elliott

et al., 2015). The role of *Dnmt1* in the development of the lower urinary tract was assessed by conditionally ablating *Dnmt1* in the epithelium of the bladder, urethra and prostate. Similar to previous studies on *Dnmt1* ablation, widespread DNA damage and p53-mediated apoptosis was observed. This was accompanied by a reduction in prostate bud formation, highlighting the role of *Dnmt1* in maintaining cell proliferation and survival of early prostate progenitors (Chapter 3). *Dnmt1* deletion in the lower urinary tract led to the breakdown of the Wolffian duct-urethra junction which was permissive for the movement of Wolffian duct cells into the urethra and bladder epithelium, where these ectopic cells reprogrammed to acquire bladder characteristics including Uroplakin expression (Joseph et al., 2018a). Studies using genetic models of DNA methyltransferase deletion have been summarized in Table 1.2.

Table 1.2 DNA methyltransferase deletion studies

Model	Phenotype	Reference
Global *DNMT1* null mice	3-fold reduction in genomic 5mC levels Recessive embryonic lethal Embryos are developmentally retarded Embryos die at mid-gestation	(Li et al., 1992)
***DNMT3A*-/- *DNMT3B*-/- mice**	*DNMT3A*-/- mice appear normal at birth but become runted and die at around 4 weeks of age *DNMT3B*-/- mice exhibit growth impairment, rostral neural tube defects and die at mid-gestation	(Okano et al., 1999)
***DNMT1*o knockout mice**	Heterozygous embryos from homozygous mutant females die during last third of gestation Loss of methylation at imprinted loci	(Howell et al., 2001)
***DNMT3L* knockout mice**	Azoospermia in homozygous males Heterozygous embryos from homozygous mutant females die during mid-gestation Loss of maternal methylation imprints	(Bourc'his et al., 2001)
***Cre*-mediated homozygous *DNMT1* deletion in fibroblasts**	*DNMT1* deletion leads to hypomethylation and aberrant expression of 10% of genes *DNMT1* depleted cells undergo p53-mediated apoptosis	(Jackson-Grusby et al., 2001)
***Cre*-mediated *DNMT1* deletion in neuroblasts**	95% of cells in the brain hypomethylated Die immediately after birth from respiratory distress; defects in neuronal respiratory control	(Fan et al., 2001)

(*CamK-cre*)		
***Cre*-mediated *DNMT1* deletion in telencephalic precursors (*Emx1-cre*)**	Mutant mice viable but undergo severe neuronal cell death from E14.5-P21 Deregulation of neuronal gene expression Defects in neuronal morphology and excitability	(Hutnick et al., 2009)
shRNA knockdown of *DNMT1* in primary human keratinocytes	*DNMT1* depleted cells exit progenitor compartment, undergo premature differentiation *DNMT1* loss results in upregulation of cyclin-dependent kinase inhibitors, cell cycle arrest and impaired proliferation	(Sen et al., 2010)
Cre-mediated *DNMT1* deletion in hematopoietic stem cells (HSC) (*Mx-cre*)	Impaired HSC self-renewal Increased cell cycling and inappropriate expression of differentiation markers in myeloid progenitor cells	(Trowbridge et al., 2009)
Cre-mediated *DNMT1* deletion in pancreatic cells (*Pdx1-cre*)	DNMT1 loss results in de-repression of p53 G2/M cell cycle arrest and apoptosis Pancreatic agenesis due to apoptosis of progenitors	(Georgia et al., 2013)
Cre-mediated *DNMT1* deletion in retinal cells (*Chx10-cre*)	Defective photoreceptor differentiation Altered cell cycle kinetics; increased proportion of G1 phase cells Increased apoptosis of post-mitotic photoreceptors and other neuronal types	(Rhee et al., 2012)
Cre-mediated *DNMT1* deletion in retinal cells (*Rx-cre*)	Mice display smaller eyes Impaired differentiation of retinal pigment epithelium Defects in photoreceptor outer segment morphogenesis	(Nasonkin et al., 2013)
Cre-mediated *DNMT1* deletion in intestinal cells (*Villin-cre*)	Mice die few weeks after birth Induction of differentiation markers in progenitor cells Impaired methylation and expression of DNA damage response genes and cell cycle regulators Increased DNA damage and apoptosis of progenitor cells	(Elliott et al., 2015)
Cre-mediated *DNMT1* deletion in Keratin 14 lineage cells (*K14-cre*)	Uneven epidermal thickness, altered hair follicle size Impaired proliferation at hair follicles, progressive alopecia with age	(Li, 2012)
Cre-mediated *DNMT1* deletion in *Shh* lineage cells (*Shh-cre*)	Mice die shortly after birth; respiratory complications arising from severe lung hypoplasia Epithelial depletion of urethral and bladder epithelium Premature differentiation and loss of bladder progenitors Cell cycle arrest and apoptosis of prostate progenitors; reduction in prostate bud number	(Joseph et al., 2018a) Chapter 3

1.6.4. DNA methylation in adult homeostasis and disease

Changes in DNA methylation are associated with the formation of specialized tissue types in the mature organism.

- ***Genome-wide methylation patterns***

CpG dinucleotides occur at a much lower frequency than expected in the genome. 60-90% of CpG dinucleotides in the mammalian genome are methylated at the 5' position of cytosine. Deamination of 5-methylcytosine to thymine makes methylated CpG dinucleotides prone to mutation, reducing their representation in the genome. Most of the methylated CpG nucleotides are scattered throughout the genome and participate in the silencing of retrotransposons and repetitive elements. Clusters of unmethylated CpGs, called CpG islands, are found at the transcription start sites of several housekeeping genes and a few tissue-specific genes. 72% of promoter sequences contain CpG islands (Saxonov et al., 2006). Most CpG islands are found at the 5' region of genes, where transcription originates. CpG islands can extend from between 500-2000 base pairs. Since CpGs within islands are unmethylated, these sites are not prone to 5'-cytosine deamination and conversion to thymine. In addition, permanent binding of transcriptional machinery and DNA-binding proteins at CpG islands prevents *de novo* methylation of CpG islands. Unmethylated CpG islands are associated with transcriptionally active genes, mostly housekeeping genes and tumor suppressors (Bird, 1986; Ghosh et al., 2010). The majority of CpG islands are unmethylated irrespective of whether the associated gene is transcriptionally active or inactive. Methylation of CpGs within CpG islands have been described and this results in the stable silencing of genes (Deaton and Bird, 2011).

- ***Tissue-specific methylation patterns***

Formation of differentiated tissue during development involves dramatic changes in DNA methylation. Tissue-specific methylation patterns established during development coordinate specialized gene expression programs in multiple tissue types. In addition, demethylation of developmentally methylated regions also contributes to the establishment of tissue-specific methylation patterns. Tissue-specific genes with CpG island promoters are usually unmethylated in all tissue types, even when the gene is inactive. In contrast, tissue specific genes with non-CpG island promoters display tissue specific methylation patterns. Broadly, DNA methylation at promoter regions is negatively correlated with gene expression (Eckhardt et al., 2006; Han et al., 2011).

There is conflicting evidence for tissue-specific differential methylation at CpG islands. Expression of known tissue specific genes do not always correlate with promoter methylation (Walsh and Bestor, 1999; Warnecke and Clark, 1999). Later studies identified tissue specific differentially methylated regions and the genes located near these regions were then assessed for tissue specific expression. This approach identified 5% of CpG islands which displayed tissue-specific methylation patterns (Song et al., 2005). Another study showed that promoters with “weak” CpG islands, which are intermediate between CpG rich promoters and non-CpG promoters, display a high frequency of methylation. These weak CpG islands are more prone to *de novo* methylation during development and contribute to the differential methylation observed between somatic and germ cells (Weber et al., 2007). Tissue-specific differentially methylated regions have also been identified in intergenic and intragenic regions of genes with non-CpG island promoters (Liang et al., 2011).

- ***Expression of DNA methyltransferases in adult tissues***

Adult tissues express lower levels of DNA methyltransferases compared to embryonic tissues. DNMT1, DNMT3A and DNMT3B expression is widespread across adult human tissues, with DNMT1 expressed at the highest level (Robertson et al., 1999). The maintenance methyltransferase DNMT1 is required for the faithful propagation of methylation patterns in proliferating adult tissues. DNMT1 expression protects against genomic hypomethylation, chromosomal instability and accumulation of mutations (Chen et al., 1998; Chen et al., 2007; Gaudet et al., 2003). In adult tissues, DNMT1 is highly expressed in rapidly dividing somatic tissues including epidermis (Sen et al., 2010) and intestine (Sheaffer et al., 2014). DNMT1 regulates the fine balance between self-renewal and differentiation in adult stem cells. Differentiation involves demethylation and activation of tissue specific genes with concomitant methylation and repression of stem cell genes. DNMT1 expression prevents differentiating cells from reverting back to an undifferentiated state (Schmidt et al., 2012). In self-renewing somatic tissues, DNMT1 methylates and suppresses differentiation gene promoters and prevents cell cycle exit in tissue progenitors (Sen et al., 2010). DNMT1 maintains methylation of intestinal stem cell enhancers for normal intestinal differentiation (Sheaffer et al., 2014). DNMT1 and DNMT3A are also highly expressed in non-proliferating post-mitotic neurons where they regulate synaptic plasticity, learning and memory (Feng, 2010). DNMT1 is highly expressed in developing prostate tissue but its expression is considerably reduced in the adult prostate. DNMT1 expression is upregulated in cycling cells from prostates of castrated mice supplemented with testosterone (Figure 1.2).

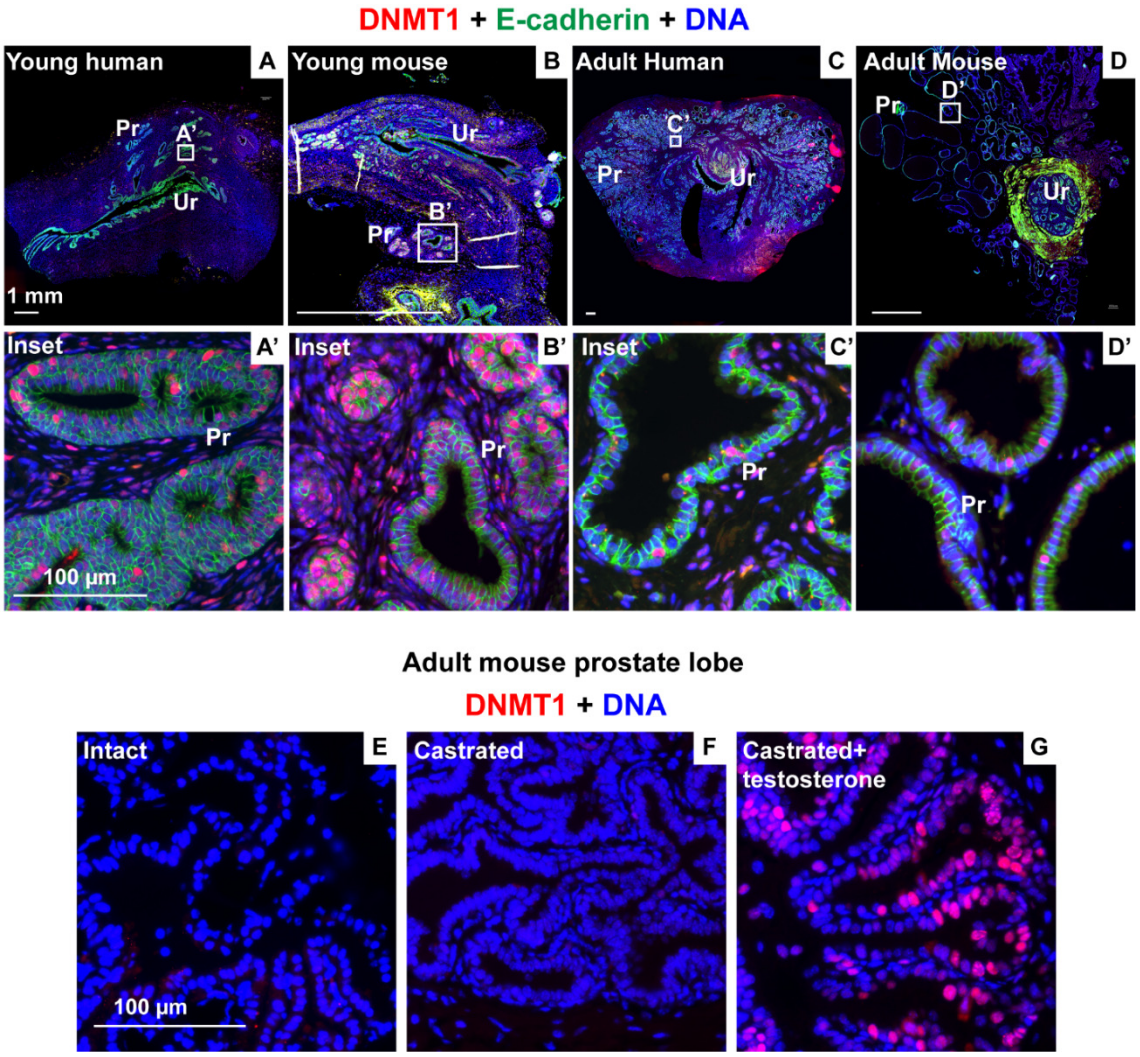

Figure 1.2 DNMT1 expression in the mouse and human prostate

Tissues sections from (A) young human (21 weeks of gestation), (B) young mouse (postnatal day 9) (C) adult human (23 years) and (D) adult mouse (7 weeks) were labeled with antibodies to DNMT1 (in red) and E-cadherin (in green). Regions enclosed in white boxes within (A), (B), (C) and (D) are magnified in (A'), (B'), (C') and (D'). Prostate tissue from (E) intact, (F) castrated and (G) castrated and testosterone supplemented mice were labeled with antibodies to DNMT1 (in red). DAPI staining is shown in blue. Abbreviations Ur: Urethra, Pr: Prostate.

- ***DNA methylation and disease***

Errors in DNA methylation contribute to several diseases including cancer, syndromes caused by imprinting errors (Prader–Willi, and Angelman syndromes), Fragile X syndrome and ICF syndrome (Robertson, 2005). Among these, the role of DNA methylation in cancer has been extensively studied. DNMT1 and DNMT3A are modestly overexpressed in several tumor tissues while DNMT3B is significantly overexpressed (Jahangiri et al., 2018; Robertson et al., 1999). Paradoxically, cancer is associated with global hypomethylation and genomic instability, with significant reduction in methylation at repetitive elements. Several cancer types display aberrant hypermethylation at promoter associated CpG islands. Hypermethylation of genes involved in apoptosis, cell cycle regulation, cell invasion and DNA repair provide cancer cells with survival advantages over normal cells. *De novo* methylation of imprint control regions can result in aberrant regulation of imprinted genes. Loss of imprinting, allowing bi-allelic expression of growth promoting genes like *Igf2*, promotes tumor growth (Robertson, 2005).

- ***DNA methylation and aging***

5-methyl cytosine (5mC) levels gradually decline over the lifetime of an organism in a process called epigenetic drift. The rate of loss of 5mC is inversely correlated with the lifespan of the organism and is determined by environmental factors like diet (Maegawa et al., 2017). Longer-lived rodents lose 5mC at a slower rate compared to rodents with a shorter life span (Wilson et al., 1987b). Accelerating the loss of 5mC by 5-azacytidine treatment or exposure to chemical carcinogens shortens the life span of *in vitro* cultured cells (Fairweather et al., 1987; Holliday, 1986; Wilson et al., 1987a). Studies in humans have shown that centenarian DNA has 7% less methylated cytosines than a newborn.

Centenarian genomes display loss of methylation at non-CpG island promoters and repetitive DNA sequences like LINE elements and LTR-retrotransposons (Heyn et al., 2012). Another cohort of elderly subjects displayed a longitudinal decline of methylation in Alu repetitive elements after repeated evaluation (Bollati et al., 2009). Sufficient DNA methylation levels are needed for healthy aging, as demonstrated using *DNMT1* haplo-insufficient mice (Liu et al., 2011).

Alteration of DNA methylation patterns with age occur from cumulative environmental exposures and lifestyle factors (Jung and Pfeifer, 2015). This is best exemplified by the phenotypic changes observed in monozygotic twins with age. Monozygotic twins possess identical genomes and epigenomes early in life but display divergence in DNA methylation and histone modifications with age (Fraga et al., 2005). Aging related changes in DNMT expression and availability of methyl donors with age contributes to epigenetic drift (Ciccarone et al., 2016; Zampieri et al., 2015). Aging fibroblasts show a downregulation of *DNMT1* and significant overexpression of *DNMT3B*. These opposing changes in *DNMT* expression may explain the global hypomethylation and site-specific hypermethylation observed in aging cells (Casillas et al., 2003; Lopatina et al., 2002). Despite widespread changes to the DNA methylome with age, it is not fully understood if these changes contribute to aging-related diseases. Changes in DNA methylation have been definitively linked to cancer, an age-related disease. Both global hypomethylation and promoter hypermethylation can result in cellular transformation (Jung and Pfeifer, 2015; Zampieri et al., 2015). Aging related hypermethylation of autophagy genes have been linked to neurodegenerative diseases and chronic inflammation (Khalil et al., 2016).

- ***DNA methylation and prostate disease***

In this section I will briefly describe two disease conditions of the prostate: Prostate cancer and Benign Prostatic Hyperplasia (BPH) and the current knowledge of the role of DNA methylation in these diseases.

Prostate cancer and DNA methylation

Prostate cancer is characterized by malignant growth of the prostate and is the third most common cancer type in the United States. Age is a significant risk factor for the development of prostate cancer. Common treatment strategies include anti-androgens (bicalutamide, flutamide, enzalutamide), androgen synthesis inhibitors (ketoconazole, abiraterone acetate), radiation therapy, surgical castration and chemical castration (LHRH agonists) (www.cancer.gov/types/prostate).

Tissue from metastatic prostate cancer, but not non-metastatic cancer, has drastically reduced 5mC levels compared to normal tissues. This correlation between metastatic capacity and 5mC content suggests that 5mC levels can be used as a biomarker to detect metastatic tumors or that the reduction in 5mC contributes to metastatic progression (Bedford and van Helden, 1987). Hypermethylation of the regulatory locus of pi-class glutathione S-transferase gene *GSTP1* is commonly observed in prostate cancer precursor lesions and prostate adenocarcinoma. *GSTP1* encodes an enzyme that catalyzes cellular detoxification reactions (Brooks et al., 1998; Lee et al., 1994). CpG island hypermethylation of multiple genes, including *APC*, *RASSF1A*, and *RUNX3*, has been detected in prostate cancer (Kang et al., 2004; Maruyama et al., 2002; Yegnasubramanian et al., 2004). Methylation status of several genes, including *APC* and *RPRM*, correlate with biochemical recurrence after radical prostatectomy (Ellinger et al.,

2008). Hypermethylation of specific CpG islands in prostate cancer correlates with hypomethylation of Alu and LINE-1 repetitive elements (Cho et al., 2007). Genome wide methylation studies have identified differentially methylated regions (DMRs) in prostate cancer compared to benign tissues. These DMRs are enriched for binding by Enhancer of zeste homolog 2 (EZH2), a key driver of prostate cancer (Kirby et al., 2017; Yang and Yu, 2013). Relatively few studies, have examined DNA methyltransferase expression in prostate cancer. One group reported upregulation of DNMT1 expression in prostate cancer cell lines and tissue (Patra et al., 2002). DNMT1 inhibition with 5-azacytidine kills prostate tumor cell lines at high doses (Patra et al., 2011) while promoting metastatic invasion at lower doses (Lee et al., 2016). In a cohort of prostate tissue samples, DNMT1 expression was highest in poorly differentiated prostate cancer and lowest in well-differentiated prostate cancer. DNMT1 expression was negatively correlated with GSTP1 and APC, which are hyper-methylated in prostate cancer. This suggests a role for DNMT1 in the methylation and repression of key tumor suppressors during prostate cancer formation (Zhang et al., 2015a).

Benign Prostatic Hyperplasia and DNA methylation

Benign Prostatic Hyperplasia (BPH) is a non-malignant enlargement of the prostate. BPH growth initiates by the age of 30 and continues throughout the individual's lifetime. The major risk factor for the development of pathological BPH is age. By the age of 50, 50% of men develop pathological BPH (Berry et al., 1984). Enlargement of the prostate in BPH constricts results in urethral constriction and manifestation of lower urinary tract symptoms (LUTS). LUTS include storage (increased frequency, urgency, nocturia) and obstructive symptoms (weak stream, incomplete voiding, urinary obstruction, overflow

incontinence) (McVary et al., 2011). BPH in association with LUTS is significant financial burden (Saigal and Joyce, 2005; Wei et al., 2005) and negatively impacts quality of life but does not lead to significant morbidity if treated. BPH is treated with three major classes of drugs, alpha adrenergic receptor blockers, 5-alpha reductase inhibitors and phosphodiesterase-5 inhibitors (Bechis et al., 2014; Kaplan and Gonzalez, 2007; Roehrborn, 2008). Alpha adrenergic receptor blockers and phosphodiesterase-5 inhibitors relax bladder and prostate smooth muscle to facilitate bladder emptying. 5-alpha reductase inhibitors lower Dihydrotestosterone (DHT) concentrations to shrink the prostate and relieve urethral constriction. If these drugs or their combinations do not alleviate LUTS, prostatectomy is performed.

Prostates with BPH have significantly lower levels of global 5mC compared to normal tissue (Bedford and van Helden, 1987). DNMT1 is expressed at low levels in BPH tissue (Zhang et al., 2015a). Although BPH is characterized by global hypomethylation, recurrent hypermethylation of the tumor suppressor gene 14-3-3Sigma occurs in BPH tissues (Henrique et al., 2005). DNMT1 regulates the methylation and repression of *SRD5A2* gene expression in BPH samples. DNMT1 expression in *SRD5A2* silenced BPH tissues is regulated by the inflammatory mediators IL-6, TNFa and NF-kB (Ge et al., 2015; Niu et al., 2011). Methylation and repression of the *SRD5A2* gene results in an androgenic to estrogenic switch. Decreased reliance of androgenic pathways in BPH could be behind the reduced efficacy of 5-alpha reductase inhibitors in some patients (Wang et al., 2017).

- ***Impact of environmental factors on DNA methylation***

DNA methylation is influenced by environmental factors including diet (Hahn et al., 2017; Yoon et al., 2017), particulate pollution (Baccarelli et al., 2009; De Prins et al., 2013;

Madrigano et al., 2011), carcinogens and benzene exposure (Bollati et al., 2007). The Developmental Origins of heath and disease hypothesis (DOHaD) states that early life environmental influences can impact adult disease. DNA methylation is one mechanism by which signatures of early life exposures can be embedded in the genome. The heritable and stable nature of DNA methylation would allow these early changes to persist into adulthood. The DOHaD hypothesis originated from observations made in low birth weight infants. Infants with low-birth weight were more prone to cardiovascular disease later in life, suggesting that poor fetal nutrition can increase adult disease susceptibility (Barker, 2007; Wadhwa et al., 2009).

Maternal diet can influence DNA methylation patterns in offspring. This is best illustrated by the seminal Agouti mouse studies. Transcription from the agouti gene locus is associated with increased obesity and yellow coat color. Viable yellow agouti mice (A^{vy}) have an IAP retrotransposon inserted at the 5' end of the agouti gene. Expression of the agouti gene is regulated by methylation of the IAP retrotransposon insert. Maternal diet enriched in methyl donors increases IAP methylation in offspring, which shuts down agouti gene transcription and produces lean mice with brown coat color. Thus, DNA methylation changes from maternal exposures completely shuts down the IAP gene and modifies offspring phenotype (Cooney et al., 2002; Waterland and Jirtle, 2003). The Dutch famine studies have demonstrated differential methylation of several metabolism genes, including the *IGF2* locus, with prenatal exposure to poor nutrition. Exposed individuals have poor metabolic regulation, increased body mass index and higher risk for developing schizophrenia (Heijmans et al., 2008; Tobi et al., 2009).

Developmental exposures to hormones and endocrine disrupting chemicals have been shown to alter prostate development. Early prostate development is dependent on androgens (testosterone and dihydrotestosterone). Disrupting androgen action or exposure to estrogenic compounds alters early prostate development with long-term consequences on the adult prostate. Commonly occurring environmental toxins like Bisphenol A (BPA), Dioxin (TCDD) and phthalates are capable of interfering with endocrine signaling and are called endocrine disruptors. Exposing pregnant mice to low doses of estrogen or estrogenic compounds (BPA or diethylstilbestrol) increases the number of prostate glands formed during fetal life and increases adult prostate size (Gupta, 2000; Timms et al., 2005; vom Saal et al., 1997). Developmental exposures to estrogens or BPA increases susceptibility to prostate cancer in rats (Ho et al., 2006). Prenatal exposure to the endocrine disruptor ethinylestradiol, found in oral contraceptives, pre-disposes male and female gerbils to prostate lesions with aging (Perez et al., 2016). Exposure to estrogenic chemicals alters DNA methylation in the prostate. Developmental exposure to estradiol and BPA alters DNA methylation patterns of several genes including phosphodiesterase type 4 variant 4 (PDE4D4), *Pitx3*, *Wnt10b*, *Paqr4*, *Sox2*, *Chst14*, *Tpd52* and *Creb3l4*. These DNA methylome changes persist into adulthood (Cheong et al., 2016; Ho et al., 2006; Tang et al., 2012). Additional research is required to ascertain whether differential regulation of these genes contributes to prostate cancer.

Maternal exposure to the persistent environmental contaminant TCDD alters prostate bud specification by disrupting Aryl hydrocarbon receptor signaling (Lin et al., 2003; Vezina et al., 2008b). Exposure to TCDD during *in utero* and lactational stages decreases adult rat

prostate size by impairing early prostate proliferation and differentiation (Roman et al., 1998). *In utero* and lactational exposure to TCDD predisposes mice to lower urinary dysfunction in later life (Ricke et al., 2016b). Early TCDD exposure can alter DNA methylation at imprinted loci in preimplantation embryos (Wu et al., 2004). Further research is required to link TCDD induced DNA methylation changes to defects in prostate growth.

DNA methyltransferase co-factor S-adenosyl methionine (SAM) is the source of methyl groups for DNA methylation. Following removal of the methyl group, SAM is converted to S-adenosyl homocysteine (SAH) and homocysteine. Homocysteine re-methylation to replenish pools of SAM requires several methyl group donors like methyl-folate, methionine and betaine. Availability of methyl donors in the diet can influence DNA methylation. This is elegantly illustrated by studies in the Agouti mouse model. Early life exposure to BPA hypomethylates the IAP retrotransposon element upstream of the agouti gene and shifts coat color to yellow. Maternal diet supplementation with methyl donors reverses BPA-induced hypomethylation and shifts coat color back to brown (Dolinoy et al., 2007b). Mice carrying the *axin fused* (*Axin^{Fu}*) allele with an insertion of the IAP retrotransposon display variable tail kinking. Maternal methyl donor supplementation increases methylation of the *Axin^{Fu}* allele and suppresses tail kinking in offspring (Waterland et al., 2006).

Dietary folate is the most well-studied methyl donor. Folates are water soluble vitamins that participate in one-carbon transfer, DNA synthesis, cell growth, hematopoiesis and metabolism. While folates occur naturally in the diet, folic acid is the synthetic form that is supplemented in fortified food stuffs or consumed as dietary supplements. Folates and

folic acid are converted to 5-methyl tetrahydrofolate which provides methyl groups for the conversion of homocysteine to methionine. Methionine is converted to SAM, the methyl donor for DNA methylation reactions. Adequate consumption of folates is required to maintain SAM pools.

In 1998, the United States mandated folic acid fortification in cereal grains. Folic acid fortification has raised serum folate levels in populations of several age groups, most significantly in children and older populations. Older populations, who are most prone to folate deficiency, showed an increase in serum folate levels from 26.2 nmol/L to 57.8 nmol/L after fortification (Pfeiffer et al., 2012; Pfeiffer et al., 2007). Maternal consumption of folic acid during the peri-conceptional period has been shown to reduce the incidence of neural tube defects (NTDs) in offspring (MRC, 1991). Post-fortification, folic acid levels have increased in women of childbearing age and resulted in a 19% reduction in the prevalence of NTDs (CDC, 2007; Honein et al., 2001; Williams et al., 2015). The exact mechanism of how folates reduce the risk of NTDs remains unknown. DNA methylation changes associated with defects in folate metabolism have been linked to NTDs. Studies in rodents have demonstrated that tissues with NTDs had lower levels of SAM and displayed genomic hypomethylation (Wang et al., 2015).

In addition to participating in methylation, folates are important players in nucleotide biosynthesis and polyamine synthesis. The complex role of folates in the body could yield protective or deleterious effects depending on the context. High gestational folic acid has been shown to have adverse effects on offspring in rodent studies (Barua et al., 2014a; Barua et al., 2016b). Multiple clinical trials have associated folic acid supplement consumption with increased risk of prostate cancer (Collin et al., 2010; de Vogel et al.,

2013; Wien et al., 2012). However, a few meta-analysis studies using combined data across multiple randomized trials have failed to identify an association between folic acid supplementation and prostate cancer risk (Qin et al., 2013; Vollset et al., 2013). Despite contradictory data, the prevalence of folic acid supplement consumption warrants further research in this area. Maternal supplementation, food grain fortification and consumption of multi-vitamin supplements have resulted in populations that have been exposed to high levels of folic acid throughout their lifetime. It is important to fully understand the consequences of folate supplementation at various stages of life and during disease processes. Studies examining the impact of folate supplementation in animal models and humans are summarized in Table 1.3.

Table 1.3 Studies examining the effects folate supplementation on development and disease

Study	Findings	Reference
Animal models of folic acid supplementation		
Pregnant rats on folic acid supplemented diet (20-fold higher than recommended)	Embryos from folic acid supplemented dams displayed lower body weight and length	(Achon et al., 1999)
Pregnant rats on folic acid supplemented diet (2.5-fold higher than recommended) Mammary tumors induced by 7,12-dimethylbenz[*a*]anthracene in female offspring	Maternal folic acid supplementation increased risk of mammary adenocarcinoma in female offspring	(Ly et al., 2011)
Pregnant rats on folic acid supplemented diet (2.5-fold higher than recommended) Colorectal cancer induced by azoxymethane in male offspring	Maternal folic acid supplementation reduced risk of colorectal cancer in male offspring Increased colorectal DNA methylation and reduced DNA damage	(Sie et al., 2011)

Pregnant mice on folic acid supplemented diet (20-fold higher than recommended)	Folic acid supplementation associated with embryonic delay, growth retardation, thinner ventricular walls	(Pickell et al., 2011)
Pregnant mice on folic acid supplemented diet (10-fold higher than recommended)	Folic acid supplementation results in embryonic loss, embryonic defects and ventricular defects	(Mikael et al., 2013)
0.4 mg/kg or 4 mg/kg folic acid throughout gestation and lifetime	Higher dose of folic acid alters gene expression in cerebellar hemispheres of offspring Higher dose of folic acid moderately affects behavior	(Barua et al., 2014a)
0.4 mg/kg or 4 mg/kg folic acid throughout gestation and lifetime	Higher dose of folic acid results in differential methylation of key developmental genes in cerebellar hemispheres Sex-specific changes in imprinted and autism linked genes	(Barua et al., 2016a, b; Barua et al., 2014b)
Pregnant mice on folic acid supplemented diet (20-fold higher than recommended)	Female offspring of folic acid supplemented dams display increased body weight and insulin resistance	(Keating et al., 2015)
Pregnant mice on folic acid supplemented diet (10-fold higher than recommended)	Offspring of dams on high folic acid diet display short term memory impairment and decreased hippocampal size	(Bahous et al., 2017)
Female mice on folic acid supplemented diet prior to mating (17-fold higher than recommended)	Offspring of females on high folic acid diet show defects in reversal learning	(Henzel et al., 2017)
Gestational folic acid supplementation during pregnancy in mouse asthma model	Airways of offspring from folic acid supplemented dams displayed airway remodeling Thicker epithelial and smooth muscle layer in airway	(Iscan et al., 2018)
4 mg/kg or 24 mg/kg folic acid throughout gestation and lifetime (12-fold higher than recommended)	Folic acid supplemented males mice show improvement of urinary symptoms in a hormone induced model of urinary obstruction	(Keil et al., 2015a)
4 mg/kg or 24 mg/kg folic acid throughout gestation and lifetime (12-fold higher than recommended)	Folic acid supplemented mice show reduced response to castration induced prostate involution. Prostates of castrated folic acid supplemented mice are larger than prostates from castrated control diet mice	(Joseph et al., 2018b)

2 mg/kg folic acid (control), 0.3 mg/kg (deficient) and 20 mg/kg (10-fold higher than recommended) fed to TRAMP mice after weaning	Folate deficient diet blocks prostate cancer progression Folate supplementation had no effect on prostate cancer growth	(Bistulfi et al., 2011)
Human studies on maternal folic acid supplementation		
Women at risk for NTDs given 4 mg folic acid/day	Infants from women given folic acid supplementation had reduced risk of NTDs	(MRC, 1991)
Women who consumed 400 ug folic acid/day during peri-conceptional period compared to women who had refrained from folic acid consumption	Offspring of women who had consumed folic acid displayed increased methylation of the *IGF2* differentially methylated region Increased *IGF2* methylation was associated with reduced birth weight	(Steegers-Theunissen et al., 2009)
Folic acid consumption through diet and supplements estimated by questionnaire in a group of 490 pregnant women	Folic acid supplement intake in late pregnancy increases risk of childhood asthma in offspring	(Whitrow et al., 2009)
Folic acid supplementation during pregnancy estimated by questionnaire	High folic acid levels associated with atopic dermatitis in offspring	(Kiefte-de Jong et al., 2012)
Women who had consumed folic acid during peri-conceptional period compared to women who had refrained from folic acid consumption	Folic acid consumption in the peri-conceptional period reduced risk of autistic disorders in offspring	(Suren et al., 2013)
Folic acid consumption estimated in women from records of prescription filling	Offspring of women who consumed folic acid during first trimester only or first trimester and later had increased risk of developing childhood asthma	(Veeranki et al., 2015)
Folic acid supplement exposure in pregnant women estimated by questionnaire	Offspring of women with high folic acid supplement exposure had increased risk of developing infant asthma	(Yang et al., 2015)
Impact of folic acid supplementation on prostate cancer		
Plasma levels of folates were tested for association with prostate cancer risk (Northern Sweden Health and disease cohort)	Increasing levels of plasma folate positively correlated with prostate cancer risk	(Hultdin et al., 2005)
Prostate cancer occurrence was assessed after folic acid supplementation	Folic acid supplementation increased the long-term probability of being diagnosed with prostate cancer	(Figueiredo et al., 2009)

(Aspirin/Folate polyp prevention study)		
Plasma levels of folates were tested for association with prostate cancer risk (ProtecT study)	Folate levels showed a positive correlation with prostate cancer risk	(Collin et al., 2010)
Serum folate levels were tested for association with prostate cancer cell proliferation in biopsies (University of Pittsburgh)	Patients with increased serum folate levels had greater cancer proliferation as measured by Ki67 positivity in biopsy tissue	(Tomaszewski et al., 2011)
Oral folic acid supplementation was tested for association with increased cancer risk (Meta-analysis of multiple studies)	Increased prostate cancer risk after folic acid supplementation compared to placebo	(Wien et al., 2012)
Serum folate levels were tested for association with prostate cancer risk (JANUS cohort, Norway)	High serum folate concentration associated with moderate increase prostate cancer risk	(de Vogel et al., 2013)
Meta-analysis of published randomized trial data to study the association of folic acid supplementation on cancer risk	Folic acid supplementation does not have a significant association with prostate cancer incidence	(Qin et al., 2013)
Meta-analysis of randomized trial data to study the association of folic acid supplementation with cancer incidence	Folic acid supplementation does not have a significant effect on prostate cancer incidence	(Vollset et al., 2013)

1.7. Addressing gaps in knowledge

The following gaps in knowledge have been addressed by the work presented in this thesis:

1.7.1. What is the role of DNA methylation in lower urinary tract development?

DNMT1 expression has been shown to be important for the development of several organs including the intestine, retina and pancreas. The role of DNA methylation in lower urinary tract development was previously unknown. In **Chapter 2**, I describe the role of

the key maintenance methyltransferase, DNMT1, during lower urinary tract development. DNMT1 expression in the urethra and bladder is required for epithelial cell survival and normal differentiation. This is a demonstration that epigenetic mechanisms in addition to classical signaling pathways are important regulators of lower urinary tract development.

1.7.2. How is the Wolffian duct-urethra junction maintained?

The Wolffian duct-urethra junction is a rare junction of epithelia from different germ layers. Several studies have described the formation of this junction by epithelial fusion. However, no studies had described mechanisms of how this junction is maintained or the consequences if it is breached. Results from **Chapter 2** show that epithelial depletion by DNMT1 deletion on one side of the junction allows cells from the other side to invade across the junction. Consequently, invading Wolffian duct cells in the bladder mesenchyme are reprogrammed to acquire bladder characteristics.

1.7.3. What is the requirement of epithelial DNMT1 in prostate budding?

Fetal exposures to endocrine disrupting chemicals found in the environment affect prostate budding and elicit changes in DNA methylation. The impact of these DNA methylation changes on prostate budding are not fully understood. In **Chapter 3**, I describe the genetic approach used to study the requirement of DNMT1 in the epithelium of the budding prostate. DNMT1 expression is required for survival and cell cycle progression of prostate progenitor cells and DNMT1 deletion reduces the number of prostate buds formed. RNA-Seq analysis showed that the expression of several genes increases multiple fold in the DNMT1 deleted prostates. Endocrine disrupting chemicals could alter DNA methylation and transcription in the developing prostate through changes in DNMT1 expression.

1.7.4. Do multiple lineages constitute prostate buds?

The adult prostate contains multiple lineages and there is increasing interest in whether these lineages originate during fetal development of the prostate. In **Chapter 3**, I show that developing prostate buds is comprised of at least two lineages by using DNMT1 deletion as a novel tool to lower the proliferation rate of a population of cells to test their incorporation into fast-growing prostate buds.

1.7.5. What is the impact of a methyl donor enriched diet on adult prostate homeostasis?

Cereal grain fortification, maternal supplementation and vitamin supplement use have caused folate levels to increase across age groups in the United States. Mice fed a folic-acid enriched diet display a reduction in symptoms associated with hormone-induced urinary dysfunction. However, the consequences of a folic acid-enriched diet on prostate homeostasis and response to androgen deprivation were unknown. In **Chapter 4**, I show that continuous exposure to a folic acid-enriched diet attenuates prostate involution in response to castration. This previously unknown interaction between folic acid and androgen deprivation has important implications for androgen deprivation therapies that are used for the treatment of prostate disease.

1.8. References

Abler, L.L., Keil, K.P., Mehta, V., Joshi, P.S., Schmitz, C.T., Vezina, C.M., 2011. A high-resolution molecular atlas of the fetal mouse lower urogenital tract. Dev. Dyn. 240, 2364-2377.

Achon, M., Reyes, L., Alonso-Aperte, E., Ubeda, N., Varela-Moreiras, G., 1999. High dietary folate supplementation affects gestational development and dietary protein utilization in rats. J. Nutr. 129, 1204-1208.

Agarwal, 1999. Urethral valves. BJU Int. 84, 570-578.

Akbal, C., Lee, S.D., Packer, S.C., Davis, M.M., Rink, R.C., Kaefer, M., 2006. Bladder augmentation with acellular dermal biomatrix in a diseased animal model. J. Urol. 176, 1706-1711.

Amir, R.E., Van den Veyver, I.B., Wan, M., Tran, C.Q., Francke, U., Zoghbi, H.Y., 1999. Rett syndrome is caused by mutations in X-linked MECP2, encoding methyl-CpG-binding protein 2. Nat. Genet. 23, 185-188.

Anumanthan, G., Makari, J.H., Honea, L., Thomas, J.C., Wills, M.L., Bhowmick, N.A., Adams, M.C., Hayward, S.W., Matusik, R.J., Brock, J.W., 3rd, Pope, J.C.t., 2008. Directed differentiation of bone marrow derived mesenchymal stem cells into bladder urothelium. J. Urol. 180, 1778-1783.

Ashley, G.R., Cathal Grace, O., Vanpoucke, G., Thomson, A.A., 2010. Identification of EphrinB1 expression in prostatic mesenchyme and a role for EphB–EphrinB signalling in prostate development. Differentiation 80, 89-98.

Atala, A., Bauer, S.B., Soker, S., Yoo, J.J., Retik, A.B., 2006. Tissue-engineered autologous bladders for patients needing cystoplasty. Lancet 367, 1241-1246.

Attia, L., Schneider, J., Yelin, R., Schultheiss, T.M., 2015. Collective cell migration of the nephric duct requires FGF signaling. Dev. Dyn. 244, 157-167.

Baccarelli, A., Wright, R.O., Bollati, V., Tarantini, L., Litonjua, A.A., Suh, H.H., Zanobetti, A., Sparrow, D., Vokonas, P.S., Schwartz, J., 2009. Rapid DNA methylation changes after exposure to traffic particles. Am. J. Respir. Crit. Care Med. 179, 572-578.

Bachman, K.E., Rountree, M.R., Baylin, S.B., 2001. Dnmt3a and Dnmt3b are transcriptional repressors that exhibit unique localization properties to heterochromatin. J. Biol. Chem. 276, 32282-32287.

Baets, J., Duan, X., Wu, Y., Smith, G., Seeley, W.W., Mademan, I., McGrath, N.M., Beadell, N.C., Khoury, J., Botuyan, M.V., Mer, G., Worrell, G.A., Hojo, K., DeLeon, J., Laura, M., Liu, Y.T., Senderek, J., Weis, J., Van den Bergh, P., Merrill, S.L., Reilly, M.M., Houlden, H., Grossman, M., Scherer, S.S., De Jonghe, P., Dyck, P.J., Klein, C.J., 2015. Defects of mutant DNMT1 are linked to a spectrum of neurological disorders. Brain 138, 845-861.

Bahous, R.H., Jadavji, N.M., Deng, L., Cosin-Tomas, M., Lu, J., Malysheva, O., Leung, K.Y., Ho, M.K., Pallas, M., Kaliman, P., Greene, N.D.E., Bedell, B.J., Caudill, M.A., Rozen, R., 2017. High dietary folate in pregnant mice leads to pseudo-MTHFR deficiency and altered methyl metabolism, with embryonic growth delay and short-term memory impairment in offspring. Hum. Mol. Genet. 26, 888-900.

Barker, D.J., 2007. The origins of the developmental origins theory. J. Intern. Med. 261, 412-417.

Barsoum, I., Yao, H.H.C., 2006. The road to maleness: from testis to Wolffian duct. Trends Endocrinol. Metab. 17, 223-228.

Bartolomei, M.S., Ferguson-Smith, A.C., 2011. Mammalian genomic imprinting. Cold Spring Harb. Perspect. Biol. 3.

Barua, S., Chadman, K.K., Kuizon, S., Buenaventura, D., Stapley, N.W., Ruocco, F., Begum, U., Guariglia, S.R., Brown, W.T., Junaid, M.A., 2014a. Increasing maternal or post-weaning folic acid alters gene expression and moderately changes behavior in the offspring. PLoS One 9, e101674.

Barua, S., Kuizon, S., Brown, W.T., Junaid, M.A., 2016a. DNA Methylation Profiling at Single-Base Resolution Reveals Gestational Folic Acid Supplementation Influences the Epigenome of Mouse Offspring Cerebellum. Front. Neurosci. 10, 168.

Barua, S., Kuizon, S., Brown, W.T., Junaid, M.A., 2016b. High Gestational Folic Acid Supplementation Alters Expression of Imprinted and Candidate Autism Susceptibility Genes in a sex-Specific Manner in Mouse Offspring. J. Mol. Neurosci. 58, 277-286.

Barua, S., Kuizon, S., Chadman, K.K., Flory, M.J., Brown, W.T., Junaid, M.A., 2014b. Single-base resolution of mouse offspring brain methylome reveals epigenome modifications caused by gestational folic acid. Epigenetics Chromatin 7, 3.

Baskin, L., DiSandro, M., Li, Y., Li, W., Hayward, S., Cunha, G., 2001. Mesenchymal-epithelial interactions in bladder smooth muscle development: effects of the local tissue environment. J. Urol. 165, 1283-1288.

Baskin, L.S., Ebbers, M.B., 2006. Hypospadias: anatomy, etiology, and technique. J. Pediatr. Surg. 41, 463-472.

Batourina, E., Tsai, S., Lambert, S., Sprenkle, P., Viana, R., Dutta, S., Hensle, T., Wang, F., Niederreither, K., McMahon, A.P., Carroll, T.J., Mendelsohn, C.L., 2005. Apoptosis induced by vitamin A signaling is crucial for connecting the ureters to the bladder. Nat. Genet. 37, 1082-1089.

Beard, C., Li, E., Jaenisch, R., 1995. Loss of methylation activates Xist in somatic but not in embryonic cells. Genes Dev. 9, 2325-2334.

Bechis, S.K., Otsetov, A.G., Ge, R., Olumi, A.F., 2014. Personalized Medicine for Management of Benign Prostatic Hyperplasia. J. Urol. 192, 16-23.

Bedford, M.T., van Helden, P.D., 1987. Hypomethylation of DNA in pathological conditions of the human prostate. Cancer Res. 47, 5274-5276.

Behringer, R.R., 1995. The mullerian inhibitor and mammalian sexual development. Philos. Trans. R. Soc. Lond. B Biol. Sci. 350, 285-288; discussion 289.

Berry, S.J., Coffey, D.S., Walsh, P.C., Ewing, L.L., 1984. The development of human benign prostatic hyperplasia with age. J. Urol. 132, 474-479.

Bestor, T., Laudano, A., Mattaliano, R., Ingram, V., 1988. Cloning and sequencing of a cDNA encoding DNA methyltransferase of mouse cells. The carboxyl-terminal domain of the mammalian enzymes is related to bacterial restriction methyltransferases. J. Mol. Biol. 203, 971-983.

Bestor, T.H., Hellewell, S.B., Ingram, V.M., 1984. Differentiation of two mouse cell lines is associated with hypomethylation of their genomes. Mol. Cell. Biol. 4, 1800-1806.

Bestor, T.H., Ingram, V.M., 1983. Two DNA methyltransferases from murine erythroleukemia cells: purification, sequence specificity, and mode of interaction with DNA. Proc. Natl. Acad. Sci. U. S. A. 80, 5559-5563.

Bird, A.P., 1978. Use of restriction enzymes to study eukaryotic DNA methylation: II. The symmetry of methylated sites supports semi-conservative copying of the methylation pattern. J. Mol. Biol. 118, 49-60.

Bird, A.P., 1986. CpG-rich islands and the function of DNA methylation. Nature 321, 209-213.

Bistulfi, G., Foster, B.A., Karasik, E., Gillard, B., Miecznikowski, J., Dhiman, V.K., Smiraglia, D.J., 2011. Dietary folate deficiency blocks prostate cancer progression in the TRAMP model. Cancer Prev. Res. (Phila.) 4, 1825-1834.

Bjerke, D.L., Peterson, R.E., 1994. Reproductive toxicity of 2,3,7,8-tetrachlorodibenzo-p-dioxin in male rats: different effects of in utero versus lactational exposure. Toxicol. Appl. Pharmacol. 127, 241-249.

Blaschko, S.D., Cunha, G.R., Baskin, L.S., 2012. Molecular mechanisms of external genitalia development. Differentiation 84, 261-268.

Bolland, F., Korossis, S., Wilshaw, S.P., Ingham, E., Fisher, J., Kearney, J.N., Southgate, J., 2007. Development and characterisation of a full-thickness acellular porcine bladder matrix for tissue engineering. Biomaterials 28, 1061-1070.

Bollati, V., Baccarelli, A., Hou, L., Bonzini, M., Fustinoni, S., Cavallo, D., Byun, H.M., Jiang, J., Marinelli, B., Pesatori, A.C., Bertazzi, P.A., Yang, A.S., 2007. Changes in DNA methylation patterns in subjects exposed to low-dose benzene. Cancer Res. 67, 876-880.

Bollati, V., Schwartz, J., Wright, R., Litonjua, A., Tarantini, L., Suh, H., Sparrow, D., Vokonas, P., Baccarelli, A., 2009. Decline in genomic DNA methylation through aging in a cohort of elderly subjects. Mech. Ageing Dev. 130, 234-239.

Bostick, M., Kim, J.K., Esteve, P.O., Clark, A., Pradhan, S., Jacobsen, S.E., 2007. UHRF1 plays a role in maintaining DNA methylation in mammalian cells. Science 317, 1760-1764.

Bouchard, M., Souabni, A., Mandler, M., Neubuser, A., Busslinger, M., 2002. Nephric lineage specification by Pax2 and Pax8. Genes Dev. 16, 2958-2970.

Bourc'his, D., Bestor, T.H., 2004. Meiotic catastrophe and retrotransposon reactivation in male germ cells lacking Dnmt3L. Nature 431, 96-99.

Bourc'his, D., Xu, G.L., Lin, C.S., Bollman, B., Bestor, T.H., 2001. Dnmt3L and the establishment of maternal genomic imprints. Science 294, 2536-2539.

Boutin, E.L., Battle, E., Cunha, G.R., 1991. The response of female urogenital tract epithelia to mesenchymal inductors is restricted by the germ layer origin of the epithelium: prostatic inductions. Differentiation 48, 99-105.

Boutin, E.L., Battle, E., Cunha, G.R., 1992. The germ layer origin of mouse vaginal epithelium restricts its responsiveness to mesenchymal inductors: uterine induction. Differentiation 49, 101-107.

Brooks, J.D., Weinstein, M., Lin, X., Sun, Y., Pin, S.S., Bova, G.S., Epstein, J.I., Isaacs, W.B., Nelson, W.G., 1998. CG island methylation changes near the GSTP1 gene in prostatic intraepithelial neoplasia. Cancer Epidemiol. Biomarkers Prev. 7, 531-536.

Buckley, J., Willingham, E., Agras, K., Baskin, L.S., 2006. Embryonic exposure to the fungicide vinclozolin causes virilization of females and alteration of progesterone receptor expression in vivo: an experimental study in mice. Environ. Health 5, 4.

Cao, M., Tasian, G., Wang, M.-H., Liu, B., Cunha, G., Baskin, L., 2010. Urothelium-derived Sonic hedgehog promotes mesenchymal proliferation and induces bladder smooth muscle differentiation. Differentiation; research in biological diversity 79, 244-250.

Casillas, M.A., Lopatina, N., Andrews, L.G., Tollefsbol, T.O., 2003. Transcriptional control of the DNA methyltransferases is altered in aging and neoplastically-transformed human fibroblasts. Mol. Cell. Biochem. 252, 33-43.

CDC, 2007. Folate status in women of childbearing age, by race/ethnicity--United States, 1999-2000, 2001-2002, and 2003-2004. MMWR Morb. Mortal. Wkly. Rep. 55, 1377-1380.

Chédin, F., Lieber, M.R., Hsieh, C.-L., 2002. The DNA methyltransferase-like protein DNMT3L stimulates de novo methylation by Dnmt3a. Proceedings of the National Academy of Sciences 99, 16916-16921.

Chen, R.Z., Pettersson, U., Beard, C., Jackson-Grusby, L., Jaenisch, R., 1998. DNA hypomethylation leads to elevated mutation rates. Nature 395, 89-93.

Chen, T., Hevi, S., Gay, F., Tsujimoto, N., He, T., Zhang, B., Ueda, Y., Li, E., 2007. Complete inactivation of DNMT1 leads to mitotic catastrophe in human cancer cells. Nat. Genet. 39, 391-396.

Chen, T., Tsujimoto, N., Li, E., 2004. The PWWP Domain of Dnmt3a and Dnmt3b Is Required for Directing DNA Methylation to the Major Satellite Repeats at Pericentric Heterochromatin. Mol. Cell. Biol. 24, 9048-9058.

Chen, T., Ueda, Y., Xie, S., Li, E., 2002. A novel Dnmt3a isoform produced from an alternative promoter localizes to euchromatin and its expression correlates with active de novo methylation. J. Biol. Chem. 277, 38746-38754.

Cheong, A., Zhang, X., Cheung, Y.Y., Tang, W.Y., Chen, J., Ye, S.H., Medvedovic, M., Leung, Y.K., Prins, G.S., Ho, S.M., 2016. DNA methylome changes by estradiol benzoate and bisphenol A links early-life environmental exposures to prostate cancer risk. Epigenetics 11, 674-689.

Chia, I., Grote, D., Marcotte, M., Batourina, E., Mendelsohn, C., Bouchard, M., 2011. Nephric duct insertion is a crucial step in urinary tract maturation that is regulated by a Gata3-Raldh2-Ret molecular network in mice. Development 138, 2089-2097.

Cho, N.Y., Kim, B.H., Choi, M., Yoo, E.J., Moon, K.C., Cho, Y.M., Kim, D., Kang, G.H., 2007. Hypermethylation of CpG island loci and hypomethylation of LINE-1 and Alu repeats in prostate adenocarcinoma and their relationship to clinicopathological features. J. Pathol. 211, 269-277.

Ciccarone, F., Malavolta, M., Calabrese, R., Guastafierro, T., Bacalini, M.G., Reale, A., Franceschi, C., Capri, M., Hervonen, A., Hurme, M., Grubeck-Loebenstein, B., Koller, B., Bernhardt, J., Schön, C., Slagboom, P.E., Toussaint, O., Sikora, E., Gonos, E.S., Breusing, N., Grune, T., Jansen, E., Dollé, M., Moreno-Villanueva, M., Sindlinger, T., Bürkle, A., Zampieri, M., Caiafa, P., 2016. Age-dependent expression of DNMT1 and DNMT3B in PBMCs from a large European population enrolled in the MARK-AGE study. Aging Cell 15, 755-765.

Collin, S.M., Metcalfe, C., Refsum, H., Lewis, S.J., Zuccolo, L., Smith, G.D., Chen, L., Harris, R., Davis, M., Marsden, G., Johnston, C., Lane, J.A., Ebbing, M., Bonaa, K.H., Nygard, O., Ueland, P.M., Grau, M.V., Baron, J.A., Donovan, J.L., Neal, D.E., Hamdy, F.C., Smith, A.D., Martin, R.M., 2010. Circulating folate, vitamin B12, homocysteine, vitamin B12 transport proteins, and risk of prostate cancer: a case-control study, systematic review, and meta-analysis. Cancer Epidemiol. Biomarkers Prev. 19, 1632-1642.

Constantinides, P.G., Jones, P.A., Gevers, W., 1977. Functional striated muscle cells from non-myoblast precursors following 5-azacytidine treatment. Nature 267, 364-366.

Constantinides, P.G., Taylor, S.M., Jones, P.A., 1978. Phenotypic conversion of cultured mouse embryo cells by aza pyrimidine nucleosides. Dev. Biol. 66, 57-71.

Cooney, C.A., Dave, A.A., Wolff, G.L., 2002. Maternal methyl supplements in mice affect epigenetic variation and DNA methylation of offspring. J. Nutr. 132, 2393s-2400s.

Cunha, G.R., Baskin, L., 2016. Mesenchymal-epithelial interaction techniques. Differentiation 91, 20-27.

Damaschke, N.A., Yang, B., Bhusari, S., Avilla, M., Zhong, W., Blute, M.L., Jr., Huang, W., Jarrard, D.F., 2017. Loss of Igf2 Gene Imprinting in Murine Prostate Promotes Widespread Neoplastic Growth. Cancer Res. 77, 5236-5247.

Davis, C.M., Constantinides, P.G., van der Riet, F., van Schalkwyk, L., Gevers, W., Parker, M.I., 1989. Activation and demethylation of the intracisternal A particle genes by 5-azacytidine. Cell Differ. Dev. 27, 83-93.

Davis, T.A., 1949. Hamartoma of the urinary bladder. Northwest Med. 48, 182-185.

De Prins, S., Koppen, G., Jacobs, G., Dons, E., Van de Mieroop, E., Nelen, V., Fierens, F., Int Panis, L., De Boever, P., Cox, B., Nawrot, T.S., Schoeters, G., 2013. Influence of ambient air pollution on global DNA methylation in healthy adults: a seasonal follow-up. Environ. Int. 59, 418-424.

de Vogel, S., Meyer, K., Fredriksen, A., Ulvik, A., Ueland, P.M., Nygard, O., Vollset, S.E., Tell, G.S., Tretli, S., Bjorge, T., 2013. Serum folate and vitamin B12 concentrations in relation to prostate cancer risk--a Norwegian population-based nested case-control study of 3000 cases and 3000 controls within the JANUS cohort. Int. J. Epidemiol. 42, 201-210.

Deaton, A.M., Bird, A., 2011. CpG islands and the regulation of transcription. Genes Dev. 25, 1010-1022.

Ding, F., Chaillet, J.R., 2002. In vivo stabilization of the Dnmt1 (cytosine-5)- methyltransferase protein. Proc. Natl. Acad. Sci. U. S. A. 99, 14861-14866.

Doherty, A.S., Bartolomei, M.S., Schultz, R.M., 2002. Regulation of stage-specific nuclear translocation of Dnmt1o during preimplantation mouse development. Dev. Biol. 242, 255-266.

Dolinoy, D.C., Huang, D., Jirtle, R.L., 2007a. Maternal nutrient supplementation counteracts bisphenol A-induced DNA hypomethylation in early development. Proc. Natl. Acad. Sci. U. S. A. 104, 13056-13061.

Dolinoy, D.C., Huang, D., Jirtle, R.L., 2007b. Maternal nutrient supplementation counteracts bisphenol A-induced DNA hypomethylation in early development. Proceedings of the National Academy of Sciences 104, 13056-13061.

Donjacour, A.A., Cunha, G.R., 1993. Assessment of prostatic protein secretion in tissue recombinants made of urogenital sinus mesenchyme and urothelium from normal or androgen-insensitive mice. Endocrinology 132, 2342-2350.

Donjacour, A.A., Cunha, G.R., 1995. Induction of prostatic morphology and secretion in urothelium by seminal vesicle mesenchyme. Development 121, 2199-2207.

Doskočil, J., Šorm, F., 1962. Distribution of 5-methylcytosine in pyrimidine sequences of deoxyribonucleic acids. Biochim. Biophys. Acta 55, 953-959.

Eckhardt, F., Lewin, J., Cortese, R., Rakyan, V.K., Attwood, J., Burger, M., Burton, J., Cox, T.V., Davies, R., Down, T.A., Haefliger, C., Horton, R., Howe, K., Jackson, D.K., Kunde, J., Koenig, C., Liddle, J., Niblett, D., Otto, T., Pettett, R., Seemann, S., Thompson, C., West, T., Rogers, J., Olek, A., Berlin, K., Beck, S., 2006. DNA methylation profiling of human chromosomes 6, 20 and 22. Nat. Genet. 38, 1378.

Elias-Assad, G., Elias, M., Kanety, H., Pressman, A., Tenenbaum-Rakover, Y., 2016. Persistent Mullerian Duct Syndrome Caused by a Novel Mutation of an Anti-Mullerian Hormone Receptor Gene: Case Presentation and Literature Review. Pediatr. Endocrinol. Rev. 13, 731-740.

Ellinger, J., Bastian, P.J., Jurgan, T., Biermann, K., Kahl, P., Heukamp, L.C., Wernert, N., Muller, S.C., von Ruecker, A., 2008. CpG island hypermethylation at multiple gene sites in diagnosis and prognosis of prostate cancer. Urology 71, 161-167.

Elliott, E.N., Sheaffer, K.L., Schug, J., Stappenbeck, T.S., Kaestner, K.H., 2015. Dnmt1 is essential to maintain progenitors in the perinatal intestinal epithelium. Development 142, 2163-2172.

Epsztejn-Litman, S., Feldman, N., Abu-Remaileh, M., Shufaro, Y., Gerson, A., Ueda, J., Deplus, R., Fuks, F., Shinkai, Y., Cedar, H., Bergman, Y., 2008. De novo DNA methylation promoted by G9a prevents reprogramming of embryonically silenced genes. Nat. Struct. Mol. Biol. 15, 1176-1183.

Espada, J., Peinado, H., Lopez-Serra, L., Setien, F., Lopez-Serra, P., Portela, A., Renart, J., Carrasco, E., Calvo, M., Juarranz, A., Cano, A., Esteller, M., 2011. Regulation of SNAIL1 and E-cadherin function by DNMT1 in a DNA methylation-independent context. Nucleic Acids Res. 39, 9194-9205.

Esteve, P.O., Chin, H.G., Smallwood, A., Feehery, G.R., Gangisetty, O., Karpf, A.R., Carey, M.F., Pradhan, S., 2006. Direct interaction between DNMT1 and G9a coordinates DNA and histone methylation during replication. Genes Dev. 20, 3089-3103.

Fairweather, D.S., Fox, M., Margison, G.P., 1987. The in vitro lifespan of MRC-5 cells is shortened by 5-azacytidine-induced demethylation. Exp. Cell Res. 168, 153-159.

Fan, G., Beard, C., Chen, R.Z., Csankovszki, G., Sun, Y., Siniaia, M., Biniszkiewicz, D., Bates, B., Lee, P.P., Kuhn, R., Trumpp, A., Poon, C., Wilson, C.B., Jaenisch, R., 2001. DNA hypomethylation perturbs the function and survival of CNS neurons in postnatal animals. J. Neurosci. 21, 788-797.

Fatemi, M., Hermann, A., Gowher, H., Jeltsch, A., 2002. Dnmt3a and Dnmt1 functionally cooperate during de novo methylation of DNA. Eur. J. Biochem. 269, 4981-4984.

Fatemi, M., Wade, P.A., 2006. MBD family proteins: reading the epigenetic code. J. Cell Sci. 119, 3033-3037.

Feng, J., 2010. Dnmt1 and Dnmt3a are required for the maintenance of DNA methylation and synaptic function in adult forebrain neurons. 13, 423-430.

Feng, Q., Zhang, Y., 2001. The MeCP1 complex represses transcription through preferential binding, remodeling, and deacetylating methylated nucleosomes. Genes Dev. 15, 827-832.

Figueiredo, J.C., Grau, M.V., Haile, R.W., Sandler, R.S., Summers, R.W., Bresalier, R.S., Burke, C.A., McKeown-Eyssen, G.E., Baron, J.A., 2009. Folic Acid and Risk of Prostate Cancer: Results From a Randomized Clinical Trial. J. Natl. Cancer Inst. 101, 432-435.

Ford, T.F., Watson, G.M., Cameron, K.M., 1985. Adenomatous metaplasia (nephrogenic adenoma) of urothelium. An analysis of 70 cases. Br. J. Urol. 57, 427-433.

Fraga, M.F., Ballestar, E., Paz, M.F., Ropero, S., Setien, F., Ballestar, M.L., Heine-Suñer, D., Cigudosa, J.C., Urioste, M., Benitez, J., Boix-Chornet, M., Sanchez-Aguilera, A., Ling, C., Carlsson, E., Poulsen, P., Vaag, A., Stephan, Z., Spector, T.D., Wu, Y.Z., Plass, C., Esteller, M., 2005. Epigenetic differences arise during the lifetime of monozygotic twins. Proc. Natl. Acad. Sci. U. S. A. 102, 10604-10609.

Friedman, N.B., Kuhlenbeck, H., 1950. Adenomatoid tumors of the bladder reproducing renal structures (nephrogenic adenomas). J. Urol. 64, 657-670.

Fritz, E.L., Papavasiliou, F.N., 2010. Cytidine deaminases: AIDing DNA demethylation? Genes Dev. 24, 2107-2114.

Fu, V.X., Dobosy, J.R., Desotelle, J.A., Almassi, N., Ewald, J.A., Srinivasan, R., Berres, M., Svaren, J., Weindruch, R., Jarrard, D.F., 2008. Aging and cancer-related loss of insulin-

like growth factor 2 imprinting in the mouse and human prostate. Cancer Res. 68, 6797-6802.

Fu, V.X., Schwarze, S.R., Kenowski, M.L., Leblanc, S., Svaren, J., Jarrard, D.F., 2004. A loss of insulin-like growth factor-2 imprinting is modulated by CCCTC-binding factor down-regulation at senescence in human epithelial cells. J. Biol. Chem. 279, 52218-52226.

Fujita, N., Watanabe, S., Ichimura, T., Tsuruzoe, S., Shinkai, Y., Tachibana, M., Chiba, T., Nakao, M., 2003. Methyl-CpG binding domain 1 (MBD1) interacts with the Suv39h1-HP1 heterochromatic complex for DNA methylation-based transcriptional repression. J. Biol. Chem. 278, 24132-24138.

Fuks, F., Hurd, P.J., Deplus, R., Kouzarides, T., 2003a. The DNA methyltransferases associate with HP1 and the SUV39H1 histone methyltransferase. Nucleic Acids Res. 31, 2305-2312.

Fuks, F., Hurd, P.J., Wolf, D., Nan, X., Bird, A.P., Kouzarides, T., 2003b. The methyl-CpG-binding protein MeCP2 links DNA methylation to histone methylation. J. Biol. Chem. 278, 4035-4040.

Gaudet, F., Hodgson, J.G., Eden, A., Jackson-Grusby, L., Dausman, J., Gray, J.W., Leonhardt, H., Jaenisch, R., 2003. Induction of tumors in mice by genomic hypomethylation. Science 300, 489-492.

Gaudet, F., Rideout, W.M., 3rd, Meissner, A., Dausman, J., Leonhardt, H., Jaenisch, R., 2004. Dnmt1 expression in pre- and postimplantation embryogenesis and the maintenance of IAP silencing. Mol. Cell. Biol. 24, 1640-1648.

Ge, R., Wang, Z., Bechis, S.K., Otsetov, A.G., Hua, S., Wu, S., Wu, C.L., Tabatabaei, S., Olumi, A.F., 2015. DNA Methyl Transferase 1 Reduces Expression of SRD5A2 in the Aging Adult Prostate. Am. J. Pathol. 185, 870-882.

Georgas, K.M., Armstrong, J., Keast, J.R., Larkins, C.E., McHugh, K.M., Southard-Smith, E.M., Cohn, M.J., Batourina, E., Dan, H., Schneider, K., Buehler, D.P., Wiese, C.B., Brennan, J., Davies, J.A., Harding, S.D., Baldock, R.A., Little, M.H., Vezina, C.M., Mendelsohn, C., 2015. An illustrated anatomical ontology of the developing mouse lower urogenital tract. Development 142, 1893-1908.

Georgia, S., Kanji, M., Bhushan, A., 2013. DNMT1 represses p53 to maintain progenitor cell survival during pancreatic organogenesis. Genes Dev. 27, 372-377.

Ghosh, S., Yates, A.J., Fruhwald, M.C., Miecznikowski, J.C., Plass, C., Smiraglia, D., 2010. Tissue specific DNA methylation of CpG islands in normal human adult somatic tissues distinguishes neural from non-neural tissues. Epigenetics 5, 527-538.

Goering, W., Ribarska, T., Schulz, W.A., 2011. Selective changes of retroelement expression in human prostate cancer. Carcinogenesis 32, 1484-1492.

Gowher, H., Jeltsch, A., 2001. Enzymatic properties of recombinant Dnmt3a DNA methyltransferase from mouse: the enzyme modifies DNA in a non-processive manner and also methylates non-CpG [correction of non-CpA] sites. J. Mol. Biol. 309, 1201-1208.

Gray, L.E., Jr., Ostby, J.S., 1995. In utero 2,3,7,8-tetrachlorodibenzo-p-dioxin (TCDD) alters reproductive morphology and function in female rat offspring. Toxicol. Appl. Pharmacol. 133, 285-294.

Grishina, I.B., Kim, S.Y., Ferrara, C., Makarenkova, H.P., Walden, P.D., 2005. BMP7 inhibits branching morphogenesis in the prostate gland and interferes with Notch signaling. Dev. Biol. 288, 334-347.

Grote, D., Souabni, A., Busslinger, M., Bouchard, M., 2006. Pax 2/8-regulated Gata 3 expression is necessary for morphogenesis and guidance of the nephric duct in the developing kidney. Development 133, 53-61.

Guioli, S., Sekido, R., Lovell-Badge, R., 2007. The origin of the Mullerian duct in chick and mouse. Dev. Biol. 302, 389-398.

Gupta, C., 2000. Reproductive malformation of the male offspring following maternal exposure to estrogenic chemicals. Proc. Soc. Exp. Biol. Med. 224, 61-68.

Hahn, M.A., Qiu, R., Wu, X., Li, A.X., Zhang, H., Wang, J., Jui, J., Jin, S.G., Jiang, Y., Pfeifer, G.P., Lu, Q., 2013. Dynamics of 5-hydroxymethylcytosine and chromatin marks in Mammalian neurogenesis. Cell reports 3, 291-300.

Hahn, O., Grönke, S., Stubbs, T.M., Ficz, G., Hendrich, O., Krueger, F., Andrews, S., Zhang, Q., Wakelam, M.J., Beyer, A., Reik, W., Partridge, L., 2017. Dietary restriction protects from age-associated DNA methylation and induces epigenetic reprogramming of lipid metabolism. Genome Biol. 18, 56.

Han, H., Cortez, C.C., Yang, X., Nichols, P.W., Jones, P.A., Liang, G., 2011. DNA methylation directly silences genes with non-CpG island promoters and establishes a nucleosome occupied promoter. Hum. Mol. Genet. 20, 4299-4310.

Harada, M., Omori, A., Nakahara, C., Nakagata, N., Akita, K., Yamada, G., 2015. Tissue-specific roles of FGF signaling in external genitalia development. Dev. Dyn. 244, 759-773.

Haraguchi, R., Mo, R., Hui, C.-c., Motoyama, J., Makino, S., Shiroishi, T., Gaffield, W., Yamada, G., 2001. Unique functions of Sonic hedgehog signaling during external genitalia development. Development 128, 4241-4250.

Hark, A.T., Schoenherr, C.J., Katz, D.J., Ingram, R.S., Levorse, J.M., Tilghman, S.M., 2000. CTCF mediates methylation-sensitive enhancer-blocking activity at the H19/Igf2 locus. Nature 405, 486-489.

Hata, K., Okano, M., Lei, H., Li, E., 2002. Dnmt3L cooperates with the Dnmt3 family of de novo DNA methyltransferases to establish maternal imprints in mice. Development 129, 1983-1993.

He, B.S., Pan, Y.Q., Zhu, C.B., 2014. [Polymorphisms of DNA methyltransferases and the risk of prostate cancer]. Zhonghua nan ke xue = National journal of andrology 20, 1077-1081.

He, Y.F., Li, B.Z., Li, Z., Liu, P., Wang, Y., Tang, Q., Ding, J., Jia, Y., Chen, Z., Li, L., Sun, Y., Li, X., Dai, Q., Song, C.X., Zhang, K., He, C., Xu, G.L., 2011. Tet-Mediated Formation of 5-Carboxylcytosine and Its Excision by TDG in Mammalian DNA. Science 333, 1303-1307.

Heijmans, B.T., Tobi, E.W., Stein, A.D., Putter, H., Blauw, G.J., Susser, E.S., Slagboom, P.E., Lumey, L.H., 2008. Persistent epigenetic differences associated with prenatal exposure to famine in humans. Proc. Natl. Acad. Sci. U. S. A. 105, 17046-17049.

Hendrich, B., Hardeland, U., Ng, H.H., Jiricny, J., Bird, A., 1999. The thymine glycosylase MBD4 can bind to the product of deamination at methylated CpG sites. Nature 401, 301-304.

Henrique, R., Jeronimo, C., Hoque, M.O., Carvalho, A.L., Oliveira, J., Teixeira, M.R., Lopes, C., Sidransky, D., 2005. Frequent 14-3-3 sigma promoter methylation in benign and malignant prostate lesions. DNA Cell Biol. 24, 264-269.

Henzel, K.S., Ryan, D.P., Schröder, S., Weiergräber, M., Ehninger, D., 2017. High-dose maternal folic acid supplementation before conception impairs reversal learning in offspring mice. Sci. Rep. 7, 3098.

Heyn, H., Li, N., Ferreira, H.J., Moran, S., Pisano, D.G., Gomez, A., Diez, J., Sanchez-Mut, J.V., Setien, F., Carmona, F.J., Puca, A.A., Sayols, S., Pujana, M.A., Serra-Musach, J., Iglesias-Platas, I., Formiga, F., Fernandez, A.F., Fraga, M.F., Heath, S.C., Valencia, A., Gut, I.G., Wang, J., Esteller, M., 2012. Distinct DNA methylomes of newborns and centenarians. Proceedings of the National Academy of Sciences 109, 10522-10527.

Hirasawa, R., Chiba, H., Kaneda, M., Tajima, S., Li, E., Jaenisch, R., Sasaki, H., 2008. Maternal and zygotic Dnmt1 are necessary and sufficient for the maintenance of DNA methylation imprints during preimplantation development. Genes Dev. 22, 1607-1616.

Ho, S.M., Tang, W.Y., Belmonte de Frausto, J., Prins, G.S., 2006. Developmental exposure to estradiol and bisphenol A increases susceptibility to prostate carcinogenesis and epigenetically regulates phosphodiesterase type 4 variant 4. Cancer Res. 66, 5624-5632.

Holliday, R., 1986. Strong effects of 5-azacytidine on the in vitro lifespan of human diploid fibroblasts. Exp. Cell Res. 166, 543-552.

Holliday, R., 1994. Epigenetics: an overview. Dev. Genet. 15, 453-457.

Holliday, R., Pugh, J., 1975. DNA modification mechanisms and gene activity during development. Science 187, 226-232.

Honein, M.A., Paulozzi, L.J., Mathews, T.J., Erickson, J.D., Wong, L.Y., 2001. Impact of folic acid fortification of the US food supply on the occurrence of neural tube defects. JAMA 285, 2981-2986.

Hou, H.A., Kuo, Y.Y., Liu, C.Y., Chou, W.C., Lee, M.C., Chen, C.Y., Lin, L.I., Tseng, M.H., Huang, C.F., Chiang, Y.C., Lee, F.Y., Liu, M.C., Liu, C.W., Tang, J.L., Yao, M., Huang, S.Y., Ko, B.S., Hsu, S.C., Wu, S.J., Tsay, W., Chen, Y.C., Tien, H.F., 2012. DNMT3A mutations in acute myeloid leukemia: stability during disease evolution and clinical implications. Blood 119, 559-568.

Howell, C.Y., Bestor, T.H., Ding, F., Latham, K.E., Mertineit, C., Trasler, J.M., Chaillet, J.R., 2001. Genomic imprinting disrupted by a maternal effect mutation in the Dnmt1 gene. Cell 104, 829-838.

Howlett, S.K., Reik, W., 1991. Methylation levels of maternal and paternal genomes during preimplantation development. Development 113, 119-127.

Hultdin, J., Van Guelpen, B., Bergh, A., Hallmans, G., Stattin, P., 2005. Plasma folate, vitamin B12, and homocysteine and prostate cancer risk: a prospective study. Int. J. Cancer 113, 819-824.

Hutnick, L.K., Golshani, P., Namihira, M., Xue, Z., Matynia, A., Yang, X.W., Silva, A.J., Schweizer, F.E., Fan, G., 2009. DNA hypomethylation restricted to the murine forebrain induces cortical degeneration and impairs postnatal neuronal maturation. Hum. Mol. Genet. 18, 2875-2888.

Iscan, B., Tuzun, F., Eroglu Filibeli, B., Cilekar Micili, S., Ergur, B.U., Duman, N., Ozkan, H., Kumral, A., 2018. Effects of maternal folic acid supplementation on airway remodeling and allergic airway disease development. J. Matern. Fetal Neonatal Med., 1-9.

J.P. Gearhart, R.D.J., 1992. Exstrophy of the bladder, epispadias, and other bladder anomalies, in: P.C. Walsh, A.B.R., T.A. Stamey, E.D. Vaughan Jr. (Ed.), Campbell's urology (6th ed.), vol. 2. W.B. Saunders Co, Philadelphia, pp. pp. 1172–1815

Jackson-Grusby, L., Beard, C., Possemato, R., Tudor, M., Fambrough, D., Csankovszki, G., Dausman, J., Lee, P., Wilson, C., Lander, E., Jaenisch, R., 2001. Loss of genomic methylation causes p53-dependent apoptosis and epigenetic deregulation. Nat. Genet. 27, 31-39.

Jackson, M., Krassowska, A., Gilbert, N., Chevassut, T., Forrester, L., Ansell, J., Ramsahoye, B., 2004. Severe global DNA hypomethylation blocks differentiation and induces histone hyperacetylation in embryonic stem cells. Mol. Cell. Biol. 24, 8862-8871.

Jacob, V., Chernyavskaya, Y., Chen, X., Tan, P.S., Kent, B., Hoshida, Y., Sadler, K.C., 2015. DNA hypomethylation induces a DNA replication-associated cell cycle arrest to block hepatic outgrowth in uhrf1 mutant zebrafish embryos. Development 142, 510-521.

Jahangiri, R., Mosaffa, F., Emami Razavi, A., Teimoori-Toolabi, L., Jamialahmadi, K., 2018. Altered DNA methyltransferases promoter methylation and mRNA expression are associated with tamoxifen response in breast tumors. J. Cell. Physiol.

Jarrard, D.F., Bussemakers, M.J., Bova, G.S., Isaacs, W.B., 1995. Regional loss of imprinting of the insulin-like growth factor II gene occurs in human prostate tissues. Clin. Cancer. Res. 1, 1471-1478.

Jin, B., Tao, Q., Peng, J., Soo, H.M., Wu, W., Ying, J., Fields, C.R., Delmas, A.L., Liu, X., Qiu, J., Robertson, K.D., 2008. DNA methyltransferase 3B (DNMT3B) mutations in ICF syndrome lead to altered epigenetic modifications and aberrant expression of genes regulating development, neurogenesis and immune function. Hum. Mol. Genet. 17, 690-709.

Jones, P.A., Taylor, S.M., 1980. Cellular differentiation, cytidine analogs and DNA methylation. Cell 20, 85-93.

Joseph, D.B., Chandrashekar, A.S., Abler, L.L., Chu, L.-F., Thomson, J.A., Mendelsohn, C., Vezina, C.M., 2018a. In vivo replacement of damaged bladder urothelium by Wolffian duct epithelial cells. Proceedings of the National Academy of Sciences 115, 8394-8399.

Joseph, D.B., Chandrashekar, A.S., Chu, L.-F., Thomson, J.A., Vezina, C.M., 2018b. A folic acid-enriched diet attenuates prostate involution in response to androgen deprivation. The Prostate 0.

Jung, M., Pfeifer, G.P., 2015. Aging and DNA methylation. BMC Biol. 13, 7.

Kafer, G.R., Li, X., Horii, T., Suetake, I., Tajima, S., Hatada, I., Carlton, P.M., 2016. 5-Hydroxymethylcytosine Marks Sites of DNA Damage and Promotes Genome Stability. Cell reports 14, 1283-1292.

Kagiwada, S., Kurimoto, K., Hirota, T., Yamaji, M., Saitou, M., 2013. Replication-coupled passive DNA demethylation for the erasure of genome imprints in mice. The EMBO Journal 32, 340-353.

Kaji, K., Nichols, J., Hendrich, B., 2007. Mbd3, a component of the NuRD co-repressor complex, is required for development of pluripotent cells. Development 134, 1123-1132.

Kaneda, M., Okano, M., Hata, K., Sado, T., Tsujimoto, N., Li, E., Sasaki, H., 2004. Essential role for de novo DNA methyltransferase Dnmt3a in paternal and maternal imprinting. Nature 429, 900-903.

Kang, G.H., Lee, S., Lee, H.J., Hwang, K.S., 2004. Aberrant CpG island hypermethylation of multiple genes in prostate cancer and prostatic intraepithelial neoplasia. J. Pathol. 202, 233-240.

Kao, C.S., Kum, J.B., Fan, R., Grignon, D.J., Eble, J.N., Idrees, M.T., 2013. Nephrogenic adenomas in pediatric patients: a morphologic and immunohistochemical study of 21 cases. Pediatr. Dev. Pathol. 16, 80-85.

Kaplan, S.A., Gonzalez, R.R., 2007. Phosphodiesterase Type 5 Inhibitors for the Treatment of Male Lower Urinary Tract Symptoms. Reviews in Urology 9, 73-77.

Kato, Y., Kaneda, M., Hata, K., Kumaki, K., Hisano, M., Kohara, Y., Okano, M., Li, E., Nozaki, M., Sasaki, H., 2007. Role of the Dnmt3 family in de novo methylation of imprinted and repetitive sequences during male germ cell development in the mouse. Hum. Mol. Genet. 16, 2272-2280.

Kay, G.F., Penny, G.D., Patel, D., Ashworth, A., Brockdorff, N., Rastan, S., 1993. Expression of Xist during mouse development suggests a role in the initiation of X chromosome inactivation. Cell 72, 171-182.

Keating, E., Correia-Branco, A., Araujo, J.R., Meireles, M., Fernandes, R., Guardao, L., Guimaraes, J.T., Martel, F., Calhau, C., 2015. Excess perigestational folic acid exposure induces metabolic dysfunction in post-natal life. J. Endocrinol. 224, 245-259.

Keil, K.P., Abler, L.L., Altmann, H.M., Wang, Z., Wang, P., Ricke, W.A., Bjorling, D.E., Vezina, C.M., 2015a. Impact of a folic acid-enriched diet on urinary tract function in mice treated with testosterone and estradiol. Am. J. Physiol. Renal Physiol. 308, F1431-1443.

Keil, K.P., Abler, L.L., Laporta, J., Altmann, H.M., Yang, B., Jarrard, D.F., Hernandez, L.L., Vezina, C.M., 2014a. Androgen receptor DNA methylation regulates the timing and androgen sensitivity of mouse prostate ductal development. Dev. Biol. 396, 237-245.

Keil, K.P., Abler, L.L., Mehta, V., Altmann, H.M., Laporta, J., Plisch, E.H., Suresh, M., Hernandez, L.L., Vezina, C.M., 2014b. DNA methylation of E-cadherin is a priming mechanism for prostate development. Dev. Biol. 387, 142-153.

Keil, K.P., Altmann, H.M., Abler, L.L., Hernandez, L.L., Vezina, C.M., 2015b. Histone acetylation regulates prostate ductal morphogenesis through a bone morphogenetic protein-dependent mechanism. Dev. Dyn.

Keil, K.P., Altmann, H.M., Mehta, V., Abler, L.L., Elton, E.A., Vezina, C.M., 2013. Catalog of mRNA expression patterns for DNA methylating and demethylating genes in developing mouse lower urinary tract. Gene Expr Patterns 13, 413-424.

Khalil, H., Tazi, M., Caution, K., Ahmed, A., Kanneganti, A., Assani, K., Kopp, B., Marsh, C., Dakhlallah, D., Amer, A.O., 2016. Aging is associated with hypermethylation of autophagy genes in macrophages. Epigenetics 11, 381-388.

Kiefte-de Jong, J.C., Timmermans, S., Jaddoe, V.W., Hofman, A., Tiemeier, H., Steegers, E.A., de Jongste, J.C., Moll, H.A., 2012. High circulating folate and vitamin B-12 concentrations in women during pregnancy are associated with increased prevalence of atopic dermatitis in their offspring. J. Nutr. 142, 731-738.

Kirby, M.K., Ramaker, R.C., Roberts, B.S., Lasseigne, B.N., Gunther, D.S., Burwell, T.C., Davis, N.S., Gulzar, Z.G., Absher, D.M., Cooper, S.J., Brooks, J.D., Myers, R.M., 2017. Genome-wide DNA methylation measurements in prostate tissues uncovers novel prostate cancer diagnostic biomarkers and transcription factor binding patterns. BMC Cancer 17, 273.

Klein, C.J., Botuyan, M.V., Wu, Y., Ward, C.J., Nicholson, G.A., Hammans, S., Hojo, K., Yamanishi, H., Karpf, A.R., Wallace, D.C., Simon, M., Lander, C., Boardman, L.A., Cunningham, J.M., Smith, G.E., Litchy, W.J., Boes, B., Atkinson, E.J., Middha, S., PJ, B.D., Parisi, J.E., Mer, G., Smith, D.I., Dyck, P.J., 2011. Mutations in DNMT1 cause hereditary sensory neuropathy with dementia and hearing loss. Nat. Genet. 43, 595-600.

Kono, T., Obata, Y., Wu, Q., Niwa, K., Ono, Y., Yamamoto, Y., Park, E.S., Seo, J.S., Ogawa, H., 2004. Birth of parthenogenetic mice that can develop to adulthood. Nature 428, 860-864.

Kroovand, R.L., Perlmutter, A.D., 1981. Congenital Anomalies of the Vas Deferens and Epididymis, in: Kogan, S.J., Hafez, E.S.E. (Eds.), Pediatric Andrology. Springer Netherlands, Dordrecht, pp. 173-180.

Kuff, E.L., Lueders, K.K., 1988. The intracisternal A-particle gene family: structure and functional aspects. Adv. Cancer Res. 51, 183-276.

Lee, E., Wang, J., Yumoto, K., Jung, Y., Cackowski, F.C., Decker, A.M., Li, Y., Franceschi, R.T., Pienta, K.J., Taichman, R.S., 2016. DNMT1 Regulates Epithelial-Mesenchymal Transition and Cancer Stem Cells, Which Promotes Prostate Cancer Metastasis. Neoplasia 18, 553-566.

Lee, W.H., Morton, R.A., Epstein, J.I., Brooks, J.D., Campbell, P.A., Bova, G.S., Hsieh, W.S., Isaacs, W.B., Nelson, W.G., 1994. Cytidine methylation of regulatory sequences near the pi-class glutathione S-transferase gene accompanies human prostatic carcinogenesis. Proc. Natl. Acad. Sci. U. S. A. 91, 11733-11737.

Lehnertz, B., Ueda, Y., Derijck, A.A., Braunschweig, U., Perez-Burgos, L., Kubicek, S., Chen, T., Li, E., Jenuwein, T., Peters, A.H., 2003. Suv39h-mediated histone H3 lysine 9 methylation directs DNA methylation to major satellite repeats at pericentric heterochromatin. Curr. Biol. 13, 1192-1200.

Lei, H., Oh, S.P., Okano, M., Juttermann, R., Goss, K.A., Jaenisch, R., Li, E., 1996. De novo DNA cytosine methyltransferase activities in mouse embryonic stem cells. Development 122, 3195-3205.

Leonhardt, H., Page, A.W., Weier, H.U., Bestor, T.H., 1992. A targeting sequence directs DNA methyltransferase to sites of DNA replication in mammalian nuclei. Cell 71, 865-873.

Ley, T.J., Ding, L., Walter, M.J., McLellan, M.D., Lamprecht, T., Larson, D.E., Kandoth, C., Payton, J.E., Baty, J., Welch, J., Harris, C.C., Lichti, C.F., Townsend, R.R., Fulton, R.S., Dooling, D.J., Koboldt, D.C., Schmidt, H., Zhang, Q., Osborne, J.R., Lin, L., O'Laughlin, M., McMichael, J.F., Delehaunty, K.D., McGrath, S.D., Fulton, L.A., Magrini, V.J., Vickery, T.L., Hundal, J., Cook, L.L., Conyers, J.J., Swift, G.W., Reed, J.P., Alldredge, P.A., Wylie, T., Walker, J., Kalicki, J., Watson, M.A., Heath, S., Shannon, W.D., Varghese, N., Nagarajan, R., Westervelt, P., Tomasson, M.H., Link, D.C., Graubert, T.A., DiPersio, J.F., Mardis, E.R., Wilson, R.K., 2010. DNMT3A mutations in acute myeloid leukemia. N. Engl. J. Med. 363, 2424-2433.

Li, E., Beard, C., Jaenisch, R., 1993. Role for DNA methylation in genomic imprinting. Nature 366, 362-365.

Li, E., Bestor, T.H., Jaenisch, R., 1992. Targeted mutation of the DNA methyltransferase gene results in embryonic lethality. Cell 69, 915-926.

Li, H., Li, W., Liu, S., Zong, S., Wang, W., Ren, J., Li, Q., Hou, F., Shi, Q., 2016. DNMT1, DNMT3 and DNMT3B Polymorphisms Associated With Gastric Cancer Risk: A Systematic Review and Meta-analysis. EBioMedicine 13, 125-131.

Li, J., 2012. Progressive alopecia reveals decreasing stem cell activation probability during aging of mice with epidermal deletion of DNA methyltransferase 1 (DNMT1). 132, 2681-2690.

Li, T., Wang, L., Du, Y., Xie, S., Yang, X., Lian, F., Zhou, Z., Qian, C., 2018. Structural and mechanistic insights into UHRF1-mediated DNMT1 activation in the maintenance DNA methylation. Nucleic Acids Res.

Li, Z., Dai, H., Martos, S.N., Xu, B., Gao, Y., Li, T., Zhu, G., Schones, D.E., Wang, Z., 2015. Distinct roles of DNMT1-dependent and DNMT1-independent methylation patterns in the genome of mouse embryonic stem cells. Genome Biol. 16.

Liang, G., Chan, M.F., Tomigahara, Y., Tsai, Y.C., Gonzales, F.A., Li, E., Laird, P.W., Jones, P.A., 2002. Cooperativity between DNA methyltransferases in the maintenance methylation of repetitive elements. Mol. Cell. Biol. 22, 480-491.

Liang, P., Song, F., Ghosh, S., Morien, E., Qin, M., Mahmood, S., Fujiwara, K., Igarashi, J., Nagase, H., Held, W.A., 2011. Genome-wide survey reveals dynamic widespread tissue-specific changes in DNA methylation during development. BMC Genomics 12, 231.

Liao, J., Karnik, R., Gu, H., Ziller, M.J., Clement, K., Tsankov, A.M., Akopian, V., Gifford, C.A., Donaghey, J., Galonska, C., Pop, R., Reyon, D., Tsai, S.Q., Mallard, W., Joung, J.K., Rinn, J.L., Gnirke, A., Meissner, A., 2015. Targeted disruption of DNMT1, DNMT3A and DNMT3B in human embryonic stem cells. Nat. Genet. 47, 469-478.

Lin, T.M., Rasmussen, N.T., Moore, R.W., Albrecht, R.M., Peterson, R.E., 2003. Region-specific inhibition of prostatic epithelial bud formation in the urogenital sinus of C57BL/6 mice exposed in utero to 2,3,7,8-tetrachlorodibenzo-p-dioxin. Toxicol. Sci. 76, 171-181.

Liu, L., Suzuki, K., Nakagata, N., Mihara, K., Matsumaru, D., Ogino, Y., Yashiro, K., Hamada, H., Liu, Z., Evans, S.M., Mendelsohn, C., Yamada, G., 2012. Retinoic acid signaling regulates sonic hedgehog and bone morphogenetic protein signalings during genital tubercle development. Birth Defects Res. B Dev. Reprod. Toxicol. 95, 79-88.

Liu, L., van Groen, T., Kadish, I., Li, Y., Wang, D., James, S.R., Karpf, A.R., Tollefsbol, T.O., 2011. Insufficient DNA methylation affects healthy aging and promotes age-related health problems. Clin. Epigenetics 2, 349-360.

Lopatina, N., Haskell, J.F., Andrews, L.G., Poole, J.C., Saldanha, S., Tollefsbol, T., 2002. Differential maintenance and de novo methylating activity by three DNA methyltransferases in aging and immortalized fibroblasts. J. Cell. Biochem. 84, 324-334.

Loughery, J.E., Dunne, P.D., O'Neill, K.M., Meehan, R.R., McDaid, J.R., Walsh, C.P., 2011. DNMT1 deficiency triggers mismatch repair defects in human cells through depletion of repair protein levels in a process involving the DNA damage response. Hum. Mol. Genet. 20, 3241-3255.

Ly, A., Lee, H., Chen, J., Sie, K.K., Renlund, R., Medline, A., Sohn, K.J., Croxford, R., Thompson, L.U., Kim, Y.I., 2011. Effect of maternal and postweaning folic acid supplementation on mammary tumor risk in the offspring. Cancer Res. 71, 988-997.

Madigan, A.A., Sobek, K.M., Cummings, J.L., Green, W.R., Bacich, D.J., O'Keefe, D.S., 2012. Activation of innate anti-viral immune response genes in symptomatic benign prostatic hyperplasia. Genes Immun. 13, 566-572.

Madrigano, J., Baccarelli, A., Mittleman, M.A., Wright, R.O., Sparrow, D., Vokonas, P.S., Tarantini, L., Schwartz, J., 2011. Prolonged exposure to particulate pollution, genes associated with glutathione pathways, and DNA methylation in a cohort of older men. Environ. Health Perspect. 119, 977-982.

Maegawa, S., Lu, Y., Tahara, T., Lee, J.T., Madzo, J., Liang, S., Jelinek, J., Colman, R.J., Issa, J.J., 2017. Caloric restriction delays age-related methylation drift. Nature communications 8, 539.

Maresca, A., Zaffagnini, M., Caporali, L., Carelli, V., Zanna, C., 2015. DNA methyltransferase 1 mutations and mitochondrial pathology: is mtDNA methylated? Frontiers in Genetics 6.

Maruyama, R., Toyooka, S., Toyooka, K.O., Virmani, A.K., Zochbauer-Muller, S., Farinas, A.J., Minna, J.D., McConnell, J., Frenkel, E.P., Gazdar, A.F., 2002. Aberrant promoter methylation profile of prostate cancers and its relationship to clinicopathological features. Clin. Cancer. Res. 8, 514-519.

Mazal, P.R., Schaufler, R., Altenhuber-Muller, R., Haitel, A., Watschinger, B., Kratzik, C., Krupitza, G., Regele, H., Meisl, F.T., Zechner, O., Kerjaschki, D., Susani, M., 2002. Derivation of nephrogenic adenomas from renal tubular cells in kidney-transplant recipients. N. Engl. J. Med. 347, 653-659.

McGrath, J., Solter, D., 1984. Completion of mouse embryogenesis requires both the maternal and paternal genomes. Cell 37, 179-183.

McVary, K.T., Roehrborn, C.G., Avins, A.L., Barry, M.J., Bruskewitz, R.C., Donnell, R.F., Foster, H.E., Jr., Gonzalez, C.M., Kaplan, S.A., Penson, D.F., Ulchaker, J.C., Wei, J.T., 2011. Update on AUA guideline on the management of benign prostatic hyperplasia. J. Urol. 185, 1793-1803.

Mehta, V., Schmitz, C.T., Keil, K.P., Joshi, P.S., Abler, L.L., Lin, T.M., Taketo, M.M., Sun, X., Vezina, C.M., 2013. Beta-catenin (CTNNB1) induces Bmp expression in urogenital sinus epithelium and participates in prostatic bud initiation and patterning. Dev. Biol. 376, 125-135.

Messerschmidt, D.M., Knowles, B.B., Solter, D., 2014. DNA methylation dynamics during epigenetic reprogramming in the germline and preimplantation embryos. Genes Dev. 28, 812-828.

Mikael, L.G., Deng, L., Paul, L., Selhub, J., Rozen, R., 2013. Moderately high intake of folic acid has a negative impact on mouse embryonic development. Birth Defects Res. A Clin. Mol. Teratol. 97, 47-52.

Miyagawa, S., Moon, A., Haraguchi, R., Inoue, C., Harada, M., Nakahara, C., Suzuki, K., Matsumaru, D., Kaneko, T., Matsuo, I., Yang, L., Taketo, M.M., Iguchi, T., Evans, S.M., Yamada, G., 2009. Dosage-dependent hedgehog signals integrated with Wnt/β-catenin signaling regulate external genitalia formation as an appendicular program. Development 136, 3969-3978.

Mohandas, T., Sparkes, R.S., Shapiro, L.J., 1981. Reactivation of an inactive human X chromosome: evidence for X inactivation by DNA methylation. Science 211, 393-396.

Moore, K.L., Persaud, T.V.N., 2003. The developing human: clinically oriented embryology 7th edition, 7th ed. Elsevier, Philadelphia.

Morgan, H.D., Dean, W., Coker, H.A., Reik, W., Petersen-Mahrt, S.K., 2004. Activation-induced cytidine deaminase deaminates 5-methylcytosine in DNA and is expressed in pluripotent tissues: implications for epigenetic reprogramming. J. Biol. Chem. 279, 52353-52360.

MRC, 1991. Prevention of neural tube defects: results of the Medical Research Council Vitamin Study. MRC Vitamin Study Research Group. Lancet 338, 131-137.

Nakamura, T., Arai, Y., Umehara, H., Masuhara, M., Kimura, T., Taniguchi, H., Sekimoto, T., Ikawa, M., Yoneda, Y., Okabe, M., Tanaka, S., Shiota, K., Nakano, T., 2007. PGC7/Stella protects against DNA demethylation in early embryogenesis. Nat. Cell Biol. 9, 64-71.

Nan, X., Ng, H.H., Johnson, C.A., Laherty, C.D., Turner, B.M., Eisenman, R.N., Bird, A., 1998. Transcriptional repression by the methyl-CpG-binding protein MeCP2 involves a histone deacetylase complex. Nature 393, 386-389.

Nanjappa, M.K., Medrano, T.I., Prins, G.S., Chen, H., Zirkin, B.R., Cooke, P.S., 2017. Transdifferentiation of adult rat stem Leydig cells into prostatic and uterine epithelium, but not epidermis. Andrology.

Nasonkin, I.O., Merbs, S.L., Lazo, K., Oliver, V.F., Brooks, M., Patel, K., Enke, R.A., Nellissery, J., Jamrich, M., Le, Y.Z., Bharti, K., Fariss, R.N., Rachel, R.A., Zack, D.J., Rodriguez-Boulan, E.J., Swaroop, A., 2013. Conditional knockdown of DNA methyltransferase 1 reveals a key role of retinal pigment epithelium integrity in photoreceptor outer segment morphogenesis. Development 140, 1330-1341.

Neubauer, B.L., Chung, L.W., McCormick, K.A., Taguchi, O., Thompson, T.C., Cunha, G.R., 1983. Epithelial-mesenchymal interactions in prostatic development. II. Biochemical observations of prostatic induction by urogenital sinus mesenchyme in epithelium of the adult rodent urinary bladder. J. Cell Biol. 96, 1671-1676.

Ng, H.H., Zhang, Y., Hendrich, B., Johnson, C.A., Turner, B.M., Erdjument-Bromage, H., Tempst, P., Reinberg, D., Bird, A., 1999. MBD2 is a transcriptional repressor belonging to the MeCP1 histone deacetylase complex. Nat. Genet. 23, 58-61.

Nimura, K., Ishida, C., Koriyama, H., Hata, K., Yamanaka, S., Li, E., Ura, K., Kaneda, Y., 2006. Dnmt3a2 targets endogenous Dnmt3L to ES cell chromatin and induces regional DNA methylation. Genes Cells 11, 1225-1237.

Niu, Y., Ge, R., Hu, L., Diaz, C., Wang, Z., Wu, C.L., Olumi, A.F., 2011. Reduced levels of 5-alpha reductase 2 in adult prostate tissue and implications for BPH therapy. Prostate 71, 1317-1324.

Norris, D.P., Patel, D., Kay, G.F., Penny, G.D., Brockdorff, N., Sheardown, S.A., Rastan, S., 1994. Evidence that random and imprinted Xist expression is controlled by preemptive methylation. Cell 77, 41-51.

Okano, M., Bell, D.W., Haber, D.A., Li, E., 1999. DNA methyltransferases Dnmt3a and Dnmt3b are essential for de novo methylation and mammalian development. Cell 99, 247-257.

Okano, M., Xie, S., Li, E., 1998. Cloning and characterization of a family of novel mammalian DNA (cytosine-5) methyltransferases. Nat. Genet. 19, 219-220.

Oottamasathien, S., Wang, Y., Williams, K., Franco, O.E., Wills, M.L., Thomas, J.C., Saba, K., Sharif-Afshar, A.R., Makari, J.H., Bhowmick, N.A., DeMarco, R.T., Hipkens, S., Magnuson, M., Brock, J.W., 3rd, Hayward, S.W., Pope, J.C.t., Matusik, R.J., 2007. Directed differentiation of embryonic stem cells into bladder tissue. Dev. Biol. 304, 556-566.

Oottamasathien, S., Williams, K., Franco, O.E., Thomas, J.C., Saba, K., Bhowmick, N.A., Staack, A., Demarco, R.T., Brock, J.W., 3rd, Hayward, S.W., Pope, J.C.t., 2006. Bladder tissue formation from cultured bladder urothelium. Dev. Dyn. 235, 2795-2801.

Orvis, G.D., Behringer, R.R., 2007. Cellular mechanisms of Müllerian duct formation in the mouse. Dev. Biol. 306, 493-504.

Ostler, K.R., Davis, E.M., Payne, S.L., Gosalia, B.B., Exposito-Cespedes, J., Le Beau, M.M., Godley, L.A., 2007. Cancer cells express aberrant DNMT3B transcripts encoding truncated proteins. Oncogene 26, 5553-5563.

Özdemir, T., Arıkan, A., 2013. Ureterocystoplasty in pediatric patients with unilateral nonfunctioning kidney. Turkish journal of urology 39, 232-236.

Palii, S.S., Van Emburgh, B.O., Sankpal, U.T., Brown, K.D., Robertson, K.D., 2008. DNA methylation inhibitor 5-Aza-2'-deoxycytidine induces reversible genome-wide DNA damage that is distinctly influenced by DNA methyltransferases 1 and 3B. Mol. Cell. Biol. 28, 752-771.

Panning, B., Jaenisch, R., 1996. DNA hypomethylation can activate Xist expression and silence X-linked genes. Genes Dev. 10, 1991-2002.

Patra, A., Deb, M., Dahiya, R., Patra, S.K., 2011. 5-Aza-2′-deoxycytidine stress response and apoptosis in prostate cancer. Clin. Epigenetics 2, 339-348.

Patra, S.K., Patra, A., Zhao, H., Dahiya, R., 2002. DNA methyltransferase and demethylase in human prostate cancer. Mol. Carcinog. 33, 163-171.

Perez, A.P., Biancardi, M.F., Caires, C.R., Falleiros-Junior, L.R., Goes, R.M., Vilamaior, P.S., Santos, F.C., Taboga, S.R., 2016. Prenatal exposure to ethinylestradiol alters the morphologic patterns and increases the predisposition for prostatic lesions in male and female gerbils during ageing. Int. J. Exp. Pathol. 97, 5-17.

Perriton, C.L., Powles, N., Chiang, C., Maconochie, M.K., Cohn, M.J., 2002. Sonic hedgehog signaling from the urethral epithelium controls external genital development. Dev. Biol. 247, 26-46.

Peuckert, C., Aresh, B., Holenya, P., Adams, D., Sreedharan, S., Porthin, A., Andersson, L., Pettersson, H., Wolfl, S., Klein, R., Oxburgh, L., Kullander, K., 2016. Multimodal Eph/Ephrin signaling controls several phases of urogenital development. Kidney Int. 90, 373-388.

Pfeifer, G.P., Kadam, S., Jin, S.-G., 2013. 5-hydroxymethylcytosine and its potential roles in development and cancer. Epigenetics & Chromatin 6, 10.

Pfeifer, G.P., Xiong, W., Hahn, M.A., Jin, S.G., 2014. The role of 5-hydroxymethylcytosine in human cancer. Cell Tissue Res. 356, 631-641.

Pfeiffer, C.M., Hughes, J.P., Lacher, D.A., Bailey, R.L., Berry, R.J., Zhang, M., Yetley, E.A., Rader, J.I., Sempos, C.T., Johnson, C.L., 2012. Estimation of Trends in Serum and RBC Folate in the U.S. Population from Pre- to Postfortification Using Assay-Adjusted Data from the NHANES 1988–2010. J. Nutr. 142, 886-893.

Pfeiffer, C.M., Johnson, C.L., Jain, R.B., Yetley, E.A., Picciano, M.F., Rader, J.I., Fisher, K.D., Mulinare, J., Osterloh, J.D., 2007. Trends in blood folate and vitamin B-12 concentrations in the United States, 1988 2004. Am. J. Clin. Nutr. 86, 718-727.

Pickell, L., Brown, K., Li, D., Wang, X.L., Deng, L., Wu, Q., Selhub, J., Luo, L., Jerome-Majewska, L., Rozen, R., 2011. High intake of folic acid disrupts embryonic development in mice. Birth Defects Res. A Clin. Mol. Teratol. 91, 8-19.

Pina-Oviedo, S., Shen, S.S., Truong, L.D., Ayala, A.G., Ro, J.Y., 2013. Flat pattern of nephrogenic adenoma: previously unrecognized pattern unveiled using PAX2 and PAX8 immunohistochemistry. Mod. Pathol. 26, 792-798.

Podlasek, C.A., Barnett, D.H., Clemens, J.Q., Bak, P.M., Bushman, W., 1999. Prostate Development Requires Sonic Hedgehog Expressed by the Urogenital Sinus Epithelium. Dev. Biol. 209, 28-39.

Prusinski, L., Al-Hendy, A., Yang, Q., 2016. Developmental exposure to endocrine disrupting chemicals alters the epigenome: Identification of reprogrammed targets. Gynecol Obstet Res 3, 1-6.

Pycha, A., Mian, C., Reiter, W.J., Brossner, C., Haitel, A., Wiener, H., Maier, U., Marberger, M., 1998. Nephrogenic adenoma in renal transplant recipients: a truly benign lesion? Urology 52, 756-761.

Qin, C., Wang, Z., Shang, J., Bekkari, K., Liu, R., Pacchione, S., McNulty, K.A., Ng, A., Barnum, J.E., Storer, R.D., 2010. Intracisternal A particle genes: Distribution in the mouse genome, active subtypes, and potential roles as species-specific mediators of susceptibility to cancer. Mol. Carcinog. 49, 54-67.

Qin, W., Wolf, P., Liu, N., Link, S., Smets, M., Mastra, F.L., Forne, I., Pichler, G., Horl, D., Fellinger, K., Spada, F., Bonapace, I.M., Imhof, A., Harz, H., Leonhardt, H., 2015. DNA methylation requires a DNMT1 ubiquitin interacting motif (UIM) and histone ubiquitination. Cell Res. 25, 911-929.

Qin, X., Cui, Y., Shen, L., Sun, N., Zhang, Y., Li, J., Xu, X., Wang, B., Xu, X., Huo, Y., Wang, X., 2013. Folic acid supplementation and cancer risk: a meta-analysis of randomized controlled trials. Int. J. Cancer 133, 1033-1041.

Rao, P.K., Burnett, A.L., 2013. Development of the Male Reproductive System, in: Kavoussi, P.K., Costabile, R.A., Salonia, A. (Eds.), Clinical Urologic Endocrinology: Principles for Men's Health. Springer London, London, pp. 11-24.

Ratnam, S., Mertineit, C., Ding, F., Howell, C.Y., Clarke, H.J., Bestor, T.H., Chaillet, J.R., Trasler, J.M., 2002. Dynamics of Dnmt1 methyltransferase expression and intracellular localization during oogenesis and preimplantation development. Dev. Biol. 245, 304-314.

Rhee, K.D., Yu, J., Zhao, C.Y., Fan, G., Yang, X.J., 2012. Dnmt1-dependent DNA methylation is essential for photoreceptor terminal differentiation and retinal neuron survival. Cell Death Dis. 3, e427.

Ricke, W.A., Lee, C.W., Clapper, T.R., Schneider, A.J., Moore, R.W., Keil, K.P., Abler, L.L., Wynder, J.L., Lopez Alvarado, A., Beaubrun, I., Vo, J., Bauman, T.M., Ricke, E.A., Peterson, R.E., Vezina, C.M., 2016a. In utero and Lactational TCDD Exposure Increases Susceptibility to Lower Urinary Tract Dysfunction in Adulthood. Toxicol. Sci.

Ricke, W.A., Lee, C.W., Clapper, T.R., Schneider, A.J., Moore, R.W., Keil, K.P., Abler, L.L., Wynder, J.L., Lopez Alvarado, A., Beaubrun, I., Vo, J., Bauman, T.M., Ricke, E.A., Peterson, R.E., Vezina, C.M., 2016b. In Utero and Lactational TCDD Exposure Increases Susceptibility to Lower Urinary Tract Dysfunction in Adulthood. Toxicol. Sci. 150, 429-440.

Riggs, A.D., 1975. X inactivation, differentiation, and DNA methylation. Cytogenet. Cell Genet. 14, 9-25.

Robertson, K.D., 2005. DNA methylation and human disease. Nature Reviews Genetics 6, 597.

Robertson, K.D., Ait-Si-Ali, S., Yokochi, T., Wade, P.A., Jones, P.L., Wolffe, A.P., 2000. DNMT1 forms a complex with Rb, E2F1 and HDAC1 and represses transcription from E2F-responsive promoters. Nat. Genet. 25, 338-342.

Robertson, K.D., Uzvolgyi, E., Liang, G., Talmadge, C., Sumegi, J., Gonzales, F.A., Jones, P.A., 1999. The human DNA methyltransferases (DNMTs) 1, 3a and 3b: coordinate mRNA expression in normal tissues and overexpression in tumors. Nucleic Acids Res. 27, 2291-2298.

Roehrborn, C.G., 2008. Current Medical Therapies for Men With Lower Urinary Tract Symptoms and Benign Prostatic Hyperplasia: Achievements and Limitations. Reviews in Urology 10, 14-25.

Roman, B.L., Timms, B.G., Prins, G.S., Peterson, R.E., 1998. In utero and lactational exposure of the male rat to 2,3,7,8-tetrachlorodibenzo-p-dioxin impairs prostate development. 2. Effects on growth and cytodifferentiation. Toxicol. Appl. Pharmacol. 150, 254-270.

Rountree, M.R., Bachman, K.E., Baylin, S.B., 2000. DNMT1 binds HDAC2 and a new co-repressor, DMAP1, to form a complex at replication foci. Nat. Genet. 25, 269-277.

Saigal, C.S., Joyce, G., 2005. Economic costs of benign prostatic hyperplasia in the private sector. J. Urol. 173, 1309-1313.

Saitou, M., Kagiwada, S., Kurimoto, K., 2012. Epigenetic reprogramming in mouse pre-implantation development and primordial germ cells. Development 139, 15-31.

Saxonov, S., Berg, P., Brutlag, D.L., 2006. A genome-wide analysis of CpG dinucleotides in the human genome distinguishes two distinct classes of promoters. Proceedings of the National Academy of Sciences 103, 1412-1417.

Schermelleh, L., Haemmer, A., Spada, F., Rösing, N., Meilinger, D., Rothbauer, U., Cardoso, M.C., Leonhardt, H., 2007. Dynamics of Dnmt1 interaction with the replication machinery and its role in postreplicative maintenance of DNA methylation. Nucleic Acids Res. 35, 4301-4312.

Schmidt, C.S., Bultmann, S., Meilinger, D., Zacher, B., Tresch, A., Maier, K.C., Peter, C., Martin, D.E., Leonhardt, H., Spada, F., 2012. Global DNA Hypomethylation Prevents Consolidation of Differentiation Programs and Allows Reversion to the Embryonic Stem Cell State. PLoS One 7, e52629.

Seifert, A.W., Bouldin, C.M., Choi, K.S., Harfe, B.D., Cohn, M.J., 2009. Multiphasic and tissue-specific roles of sonic hedgehog in cloacal septation and external genitalia development. Development 136, 3949-3957.

Seifert, A.W., Harfe, B.D., Cohn, M.J., 2008. Cell lineage analysis demonstrates an endodermal origin of the distal urethra and perineum. Dev. Biol. 318, 143-152.

Sen, G.L., Reuter, J.A., Webster, D.E., Zhu, L., Khavari, P.A., 2010. DNMT1 maintains progenitor function in self-renewing somatic tissue. Nature 463, 563-567.

Shah, M.Y., Vasanthakumar, A., Barnes, N.Y., Figueroa, M.E., Kamp, A., Hendrick, C., Ostler, K.R., Davis, E.M., Lin, S., Anastasi, J., Le Beau, M.M., Moskowitz, I.P., Melnick, A., Pytel, P., Godley, L.A., 2010. DNMT3B7, a truncated DNMT3B isoform expressed in human tumors, disrupts embryonic development and accelerates lymphomagenesis. Cancer Res. 70, 5840-5850.

Sheaffer, K.L., Kim, R., Aoki, R., Elliott, E.N., Schug, J., Burger, L., Schubeler, D., Kaestner, K.H., 2014. DNA methylation is required for the control of stem cell differentiation in the small intestine. Genes Dev. 28, 652-664.

Sie, K.K., Medline, A., van Weel, J., Sohn, K.J., Choi, S.W., Croxford, R., Kim, Y.I., 2011. Effect of maternal and postweaning folic acid supplementation on colorectal cancer risk in the offspring. Gut 60, 1687-1694.

Smith, F.M., Garfield, A.S., Ward, A., 2006. Regulation of growth and metabolism by imprinted genes. Cytogenet. Genome Res. 113, 279-291.

Song, F., Smith, J.F., Kimura, M.T., Morrow, A.D., Matsuyama, T., Nagase, H., Held, W.A., 2005. Association of tissue-specific differentially methylated regions (TDMs) with differential gene expression. Proc. Natl. Acad. Sci. U. S. A. 102, 3336-3341.

Steegers-Theunissen, R.P., Obermann-Borst, S.A., Kremer, D., Lindemans, J., Siebel, C., Steegers, E.A., Slagboom, P.E., Heijmans, B.T., 2009. Periconceptional maternal folic acid use of 400 microg per day is related to increased methylation of the IGF2 gene in the very young child. PLoS One 4, e7845.

Storebjerg, T.M., Strand, S.H., Hoyer, S., Lynnerup, A.S., Borre, M., Orntoft, T.F., Sorensen, K.D., 2018. Dysregulation and prognostic potential of 5-methylcytosine (5mC), 5-hydroxymethylcytosine (5hmC), 5-formylcytosine (5fC), and 5-carboxylcytosine (5caC) levels in prostate cancer. Clin. Epigenetics 10, 105.

Stroud, H., Feng, S., Morey Kinney, S., Pradhan, S., Jacobsen, S.E., 2011. 5-Hydroxymethylcytosine is associated with enhancers and gene bodies in human embryonic stem cells. Genome Biol. 12, R54.

Stuhrmann, M., Dork, T., 2000. CFTR gene mutations and male infertility. Andrologia 32, 71-83.

Subramaniam, R., 2017. Regenerative Medicine in Bladder Reconstructive Surgery. European Urology Supplements 16, 23-29.

Surani, M.A., Barton, S.C., Norris, M.L., 1984. Development of reconstituted mouse eggs suggests imprinting of the genome during gametogenesis. Nature 308, 548-550.

Suren, P., Roth, C., Bresnahan, M., Haugen, M., Hornig, M., Hirtz, D., Lie, K.K., Lipkin, W.I., Magnus, P., Reichborn-Kjennerud, T., Schjolberg, S., Davey Smith, G., Oyen, A.S., Susser, E., Stoltenberg, C., 2013. Association between maternal use of folic acid supplements and risk of autism spectrum disorders in children. JAMA 309, 570-577.

Suzuki, K., Matsumaru, D., Matsushita, S., Murashima, A., Ludwig, M., Reutter, H., Yamada, G., 2017. Epispadias and the associated embryopathies: genetic and developmental basis. Clin. Genet. 91, 247-253.

Szyf, M., Kaplan, F., Mann, V., Giloh, H., Kedar, E., Razin, A., 1985. Cell cycle-dependent regulation of eukaryotic DNA methylase level. J. Biol. Chem. 260, 8653-8656.

Tahiliani, M., Koh, K.P., Shen, Y., Pastor, W.A., Bandukwala, H., Brudno, Y., Agarwal, S., Iyer, L.M., Liu, D.R., Aravind, L., Rao, A., 2009. Conversion of 5-Methylcytosine to 5-Hydroxymethylcytosine in Mammalian DNA by MLL Partner TET1. Science 324, 930-935.

Tan, A.Y., Manley, J.L., 2009. The TET Family of Proteins: Functions and Roles in Disease. J. Mol. Cell. Biol. 1, 82-92.

Tang, W.Y., Morey, L.M., Cheung, Y.Y., Birch, L., Prins, G.S., Ho, S.M., 2012. Neonatal exposure to estradiol/bisphenol A alters promoter methylation and expression of Nsbp1 and Hpcal1 genes and transcriptional programs of Dnmt3a/b and Mbd2/4 in the rat prostate gland throughout life. Endocrinology 153, 42-55.

Tao, R., Chen, Z., Wu, P., Liu, C., Peng, Y., Zhao, W., Hu, C., Feng, J., 2015. The possible role of EZH2 and DNMT1 polymorphisms in sporadic triple-negative breast carcinoma in southern Chinese females. Tumour Biol. 36, 9849-9855.

Tasian, G., Cunha, G., Baskin, L., 2010. Smooth muscle differentiation and patterning in the urinary bladder. Differentiation 80, 106-117.

Taylor, R.A., Wang, H., Wilkinson, S.E., Richards, M.G., Britt, K.L., Vaillant, F., Lindeman, G.J., Visvader, J.E., Cunha, G.R., St John, J., Risbridger, G.P., 2009. Lineage enforcement by

inductive mesenchyme on adult epithelial stem cells across developmental germ layers. Stem Cells 27, 3032-3042.

Taylor, S.M., Jones, P.A., 1979. Multiple new phenotypes induced in 10T1/2 and 3T3 cells treated with 5-azacytidine. Cell 17, 771-779.

Taylor, S.M., Jones, P.A., 1982. Changes in phenotypic expression in embryonic and adult cells treated with 5-azacytidine. J. Cell. Physiol. 111, 187-194.

Thomson, A.A., Cunha, G.R., 1999. Prostatic growth and development are regulated by FGF10. Development 126, 3693-3701.

Timms, B.G., Howdeshell, K.L., Barton, L., Bradley, S., Richter, C.A., vom Saal, F.S., 2005. Estrogenic chemicals in plastic and oral contraceptives disrupt development of the fetal mouse prostate and urethra. Proc. Natl. Acad. Sci. U. S. A. 102, 7014-7019.

Tobi, E.W., Lumey, L.H., Talens, R.P., Kremer, D., Putter, H., Stein, A.D., Slagboom, P.E., Heijmans, B.T., 2009. DNA methylation differences after exposure to prenatal famine are common and timing- and sex-specific. Hum. Mol. Genet. 18, 4046-4053.

Tomaszewski, J.J., Cummings, J.L., Parwani, A.V., Dhir, R., Mason, J.B., Nelson, J.B., Bacich, D.J., O'Keefe, D.S., 2011. Increased cancer cell proliferation in prostate cancer patients with high levels of serum folate. Prostate 71, 1287-1293.

Tong, G.X., Melamed, J., Mansukhani, M., Memeo, L., Hernandez, O., Deng, F.M., Chiriboga, L., Waisman, J., 2006. PAX2: a reliable marker for nephrogenic adenoma. Mod. Pathol. 19, 356-363.

Tong, G.X., Weeden, E.M., Hamele-Bena, D., Huan, Y., Unger, P., Memeo, L., O'Toole, K., 2008. Expression of PAX8 in nephrogenic adenoma and clear cell adenocarcinoma of the lower urinary tract: evidence of related histogenesis? Am. J. Surg. Pathol. 32, 1380-1387.

Trowbridge, J.J., Snow, J.W., Kim, J., Orkin, S.H., 2009. DNA Methyltransferase 1 is essential for and uniquely regulates hematopoietic stem and progenitor cells. Cell stem cell 5, 442-449.

Tsai, C.C., Su, P.F., Huang, Y.F., Yew, T.L., Hung, S.C., 2012. Oct4 and Nanog directly regulate Dnmt1 to maintain self-renewal and undifferentiated state in mesenchymal stem cells. Mol. Cell 47, 169-182.

Unterberger, A., Andrews, S.D., Weaver, I.C., Szyf, M., 2006. DNA methyltransferase 1 knockdown activates a replication stress checkpoint. Mol. Cell. Biol. 26, 7575-7586.

Veeranki, S.P., Gebretsadik, T., Mitchel, E.F., Tylavsky, F.A., Hartert, T.V., Cooper, W.O., Dupont, W.D., Dorris, S.L., Hartman, T.J., Carroll, K.N., 2015. Maternal Folic Acid Supplementation During Pregnancy and Early Childhood Asthma. Epidemiology 26, 934-941.

Vezina, C.M., Allgeier, S.H., Fritz, W.A., Moore, R.W., Strerath, M., Bushman, W., Peterson, R.E., 2008a. Retinoic acid induces prostatic bud formation. Dev. Dyn. 237, 1321-1333.

Vezina, C.M., Allgeier, S.H., Moore, R.W., Lin, T.M., Bemis, J.C., Hardin, H.A., Gasiewicz, T.A., Peterson, R.E., 2008b. Dioxin causes ventral prostate agenesis by disrupting dorsoventral patterning in developing mouse prostate. Toxicol. Sci. 106, 488-496.

Vollset, S.E., Clarke, R., Lewington, S., Ebbing, M., Halsey, J., Lonn, E., Armitage, J., Manson, J.A.E., Hankey, G.J., Spence, J.D., Galan, P., Bønaa, K.H., Jamison, R., Gaziano, J.M., Guarino, P., Baron, J.A., Logan, R.F.A., Giovannucci, E.L., den Heijer, M., Ueland, P.M., Bennett, D., Collins, R., Peto, R., 2013. Effects of folic acid on overall and site-specific cancer incidence during the randomised trials: meta-analyses of data on 50 000 individuals. Lancet 381.

vom Saal, F.S., Timms, B.G., Montano, M.M., Palanza, P., Thayer, K.A., Nagel, S.C., Dhar, M.D., Ganjam, V.K., Parmigiani, S., Welshons, W.V., 1997. Prostate enlargement in mice due to fetal exposure to low doses of estradiol or diethylstilbestrol and opposite effects at high doses. Proc. Natl. Acad. Sci. U. S. A. 94, 2056-2061.

Waddington, C.H., 2012. The epigenotype. 1942. Int. J. Epidemiol. 41, 10-13.

Wadhwa, P.D., Buss, C., Entringer, S., Swanson, J.M., 2009. Developmental Origins of Health and Disease: Brief History of the Approach and Current Focus on Epigenetic Mechanisms. Semin. Reprod. Med. 27, 358-368.

Walsh, C.P., Bestor, T.H., 1999. Cytosine methylation and mammalian development. Genes Dev. 13, 26-34.

Walsh, C.P., Chaillet, J.R., Bestor, T.H., 1998. Transcription of IAP endogenous retroviruses is constrained by cytosine methylation. Nat. Genet. 20, 116-117.

Wang, X., Guan, Z., Chen, Y., Dong, Y., Niu, Y., Wang, J., Zhang, T., Niu, B., 2015. Genomic DNA Hypomethylation Is Associated with Neural Tube Defects Induced by Methotrexate Inhibition of Folate Metabolism. PLoS One 10, e0121869.

Wang, Z., Hu, L., Salari, K., Bechis, S.K., Ge, R., Wu, S., Rassoulian, C., Pham, J., Wu, C.L., Tabatabaei, S., Strand, D.W., Olumi, A.F., 2017. Androgenic to oestrogenic switch in the human adult prostate gland is regulated by epigenetic silencing of steroid 5alpha-reductase 2. J. Pathol. 243, 457-467.

Warnecke, P.M., Clark, S.J., 1999. DNA methylation profile of the mouse skeletal alpha-actin promoter during development and differentiation. Mol. Cell. Biol. 19, 164-172.

Waterland, R.A., Dolinoy, D.C., Lin, J.R., Smith, C.A., Shi, X., Tahiliani, K.G., 2006. Maternal methyl supplements increase offspring DNA methylation at Axin Fused. Genesis 44, 401-406.

Waterland, R.A., Jirtle, R.L., 2003. Transposable elements: targets for early nutritional effects on epigenetic gene regulation. Mol. Cell. Biol. 23, 5293-5300.

Waterston, R.H., Lindblad-Toh, K., Birney, E., Rogers, J., Abril, J.F., Agarwal, P., Agarwala, R., Ainscough, R., Alexandersson, M., An, P., Antonarakis, S.E., Attwood, J., Baertsch, R., Bailey, J., Barlow, K., Beck, S., Berry, E., Birren, B., Bloom, T., Bork, P., Botcherby, M., Bray, N., Brent, M.R., Brown, D.G., Brown, S.D., Bult, C., Burton, J., Butler, J., Campbell,

R.D., Carninci, P., Cawley, S., Chiaromonte, F., Chinwalla, A.T., Church, D.M., Clamp, M., Clee, C., Collins, F.S., Cook, L.L., Copley, R.R., Coulson, A., Couronne, O., Cuff, J., Curwen, V., Cutts, T., Daly, M., David, R., Davies, J., Delehaunty, K.D., Deri, J., Dermitzakis, E.T., Dewey, C., Dickens, N.J., Diekhans, M., Dodge, S., Dubchak, I., Dunn, D.M., Eddy, S.R., Elnitski, L., Emes, R.D., Eswara, P., Eyras, E., Felsenfeld, A., Fewell, G.A., Flicek, P., Foley, K., Frankel, W.N., Fulton, L.A., Fulton, R.S., Furey, T.S., Gage, D., Gibbs, R.A., Glusman, G., Gnerre, S., Goldman, N., Goodstadt, L., Grafham, D., Graves, T.A., Green, E.D., Gregory, S., Guigo, R., Guyer, M., Hardison, R.C., Haussler, D., Hayashizaki, Y., Hillier, L.W., Hinrichs, A., Hlavina, W., Holzer, T., Hsu, F., Hua, A., Hubbard, T., Hunt, A., Jackson, I., Jaffe, D.B., Johnson, L.S., Jones, M., Jones, T.A., Joy, A., Kamal, M., Karlsson, E.K., Karolchik, D., Kasprzyk, A., Kawai, J., Keibler, E., Kells, C., Kent, W.J., Kirby, A., Kolbe, D.L., Korf, I., Kucherlapati, R.S., Kulbokas, E.J., Kulp, D., Landers, T., Leger, J.P., Leonard, S., Letunic, I., Levine, R., Li, J., Li, M., Lloyd, C., Lucas, S., Ma, B., Maglott, D.R., Mardis, E.R., Matthews, L., Mauceli, E., Mayer, J.H., McCarthy, M., McCombie, W.R., McLaren, S., McLay, K., McPherson, J.D., Meldrim, J., Meredith, B., Mesirov, J.P., Miller, W., Miner, T.L., Mongin, E., Montgomery, K.T., Morgan, M., Mott, R., Mullikin, J.C., Muzny, D.M., Nash, W.E., Nelson, J.O., Nhan, M.N., Nicol, R., Ning, Z., Nusbaum, C., O'Connor, M.J., Okazaki, Y., Oliver, K., Overton-Larty, E., Pachter, L., Parra, G., Pepin, K.H., Peterson, J., Pevzner, P., Plumb, R., Pohl, C.S., Poliakov, A., Ponce, T.C., Ponting, C.P., Potter, S., Quail, M., Reymond, A., Roe, B.A., Roskin, K.M., Rubin, E.M., Rust, A.G., Santos, R., Sapojnikov, V., Schultz, B., Schultz, J., Schwartz, M.S., Schwartz, S., Scott, C., Seaman, S., Searle, S., Sharpe, T., Sheridan, A., Shownkeen, R., Sims, S., Singer, J.B., Slater, G., Smit, A., Smith, D.R., Spencer, B., Stabenau, A., Stange-Thomann, N., Sugnet, C., Suyama, M., Tesler, G., Thompson, J., Torrents, D., Trevaskis, E., Tromp, J., Ucla, C., Ureta-Vidal, A., Vinson, J.P., Von Niederhausern, A.C., Wade, C.M., Wall, M., Weber, R.J., Weiss, R.B., Wendl, M.C., West, A.P., Wetterstrand, K., Wheeler, R., Whelan, S., Wierzbowski, J., Willey, D., Williams, S., Wilson, R.K., Winter, E., Worley, K.C., Wyman, D., Yang, S., Yang, S.P., Zdobnov, E.M., Zody, M.C., Lander, E.S., 2002. Initial sequencing and comparative analysis of the mouse genome. Nature 420, 520-562.

Weber, M., Hellmann, I., Stadler, M.B., Ramos, L., Pääbo, S., Rebhan, M., Schübeler, D., 2007. Distribution, silencing potential and evolutionary impact of promoter DNA methylation in the human genome. Nat. Genet. 39, 457.

Wei, J.T., Calhoun, E., Jacobsen, S.J., 2005. Urologic diseases in America project: benign prostatic hyperplasia. J. Urol. 173, 1256-1261.

Weiss, A.C., Airik, R., Bohnenpoll, T., Greulich, F., Foik, A., Trowe, M.O., Rudat, C., Costantini, F., Adams, R.H., Kispert, A., 2014. Nephric duct insertion requires EphA4/EphA7 signaling from the pericloacal mesenchyme. Development 141, 3420-3430.

Whitrow, M.J., Moore, V.M., Rumbold, A.R., Davies, M.J., 2009. Effect of supplemental folic acid in pregnancy on childhood asthma: a prospective birth cohort study. Am. J. Epidemiol. 170, 1486-1493.

Wien, T.N., Pike, E., Wisløff, T., Staff, A., Smeland, S., Klemp, M., 2012. Cancer risk with folic acid supplements: a systematic review and meta-analysis. BMJ Open 2.

Williams, J., Mai, C.T., Mulinare, J., Isenburg, J., Flood, T.J., Ethen, M., Frohnert, B., Kirby, R.S., 2015. Updated estimates of neural tube defects prevented by mandatory folic Acid fortification - United States, 1995-2011. MMWR Morb. Mortal. Wkly. Rep. 64, 1-5.

Wilson, V.L., Smith, R.A., Longoria, J., Liotta, M.A., Harper, C.M., Harris, C.C., 1987a. Chemical carcinogen-induced decreases in genomic 5-methyldeoxycytidine content of normal human bronchial epithelial cells. Proc. Natl. Acad. Sci. U. S. A. 84, 3298-3301.

Wilson, V.L., Smith, R.A., Ma, S., Cutler, R.G., 1987b. Genomic 5-methyldeoxycytidine decreases with age. J. Biol. Chem. 262, 9948-9951.

Winkelmann, J., Lin, L., Schormair, B., Kornum, B.R., Faraco, J., Plazzi, G., Melberg, A., Cornelio, F., Urban, A.E., Pizza, F., Poli, F., Grubert, F., Wieland, T., Graf, E., Hallmayer, J., Strom, T.M., Mignot, E., 2012. Mutations in DNMT1 cause autosomal dominant cerebellar ataxia, deafness and narcolepsy. Hum. Mol. Genet. 21, 2205-2210.

Wu, C., Morris, J.R., 2001. Genes, genetics, and epigenetics: a correspondence. Science 293, 1103-1105.

Wu, Q., Ohsako, S., Ishimura, R., Suzuki, J.S., Tohyama, C., 2004. Exposure of mouse preimplantation embryos to 2,3,7,8-tetrachlorodibenzo-p-dioxin (TCDD) alters the methylation status of imprinted genes H19 and Igf2. Biol. Reprod. 70, 1790-1797.

Xu, K., Wu, X., Shapiro, E., Huang, H., Zhang, L., Hickling, D., Deng, Y., Lee, P., Li, J., Lepor, H., Grishina, I., 2012. Bmp7 functions via a polarity mechanism to promote cloacal septation. PLoS One 7, e29372.

Yamada, G., Satoh, Y., Baskin, L.S., Cunha, G.R., 2003. Cellular and molecular mechanisms of development of the external genitalia. Differentiation 71, 445-460.

Yang, H., Liu, Y., Bai, F., Zhang, J.Y., Ma, S.H., Liu, J., Xu, Z.D., Zhu, H.G., Ling, Z.Q., Ye, D., Guan, K.L., Xiong, Y., 2013. Tumor development is associated with decrease of TET gene expression and 5-methylcytosine hydroxylation. Oncogene 32, 663-669.

Yang, L., Jiang, L., Bi, M., Jia, X., Wang, Y., He, C., Yao, Y., Wang, J., Wang, Z., 2015. High dose of maternal folic acid supplementation is associated to infant asthma. Food Chem. Toxicol. 75, 88-93.

Yang, Y.A., Yu, J., 2013. EZH2, an epigenetic driver of prostate cancer. Protein & cell 4, 331-341.

Yegnasubramanian, S., Kowalski, J., Gonzalgo, M.L., Zahurak, M., Piantadosi, S., Walsh, P.C., Bova, G.S., De Marzo, A.M., Isaacs, W.B., Nelson, W.G., 2004. Hypermethylation of CpG islands in primary and metastatic human prostate cancer. Cancer Res. 64, 1975-1986.

Yen, R.W., Vertino, P.M., Nelkin, B.D., Yu, J.J., el-Deiry, W., Cumaraswamy, A., Lennon, G.G., Trask, B.J., Celano, P., Baylin, S.B., 1992. Isolation and characterization of the cDNA encoding human DNA methyltransferase. Nucleic Acids Res. 20, 2287-2291.

Yoon, A.R., Tammen, S.A., Park, S., Han, S.N., Choi, S.W., 2017. Genome-wide hepatic DNA methylation changes in high-fat diet-induced obese mice. Nutr. Res. Pract. 11, 105-113.

Zampieri, M., Ciccarone, F., Calabrese, R., Franceschi, C., Bürkle, A., Caiafa, P., 2015. Reconfiguration of DNA methylation in aging. Mech. Ageing Dev. 151, 60-70.

Zhang, W., Jiao, H., Zhang, X., Zhao, R., Wang, F., He, W., Zong, H., Fan, Q., Wang, L., 2015a. Correlation between the expression of DNMT1, and GSTP1 and APC, and the methylation status of GSTP1 and APC in association with their clinical significance in prostate cancer. Mol Med Rep 12, 141-146.

Zhang, Z.-M., Liu, S., Lin, K., Luo, Y., Perry, J.J., Wang, Y., Song, J., 2015b. Crystal Structure of Human DNA Methyltransferase 1. J. Mol. Biol. 427, 2520-2531.

CHAPTER 2. IN VIVO REPLACEMENT OF DAMAGED BLADDER UROTHELIUM BY WOLFFIAN DUCT EPITHELIAL CELLS

Adapted from **Diya B Joseph**, Anoop S Chandrashekar, Lisa L Abler, Li-Fang Chu, James A Thomson, Cathy Mendelsohn and Chad M Vezina

In vivo replacement of damaged bladder urothelium by Wolffian duct epithelial cells. Proceedings of the National Academy of Sciences (2018) August 14, 115 (33) 8394-8399; https://doi.org/10.1073/pnas.1802966115

2.1. Introduction

The bladder's specialized epithelium, or urothelium, consists of basal, intermediate and superficial cell layers which collaborate to establish and maintain a protective barrier against water, ions and pathogens (Georgas et al., 2015). Uroplakins, expressed on apical surfaces of terminally differentiated superficial cells, form crystalline plaques to establish a permeability barrier. Breach of this barrier exposes bladder mucosa, musculature and surrounding nerve fibers to urinary irritants, causing pain and voiding dysfunction (Khandelwal et al., 2009). Although bladder urothelium has a slow turnover rate, it rapidly regenerates in response to injury or infection. Bladder urothelium regenerates from basal and intermediate cell progenitors specified during embryonic development (Gandhi, 2013; Papafotiou et al., 2016; Shin et al., 2011). There is a clear role for retinoid (Gandhi, 2013) and other classical developmental signaling pathways (Shin et al., 2011) in progenitor specification, but the role of epigenetic factors is poorly understood. Highlighting the importance of epigenetics in bladder development, a recent study demonstrated that the Polycomb repressor complex 2, which has histone methyltransferase activity, is essential for maintenance of embryonic and adult urothelial progenitors (Guo et al., 2017). The initial purpose of this study was to investigate whether DNA methylation is required in lower urinary tract development and specifically in bladder urothelial development. The key maintenance methyltransferase, DNA methyltransferase-1 (*Dnmt1*) coordinates many aspects of organogenesis (Elliott et al., 2015; Georgia et al., 2013) and maintains progenitors required for tissue regeneration (Sen et al., 2010). *Dnmt1* is required for progenitor survival, cell differentiation and lineage commitment in developing intestine (Elliott et al., 2015), retina (Nasonkin et al., 2013) and

pancreas (Georgia et al., 2013), but its requirement in bladder and urethral development has not been examined.

We used a *Shh*^{cre} (Harfe et al., 2004) driver to conditionally delete *Dnmt1* in embryonic mouse urethral and bladder epithelium, where it is highly expressed (Keil et al., 2013) . Embryonic day (E) 18.5 mutants harbored an abnormally thin bladder urothelium characterized by discontinuous Uroplakin expression, fewer basal and intermediate cells, and widespread apoptosis. At earlier developmental stages, *Dnmt1* depleted urethral and bladder epithelium lost DNA methylation, progressively activated the DNA damage response and P53, and underwent apoptosis at E15.5. By following *Shh* lineage marked cells in urethra and bladder at this stage, our initial focus on DNA methylation gave rise to a far more important discovery: that Wolffian duct epithelial cells migrate into the damaged lower urinary tract of mutant mice and reprogram to acquire urethral and bladder epithelial markers (FOXA1, Keratin 5, P63 and Uroplakin). Our results establish a new paradigm for bladder regeneration: depletion of urothelial progenitors can trigger recruitment of Wolffian duct epithelial cells into the urethra and bladder, where they expand and reprogram to restore the Uroplakin barrier. This previously unknown function of Wolffian duct epithelium as a reservoir for bladder replacing cells has important implications for bladder regenerative therapies.

2.2. Materials and Methods

Data dissemination

Raw image files and other data generated as part of this study can be found at GUDMAP Consortium https://doi.org/10.25548/W-QXXC (Vezina, 2018). RNA-Seq data was

deposited in Gene Expression Omnibus (www.ncbi.nlm.nih.gov/geo/) Accession number: GSE115477.

Conditional urogenital tract endodermal *Dnmt1* knockout embryos (*Dnmt1*cKO)

Mice were housed as previously described (Mehta et al., 2011) in clear plastic cages containing corn cob bedding and maintained on a 12-hr light and dark cycle at 25+5ºC and 20–50% relative humidity. Feed (Diet 2019 for males and Diet 7002 for pregnant females, Harlan Teklad, Madison, WI) and water were available *ad libitum*. All procedures performed on mice were approved by the University of Wisconsin-Madison Animal Care and Use Committee and were carried out in accordance with the Guide for the Care and Use of Laboratory Animals. Mice carrying the *Dnmt1Flox* allele (B6.129S4-*Dnmt1*$^{tm2Jae/Mmucd}$) were from the Mutant Mouse Research and Resource Centers at the University of California, Davis (MMRRC, 014114-UCD). Genotyping for the *Dnmt1Flox* allele was carried out as described previously (Jackson-Grusby et al., 2001). Mice carrying the *Shh*^{cre} allele (B6.Cg*Shh*$^{tm1(EGFP/cre)Cjt/J}$, The Jackson Laboratory, 005622) were genotyped as described previously (Harfe et al., 2004). Mice carrying the Cre inducible *R26R-LacZ* reporter allele (B6;129S4-*Gt(ROSA)26*$^{Sortm1Sor/J}$, The Jackson Laboratory, 003309) were genotyped using the following primers: 5'-AAAGTCGCTCTGAGTTGTTAT -3' and 5'-GCGAAG AGTTTGTCCTCAACC-3' (Soriano, 1999). Mice carrying the *R26R-EYFP* reporter allele (B6.129X1-*Gt(ROSA)26*$^{Sortm1(EYFP)Cos/J}$, The Jackson Laboratory, 006148) were genotyped using the following primers: 5'-AAAGTCGCTCTGAGTTGTTAT -3' and 5'-AAGACCGCGAAGAGTTTGTC -3' (Srinivas et al., 2001). *Dnmt1Flox* mice were bred to mice carrying either the *R26R-LacZ* or *R26R-EYFP* alleles to obtain *Dnmt1Flox/Flox;*

R26R/R26R females. These females were crossed with *Shhcre/+; Dnmt1Flox/+* males in timed matings. The mating pair was placed together in a microisolator cage between 4-6 pm in the evening. Females were removed to a separate cage between 6-7 am on the morning of the next day after confirming the presence of a copulatory plug. Noon of the same day was considered to be embryonic day (E) 0.5. Dams were euthanized by CO_2 asphyxiation to harvest embryos at different embryonic stages. Of the resulting offspring, *Shhcre/+; Dnmt1Flox/+; R26R/+* embryos (Control) were used as controls and compared to age-matched mutant litter mates of the genotype *Shhcre/+; Dnmt1Flox/Flox; R26R/+* (*Dnmt1*cKO). Male and female embryos prior to gonadal differentiation were identified by genotyping for the *Sry* gene locus with the following primers: 5'-TGCAGCTCTACTCCAGTCTTG-3' and 5′-GATCTTGATTTTTAGTGTTC-3′ (Kim et al., 2011). For each analysis $n \geq 3$ litter independent male or female embryos of each genotype were used.

Fluorescent Immunohistochemistry

Fluorescent immunohistochemistry was performed as described previously (Abler et al., 2011a). In brief, 5 µm paraffin sections were deparaffinized in xylene and hydrated through a series of ethanol washes. Heat mediated antigen retrieval was performed by boiling slides in 10 mM sodium citrate (pH 6.0) for 20 mins in a conventional microwave oven. Tissues were washed with a solution containing 25 mM Tris-HCl, pH 7.5, 140 mM NaCl, 2.7 mM KCl, and 0.1% Tween-20 (TBSTw) and non-specific binding sites were blocked for 1 hr in TBSTw containing 1% Blocking Reagent (Roche Diagnostics, Indianapolis, IN), 5% normal goat sera, and 1% bovine serum albumin fraction 5 (RGBTw). Tissues were incubated overnight at 4^0C with primary antibodies diluted in

RGBTw. Following primary antibody incubation, tissues were washed several times in TBSTw and incubated with secondary antibodies diluted in RGBTw for 1 hour at room temperature. Images were obtained using a Leica SP8 Confocal Microscope fitted with a 20X oil immersion objective (HC PL Apo CS2 NA = 0.75) (Leica, Wetzlar, Germany) or a Nikon Eclipse E600 compound microscope fitted with 10X (Plan Fluor NA = 0.30) and 20X (Plan Fluor NA = 0.50) (Nikon Instruments Inc., Tokyo, Japan) or a Keyence BZ-X710 microscope (Keyence, Osaka, Japan). Sections from both experimental groups were imaged using the same exposure settings or laser power for a given antibody combination. The tile-scanning function was used to obtain images of entire tissue sections containing the urethra and bladder to reduce sampling bias. For primary and secondary antibody information see Table 2.1.

Hematoxylin-Eosin staining

5 µm paraffin sections were washed in xylene and rehydrated through a series of graded ethanol washes. Slides were washed in water and a drop of Hematoxylin QS (Vector Laboratories, Burlingame, CA, US) was placed over the tissue for 8 minutes. Slides were washed in tap water and phosphate buffered saline to develop stain. Slides were then washed in a 50% ethanol solution followed by a 75% ethanol solution. Slides were incubated in Eosin working solution (0.25% Eosin, 60% ethanol, 0.5% glacial acetic acid) for 2 minutes and dehydrated through a series of graded ethanol washes. Slides were washed in xylene and mounted with Richard-Allan Scientific™ Mounting Medium (Thermo Fisher Scientific, Waltham, MA, USA) before coverslips were applied. Images were obtained using an Eclipse 80i compound microscope.

RNA *in situ* Hybridization

In situ hybridization for tissue sections was carried out as described previously (Abler et al., 2011b; Keil et al., 2012). For *in situ* hybridization, tissues were fixed overnight in phosphate buffered saline containing 4% paraformaldehyde, embedded in OCT embedding medium, cut into 10 µm sections and mounted on glass slides. Slides were air-dried for 15 mins and fixed for 1 hour in 4% paraformaldehyde. Slides were washed in phosphate buffered saline containing 0.1% Tween20 (PBSTw) and incubated for 20 mins in PBSTw containing 6% hydrogen peroxide. Following PBSTw washes, slides were incubated in PBSTw containing 5 ng/µl Proteinase K for 8 mins. After proteinase digestion, slides were fixed for 10 mins in a 0.2% glutaraldehyde, 4% paraformaldehyde solution. Following this, slides were incubated in acetylation solution (0.1M Triethanolamine, 0.078M HCl, 0.25% acetic anhydride) for 10 mins. Slides were incubated in prehybridization solution (50% formamide, 25% SSC, 1% Roche blocking reagent #11096176001, 10 µg/ml yeast tRNA, 10 µg/ml heparin) for 1 hour and hybridized with 0.2 µg/ml of digoxygenin conjugated RNA probe overnight at 60.5 C. After overnight incubation with probes, slides were washed with formamide containing solutions, treated with RNase solution and blocked in 10% sheep serum, 1% Roche blocking reagent and 1% BSA for 2 hours. Slides were incubated overnight with anti-digoxygenin alkaline phosphatase conjugated antibodies (Roche #11093274910). Following overnight antibody incubation, slides were washed and incubated in BM purple alkaline phosphatase precipitating substrate (Roche #11442074001). After completion of the colorimetric reaction, tissues were fixed overnight in phosphate buffered saline containing 4% paraformaldehyde before imaging using a Nikon Eclipse 80i compound microscope.

For primer sequences using for making RNA probes and complete probe sequences see Table 2.1.

Assay for β-galactosidase activity

β-galactosidase activity was assessed as previously described by (Cheng et al., 1993) with modifications described by (Mehta et al., 2013). Briefly, freshly dissected tissues were fixed for 20 minutes on ice in phosphate buffered saline (PBS) containing 4% paraformaldehyde, rinsed with cold PBS and incubated in a solution containing 5 mM $K_3Fe(CN)_3$,5 mM $K_4Fe(CN)_6$, 2 mM $MgCl_2$, 0.02% NP-40, 0.01% sodium deoxycholate, and 1mg/ml X-Gal. Tissues were light protected and incubated for 3 hours at 37 C on a rocking platform. Tissues were fixed overnight in PBS containing 4% paraformaldehyde before imaging.

Wolffian duct epithelium/bladder mesenchyme recombinants

Wolffian ducts were dissected from E14.5 CD-1 wildtype embryos. Bladders were dissected from embryos heterozygous for UBC-GFP (ubiquitous GFP). Epithelium and mesenchyme were separated by incubation in 1% Trypsin (in Hanks Balanced Salt Solution containing 7.5% NaHCO3) for 90 mins at 4 C followed by microdissection. Isolated Wolffian duct epithelium was placed on top of bladder mesenchyme on a sterile filter placed in the well of a 6-well dish containing 1 ml of DMEM/F12 (Fisher #SH30271.01) with 6.7 ng/ml Sodium Selenite, 10 µg/ml Insulin, 5.5 µg/ml Transferrin, 1 ng/ml Dihydrotestosterone and antibiotics (Penicillin/Streptomycin/Fungizone Fisher #SV30079.01). Tissue recombinants were allowed to adhere for 24 hours and grafted under the renal capsule of athymic nude mice. Grafts were harvested after 3 weeks, fixed overnight in 4% paraformaldehyde and processed for immunohistochemistry.

E14.5 Bladder grafts

Lower urinary tracts were dissected from E14.5 Control and *Dnmt1*cKO embryos obtained through timed matings. Bladders were severed from the urethra and Wolffian ducts and grafted under the renal capsule of athymic nude mice. Grafts were harvested after 3 weeks, fixed overnight in 4% paraformaldehyde and processed for immunohistochemistry.

Bladder urothelium thickness measurements

Hematoxylin-eosin stained tissue sections were imaged for measuring thickness of bladder compartments namely the urothelial layer, lamina propria and muscularis propria. Image analysis was performed using *ImageJ v1.51k*. For urothelium, the shortest distance between the lamina propria and bladder lumen were measured across five different regions using the *Straight-line tool*. Three litter independent samples per genotype were analyzed.

Cell density counts for bladder layers

5 μm bladder sections were fluorescently labeled with antibodies to E-cadherin (CDH1) and Smooth muscle actin alpha and the nuclear dye DAPI as described above. The unlabeled region between E-cadherin labeled urothelium and Smooth muscle actin labeled muscularis propria was defined as the lamina propria. Image analysis was performed using *ImageJ v1.51k*. The *Freehand selection tool* was used to select the lamina propria region. The *Measure* function was used to determine the selected area. The *Clear Outside* function was used to clear from the image regions residing outside the lamina propria. The *Split Channels* option was used to isolate DAPI staining. Individual lamina propria nuclei were counted using the *Analyze particles* function. Lamina propria

cell density was computed as the number of nuclei per mm squared of lamina propria area. Three litter independent samples per genotype were analyzed.

Pixel staining intensity for COL1A1 antibody

5 µm bladder sections were fluorescently labeled with antibodies against COL1A1, CDH1 and the nuclear dye DAPI as described above. Image analysis was performed using *ImageJ v1.51k*. The *Freehand selection tool* was used to select the lamina propria region where the COL1A1 antibody staining was localized. The *Measure* function was used to find the area of the selection. The *Clear Outside* function was used to clear regions outside the lamina propria. The *Split Channels* option was applied to isolate COL1A1 staining. Thresholding was applied, and the area covered by thresholded pixels was measured using *Analyze>Measure* functions. Pixel density was computed as the area of antibody stained pixels to the total selection area. Results were presented as a percentage value. Three litter independent samples per genotype were analyzed.

Cell counts for differentiation markers, cleaved caspase-3

5 µm bladder sections were fluorescently labeled with antibodies to various cellular proteins. Image analysis was performed using *ImageJ v1.51k*. Cells positive for various markers were counted manually using the *Cell Counter* plugin. Three litter independent samples per genotype were analyzed.

Statistical Analysis

Statistical analysis was carried out using *R* version 3.2.4. Homogeneity of variance was determined using Bartlett's test or Levene's test using R packages. Student's t-test was performed on parametric data with two groups. One-way ANOVA was performed on parametric data with more than two groups. P values less than 0.05 were considered

statistically significant. Results are presented as mean ± standard error of the mean (SEM) from at least three litter independent samples per genotype. NS: Not significant, * $p<0.05$, ** $p<0.01$, *** $p<0.001$.

RNA-Seq

E15.5 Control and *Dnmt1*cKO bladder epithelium was isolated by trypsin digestion as described previously (Cunha and Baskin, 2016). Dissected tissues were placed directly into RLT Plus lysis buffer (Qiagen) for later processing. For each batch of harvest, dissected tissues from multiple embryos were pooled into one lysate. Total RNA was purified from the RLT Plus lysates using the RNeasy Plus Micro Kit (Qiagen) according to manufacturer's instructions. For constructing the RNA-Seq library, total RNA from each batch of samples (using an input of ~100 ng total RNA) were used following the LM-seq protocol (Hou et al., 2015). The reads generated from the Illumina HiSeq 3000 (69 cycles of insert read and 10 cycles of index read) were processed with CASAVA-1.8.2 basecalling software (Illumina). The demultiplexing step allotted approximately 333 million total reads across the all the samples, ranging from ~0.3 million to ~13.6 million reads assigned per sample. Reads were mapped to Mus musculus reference mm10 assembly with an average of ~74.5% mapping rate using Bowtie (Langmead et al., 2009), and gene expression estimates were obtained using RSEM (Li and Dewey, 2011). Differentially expressed genes were identified using the *DESeq2* package (Love et al., 2014). Independent filtering was performed to eliminate genes with less than 10 reads in all samples combined. Genes with adjusted p-value or False discovery rate (FDR) <0.1 were considered to be differentially expressed. Gene Ontology enrichment analysis for biological processes was conducted using WebGestalt (Wang et al., 2017).

2.3. Results

Dnmt1 deletion in *Shh* lineage cells leads to neonatal lethality

Mice carrying one copy of the *Shh*^{cre} transgene and one copy of a *Dnmt1flox* allele (Jackson-Grusby et al., 2001) served as experimental controls for mice carrying one copy of the *Shh*^{cre} allele and two copies of the *Dnmt1flox* allele (*Dnmt1*cKO). Initial observation of *Dnmt1*cKO neonates revealed severe lung hypoplasia, cyanosis and death at postnatal day 0 (Figure S 2.1 A-B). Subsequent studies with embryos examined at or before E18.5, prior to development of respiratory complications, revealed viable *Dnmt1*cKO embryos with a normal external appearance and a crown-rump length comparable to controls (Figure S 2.1 C). Cre recombination, evaluated by inducible *R26R-LacZ* or *R26R-EYFP* lineage reporters, localized to bladder and urethral epithelium but not caudal Wolffian or Müllerian duct epithelium (Figure 2.1 A, S 2.3 C). All subsequent Figure panels are from male embryos unless otherwise specified.

Wolffian duct epithelial cells are recruited into the *Dnmt1* depleted lower urinary tract

We first tested whether DNMT1 protein abundance and global DNA methylation were reduced in E18.5 *Dnmt1*cKO mutants. DNMT1 and 5-methylcytosine (5mC) were not detected in *Shh* lineage (EYFP+) epithelial cells in *Dnmt1*cKO mutants. The most surprising finding was the presence of many EYFP-, DNMT1+, 5mC+ cells in *Dnmt1*cKO urethra and bladder (Figure 2.1 A-B, S 2.1 D-E). We used a different lineage reporter (*R26R-LacZ*) to evaluate *Shh* lineage cell distribution. A sizeable cluster of lineage negative (non-stained with X-Gal) epithelial cells accumulated between the bladder neck and Wolffian duct of *Dnmt1*cKO mutants (Figure 2.1 C-D). Presence of *Shh* lineage

negative cells in this region is unusual considering that the entire epithelium of the urethra and bladder derives from *Shh* lineage cells (Seifert et al., 2008).

Incomplete Cre mediated recombination could cause *Shh* lineage negative cells to accumulate but this is unlikely given these cells are not randomly distributed but instead restricted to a discrete anatomical region. In addition, 100% Cre recombination was observed in controls (Figure S 2.1 F-N). We then contemplated the unusual possibility that *Shh* lineage negative cells are recruited to the *Dnmt1*cKO urethra from a different source. Wolffian duct epithelium, marked by Paired Box 2 (PAX2) and Paired Box 8 (PAX8) (Bouchard et al., 2002), is the closest non-endodermal epithelial source and derives from a *Shh* negative lineage (intermediate mesoderm). PAX2+, PAX8+ cells were restricted to control mouse Wolffian ducts as expected but surprisingly extended into *Dnmt1*cKO urethra and bladder (Figure 2.1 E-F). *Pax2* and *Pax8* mRNAs were expressed in patterns resembling their protein expression (Figure S 2.2 A-D) and we confirmed PAX8+ cells were indeed integrated into *Dnmt1*cKO urethral epithelium because they were externally bounded by a continuous laminin a1 (LAMA1) stained basement membrane (Figure S 2.2 E-F). Collectively, these results support the hypothesis that Wolffian duct epithelial cells are recruited into *Dnmt1*cKO urethra and bladder and that cell recruitment is unidirectional (urethra/bladder epithelial cells do not invade Wolffian duct epithelium). Ureters and Müllerian ducts could be additional sources of PAX2+, PAX8+ cells but there was no evidence of cell movement from either of these tissues into the urethra and bladder (Figure S 2.2 I-J and K-L). Further, when *Dnmt1*cKO bladders are severed from the Wolffian ducts and grafted, no PAX2+ cells appear in bladder (Figure S 2.2 M-N).

We examined multiple developmental stages, spanning E12.5-E18.5, to pinpoint when Wolffian duct cells are recruited into *Dnmt1*cKO urethra and bladder. Between E12.5-E14.5, no PAX2+ Wolffian duct cells were observed in urethra or bladder of either genotype (Figure 2.1 G-J, S 2.2 G-H). The Wolffian ducts were separated from the urethra and bladder by the urogenital sinus (UGS) ridge, an epithelial thickening on the urethral side of the Wolffian duct-urethra junction. The UGS ridge was present and its size comparable between genotypes at E13.5 and E14.5 (Figure 2.1 G-J). At E15.5, the *Dnmt1*cKO UGS ridge was smaller than controls and was completely absent by E18.5 (Figure 2.1 K-N). Wolffian duct cells colonized the male *Dnmt1*cKO urethra at the onset of UGS ridge depletion at E15.5 and progressively expanded into the bladder. None of the ectopic PAX2+ Wolffian duct cells expressed the *Shh* lineage label, indicating these cells do not acquire *Shh* expression or lose DNMT1 within urethra or bladder (Figure S 2.1 N-O).

Onset of Wolffian duct cell recruitment at E15.5 excludes the possibility that these cells are remnants of the transitory Wolffian duct derivative, the common nephric duct. The common nephric duct typically recedes at E11.5 (Batourina et al., 2005) and there was no evidence of Wolffian duct cell recruitment into the urethra until E15.5. We also found that Wolffian duct cells are recruited to the female *Dnmt1*cKO urethra at E15.5, prior to Wolffian duct degradation at E16.5 (Figure S 2.3), suggesting this phenomenon occurs in both sexes.

Wolffian duct cells recruited to the *Dnmt1* depleted lower urinary tract acquire bladder epithelial characteristics

We found that bladder mesenchyme can instructively reprogram Wolffian duct epithelium when the tissues are combined and grafted under the kidney capsule for continued development (Figure S 2.4 G-J). We tested whether similar reprogramming occurs in Wolffian duct cells recruited to the bladder. During normal development and differentiation, bladder epithelium initially expresses the definitive endoderm marker FOXA1 and then acquires Keratin 5 (KRT5), P63 and Uroplakin (UPK) to generate basal (KRT5+, P63+, UPK-), intermediate (KRT5-, P63+, UPK+) and superficial (KRT5-, P63-, UPK+) cells (Gandhi, 2013). During embryonic development in control mice, Wolffian duct epithelium exhibits a columnar morphology in contrast to the cuboidal morphology of urethral epithelium and does not express FOXA1, KRT5, P63 or Uroplakins. At the onset of Wolffian duct epithelial cell recruitment into the *Dnmt1cKO* lower urinary tract (E15.5), only a few PAX2+ cells were present in the urethra and these cells expressed FOXA1 but not KRT5 or P63 (Figure S 2.4). At E18.5, many PAX2+ cells resided in the *Dnmt1*cKO urethra and bladder and all co-expressed FOXA1 (Figure 2.2 A-B). PAX2+, PAX8+ cells residing closest to the Wolffian duct-urethra junction were KRT5-, P63- and those in the bladder neck and bladder were KRT5+, P63+ (Figure 2.2 C-J). These results indicate that recruited Wolffian duct epithelial cells progressively differentiate as they migrate away from the Wolffian duct and into bladder. Consistent with this hypothesis, recruited Wolffian duct cells near the E18.5 *Dnmt1*cKO Wolffian duct had a columnar morphology resembling Wolffian duct epithelia while those in the bladder had a cuboidal morphology resembling bladder epithelia (Figure 2.2 O).

Cell counts show that 100% of Wolffian duct cells (*Shh* lineage negative) in the urethra express PAX2 whereas only 64% of Wolffian duct cells in the bladder express PAX2

(346/537 cells counted) (Figure S 2.1 N). We hypothesized that Wolffian duct cells enter the bladder from the urethra as a homogenous population and some lose PAX2 expression upon differentiation. We tested and confirmed that bladder-recruited Wolffian duct cells (*Shh* lineage negative, EYFP- cells) achieved expression of Uroplakin (UPK), the defining marker of bladder superficial cells (Figure 2.2 P-Q). These UPK+ Wolffian duct cells appeared to be PAX8- (Figure 2.2 K-N) although adjacent basal cells were PAX8+. We interpret these results as evidence that Wolffian duct cells partially retain their identity when reprogrammed to basal cells but lose their Wolffian duct identity when reprogrammed to superficial cells.

Dnmt1 **depleted lower urinary tract epithelia differentiate inappropriately and are abnormally thin**

Having characterized Wolffian duct cell recruitment and reprogramming in *Dnmt1*cKO lower urinary tracts, we turned our attention to the *Dnmt1* depleted epithelium into which they are recruited. *Dnmt1*cKO urethras exhibited abnormal dorsal-ventral patterning and disorganization, with acellular holes in the epithelium (Figure 2.3 A-F). *Dnmt1*cKO bladders were abnormally large, filled with urine (Figure S 2.5 A-B), and featured a thinner epithelium than controls (Figure 2.3 G-I).

We hypothesized *Dnmt1* deficiency causes inappropriate epithelial differentiation and cell depletion, creating a permissive environment for colonization by Wolffian duct cells. We focused on the bladder apex region because it is least contaminated by recruited Wolffian duct cells (Figure 2.1 A-B) and made three observations supporting inappropriate differentiation of *Dnmt1* depleted bladder epithelial cells. First, I noted a precocious appearance of KRT5+, P63+ basal epithelial cells in E15.5 *Dnmt1*cKOs compared to

controls (Figure 2.3 J-K, 2.3 R, S 2.5 I). Second, E18.5 *Dnmt1*cKO bladders had fewer KRT5+, P63+ basal cells than controls and were characterized by weak and discontinuous UPK expression, consistent with impaired barrier function (Figure 2.3 L-O, 2.3 R). Third, E18.5 *Dnmt1*cKO bladder cells ectopically expressed the squamous epithelial marker Keratin 17 (KRT17) (Guo et al., 2017) which was absent in control bladder cells (Figure 2.3 P-Q) and Wolffian duct derived bladder epithelium (Figure S 2.6 Q-T). The proportion of basal, intermediate and superficial cells in *Dnmt1*cKO bladder epithelium was also different than controls (Figure 2.3 R). An increased frequency of superficial cells at the expense of basal and intermediate populations supports the hypothesis that *Dnmt1* deficiency drives premature cell differentiation and depletes bladder progenitors. Bladder development is dependent on reciprocal signaling between the epithelium and mesenchyme. Non-cell autonomous effects of epithelial DNMT1 deletion were observed in *Dnmt1*cKO bladder mesenchyme including reduced lamina propria cell density and decreased COL1A1 expression (Figure S 2.5 C-H). The expression profile of Wolffian duct derived bladder epithelium closely resembled control bladder urothelium but the proportion of bladder epithelial sub-types was changed (Figure S 2.6). UPK staining was discontinuous where *Dnmt1* was depleted (EYFP+) but continuous where Wolffian duct cells (EYFP-) replaced the damaged epithelium (Figure S 2.6 U-X, S 2.7). This is evidence that recruited Wolffian duct cells not only differentiate towards a bladder fate, but also restore the UPK barrier.

Dnmt1 **depleted lower urinary tract cells are hypomethylated and undergo apoptosis**

To understand the mechanisms underlying epithelial depletion and disorganization, we performed RNA-Seq analysis of isolated E15.5 bladder epithelium (at onset of Wolffian duct migration). We observed increased abundance of P53 targets including *Cdkn1a1*, *Ccng1* and *Pmaipi1* (*Noxa*) (Figure S 2.8). Previous studies in developing intestine and pancreas associated *Dnmt1* depletion with DNA hypomethylation and P53-mediated apoptosis characterized by Gamma-H2AX activation (DNA damage marker), P53 activation (Ser15 phosphorylation) and Caspase 3 cleavage (Elliott et al., 2015; Georgia et al., 2013). We examined whether a similar series of events precipitates apoptosis of *Dnmt1*cKO urethra and bladder epithelium. Loss of DNMT1 protein and 5mC labeling was detected as early as E13.5 in *Dnmt1*cKO urethra and bladder (Figure S 2.9 A-D). Immunolabeling showed that Phospho-Gamma-H2AX (Figure 2.4 A-H) and Phospho-P53 Serine 15 (Figure 2.4 I-P) were increased in *Dnmt1*cKO urethra and bladder starting at least as early as E13.5. Phospho-P53 Serine 15 appeared to localize to mitochondria, was restricted to *Dnmt1* depleted (EYFP+) cells and was absent from recruited Wolffian duct cells (EYFP-) (Figure S 2.9 E-P).

We next tested whether DNA damage and P53 phosphorylation triggered apoptosis in *Dnmt1*cKO epithelial cells. Cleaved Caspase 3 positive lower urinary tract epithelial cells were rare and their frequency did not differ between genotypes at E13.5 and E14.5 (Figure 2.4 Q-T). By E15.5 and continuing through E18.5, cleaved Caspase 3 positive epithelial cells were significantly more frequent in *Dnmt1*cKOs than controls (Figure 2.4 U-Z). Cleaved Caspase 3 staining in *Dnmt1*cKOs was confined to *Dnmt1* depleted *Shh* lineage (EYFP+) cells and was absent from recruited Wolffian duct (EYFP-) cells (Figure S 2.10). Thus, DNA hypomethylation, DNA damage and P53 activation precede apoptosis

in *Dnmt1*cKO urethra and bladder epithelia at E15.5, and apoptosis coincides with Wolffian duct cell recruitment. Because Wolffian duct cells are not recruited into the lower urinary tract until *Dnmt1* deficient cells undergo apoptosis, I conclude Wolffian duct cell recruitment is a consequence of *Dnmt1* ablation.

2.4. Discussion

Our results support the model in Figure 2.5. *Dnmt1* ablation in urethral and bladder epithelium causes global DNA hypomethylation, initiates a DNA damage response and drives P53-mediated apoptosis. Urethral and bladder epithelial cell depletion and UGS ridge breakdown are triggers for Wolffian duct cell recruitment. Recruited cells migrate into the bladder, acquire bladder-specific markers and restore the bladder's Uroplakin barrier. These results identify Wolffian duct epithelium as a new reservoir for bladder epithelial cell replacement.

This is the first study to investigate the role of DNMT1 in urethra and bladder development. *Dnmt1* deletion in the lower urinary tract caused extensive epithelial damage as evidenced by acellular holes in the epithelium, increased frequency of apoptotic cells, thinning of bladder epithelium and discontinuous Uroplakin staining. DNA hypomethylation is accompanied by activation of the DNA damage response, P53 accumulation and apoptosis. The sequence of molecular events leading to *Dnmt1* deficient bladder cell apoptosis matches that described in *Dnmt1* depletion studies in the developing intestine (Elliott et al., 2015) but the outcome is unique: *Dnmt1* ablation in lower urinary tract epithelium triggers cell movement events that were not detected in previous conditional *Dnmt1* mutant studies. Together, our results demonstrate a

requirement for *Dnmt1* in maintaining global DNA methylation and progenitor cell survival in the developing bladder epithelium.

Early in embryonic development, Wolffian ducts elongate along the anteroposterior axis, turn towards the midline and fuse with the cloacal epithelium (precursor of urethral and bladder epithelia). The timing of Wolffian duct-urethra junction formation is critical and the mechanism has been thoroughly characterized (Chia et al., 2011), but it was not known how this junction is maintained during lower urinary tract development and maturation. Our study reveals a novel and unexpected role of cell survival mediated by *Dnmt1* in maintaining the junction by preventing the intermixing of Wolffian duct and urethral cells. Although the Wolffian duct-urethra junction is formed normally in *Dnmt1* mutants, it is not maintained. Our results demonstrate for the first time that the Wolffian duct-urethral junction can be destabilized and breached by epithelial depletion/injury of the urethral epithelium. Other instances of epithelial injury to the urethra could potentially cause this to happen in humans.

Wolffian duct cell recruitment into the urethra and bladder is a novel and unprecedented observation, but I only examined embryonic stages due to neonatal lethality of *Dnmt1*cKO mutants. Our results raise new questions about whether postnatal Wolffian duct derivatives (vas deferens, seminal vesicle) retain the capacity to invade the postnatal urethra and bladder. Intriguing support for this possibility exists in patients with the rare condition of nephrogenic adenoma, a benign lesion of the bladder or urethra observed most frequently in patients with a history of bladder injury, inflammation, infection, kidney stones or urogenital surgeries (Ford et al., 1985; Mazal et al., 2002). Presence of PAX2 and PAX8 immuno-positive cells in bladder and urethral biopsies is diagnostic for

nephrogenic adenoma (Pina-Oviedo et al., 2013), but the source of these cells is not completely known. One study demonstrated that exfoliated kidney epithelial cells from donors colonize bladders of kidney transplant recipients who later developed nephrogenic adenoma (Mazal et al., 2002). Whether other cell types, including Wolffian duct epithelium, can also be recruited to the postnatal bladder has not been examined. The adult regenerative capacity of Wolffian duct derivatives is an important avenue to pursue. Our study and nephrogenic adenoma demonstrate the ability of injured bladder epithelium to recruit non-bladder cells to repair itself. These non-bladder cells could behave differently from normal bladder epithelium in disease contexts and could contribute to disease in the long-term.

One of the most surprising observations from this study is the newly recognized capacity of mesodermal Wolffian duct epithelial cells to acquire endodermal bladder epithelial characteristics after invading *Dnmt1*cKO bladder epithelium. Tissue recombination studies using *in vivo* grafting of tissue recombinants have identified the inductive capacities of embryonic bladder mesenchyme. Embryonic bladder mesenchyme induces urothelial differentiation when recombined with adult bladder epithelium (Oottamasathien et al., 2006) or adult mesenchymal stem cells (Anumanthan et al., 2008), and I report here for the first time that the bladder mesenchyme can instructively reprogram Wolffian duct epithelium. The presence of Wolffian duct epithelial cells in the inductive bladder mesenchyme niche of *Dnmt1*cKO mutants provides a unique opportunity to study Wolffian duct epithelial reprogramming by bladder mesenchyme *in vivo*. Once in the bladder, recruited Wolffian duct epithelial cells acquire expression of KRT5, P63 and Uroplakin, signifying urothelial differentiation. Progressive differentiation of recruited

Wolffian duct cells as they move from urethra to bladder suggests that the degree of reprogramming could depend on the time spent in the new niche or relative location within this niche.

Bladder basal and intermediate cells had been considered the only populations to participate in bladder regeneration after injury (Gandhi, 2013; Papafotiou et al., 2016). Here we demonstrate that Wolffian duct epithelial cells can also repopulate injured bladders and restore a Uroplakin barrier. This capacity can potentially be leveraged for bladder regeneration therapies. Currently, intestinal epithelium is used as a source of tissue for creating neo-bladders for urine repositories. However, disparate functions of intestinal and bladder epithelium lead to complications, which include excess mucous production that increases urine viscosity and impairs neo-bladder emptying (N'Dow et al., 2001). Alternate strategies for bladder replacement include the use of acellular matrices as scaffolds to guide regeneration (Lin et al., 2015). Our results support the possibility that Wolffian duct-derived tissue may be another cell source for autologous bladder regeneration. Crucial to future studies is a determination of whether Wolffian duct derivatives retain the capacity to reprogram into bladder epithelial cells during postnatal stages or in adulthood.

2.5. Figures and Tables

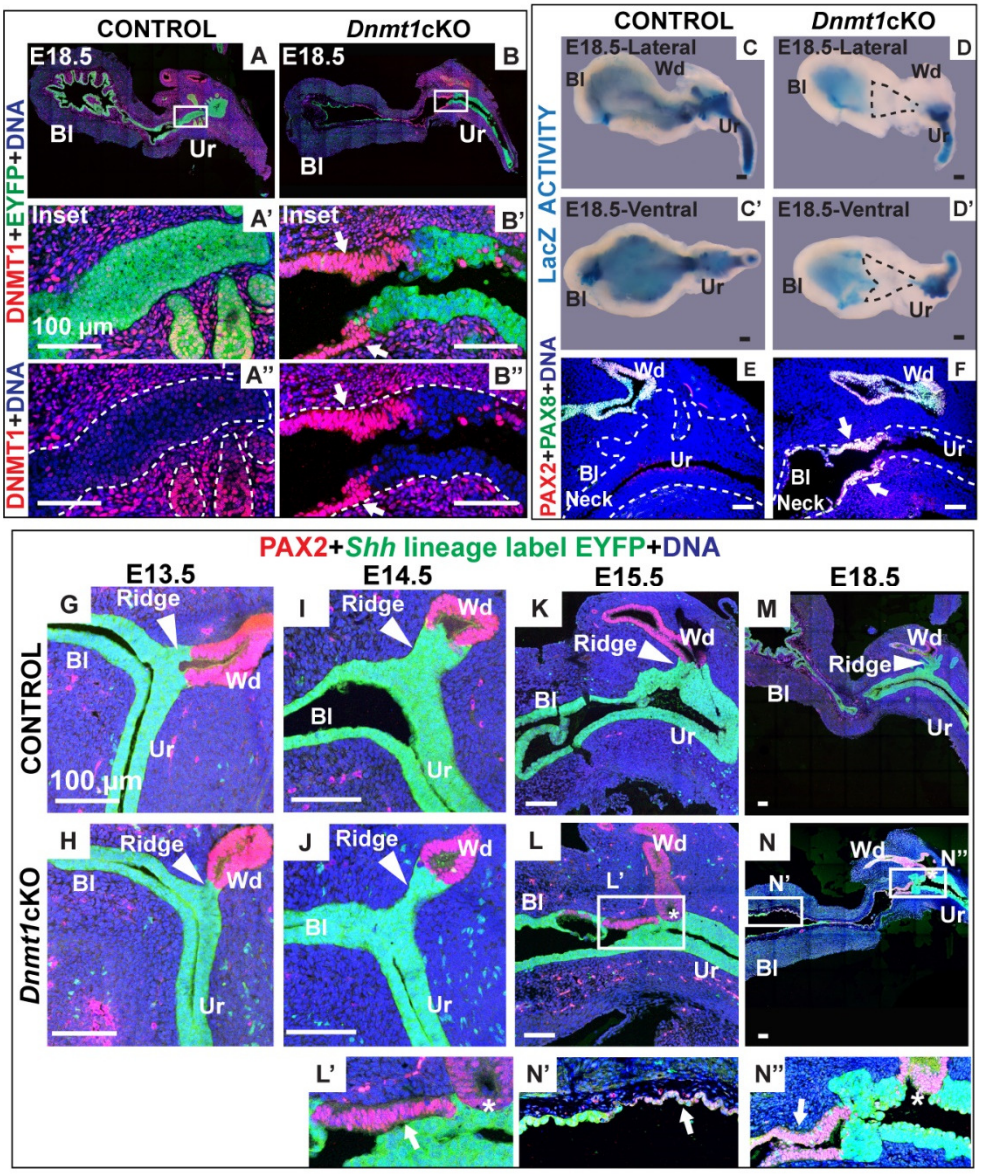

Figure 2.1 Wolffian duct-derived epithelial cells are recruited into *Dnmt1* conditional knockout (*Dnmt1*cKO) lower urinary tracts

(A-B) Lower urinary tract sagittal sections labeled with antibodies against DNMT1 (red) and EYFP (green, labels *Shh* lineage cells). DNMT1+, EYFP- cells in *Dnmt1*cKO urethras are indicated by white arrows. Boxed areas in (A) and (B) are magnified in (A'), (A'') and

(B’), (B’’). (C-D) Lateral views and (C’-D’) ventral views of lower urinary tracts treated with X-Gal to reveal LacZ activity (blue) in *Shh* lineage cells. A wedge of LacZ- cells is enclosed with black dashed lines. (E-F) Lower urinary tract sagittal sections labeled with antibodies against Wolffian duct epithelial markers PAX2 (red) and PAX8 (green). PAX2+, PAX8+ cells in *Dnmt1*cKO UGS epithelium indicated by white arrows. (G-N) Lower urinary tract sagittal sections from sequentially staged Control and *Dnmt1*cKO embryos labeled with antibodies against PAX2 (red) and EYFP (green, labels *Shh* lineage cells). White arrowheads indicate the UGS ridge and asterisks indicate a deficient UGS ridge in *Dnmt1*cKO embryos. White arrows mark PAX2+, EYFP- cells in *Dnmt1*cKO urethra and bladder. DAPI staining shown in blue. Scale bar: 100 μm. Abbreviations: Wd: Wolffian Duct, Ur: Urethra, Bl: Bladder, Bl Neck: Bladder Neck.

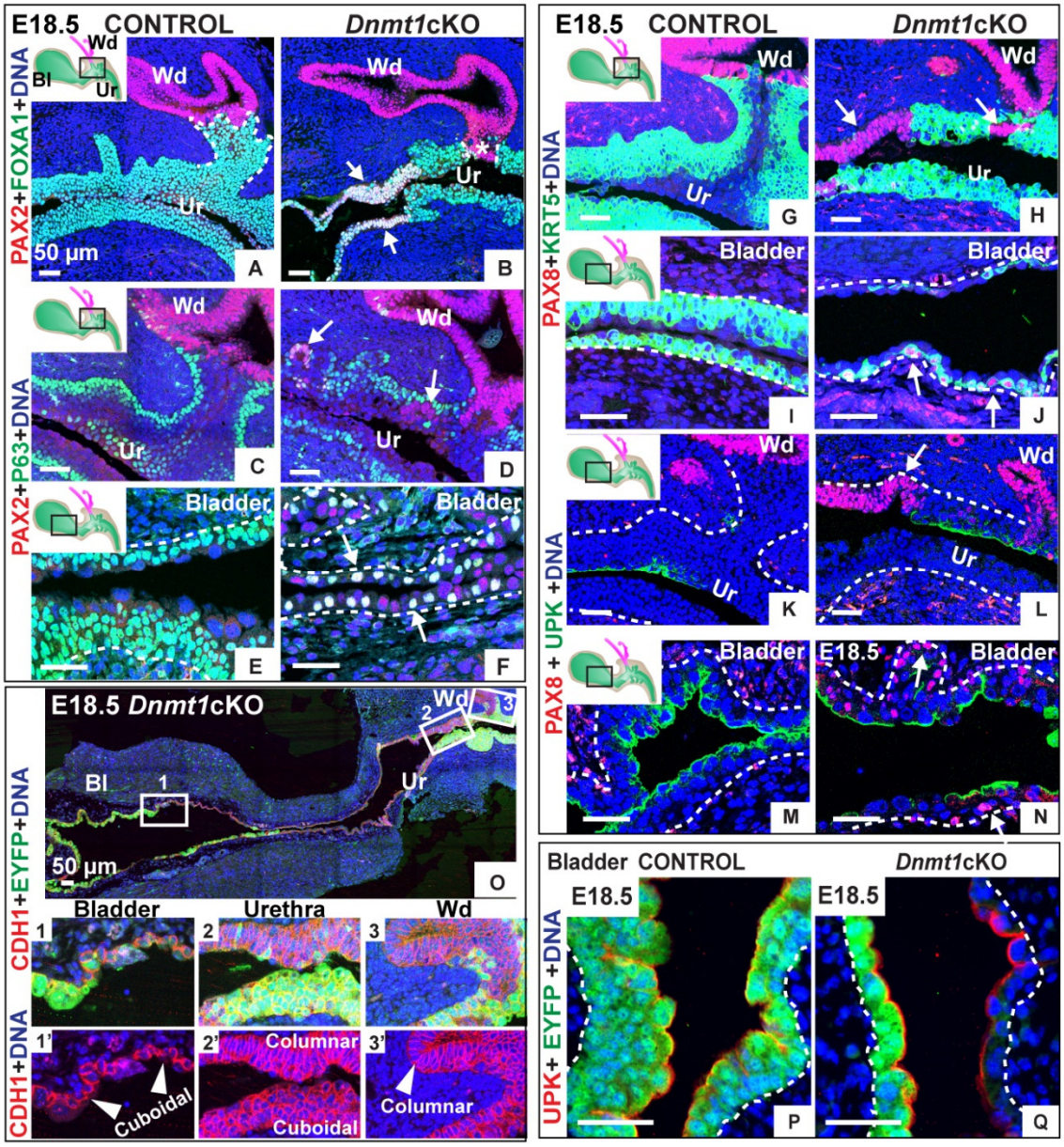

Figure 2.2 Recruited Wolffian duct cells acquire bladder characteristics as they expand into the *Dnmt1*cKO urethra and bladder.

E18.5 male lower urinary tract sagittal sections labeled with antibodies against (A-B) FOXA1 (green) and PAX2 (red, labels Wolffian duct epithelium), (C-F) PAX2 (red) and P63 (green, labels basal epithelium), (G-J) PAX8 (red, labels Wolffian duct epithelium) and KRT5 (green, labels basal epithelium), (K-N) PAX8 (red) and UPK (green, labels

superficial epithelium). White arrows indicate PAX2+ or PAX8+ cells in *Dnmt1*cKO urethra and bladder epithelia. The anatomical region shown in each panel (urethra or bladder) is depicted in the schematic diagram. (O) E18.5 male *Dnmt1*cKO lower urinary tract labeled with CDH1 (red, labels epithelial cells) and EYFP (green, labels *Shh* lineage cells). (P-Q) E18.5 bladders sections labeled with antibodies against PAX8 (red) and UPK (green). White dotted lines mark the bladder epithelial-stromal interface. DAPI staining shown in blue. Scale bar: 50 μm. Abbreviations: same as Figure 2.1.

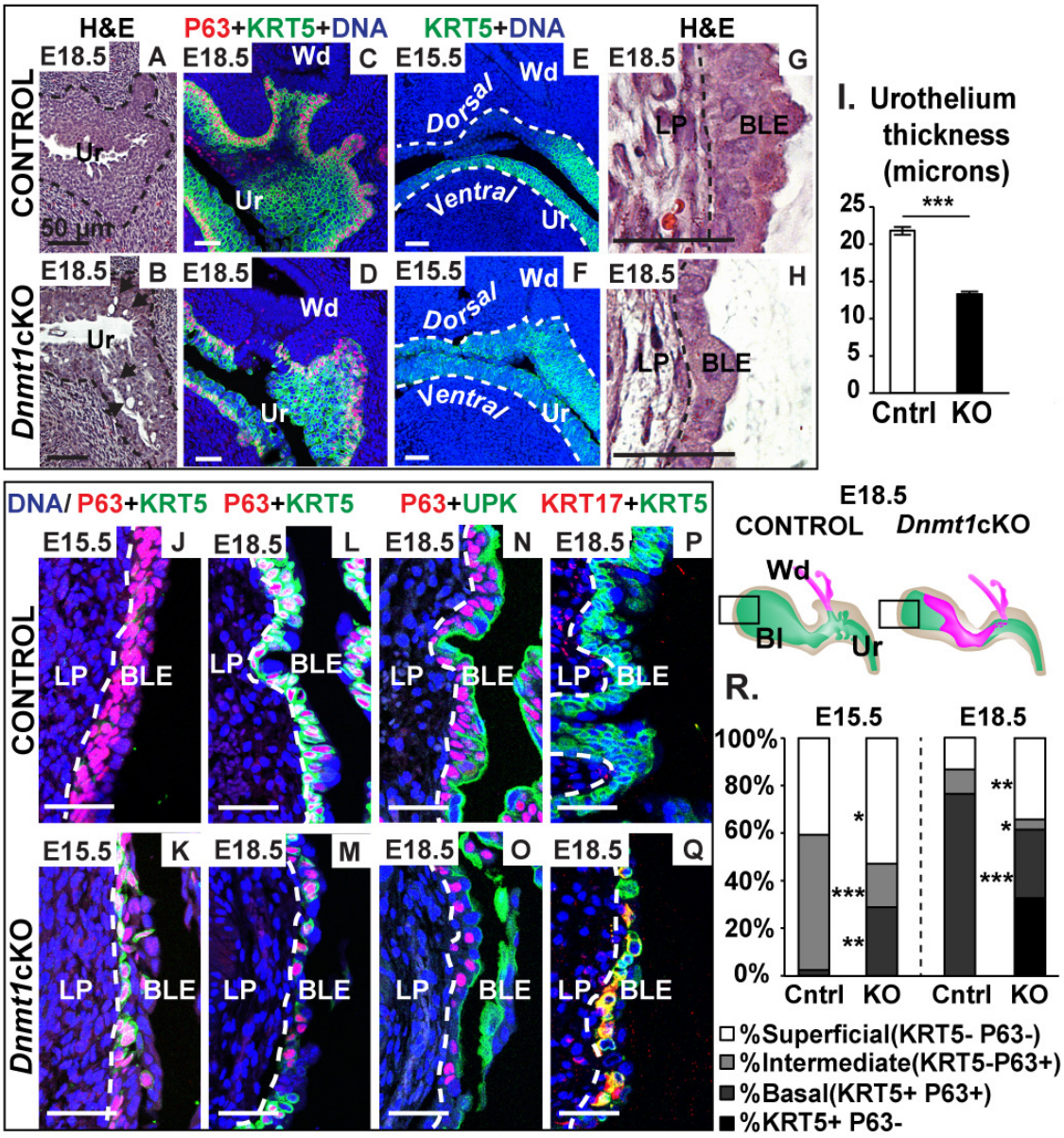

Figure 2.3 *Dnmt1* depleted lower urinary tract epithelial cells precociously differentiate and disorganize beginning at E15.5.

(A-B) H&E stained E18.5 urethral sections. Black arrows indicate acellular holes in *Dnmt1*cKO urethral epithelium. (C-D) E18.5 urethral sections labeled with basal markers KRT5 (green) and P63 (red). (E-F) E15.5 urethra sections labeled with KRT5 (green) (G-H) H&E stained E18.5 bladder sections used to quantify (I) Bladder epithelial thickness.

(J-K) E15.5 bladder sections stained with antibodies against P63 (red) and KRT5 (green). E18.5 bladder sections from region depicted in diagram stained with (L-M) P63 (red) and KRT5 (green) (N-O) P63(red) and UPK (green), or (P-Q) KRT17 (red) and KRT5 (green). (R) Percentages of basal, intermediate and superficial bladder epithelial cells at E15.5 and E18.5. Dashed lines demarcate the epithelial-mesenchymal interface. DAPI staining shown in blue. Scale bar: 50 μm. Graphical data are reported as mean ± SEM of at least three male mice/genotype. Student's t-test * $p<0.05$, ** $p<0.01$, *** $p<0.001$. Abbreviations: Same as Figure 2.1. in addition to LP: Lamina propria, BLE: Bladder Epithelium, Cntrl: Control, KO: *Dnmt1*cKO

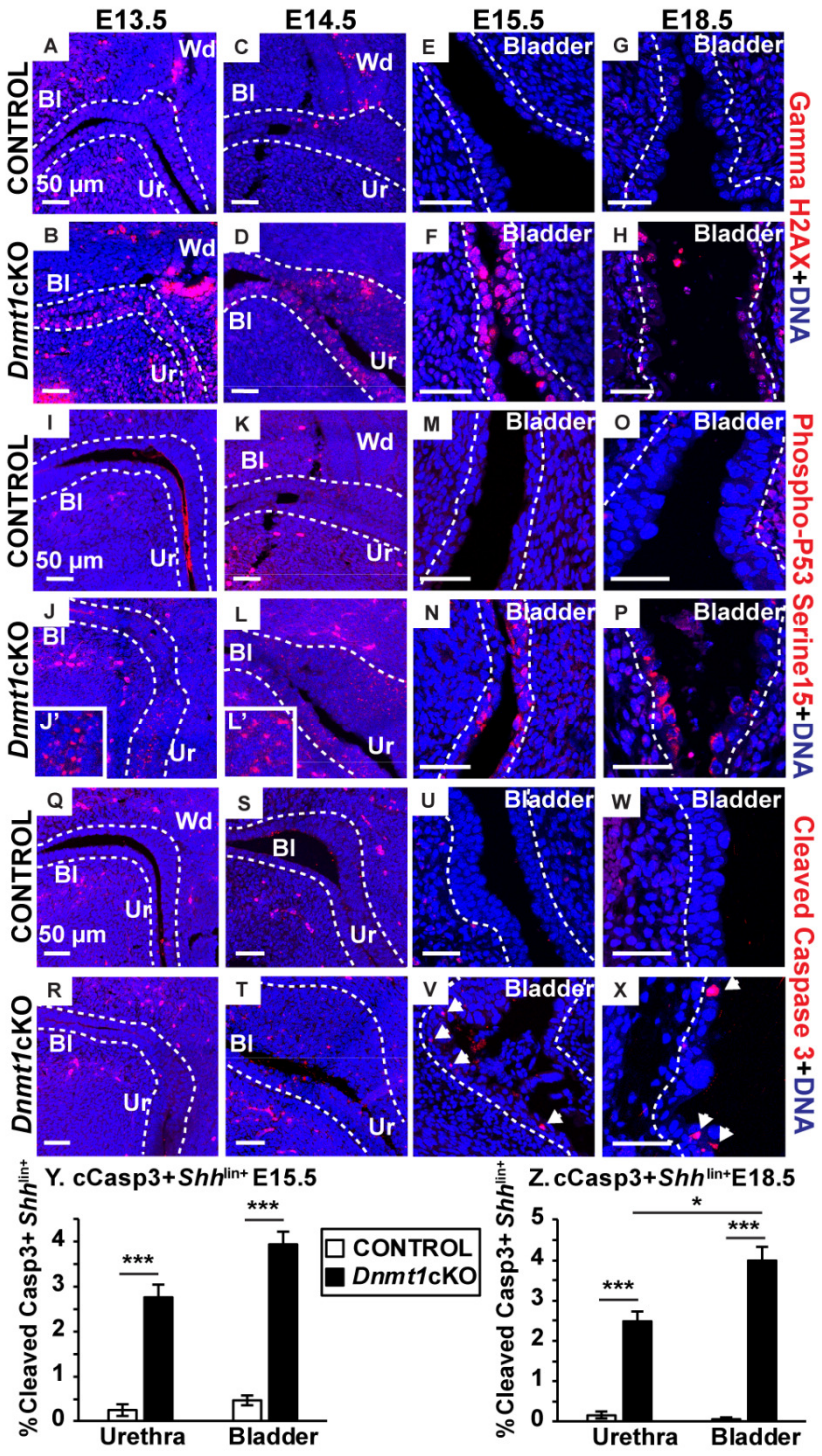

Figure 2.4 Hypomethylation triggers DNA damage and P53-mediated apoptosis in *Dnmt1*cKO urethra and bladder.

E13.5-E18.5 lower urinary tract sections were labeled with antibodies against: (A-H) Gamma H2AX (red, marker of DNA damage response) and (I-P) Phospho-P53 Serine 15 (red, marks active P53). (J') and (L') are magnified regions from (J) and (L). (Q-X) Cleaved Caspase 3 (red, marks apoptotic cells) and EYFP (*Shh* lineage label, not shown to better visualize red labeling). Percentage of Cleaved Caspase 3+ *Shh* lineage cells determined at (Y) E15.5 and (Z) E18.5. White arrows indicate apoptotic cells. White dashed lines demarcate the epithelial-mesenchymal interface. DAPI staining in blue. Scale bar: 50 μm. Graphical data are reported as mean ± SEM of at least three male mice/genotype. Student's t-test * $p<0.05$, ** $p<0.01$, *** $p<0.001$. Abbreviations: Same as Figure 2.1.

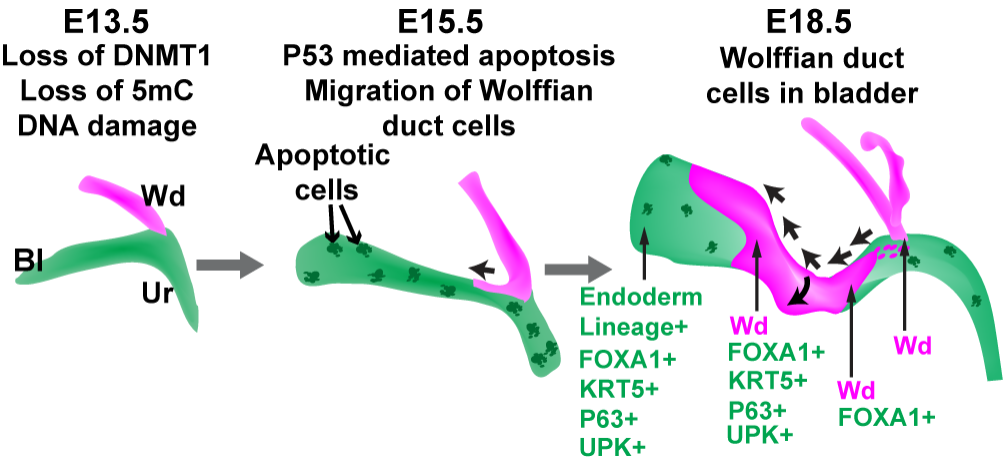

Figure 2.5 Model of Wolffian duct cell recruitment and reprogramming in *Dnmt1*cKO mice.

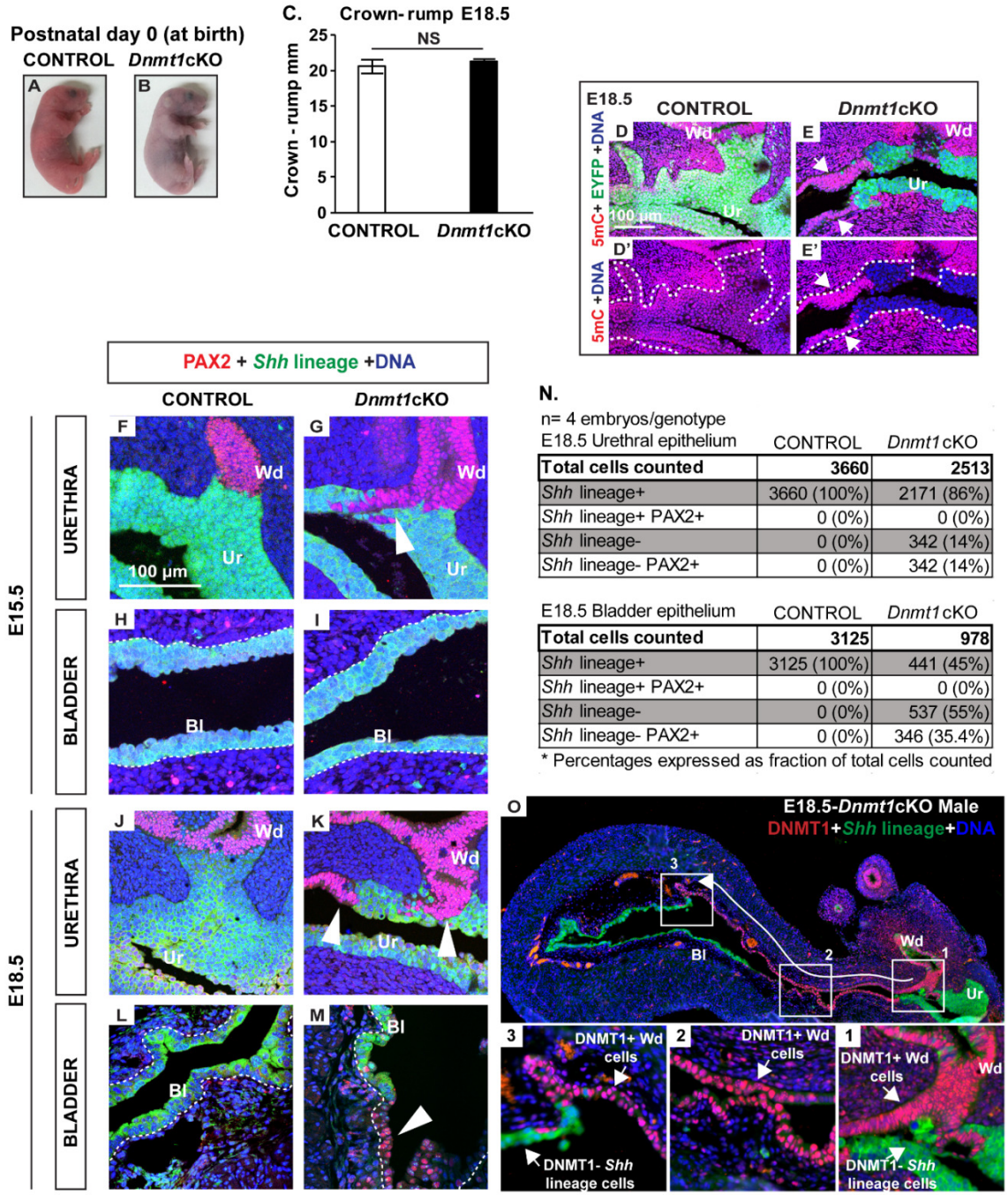

Figure S 2.1 *Shh* lineage negative Wolffian duct epithelial cells are embedded in E18.5 *Dnmt1*cKO urethral epithelium.

(A-B) Images of Control and *Dnmt1*cKO pups at Postnatal day 0 (shortly after birth). *Dnmt1*cKO pups are cyanotic and die shortly after birth. (C) Crown-rump length (mm)

was determined for E18.5 Control and *Dnmt1*cKO embryos. Crown-rump length was 20.5 ± 1 mm in controls and 21.2 ± 0.2 mm in *Dnmt1*cKOs, (n=3/genotype, Student's t-test p=0.62). Results are represented as mean± SEM. NS: Not significant. (D-E) E18.5 male urethras immunolabeled with antibodies against 5-methylcytosine (red) and EYFP (green, *Shh* lineage label). (B'-C') show the isolated red channel. White arrows identify 5mC+ EYFP- cells. (F-I) E15.5 and (J-M) E18.5 urethra and bladder sections immunolabeled with antibodies to PAX2 (red, labels Wolffian duct epithelium) and *Shh* lineage label (LacZ or EYFP). White arrowheads indicate PAX2+ cells in urethra or bladder epithelium. (N) Cell counts for PAX2+ and *Shh* lineage label+ cells in E18.5 urethra and bladder. (O) E18.5 male *Dnmt1*cKO lower urinary tract labeled with DNMT1 (red) and EYFP (green, labels *Shh* lineage cells). Long white arrow indicates path taken by Wolffian duct epithelial cells into the bladder. White dashed lines demarcate the epithelial-mesenchymal interface. DAPI staining is shown in blue. Graphical data are reported as mean ± SEM. Student's t-test NS: Not significant. Scale bar is 100 μm. Abbreviations Wd: Wolffian Duct, Ur: Urethra, Bl: Bladder.

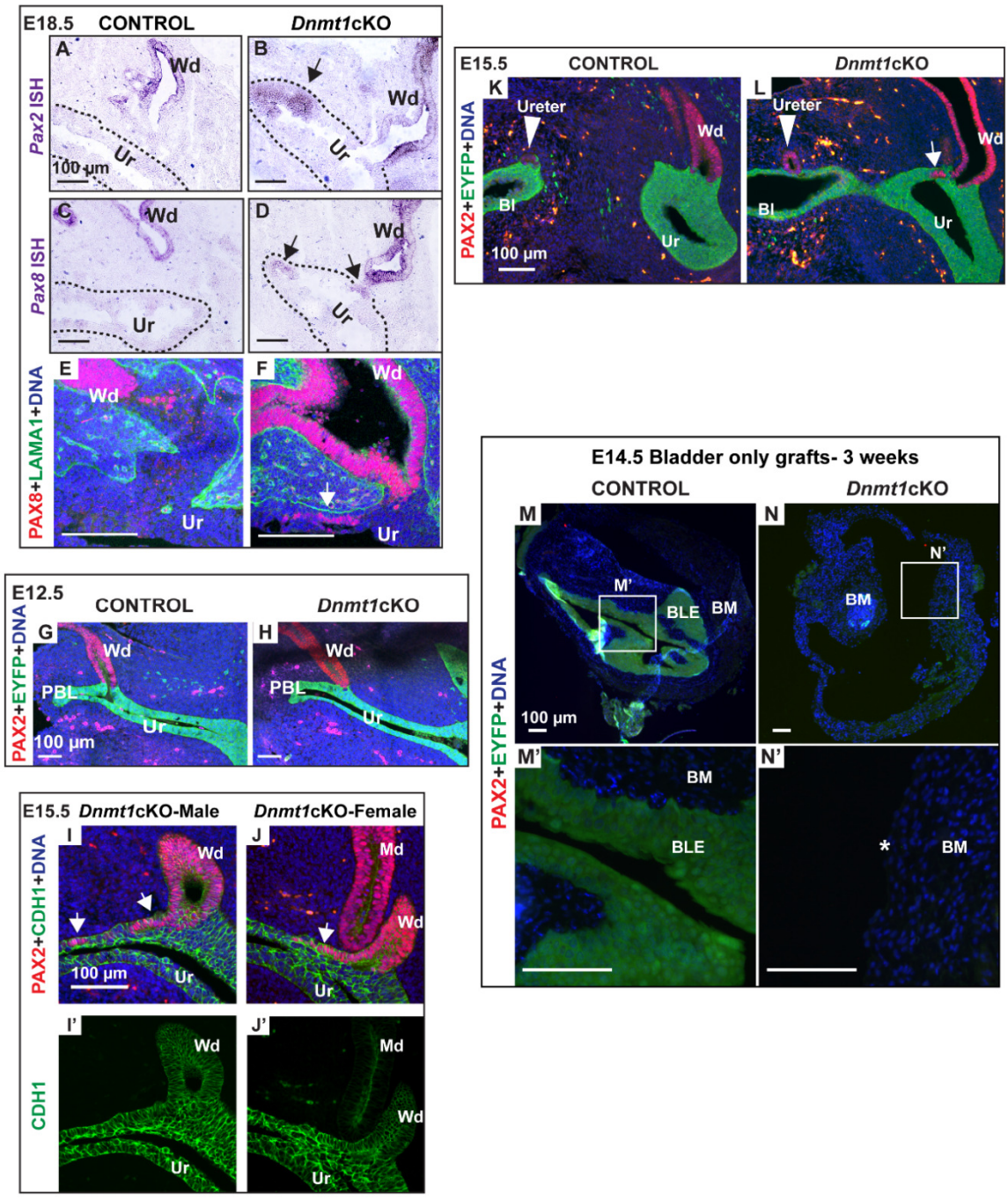

Figure S 2.2 Wolffian duct epithelium is the source of PAX2/PAX8+ cells in *Dnmt1*cKO urethra and bladder.

(A-D) *Pax2* and *Pax8* mRNA staining evaluated by *in situ* hybridization was undetectable in urethral sections from Control embryos but detected in *Dnmt1*cKO urethral epithelium

(indicated by black arrows). (E-F) E18.5 male urethral sections were labeled with antibodies against LAMA1 (green, marks basement membrane) and PAX8 (red, labels Wolffian duct epithelium). White arrows indicate PAX8+ cells in *Dnmt1*cKO urethral epithelium. (G-H) E12.5 male lower urinary tract sections were labeled with antibodies against PAX2 (red, labels Wolffian duct epithelium) and EYFP (green, *Shh* lineage label). There is no apparent persistent common nephric duct in *Dnmt1c*KO lower urinary tract. (I-J) E15.5 urethral sections from male and female *Dnmt1*cKO embryos labeled with PAX2 and CDH1 (green, labels epithelial cells). (I') and (J') represent (I) and (J) with green channel isolated. White arrows indicate PAX2+ cells in *Dnmt1*cKO urethral epithelium. (K-L) E15.5 male lower urinary tract sections were labeled with antibodies against PAX2 (red) and EYFP (green, *Shh* lineage label). White arrows indicate PAX2+ cells in *Dnmt1*cKO urethral epithelium. White arrowheads indicate location of ureters. (M-N) E14.5 control and *Dnmt1*cKO bladders were separated from Wolffian ducts and urethra and grafted under the renal capsule of athymic nude mice for 3 weeks. Tissue sections were labeled with antibodies against PAX2 (red) and EYFP (green, *Shh* lineage label). Boxed areas in (M) and (N) are magnified in (M') and (N'). Asterisk indicates absence of bladder epithelium. Dashed lines demarcate the epithelial-mesenchymal interface. DAPI staining is shown in blue. Scale bar is 100 μm. Abbreviations Wd: Wolffian Duct, Ur: Urethra, Bl: Bladder, PBL: Primitive bladder, Md: Müllerian duct, BLE: Bladder epithelium, BM: Bladder mesenchyme

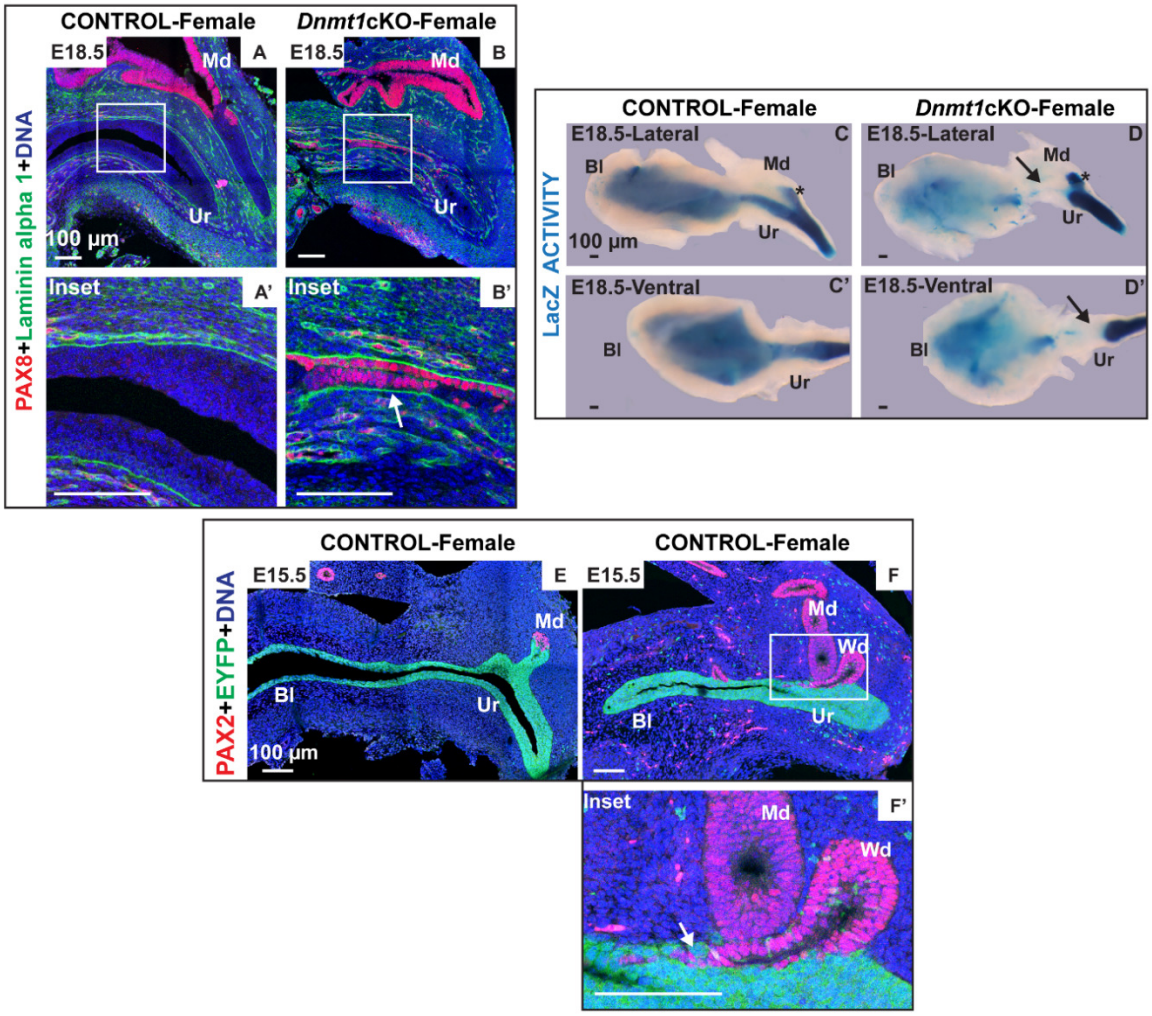

Figure S 2.3 Wolffian duct epithelium is the source of PAX2+, PAX8+ cells in *Dnmt1*cKO female urethra and bladder.

(A-B) E18.5 female lower urinary tracts were labeled with antibodies against PAX8 (red, labels Wolffian and Müllerian duct epithelium) and LAMA1 (green, basement membrane marker). Boxed areas are magnified in A' and B'. White arrows indicate PAX8+ cells invading female urethral epithelium. (C-D) Lateral views and (C'-D') ventral views of E18.5 female lower urinary tracts stained with X-Gal to reveal LacZ activity (blue) in *Shh* lineage cells. All control mouse bladder and urethral epithelial cells were LacZ+ but in

*Dnmt1*cKOs, a wedge of LacZ- cells (*Shh* lineage negative) spanned from the urethra through the bladder neck. Black arrows indicate regions lacking LacZ activity. Asterisks indicate the Sinus vagina, the endodermal region where the Müllerian ducts meet the urethra. (E-F) E15.5 female urogenital sinuses were immunolabeled with antibodies against PAX2 (red, labels Wolffian and Müllerian duct epithelium) and EYFP (green). Boxed areas in (F) are magnified in (F'). White arrows indicate Wolffian duct epithelial cells invading female urethral epithelium. DAPI staining is shown in blue. Scale bar is 100 μm. Abbreviations: Wd: Wolffian duct, Md: Müllerian duct, Ur: Urethra, Bl: Bladder

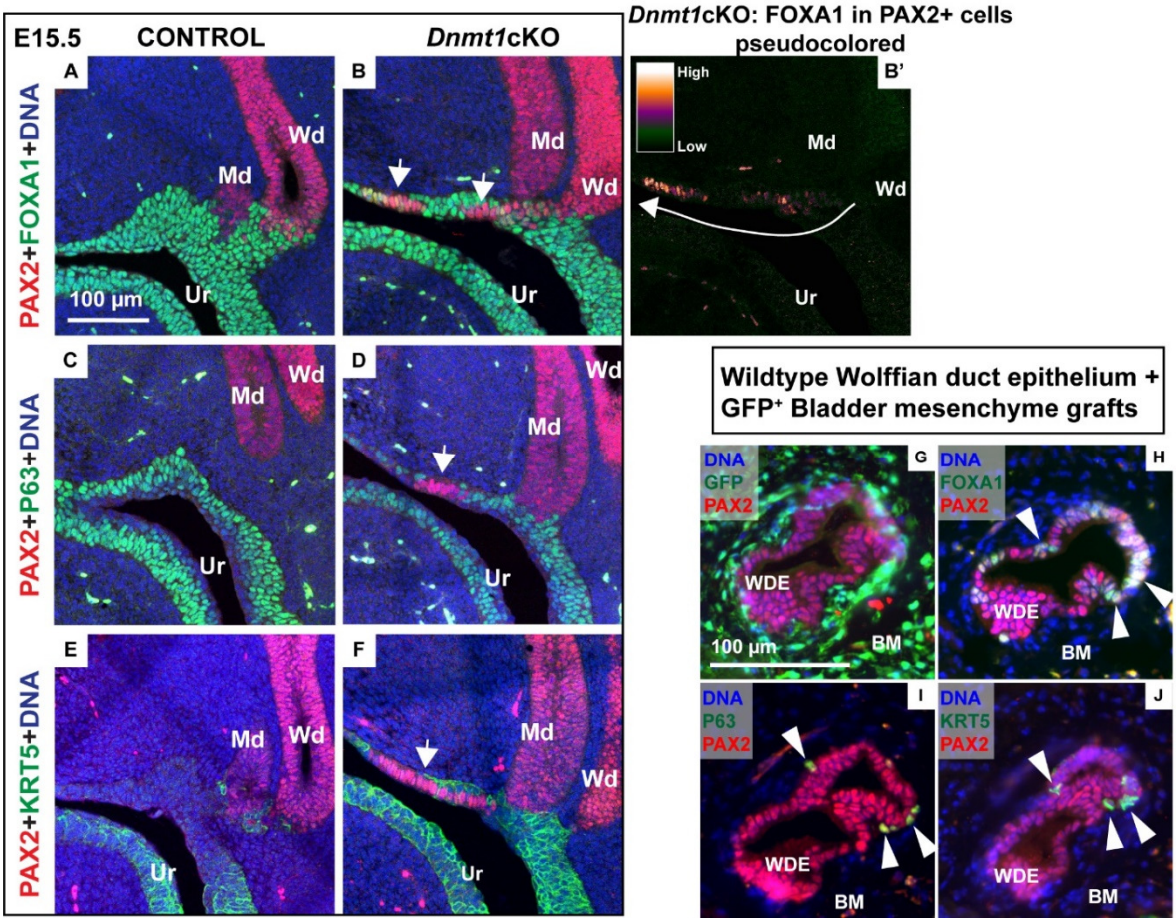

Figure S 2.4 At E15.5, Wolffian duct-derived epithelial cells acquire the endodermal marker FOXA1 but not P63 or Keratin 5; Wolffian duct epithelial reprogramming by bladder mesenchyme in tissue recombinants.

E15.5 male lower urinary tract sagittal sections were labeled with antibodies against (A-B) PAX2 (red, labels Wolffian duct epithelium) and FOXA1 (green, labels endoderm derived tissues) (B') Pixels with FOXA1 and PAX2 labeling were isolated and pseudo colored from (B) for assessing FOXA1 expression in invading Wolffian duct cells. (C-D) PAX2 (red) and P63 (green, labels basal epithelium) and (E-F) PAX2 (red) and KRT5 (green, labels basal epithelium). White arrows indicate PAX2+ cells in *Dnmt1*cKO urethra and bladder epithelia. Heterotypic tissue recombinants of isolated E14.5 wildtype Wolffian

duct epithelium and E14.5 GFP expressing bladder mesenchyme were grafted under the renal capsule of athymic nude. Tissue sections from 3-week old grafts were labeled with antibodies against (G) PAX2 (red) and GFP (green, expressed in bladder mesenchyme) (H) PAX2 (red) and FOXA1 (green) (I) PAX2 (red) and P63 (green) (J) PAX2 (red) and KRT5 (green) White arrowheads indicate PAX2+ cells that acquired FOXA1, P63 or KRT5. DAPI staining is shown in blue. Scale bar is 100 μm. Abbreviations Wd: Wolffian duct, Md: Müllerian, Ur: Urethra, WDE: Wolffian duct epithelium, BM: Bladder mesenchyme

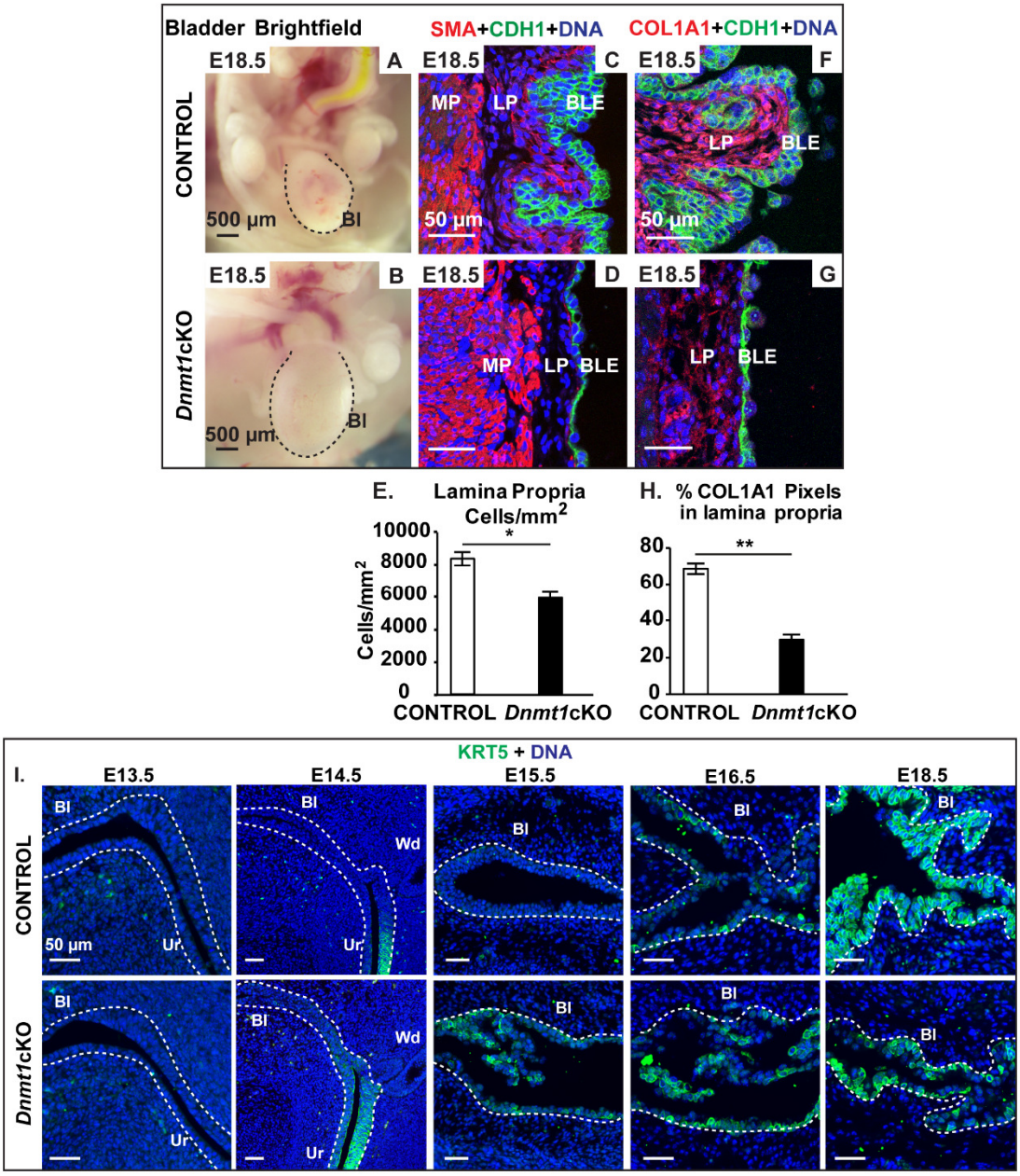

Figure S 2.5 *Dnmt1*cKO bladders are enlarged, display stromal defects and impaired epithelial differentiation.

(A-B) Brightfield microscope images of E18.5 male control and *Dnmt1*cKO bladders. Black dashed lines enclose the bladder. Scale bar is 500 µm. (C-D) E18.5 male bladders were labeled with antibodies against SMA (red, labels smooth muscle actin) and CDH1

(green, labels epithelial cells). Scale bar is 50 μm. (E) Lamina propria cell density quantified from images represented in (C) and (D). (F-G) E18.5 male bladders were labeled with antibodies against COL1A1 (red, labels Collagen 1a1) and CDH1 (green, labels epithelial cells). Scale bar is 50 μm. (H) COL1A1 staining intensity in the lamina propria quantified from images represented in (F) and (G) (I) Sections from E13.5-E18.5 bladders stained with KRT5 (green, basal epithelial marker). White dashed lines indicate the epithelial-mesenchymal interface. Scale bar is 50 μm. DAPI staining is shown in blue. Graphical data are reported as mean ± SEM. Student's t-test NS: Not significant. Abbreviations Wd: Wolffian duct, Ur: Urethra, Bl: Bladder, MP: Muscularis propria, LP: Lamina propria, BLE: Bladder Epithelium

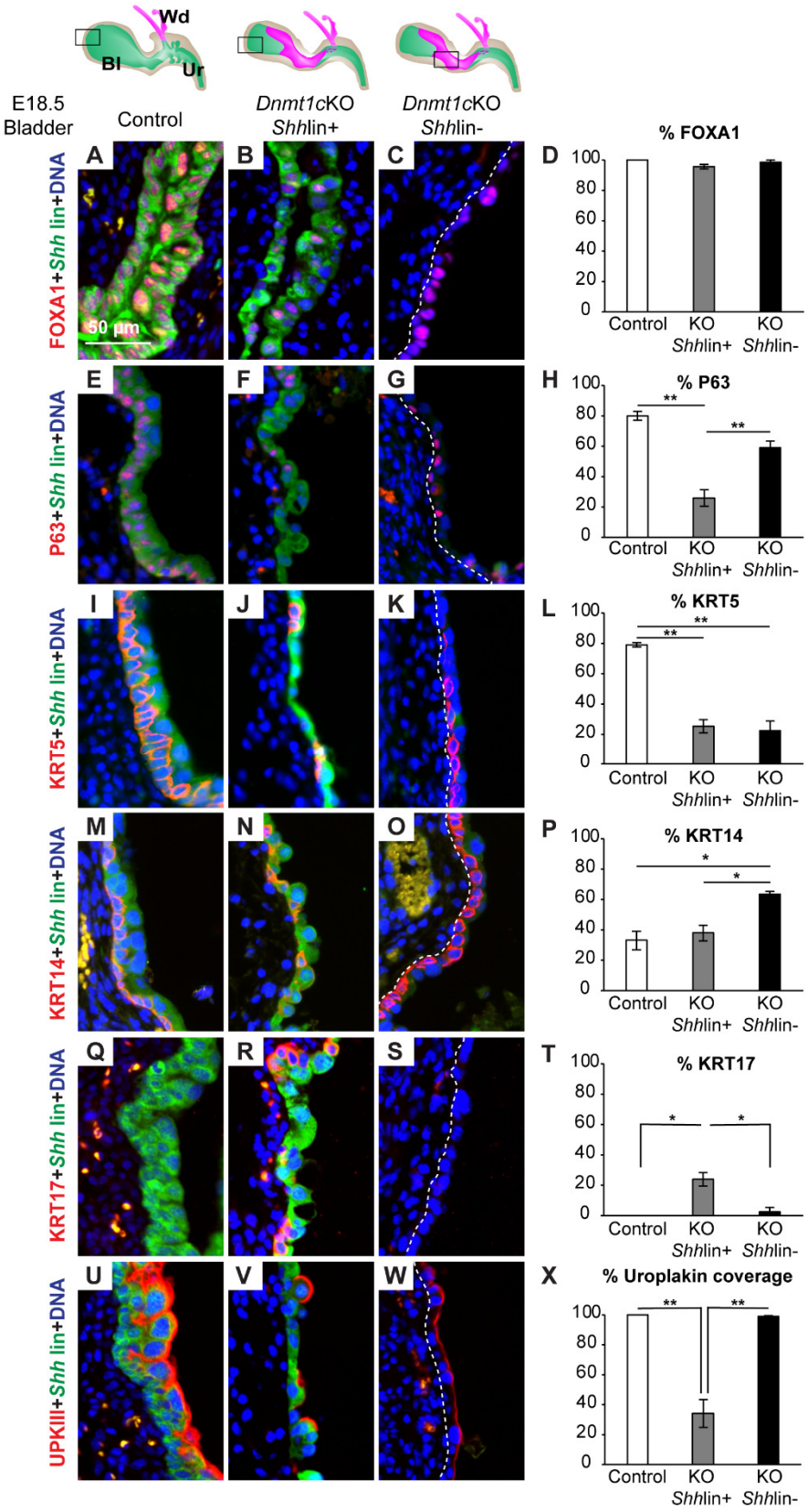
Wd
Bl
Ur
E18.5 Bladder
Control
Dnmt1cKO Shhlin+
Dnmt1cKO Shhlin-
FOXA1+Shh lin+DNA
P63+Shh lin+DNA
KRT5+Shh lin+DNA
KRT14+Shh lin+DNA
KRT17+Shh lin+DNA
UPKIII+Shh lin+DNA
A
B
C
D
E
F
G
H
I
J
K
L
M
N
O
P
Q
R
S
T
U
V
W
X
50 µm
% FOXA1
% P63
% KRT5
% KRT14
% KRT17
% Uroplakin coverage
100
80
60
40
20
0
**
*
Control
KO Shhlin+
KO Shhlin-

Figure S 2.6 Comparison of *Dnmt1* ablated bladder epithelium (*Shh* lineage positive) and invading Wolffian duct epithelial cells (*Shh* lineage negative) lining the bladder

Figures in a column depict region of interest depicted in diagram above it. E18.5 bladder sections were labeled with antibodies to *Shh* lineage label EYFP (green) and (A-C) FOXA1 (red) (D) Quantification of percentage FOXA1+ bladder epithelial cells (E-G) P63 (red) (H) Quantification of percentage P63+ bladder epithelial cells (I-K) KRT5 (red) (L) Quantification of percentage KRT5+ bladder epithelial cells (M-O) KRT14 (red) (P) Quantification of percentage KRT14+ bladder epithelial cells (Q-S) KRT17 (red) (T) Quantification of percentage KRT17+ bladder epithelial cells (U-W) UPKIII (red) (X) Percentage of bladder apical surface covered by Uroplakin **.** White dashed lines indicate the epithelial-mesenchymal interface. Scale bar is 50 μm. DAPI staining is shown in blue. Graphical data are reported as mean ± SEM. ANOVA * $p<0.05$, ** $p<0.01$, *** $p<0.001$. Abbreviations KO *Shh*lin+: *Dnmt1*cKO *Shh* lineage positive cells, KO *Shh*lin-: *Dnmt1*cKO *Shh* lineage negative cells.

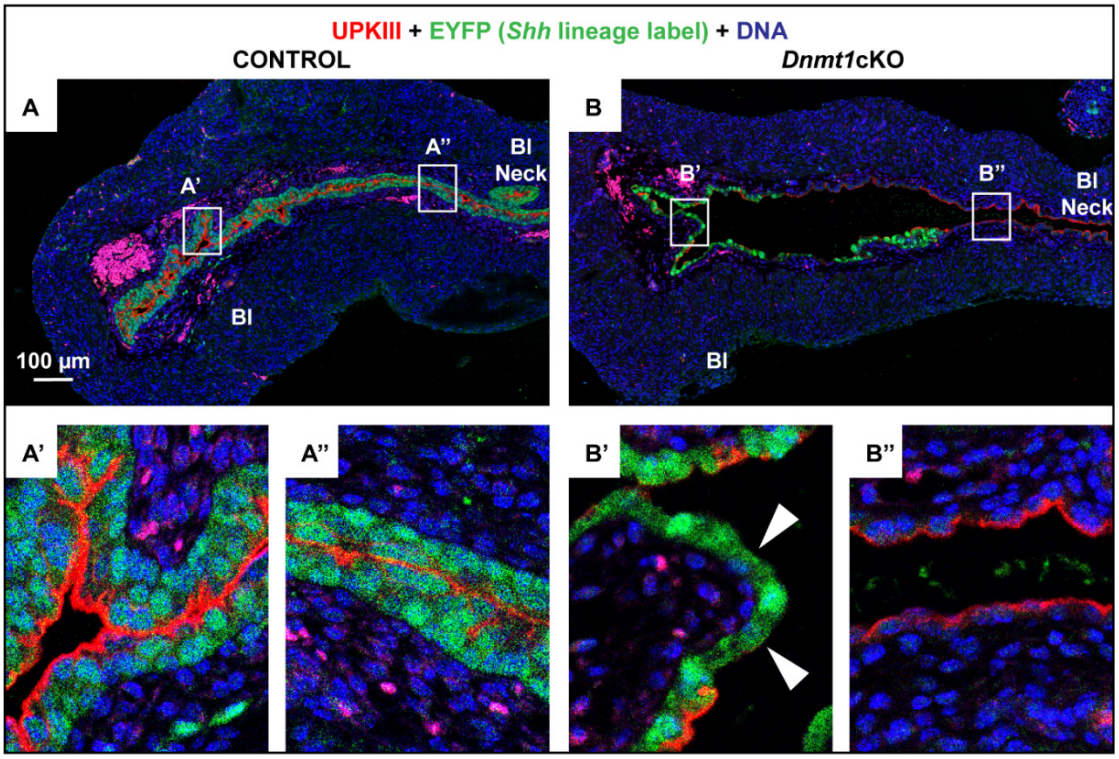

Figure S 2.7 *Dnmt1* ablated bladder epithelium (*Shh* lineage positive) has discontinuous Uroplakin barrier while invading Wolffian duct epithelial cells (*Shh* lineage negative) lining the bladder have continuous Uroplakin barrier

(A-B) E18.5 male bladder sagittal sections were labeled with antibodies against Uroplakin III (red, marks Uroplakin barrier) and EYFP (green, marks *Shh* lineage cells). Boxed areas in A and B are magnified in A', A'' and B', B''. White arrows indicate regions lacking Uroplakin III labeling. DAPI staining is shown in blue. Scale bar is 100 µm. Abbreviations Bl Neck: Bladder Neck, Bl: Bladder

A. PCA Score plot: E15.5 Bladder epithelium

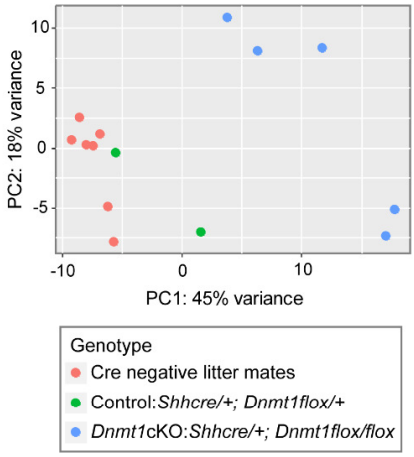

B. Summary of differential gene expression between genotypes

Comparison	Differentially expressed genes (FDR<0.1)	Upregulated	Downregulated
Dnmt1 cKO vs Control	n= 156	n= 100	n= 56
Dnmt1 cKO vs Cre negative	n= 846	n= 472	n= 374
Control vs Cre negative	n= 23	n= 15	n= 8

C. GO Terms enriched in differentially expressed genes upregulated in *Dnmt1*cKO versus Control

GO ID Biological Process	Category	FDR
GO:0007283	Spermatogenesis	3.76E-05
GO:0048232	Male gamete generation	3.76E-05
GO:0044702	Single organism reproductive process	4.82E-05
GO:0007276	Gamete generation	5.18E-05
GO:0022414	Reproductive process	9.11E-05
GO:0007126	Meiotic nuclear division	1.85E-04

D. Heatmap of selected Differentially expressed genes upregulated in *Dnmt1*cKO versus Control

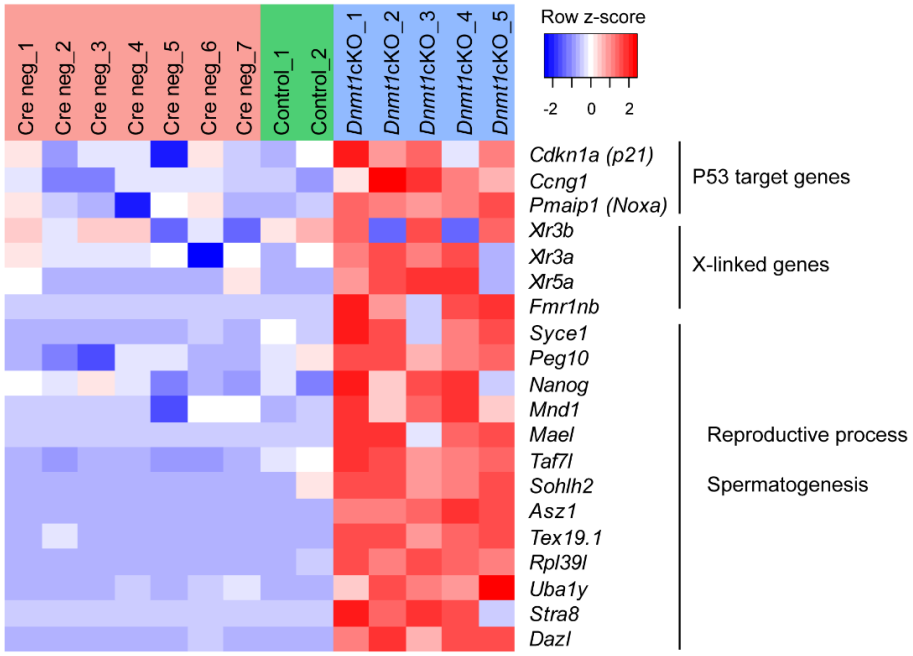

Figure S 2.8 RNA-Seq analysis shows upregulation of P53 target genes in E15.5 *Dnmt1*cKO bladder epithelium compared to Control bladder epithelium.

Isolated E15.5 bladder epithelia from Control and *Dnmt1*cKO embryos were used for RNA-seq analysis. (A) Principal components analysis of samples (B) Summary of differential gene expression between genotypes. (C) Biological processes enriched in upregulated genes from *Dnmt1*cKO bladder epithelium. (D) Heatmap of selected upregulated genes in *Dnmt1*cKO vs Control bladder epithelium. Abbreviations FDR: False Discovery Rate

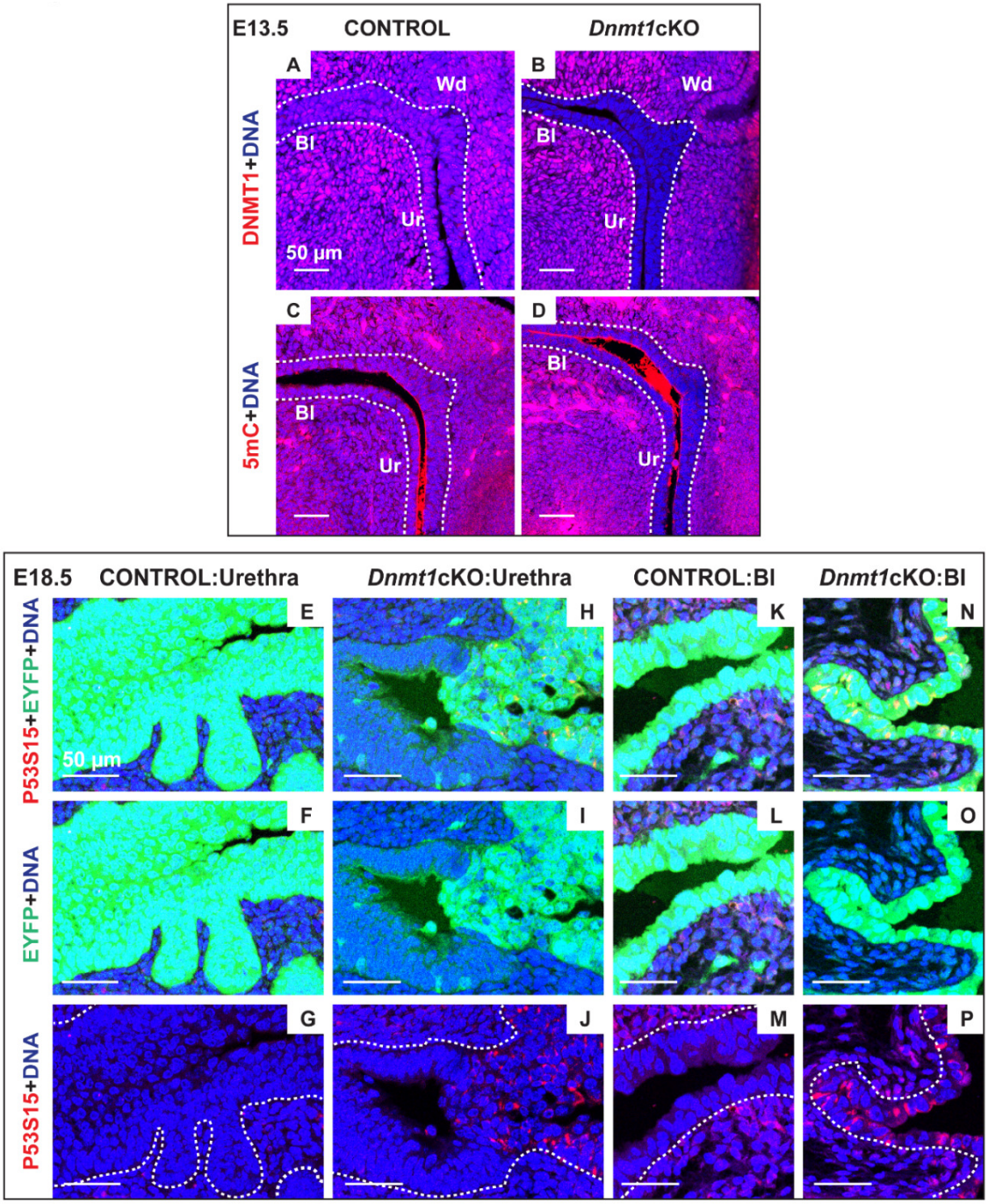

Figure S 2.9 P53 activation in *Dnmt1*cKO lower urinary tracts occurs specifically in DNMT1- *Shh* lineage cells and not invading DNMT1+ Wolffian duct epithelial cells.

E13.5 male lower urinary tracts were labeled with antibodies against (A-B) DNMT1 (red) or (C-D) 5-methylcytosine (red) (E-P) E18.5 male lower urinary tracts were labeled with

antibodies against Phospho-P53 Serine 15 (red, marker of activated P53) and EYFP (green, labels *Shh* lineage cells). P53 immunostaining is punctate (likely associated with mitochondria) and to aide visualization, green and red channels are overlaid in E, H, K, and N; the green channel is isolated in F, I, L, O, and the red channel is isolated in G, J, M, P. White dashed lines demarcate the epithelial-mesenchymal interface. DAPI staining is shown in blue. Scale bar is 50 μm. Abbreviations Ur: Urethra, Wd: Wolffian duct, Bl: Bladder.

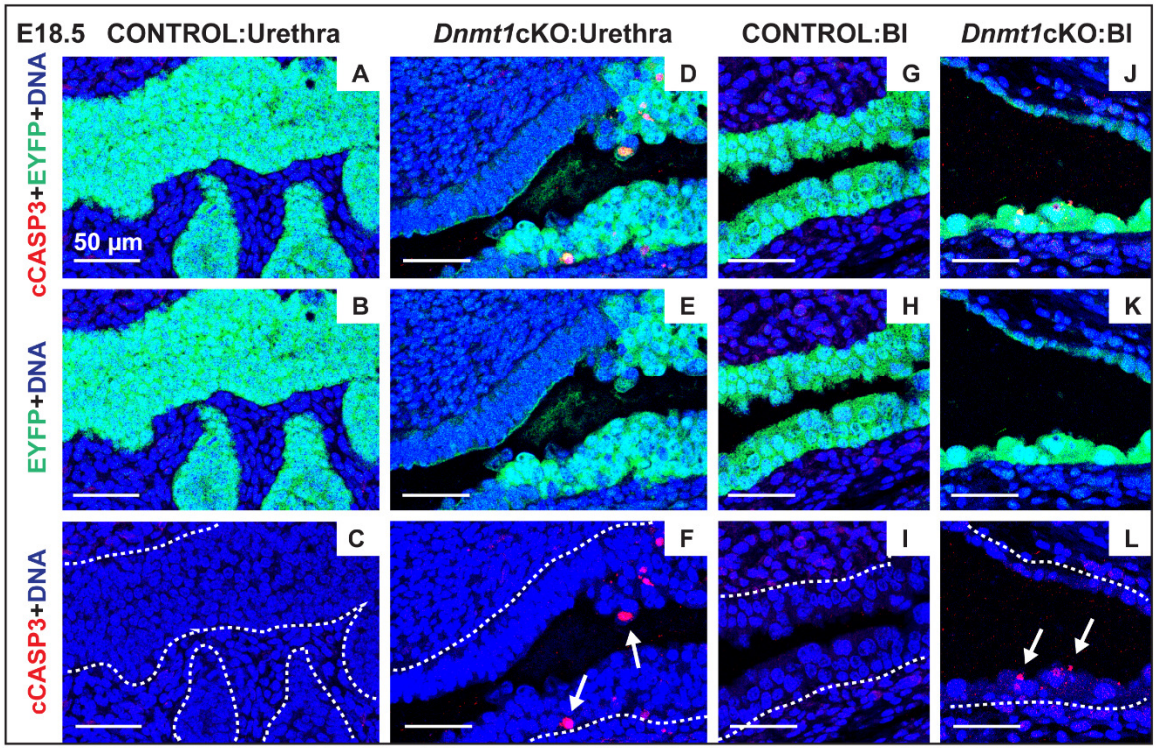

Figure S 2.10 Apoptosis in *Dnmt1*cKO lower urinary tracts occurs specifically in DNMT1- *Shh* lineage cells and not invading DNMT1+ Wolffian duct epithelial cells.

(A-L) E18.5 control and *Dnmt*1cKO male lower urinary tracts were labeled with antibodies against Cleaved Caspase 3 (red, apoptotic marker) and EYFP (green, *Shh* lineage label). Cleaved Caspase 3 staining is punctate and to aide visualization, green and red channels

are overlaid in A, D, G, and J; the green channel is isolated in B, E, H, K, and the red channel is isolated in C, F, I, L. Dashed white lines demarcate the epithelial-mesenchymal interface. White arrows indicate cleaved Caspase 3 positive cells. DAPI staining is shown in blue. Scale bar is 50 μm. Ur: Urethra, Bl: Bladder.

Table 2.1 Reagents and resources

Reagent or Resource	Source/Reference	Identifier
Antibodies		
Mouse monoclonal anti-5 methyl cytosine	Abcam	Cat#ab10805; RRID:AB_442823
Mouse monoclonal anti-CDH1	BD Transduction Labs	Cat#610181; RRID:AB_397580
Rabbit monoclonal anti-CDH1	Cell Signaling	Cat#3195S
Rabbit monoclonal anti-Cleaved Casp3 (Asp 175)	Cell Signaling	Cat#9664; RRID:AB_2070042
Mouse monoclonal anti-COL1A1	Novus Biologicals	Cat#NB600-450; RRID:AB_10124390
Rabbit monoclonal anti-DNMT1	Cell Signaling	Cat#D63A6; RRID:AB_10828695
Mouse monoclonal anti-FOXA1	Millipore	Cat#05-1466; RRID:AB_1977191
Chicken polyclonal anti-GFP	Abcam	Cat#ab13970; RRID:AB_300798
Rabbit polyclonal anti-GFP	Rockland Immunochemicals	Cat# 600-401-215, RRID:AB_828167
Rabbit polyclonal anti-Histone H2AX (phospho Ser139)	Cell Signaling	Cat#2577; RRID:AB_2118011
Chicken polyclonal anti-KRT5	Biolegend	Cat#905901; AB_2565054
Mouse monoclonal anti-KRT14	Thermo Fisher Scientific	Cat# MS-115-P0, RRID:AB_63786
Rabbit monoclonal anti-KRT17	Abcam	Cat#ab109725; RRID:AB_10889888
Chicken polyclonal anti-LacZ	Abcam	Cat# ab9361, RRID:AB_307210
Rabbit polyclonal anti-Laminin	Sigma	Cat#L9393-.2ml; RRID:AB_477163
Mouse monoclonal anti-P53 (phospho Ser15) 16G8	Cell Signaling	Cat#9286; RRID:AB_331741
Mouse monoclonal anti-P63	Biocare Medical	Cat#CM163A; RRID:AB_10582730
Rabbit polyclonal anti-PAX2	Covance	Cat#PRB-276P-200; RRID:AB_291611
Mouse monoclonal anti-PAX8	Thermo Fisher Scientific	Cat# MA1-117; RRID:AB_2536828
Mouse monoclonal anti-Smooth muscle actin alpha	Leica	Cat#ncl-sma; RRID:AB_442134

Rabbit polyclonal anti-UPK (pan)	Tung-Tien Sun, New York University	
Mouse monoclonal anti-UPKIII	Fitzgerald Industries International	Cat# 10R-U103a, RRID:AB_1289312
Goat polyclonal anti-Chicken Alexa488 conjugated	Jackson Immunoresearch	Cat#103-545-155; RRID:AB_2337390
Goat polyclonal anti-Mouse Alexa488 conjugated	Jackson Immunoresearch	Cat# 115-547-003; RRID:AB_2338869
Goat polyclonal anti-Rabbit Alexa488 conjugated	Jackson Immunoresearch	Cat# 111-547-003; RRID:AB_2338058
Goat polyclonal anti-Mouse Alexa594 conjugated	Jackson Immunoresearch	Cat# 115-585-062; RRID:AB_2338876
Goat polyclonal anti-Rabbit Alexa594 conjugated	Jackson Immunoresearch	Cat# 111-586-045; RRID:AB_2338067
Sheep polyclonal anti-Digoxygenin Alkaline phosphatase conjugated	Roche	Cat#11093274910; RRID:AB_514497
Experimental Models: Organisms/Strains		
Mouse: B6.129S4-*Dnmt1*$^{tm2Jae/Mmucd}$	MMRRC, UC Davis	Stock#014114-UCD; RRID:MMRRC_014114-UCD
Mouse: B6.Cg*Shh*$^{tm1(EGFP/cre)Cjt/J}$	Jackson Laboratory	Stock#005622; RRID:IMSR_JAX:005622
Mouse: B6;129S4-*Gt(ROSA)26*$^{Sortm1Sor/J}$	Jackson Laboratory	Stock#003309; RRID:IMSR_JAX:003309
Mouse: B6.129X1-*Gt(ROSA)26*$^{Sortm1(EYFP)Cos/J}$	Jackson Laboratory	Stock#006148; RRID:IMSR_JAX:006148
Mouse: CD-1 IGS mouse (wildtype)	Charles Rives	Stock#022
Mouse: C57BL/6-Tg(UBC-GFP)30Scha/J	Jackson Laboratory	Stock#004353, RRID:IMSR_JAX:004353
Mouse: Athymic nude nu/nu	Jackson Laboratory	Stock#002019
Sequence-Based Reagents		
Mouse *Pax2* ISH probe Forward primer 5'-TGGAGACTCCCAGAGTGGTG-3'	This paper	N/A
Mouse *Pax2* ISH probe Reverse primer 5'-CGATGTTAATACGACTCACTATAGGGCCTGAAGC TTGATGTGGTC-3' (T7 binding site underlined)	This paper	N/A
Mouse *Pax8* ISH probe Forward primer 5'-CCCAGAGAGTCACACAAAGG-3'	This paper	N/A
Mouse *Pax8* ISH probe Reverse primer 5'-CGATGTTAATA CGACTCACTATAGGGGGTAGCCACTGG TTGAGAGG-3' (T7 binding site underlined)	This paper	N/A
Pax2 ISH probe binding site	This paper	NM_011037.4
Pax8 ISH probe binding site	This paper	NM_011040.4
Software and Algorithms		
ImageJ	imagej.nih.gov	Version 1.51k
R for Windows	cran.r-project.org	Version 3.2.4

Adobe Illustrator	adobe.com	CC2017
Adobe Photoshop	adobe.com	CC2017
Deposited Sequence data		
RNA-Seq data (14 samples) deposited in Gene Expression Omnibus (GEO)	This paper	GEO Accession: GSE115477

2.6. References

Abler, L.L., Keil, K.P., Mehta, V., Joshi, P.S., Schmitz, C.T., Vezina, C.M., 2011a. A high-resolution molecular atlas of the fetal mouse lower urogenital tract. Dev. Dyn. 240, 2364-2377.

Abler, L.L., Mehta, V., Keil, K.P., Joshi, P.S., Flucus, C.L., Hardin, H.A., Schmitz, C.T., Vezina, C.M., 2011b. A high throughput in situ hybridization method to characterize mRNA expression patterns in the fetal mouse lower urogenital tract. J Vis Exp.

Anumanthan, G., Makari, J.H., Honea, L., Thomas, J.C., Wills, M.L., Bhowmick, N.A., Adams, M.C., Hayward, S.W., Matusik, R.J., Brock, J.W., 3rd, Pope, J.C.t., 2008. Directed differentiation of bone marrow derived mesenchymal stem cells into bladder urothelium. J. Urol. 180, 1778-1783.

Batourina, E., Tsai, S., Lambert, S., Sprenkle, P., Viana, R., Dutta, S., Hensle, T., Wang, F., Niederreither, K., McMahon, A.P., Carroll, T.J., Mendelsohn, C.L., 2005. Apoptosis induced by vitamin A signaling is crucial for connecting the ureters to the bladder. Nat. Genet. 37, 1082-1089.

Bouchard, M., Souabni, A., Mandler, M., Neubuser, A., Busslinger, M., 2002. Nephric lineage specification by Pax2 and Pax8. Genes Dev. 16, 2958-2970.

Cheng, T.C., Wallace, M.C., Merlie, J.P., Olson, E.N., 1993. Separable regulatory elements governing myogenin transcription in mouse embryogenesis. Science 261, 215-218.

Chia, I., Grote, D., Marcotte, M., Batourina, E., Mendelsohn, C., Bouchard, M., 2011. Nephric duct insertion is a crucial step in urinary tract maturation that is regulated by a Gata3-Raldh2-Ret molecular network in mice. Development 138, 2089-2097.

Cunha, G.R., Baskin, L., 2016. Mesenchymal-epithelial interaction techniques. Differentiation 91, 20-27.

Elliott, E.N., Sheaffer, K.L., Schug, J., Stappenbeck, T.S., Kaestner, K.H., 2015. Dnmt1 is essential to maintain progenitors in the perinatal intestinal epithelium. Development 142, 2163-2172.

Ford, T.F., Watson, G.M., Cameron, K.M., 1985. Adenomatous metaplasia (nephrogenic adenoma) of urothelium. An analysis of 70 cases. Br. J. Urol. 57, 427-433.

Gandhi, D., 2013. Retinoid-signaling in progenitors controls specification and regeneration of the urothelium. 26, 469-482.

Georgas, K.M., Armstrong, J., Keast, J.R., Larkins, C.E., McHugh, K.M., Southard-Smith, E.M., Cohn, M.J., Batourina, E., Dan, H., Schneider, K., Buehler, D.P., Wiese, C.B., Brennan, J., Davies, J.A., Harding, S.D., Baldock, R.A., Little, M.H., Vezina, C.M., Mendelsohn, C., 2015. An illustrated anatomical ontology of the developing mouse lower urogenital tract. Development 142, 1893-1908.

Georgia, S., Kanji, M., Bhushan, A., 2013. DNMT1 represses p53 to maintain progenitor cell survival during pancreatic organogenesis. Genes Dev. 27, 372-377.

Guo, C., Balsara, Z.R., Hill, W.G., Li, X., 2017. Stage- and subunit-specific functions of polycomb repressive complex 2 in bladder urothelial formation and regeneration. Development 144, 400-408.

Harfe, B.D., Scherz, P.J., Nissim, S., Tian, H., McMahon, A.P., Tabin, C.J., 2004. Evidence for an expansion-based temporal Shh gradient in specifying vertebrate digit identities. Cell 118, 517-528.

Hou, Z., Jiang, P., Swanson, S.A., Elwell, A.L., Nguyen, B.K., Bolin, J.M., Stewart, R., Thomson, J.A., 2015. A cost-effective RNA sequencing protocol for large-scale gene expression studies. Sci. Rep. 5, 9570.

Jackson-Grusby, L., Beard, C., Possemato, R., Tudor, M., Fambrough, D., Csankovszki, G., Dausman, J., Lee, P., Wilson, C., Lander, E., Jaenisch, R., 2001. Loss of genomic methylation causes p53-dependent apoptosis and epigenetic deregulation. Nat. Genet. 27, 31-39.

Keil, K.P., Altmann, H.M., Mehta, V., Abler, L.L., Elton, E.A., Vezina, C.M., 2013. Catalog of mRNA expression patterns for DNA methylating and demethylating genes in developing mouse lower urinary tract. Gene Expr Patterns 13, 413-424.

Keil, K.P., Mehta, V., Abler, L.L., Joshi, P.S., Schmitz, C.T., Vezina, C.M., 2012. Visualization and quantification of mouse prostate development by in situ hybridization. Differentiation 84, 232-239.

Khandelwal, P., Abraham, S.N., Apodaca, G., 2009. Cell biology and physiology of the uroepithelium. Am. J. Physiol. Renal Physiol. 297, F1477-1501.

Kim, B., Kim, Y., Sakuma, R., Hui, C.-C., Rüther, U., Jorgensen, J.S., 2011. Primordial germ cell proliferation is impaired in Fused Toes mutant embryos. Dev. Biol. 349, 417-426.

Langmead, B., Trapnell, C., Pop, M., Salzberg, S.L., 2009. Ultrafast and memory-efficient alignment of short DNA sequences to the human genome. Genome Biol. 10, R25.

Li, B., Dewey, C.N., 2011. RSEM: accurate transcript quantification from RNA-Seq data with or without a reference genome. BMC Bioinformatics 12, 323.

Lin, H.K., Madihally, S.V., Palmer, B., Frimberger, D., Fung, K.M., Kropp, B.P., 2015. Biomatrices for bladder reconstruction. Adv Drug Deliv Rev 82-83, 47-63.

Love, M.I., Huber, W., Anders, S., 2014. Moderated estimation of fold change and dispersion for RNA-seq data with DESeq2. Genome Biol. 15, 550.

Mazal, P.R., Schaufler, R., Altenhuber-Muller, R., Haitel, A., Watschinger, B., Kratzik, C., Krupitza, G., Regele, H., Meisl, F.T., Zechner, O., Kerjaschki, D., Susani, M., 2002. Derivation of nephrogenic adenomas from renal tubular cells in kidney-transplant recipients. N. Engl. J. Med. 347, 653-659.

Mehta, V., Abler, L.L., Keil, K.P., Schmitz, C.T., Joshi, P.S., Vezina, C.M., 2011. Atlas of Wnt and R-spondin gene expression in the developing male mouse lower urogenital tract. Dev. Dyn. 240, 2548-2560.

Mehta, V., Schmitz, C.T., Keil, K.P., Joshi, P.S., Abler, L.L., Lin, T.M., Taketo, M.M., Sun, X., Vezina, C.M., 2013. Beta-catenin (CTNNB1) induces Bmp expression in urogenital sinus epithelium and participates in prostatic bud initiation and patterning. Dev. Biol. 376, 125-135.

N'Dow, J., Robson, C.N., Matthews, J.N., Neal, D.E., Pearson, J.P., 2001. Reducing mucus production after urinary reconstruction: a prospective randomized trial. J. Urol. 165, 1433-1440.

Nasonkin, I.O., Merbs, S.L., Lazo, K., Oliver, V.F., Brooks, M., Patel, K., Enke, R.A., Nellissery, J., Jamrich, M., Le, Y.Z., Bharti, K., Fariss, R.N., Rachel, R.A., Zack, D.J., Rodriguez-Boulan, E.J., Swaroop, A., 2013. Conditional knockdown of DNA methyltransferase 1 reveals a key role of retinal pigment epithelium integrity in photoreceptor outer segment morphogenesis. Development 140, 1330-1341.

Oottamasathien, S., Williams, K., Franco, O.E., Thomas, J.C., Saba, K., Bhowmick, N.A., Staack, A., Demarco, R.T., Brock, J.W., 3rd, Hayward, S.W., Pope, J.C.t., 2006. Bladder tissue formation from cultured bladder urothelium. Dev. Dyn. 235, 2795-2801.

Papafotiou, G., Paraskevopoulou, V., Vasilaki, E., Kanaki, Z., Paschalidis, N., Klinakis, A., 2016. KRT14 marks a subpopulation of bladder basal cells with pivotal role in regeneration and tumorigenesis. Nature communications 7, 11914.

Pina-Oviedo, S., Shen, S.S., Truong, L.D., Ayala, A.G., Ro, J.Y., 2013. Flat pattern of nephrogenic adenoma: previously unrecognized pattern unveiled using PAX2 and PAX8 immunohistochemistry. Mod. Pathol. 26, 792-798.

Seifert, A.W., Harfe, B.D., Cohn, M.J., 2008. Cell lineage analysis demonstrates an endodermal origin of the distal urethra and perineum. Dev. Biol. 318, 143-152.

Sen, G.L., Reuter, J.A., Webster, D.E., Zhu, L., Khavari, P.A., 2010. DNMT1 maintains progenitor function in self-renewing somatic tissue. Nature 463, 563-567.

Shin, K., Lee, J., Guo, N., Kim, J., Lim, A., Qu, L., Mysorekar, I.U., Beachy, P.A., 2011. Hedgehog/Wnt feedback supports regenerative proliferation of epithelial stem cells in bladder. Nature 472, 110.

Soriano, P., 1999. Generalized lacZ expression with the ROSA26 Cre reporter strain. Nat. Genet. 21, 70-71.

Srinivas, S., Watanabe, T., Lin, C.-S., William, C.M., Tanabe, Y., Jessell, T.M., Costantini, F., 2001. Cre reporter strains produced by targeted insertion of EYFP and ECFP into the ROSA26 locus. BMC Dev. Biol. 1, 4-4.

Vezina, C.M., 2018. GUDMAP Consortium https://doi.org/10.25548/W-QXXC.

Wang, J., Vasaikar, S., Shi, Z., Greer, M., Zhang, B., 2017. WebGestalt 2017: a more comprehensive, powerful, flexible and interactive gene set enrichment analysis toolkit. Nucleic Acids Res. 45, W130-W137.

CHAPTER 3. EPITHELIAL DNA METHYLTRANSFERASE-1 REGULATES CELL SURVIVAL, GROWTH AND MATURATION IN DEVELOPING PROSTATIC BUDS

Adapted from **Diya B Joseph**, Anoop S Chandrashekar, Lisa L Abler, Li-Fang Chu, James A Thomson and Chad M Vezina

(Manuscript under review at Developmental Biology)

3.1. Introduction

Prostatic buds arise from the urethral epithelium in response to androgen signaling in adjacent mesenchyme. Coordinated epithelial-mesenchymal interactions guide morphogenesis in the developing prostate as in other budding organ systems. While morphogens, growth factors and their receptors have been a major focus of mechanistic studies, few studies have examined how epigenetic processes engage in morphogenesis. DNA methyltransferase-1 (DNMT1) carries out cytosine methylation of unmethylated daughter strands in newly replicated DNA (Monk et al., 1987; Reik et al., 2001). *Dnmt1* knockout mice die at mid-gestation, highlighting a critical role in early embryonic development (Li et al., 1992). We previously reported that *Dnmt1* expression domains change synchronously with prostatic bud specification and initiation. *Dnmt1* expression is widespread in urethral epithelium and stroma prior to bud formation at E16.5 and restricts to highly proliferative basal epithelial cells during prostatic bud specification and initiation (Keil et al., 2013). DNA methylation regulates prostate morphogenesis through diverse molecular processes including epithelial adhesion and androgen receptor signaling. We found that DNA methylation decreases prior to prostatic bud initiation at the androgen receptor (*Ar*) locus and increases during prostatic bud outgrowth at the E-cadherin (*Cdh1*) locus. By selectively inhibiting DNA methylation with the DNMT1 inhibitor 5-aza-2'-deoxycytidine (5AzadC) at key developmental stages, we either increased *Ar* abundance and accelerated prostatic bud formation or increased *Cdh1* abundance and interfered with bud outgrowth (Keil et al., 2014a; Keil et al., 2014b).

Our previous findings revealed essential roles of DNA methylation in prostatic bud morphogenesis, but we did not pinpoint whether prostatic bud formation requires DNMT1

in the mesenchyme or epithelium because it was not possible to deliver 5AzadC in a cell-specific manner. We were also unable to examine the requirement for DNMT1 *in vivo* because 5AzadC is a lethal teratogen (Bulut et al., 1999) which interacts non-specifically with other epigenetic processes (Wozniak et al., 2007), and interferes with testicular development and androgen synthesis (Choi et al., 2013; Cisneros and Branch, 2003).

To circumvent limitations of pharmacological DNMT1 inhibition, we employed targeted genetic approaches to delete *Dnmt1* in the urethral epithelium that gives rise to prostatic buds. Targeted genetic approaches have been used previously to interrogate the role of DNMT1 in the developing bladder (Joseph et al., 2018), intestine (Elliott et al., 2015), retina (Nasonkin et al., 2013) and pancreas (Georgia et al., 2013), but the prostate has not been studied in this context. We used a *Shhcre* driver (Harfe et al., 2004) to conditionally delete *Dnmt1* across urethral epithelium from which prostatic buds emerge (c*Dnmt1*KOs) and discovered that DNMT1 is required for prostatic bud formation and elongation and maintains urethral epithelial cell integrity, cell cycle progression and survival. DNMT1 depleted cells undergo G2/M cell cycle arrest and apoptosis. c*Dnmt1*KO urethras, rescued from embryos and grafted under the kidney capsule for continued development, are devoid of mature prostate glands. These findings establish a critical role for DNMT1 in regulating prostate budding by maintaining survival of urethral epithelial cells from which prostate buds emerge.

The exact identity of urethral epithelial cells that give rise to prostate buds remains unclear. It was initially believed that a single urethral epithelial cell type, characterized by expression of basal epithelial cell markers KRT14 and TRP63, gave rise to prostatic bud and ductal epithelium (Kurita et al., 2004; Signoretti and Loda, 2006; Signoretti et al.,

2005). Recent results indicate these factors are not ubiquitous across the prostatic bud. KRT14 and TRP63 are more abundant in epithelial cells of the lateral and distal portions of prostatic buds (margin cells) than inner (core) prostatic bud epithelial cells (Abler et al., 2011a; Mehta et al., 2013). Whether molecular differences extend to functional or physiological differences between prostatic bud epithelial cell populations has not been examined. A greater understanding of these molecular differences and how it is established could resolve which developmental processes (oriented cell division, convergent extension, collective cell migration, epithelial-to-mesenchymal cell transition) underlie prostatic bud elongation. In this study, we show that prostatic bud epithelial cells divide parallel and perpendicular to the bud axis to elongate and widen prostatic buds.

Having demonstrated oriented cell division in prostatic buds and the requirement for DNMT1 in cell survival, we leveraged our new findings to pinpoint the contribution of cell proliferation to prostate bud elongation. Specifically, we used *Dnmt1* deletion as tool to determine whether DNA methylation-dependent cell proliferation is equally required in all epithelial cells within the prostate bud. The approach involved a *Shh*^{creErt2} driver to achieve *Dnmt1* inactivation in a subset (mosaic) of urethral epithelium (i*Dnmt1*LOFs). Though prostatic bud development proceeds normally in i*Dnmt1*LOF mice, DNMT1- cells are not randomly distributed in prostate buds. Replication competent DNMT1+ cells accumulate preferentially in prostatic bud margins and tips while DNMT1- replication impeded cells are excluded from bud margins and tips, accumulating instead in prostatic bud cores. These results are consistent with differing cell proliferation requirements in prostatic bud margin versus core epithelial cells and allow for the possibility that prostatic bud core cells arise from a non-proliferative mechanism such as cell migration.

3.2. Materials and Methods

Animals

Mice were housed as previously described (Mehta et al., 2011). All procedures performed on mice were approved by the University of Wisconsin-Madison Animal Care and Use Committee and were carried out in accordance with the Guide for the Care and Use of Laboratory Animals. All embryos used in this study were obtained from timed matings. Mice carrying the *Dnmt1Flox* allele (B6.129S4-*Dnmt1*$^{tm2Jae/Mmucd}$) were from the Mutant Mouse Research and Resource Centers at the University of California, Davis (MMRRC, 014114-UCD). Genotyping for the *Dnmt1Flox* allele was carried out as described previously (Jackson-Grusby et al., 2001). Mice carrying the *Shh*^{creErt2} allele (B6.129S6-*Shh*$^{tm2(cre/ERT2)Cjt/J}$, The Jackson Laboratory, 005623) and the *Shhcre* allele (B6.Cg-*Shh*$^{tm1(EGFP/cre)Cjt/J}$, The Jackson Laboratory, 005622) were genotyped as described previously (Harfe et al., 2004; Mehta et al., 2013). Mice carrying the Cre inducible *R26R-LacZ* reporter allele (B6;129S4-*Gt(ROSA)26*$^{Sortm1Sor/J}$, The Jackson Laboratory, 003309) were genotyped as described previously (Soriano, 1999). Mice carrying the *R26R-EYFP* reporter allele (B6.129X1-*Gt(ROSA)26*$^{Sortm1(EYFP)Cos/J}$, The Jackson Laboratory, 006148) were genotyped as previously described (Srinivas et al., 2001). *Dnmt1Flox* mice were bred to mice carrying either the *R26R-LacZ* or *R26R-EYFP* alleles to obtain *Dnmt1Flox/Flox; R26R/R26R* females. These females were used for timed matings with *Shhcre/+; Dnmt1Flox/+* or *ShhcreErt2/+; Dnmt1Flox/+* males. Dams were euthanized by CO_2 asphyxiation to harvest embryos. Of the resulting male offspring, *cre/+; Dnmt1Flox/+; R26R/+* embryos were used as controls and compared to litter mates of the genotype

cre/+; Dnmt1Flox/Flox; R26R/+. Wildtype C57Bl6/J or CD-1 mice were obtained from the Jackson laboratory or Charles River laboratories respectively.

Tamoxifen administration

Pregnant dams were dosed intra-peritoneally with sterile corn oil (2.5 ml/kg) containing 10% ethanol, tamoxifen (200 mg/kg mouse weight, Sigma #T56482, St. Louis MO) and progesterone (75 mg/kg mouse weight, Watson #NDC0591-3128-79, Corona CA) on embryonic day 9.5 to activate Cre recombinase in embryos carrying the $Shh^{creErt2}$ allele. Dams were euthanized by CO_2 asphyxiation and embryos were collected at embryonic day 18.5.

Renal grafting

Embryonic day 18.5 urogenital sinuses were placed under the renal capsule of 6-12 week intact male athymic *nu/nu* mice (The Jackson Laboratory, 002019). Grafts were grown for 1 month before tissues were collected.

Fluorescent Immunohistochemistry

Fluorescent immunohistochemistry was performed as described previously (Abler et al., 2011a). Dissected tissues were fixed overnight in 4% paraformaldehyde and processed to obtain paraffin sections. 5 µm paraffin sections were deparaffinized in xylene and hydrated through a series of ethanol washes. Heat mediated antigen retrieval was performed by boiling slides in 10 mM sodium citrate (pH 6.0) for 20 mins in a conventional microwave oven. Tissues were washed with a solution containing 25 mM Tris-HCl, pH 7.5, 140 mM NaCl, 2.7 mM KCl, and 0.1% Tween-20 (TBSTw) and non-specific binding sites were blocked for 1 hr in TBSTw containing 1% Blocking Reagent (Roche

Diagnostics, Indianapolis, IN), 5% normal goat sera, and 1% bovine serum albumin fraction 5 (RGBTw). Tissues were incubated overnight at 4^0C with primary antibodies diluted in RGBTw. Following primary antibody incubation, tissues were washed several times in TBSTw and incubated with secondary antibodies diluted in RGBTw for 1 hour at room temperature. Tissues were washed in TBSTw and labeled with 4',6-diamidino-2-phenylindole, dilactate (DAPI) to visualize cell nuclei and mounted in phosphate buffered saline containing 80% glycerol and 0.2% n-propyl gallate. Images were obtained using a Leica SP8 Confocal Microscope fitted with a 20X oil immersion objective (HC PL Apo CS2 NA = 0.75) (Leica, Wetzlar, Germany) or a Nikon Eclipse E600 compound microscope fitted with 10X (Plan Fluor NA = 0.30) and 20X objectives (Plan Fluor NA = 0.50) (Nikon Instruments Inc., Tokyo, Japan). Sections from both experimental groups were imaged using the same exposure settings or laser power for a given antibody combination. The tile-scanning function was used to obtain images of entire tissue sections containing the urethra to reduce sampling bias. For primary and secondary antibody information see Table 3.1.

EdU Proliferation assay

5-ethynyl-2'-deoxyuridine (Thermo Fisher Cat #A10044-50 mg) was dissolved in sterile saline to a concentration of 1 mg/ml. Timed pregnant females were dosed intraperitoneally at 5 mg EdU/kg body weight two hours prior to euthanasia to label S phase cells in embryos. Tissue sections from EdU dosed embryos were labeled using the Click-iT EdU Alexa Fluor 488 Imaging kit (Thermo Fisher Cat #C10337).

Mitotic spindle angle measurements

Mitotic spindles in tissue sections were labeled using antibodies to Gamma tubulin (Abcam #ab11317). Spindle angles were computed with respect to a tangent drawn to the closest bud edge using *ImageJ v3.3.1* as previously described (Feng et al., 2013). Spindle angles were binned into 3 categories: 0-30 degrees (parallel to axis of bud extension), 30-60 degrees (random) and 60-90 degrees (perpendicular to axis of bud extension).

RNA *in situ* Hybridization

In situ hybridization for whole tissues was carried out as described previously (Abler et al., 2011b; Keil et al., 2012a). For *in situ* hybridization on tissue sections, lower urinary tracts fixed overnight in phosphate buffered saline containing 4% paraformaldehyde were embedded in OCT embedding medium and cut into 10-micron sections before probe hybridization. Sequences for primers used in riboprobe synthesis are as follows: Mouse *Nkx3-1* 5'- CAGTGGCTGATGTCAAGG-3' and 5'- CGATGTTAATACGACTCACTATAGGGCTAAGCAGGA AGGGCAGGAG-3'. After completion of the colorimetric reaction, tissues were fixed overnight in phosphate buffered saline containing 4% paraformaldehyde before imaging using a Nikon Eclipse 80i compound microscope or an Olympus SZX10 dissecting microscope.

Hematoxylin-eosin staining

5-micron paraffin sections were washed in xylene and rehydrated through a series of graded ethanol washes. Slides were washed in water, Hematoxylin QS (Vector Laboratories, Burlingame, CA, US) was added dropwise to cover tissue sections and tissues were stained for 8 minutes. Slides were washed in tap water and phosphate

buffered saline to develop stain. Slides were then washed in a 50% ethanol solution followed by a 75% ethanol solution. Slides were incubated in eosin working solution (0.25% eosin, 60% ethanol, 0.5% glacial acetic acid) for 2 minutes and dehydrated through a series of graded ethanol washes. Slides were washed in xylene and mounted with Richard-Allan Scientific™ Mounting Medium (Thermo Fisher Scientific, Waltham, MA, USA) before coverslips were applied. Images were obtained using a Nikon eclipse 80i compound microscope.

Whole-mount tissue staining

Lower urinary tract tissue was harvested from E18.5 embryos. Tissues were briefly washed in cold phosphate buffered saline and fixed in 4% paraformaldehyde solution for 20 mins on ice. Tissues were washed in 25 mM Tris-HCl, pH 7.5, 140 mM NaCl, 2.7 mM KCl, and 0.1% Triton-X100 (TBSTx). Tissues were then digested with 1 mg/ml Collagenase from *Clostridium histolyticum*, washed and post-fixed in 4% paraformaldehyde for 20 mins. Tissues were washed and blocked for 1 hr in TBSTx containing 1% Blocking Reagent (Roche Diagnostics, Indianapolis, IN), 5% normal goat sera, and 1% bovine serum albumin fraction 5 (RGBTx) with 0.5% Triton X-100 and 1% dimethyl sulfoxide. After blocking, tissues were incubated in RGBTx containing primary antibodies overnight at room temperature. Tissues were washed 5 times for 1 hour in TBSTx and incubated with secondary antibodies diluted in RGBTx (overnight at 4°C). Tissues were washed 5 times for 1 hour each in TBSTx and cleared in Citifluor (Electron Microscopy Sciences). Images were obtained using a Leica SP8 Confocal Microscope.

RNA-Seq

Urethral epithelia were isolated by trypsin digestion as described previously (Cunha and Baskin, 2016). Dissected tissues were placed directly into RLT Plus lysis buffer (Qiagen) for later processing. Dissected tissues from multiple embryos were pooled into one lysate. Total RNA was purified from the RLT Plus lysates using the RNeasy Plus Micro Kit (Qiagen) according to manufacturer's instructions. For constructing the RNA-Seq library, total RNA from each batch of samples (using an input of ~100 ng total RNA) was used following the LM-seq protocol (Hou et al., 2015). The reads generated from the Illumina HiSeq 3000 (69 cycles of insert read and 10 cycles of index read) were processed with CASAVA basecalling software (Illumina). The demultiplexing step allotted approximately 124.7 million total reads across the all the samples, ranging from ~0.7 million to ~18.9 million reads assigned per sample. Reads were mapped to Mus musculus reference mm10 assembly with an average of ~66% mapping rate using Bowtie (Langmead et al., 2009), and gene expression estimates were obtained using RSEM (Li and Dewey, 2011). Differentially expressed genes were identified using the *DESeq2* package (Love et al., 2014). Independent filtering was performed to eliminate genes with less than 10 reads in all samples combined. Genes with adjusted p-value or False discovery rate (FDR) <0.05 were categorized as differentially expressed. Gene Ontology enrichment analysis for biological processes was conducted using WebGestalt (Wang et al., 2017). RNA-Seq data was deposited in Gene Expression Omnibus (www.ncbi.nlm.nih.gov/geo/) Accession number: GSE121086.

Real-time quantitative PCR

Quantitative PCR was carried out as previously described (Keil et al., 2014a; Keil et al., 2012b). Relative mRNA abundance was determined using the ΔCt method (Yuan et al.,

2006) and normalized to the abundance of housekeeping gene *Ppia*. Urethral tissue from four embryos was used for analysis. Primers sequences are provided in the Key resource table.

Statistical Analysis

Statistical analysis was conducted using *R* version 3.3.1. Two tailed Student's t-test was performed on untransformed data that passed the Bartlett's test for homogeneity of variance. P values less than 0.05 were considered statistically significant (* $p<0.05$, ** $p<0.01$, *** $p<0.001$). Results are presented as mean ± standard error of mean (SEM) from at least 3 litter independent male embryos per genotype.

3.3. Results

Epithelial DNMT1 is required for prostate bud formation

We used *Shhcre* and *Dnmt1Flox* alleles to test whether *Dnmt1* deletion from urethral epithelium reduces prostatic budding. The *Shhcre* allele expresses Cre recombinase throughout the urethral epithelium starting as early as E10.5, which is prior to the onset of prostate bud formation at E16.5 (Seifert et al., 2008). We compared embryos carrying one copy of the *Shhcre* allele and one copy of the *Dnmt1Flox* allele (control) to those carrying one copy of the *Shhcre* allele and two copies of the *Dnmt1Flox* allele (c*Dnmt1*KO). Cre inducible R26R-LacZ or R26R-EYFP alleles were also incorporated to visualize Cre-mediated recombination.

c*Dnmt1*KO newborns do not survive more than a few minutes, are cyanotic and have severely hypoplastic lungs compared to controls (Joseph et al., 2018). DNMT1 protein is detectable in most urethral epithelial cells and is especially abundant in prostatic bud

epithelial cells of control mice but is undetectable in *Shh* lineage labeled c*Dnmt1*KO urethral epithelium (Figure S 3.1 A-B). 5-methylcytosine (5mC) immunoreactivity is abundant in control urethral epithelium but is undetectable in c*Dnmt1*KO urethral epithelium (Figure S 3.1 C-D).

We tested whether prostate bud formation is impaired by labeling isolated E18.5 urethras with an *in-situ* hybridization probe against NK3 homeobox 1 (*Nkx3-1*) and counting labeled buds. c*Dnmt1*KO fetuses have fewer total prostatic buds (Figure 3.1 A-C) and specifically fewer dorsal and anterior prostatic buds than controls (Figure S 3.2 A). c*Dnmt1*KO prostatic buds are unusually short and wide compared to control buds (Figure 3.1 D-E). We also show that deleting a single *Dnmt1* allele (controls) does not affect the quantity of prostatic buds compared to *cre* negative mice (Figure S 3.2 B), thereby validating single *Dnmt1flox* mice as appropriate controls for subsequent experiments.

To summarize, DNMT1 expression in the urethral epithelium maintains DNA methylation and is required for prostate bud formation and elongation.

DNMT1 maintains urethral and prostatic epithelial cell organization

We performed immunolabeling with an antibody against Keratin 5 (KRT5) to assess basal epithelial surface integrity across the budding prostatic urethra. KRT5 labeling in the basal layer is discontinuous in c*Dnmt1*KO tissues while control tissues appear normal with a continuous KRT5 layer (Figure 3.1 F-G). The tight-junction protein ZO-1 was visualized as a secondary epithelial integrity measure and is apically localized and continuous in control urethral epithelium but noticeably less abundant and non-apically distributed, especially around acellular holes of c*Dnmt1*KOs (Figure 3.1 H-I). Our results indicate that

Dnmt1 expression is required for maintaining urethral and prostatic basal epithelial organization and tight junctions.

DNMT1 is required for normal cell cycle progression in urethral and prostatic epithelium

We used Ki67 immunostaining to test whether a cell proliferation defect underlies impaired prostatic budding in c*Dnmt1*KOs. Nuclear Ki67 is expressed in active phases of the cell cycle. We were surprised to observe a higher percentage of Ki67 positive urethral epithelial cells in c*Dnmt1*cKOs than in controls, despite reduced prostate bud formation in c*Dnmt1*KOs. (Figure 3.2 A-C). To further investigate this counterintuitive finding, we decided to examine cell proliferation within the urethral epithelium in greater detail. We performed a short pulse labeling with EdU to compare S-phase cell frequencies between genotypes. Despite a greater frequency of cells entering the cycle (Ki67+), the frequency of cells progressing to S-phase is significantly lower in *Dnmt1*cKOs compared to controls (Figure 3.2 D-F).

We hypothesized that cell cycle arrest at later stages promotes Ki67+ epithelial cell accumulation in *Dnmt1*cKO urethral epithelium. Phospho-histone H3 Serine 10 immunostaining was used to calculate percentages of G2 and M phase cells. G2 phase nuclei have speckled Phospho-histone H3 Serine 10 labeling while M phase nuclei are intensely and homogeneously labeled (Ozawa, 2008). The percentage of G2 phase cells is greater in c*Dnmt1*KOs than controls while the percentage of M phase cells does not differ between groups (Figure 3.2 G-I). Together these results indicate that c*Dnmt1*KO urethral and prostatic bud epithelia undergo G2/M cell cycle arrest.

DNMT1 suppresses DNA damage, p53 activation and apoptosis in the developing urethral and prostatic bud epithelium

We used RNA-Seq to identify molecular mechanisms contributing to G2/M cell cycle arrest in c*Dnmt1*KO urethras. Urethral epithelia were isolated at E15.5, prior to prostate bud outgrowth. We found that 434 genes are more abundant and 602 genes less abundant in c*Dnmt1*KOs compared to controls (Figure 3.3 A-B). Among genes upregulated in c*Dnmt1*KOs are those involved in DNA methylation and the intrinsic apoptotic signaling pathway, including the p53 target gene cyclin dependent kinase inhibitor 1a (*Cdkn1a*, also known as p21) (Fischer, 2017) (Figure 3.3 C-D). *Cdkn1a* controls the G2/M cell cycle checkpoint (Agarwal et al., 1995; Niculescu et al., 1998) and its increased abundance in c*Dnmt1*KOs is consistent with G2/M arrest. We used real-time RT-PCR to confirm *Cdkn1a* mRNA is also significantly more abundant in E18.5 c*Dnmt1*KO whole prostatic urethras (epithelium+mesenchyme) than in controls (Figure 3.4 A).

Checkpoints prevent cells with incomplete DNA replication or DNA damage from passing incomplete or abnormal genetic material to daughter cells. In Figure S1, we show that depleting DNMT1 diminishes 5mC. DNA hypomethylation is a trigger for the DNA damage response (Elliott et al., 2015; Palii et al., 2008), which involves activation of ATM kinases that phosphorylate and stabilize p53 to induce apoptosis (Banin et al., 1998; Georgia et al., 2013; Jackson-Grusby et al., 2001). There are more cells immune-positive for the DNA damage marker gamma H2AX in c*Dnmt1*KO urethral epithelia than in control epithelia (Figure 3.4 B-C) and p53 phosphorylated at Serine 15 accumulates c*Dnmt1*KO urethral epithelia (Figure 3.4 D-E). We also show there are more cleaved caspase 3

positive apoptotic cells in c*Dnmt1*KO urethral epithelia compared to that of controls (Figure 3.4 F-H). Thus, loss of DNMT1 protein leads to DNA hypomethylation, which triggers a DNA damage induced, p53-mediated apoptotic cell death pathway in c*Dnmt1*KO urethral epithelium. Collectively, we found that DNMT1 maintains DNA methylation and cell survival in urethral and prostatic bud epithelia.

DNMT1 expression is required for prostate glandular development

Prostatic gland genesis is not complete until approximately one month after birth but c*Dnmt1*KO pups die soon after birth (Joseph et al., 2018). We therefore rescued E18.5 prostatic urethras from control and c*Dnmt1*KO embryos and grafted them under the kidney capsule of intact male athymic nude mice for continued growth and development. Grafts from control and c*Dnmt1*KO embryos do not differ in size (Figure 3.5 A-B). Control grafts contain glandular structures resembling mature prostatic ducts and seminal vesicles, both with visible intra-luminal secretions. Seminal vesicle tissue is expected in grafts, as the fetal material used for grafting contains seminal vesicle remnants despite removal of much of the tissue by dissection. However, c*Dnmt1*KO grafts are completely devoid of prostatic glands and instead only contain seminal vesicle tissue (Figure 3.5 C-D).

As further evidence for impaired prostate gland genesis in c*Dnmt1*KO mutants, we used immunohistochemistry to visualize the seminal vesicle epithelial cell marker PAX2 (Quick et al., 2010) and the endodermal marker FOXA1 (Hou et al., 2007; Taube et al., 2010). Most of control graft glandular epithelia is FOXA1+, consistent with the endodermal origin of prostate tissue. In contrast, glandular epithelia in c*Dnmt1*KO grafts are devoid of

FOXA1+ cells and instead harbor PAX2+ cells, consistent with seminal vesicle identity (Figure 3.5 E-H).

We visualized the Cre inducible EYFP reporter to test whether glandular epithelia in grafts derive from an endodermal (EYFP+, prostate) or an intermediate mesoderm origin (PAX2+, EYFP-, ejaculatory duct and seminal vesicle). Most control graft glandular epithelial cells are EYFP+. In contrast, c*Dnmt1*KO graft glandular epithelia are PAX2+, EYFP-, indicating seminal vesicle epithelium (Figure 3.5 I-L). Although c*Dnmt1*KO grafts do not contain prostate glands, presence of mature seminal vesicle tissue confirms that grafting was successful. We conclude that DNMT1 expression in fetal prostate epithelia is required for prostate glandular development and maturation.

Conditional DNMT1 depletion is a new strategy for examining cell replication requirements in epithelial morphogenesis

Prostatic buds have been postulated to elongate through a combination of oriented cell division and epithelial-mesenchymal transition, yet there is little direct evidence supporting either mechanism (Grant and Kyprianou, 2013). We observe that prostatic bud epithelial cells divide in an oriented manner, with mitotic spindles aligned parallel or perpendicular to the axis of bud elongation (Figure 3.6 A-C).

In previous figures, we show that DNMT1 depleted cells undergo cell cycle arrest and are ‘replication impeded’ while DNMT1 expressing cells are ‘replication competent’. We leveraged these observations to examine the requirement for cell replication across prostatic bud epithelial cells. We used an inducible *Shh*^{creErt2} allele to delete *Dnmt1* in a

subset of urethral epithelial cells, creating a mosaic urethral epithelium containing replication impeded (DNMT1-) and replication competent (DNMT1+) cells.

Embryos carrying one copy of the *Shh*^{creErt2} allele and one copy of the *Dnmt1Flox* allele (control) were compared to embryos carrying one copy of the *Shh*^{creErt2} allele and two copies of the *Dnmt1Flox* allele (i*Dnmt1*LOF). Pregnant dams were dosed with tamoxifen at E9.5 to activate Cre recombination in the urethral epithelium prior to the onset of prostate budding. Prostatic bud number does not differ significantly between control and i*Dnmt1*LOF embryos (Figure 3.6 D-F). The Cre inducible LacZ reporter protein is expressed in a patchy pattern in i*Dnmt1*LOFs (Figure 3.6 G-H) and Cre recombination causes DNMT1 ablation and loss of methylation (Figure 3.6 I-J).

Replication competent DNMT1+ cells accumulate in prostatic bud tips while replication impeded DNMT1- cells accumulate in the prostatic bud core

Because *Dnmt1* expression in urethral epithelia is required for prostatic bud formation, we hypothesized that i*Dnmt1*KO prostatic buds would selectively accumulate replication competent cells (DNMT1+, 5mC+) and exclude replication impeded (DNMT1-, 5mC-) cells. Antibodies to the basal protein Keratin 14 (K14) were used to label the basal layer of urethral epithelium and developing prostatic buds. An antibody to 5mC was used to identify replication competent (5mC+) and replication impeded cells (5mC-). All cells in control urethral epithelia are 5mC+. In i*Dnmt1*LOF urethras, the K14+ (basal layer and prostatic buds) had a higher percentage of 5mC+ cells compared to the K14- cell layer (intermediate/superficial layers) (Figure 3.7 A-C). This suggests that DNMT1-, 5mC- replication impeded cells are excluded from K14+ basal and prostatic bud layers.

Our results also show that 5mC- cells are not entirely excluded from prostatic buds but can instead accumulate in the core of prostatic buds (Figure 3.7 A-C). This finding suggests there are two discrete populations of prostatic bud epithelia that contribute to prostatic bud formation by distinct mechanisms. Cells at the margins and tips of prostatic buds elongate buds axes by cell proliferation, a notion supported by the observation that complete ablation of *Dnmt1* in urethral epithelium results in fewer and shorter buds (Figure 3.1 A-C). However, accumulation of replication impeded DNMT1- cells in prostatic bud cores from mosaic i*Dnmt1*LOF mutants suggest these cells participate in prostatic bud growth by a proliferation independent mechanism, potentially via cell migration from the intermediate and superficial layers of the urethra.

3.4. Discussion

This study is the first to examine the requirement of DNMT1 in prostate bud formation. *Nkx3-1* positive prostatic bud formation is impaired in c*Dnmt1*KO embryos, accompanied by defects in prostatic bud shape, abnormal distribution of Keratin 5 and ZO-1 indicating epithelial disorganization, and evidence of DNA damage and p53 activation. These changes are associated with increased expression of the p53 target gene *Cdkn1a*, G2/M cell cycle arrest and apoptosis. Collectively, these defects are the likely mechanism for impaired prostate bud formation and gland genesis in c*Dnmt1*KO mutants.

In contrast to pharmacological agents that act globally, our model specifically induces cell cycle arrest in the epithelial cells of the urethra and developing prostate without affecting the surrounding mesenchyme. *Dnmt1* ablation results in a ‘replication impeded’ cell, which we define as cell cycle arrested. We show that *Dnmt1* depleted cells are hypomethylated, exhibit a DNA damage response and arrest in the G2 phase of the cell

cycle. *Dnmt1* deleted cells can escape arrest but undergo apoptosis in the M-phase or after re-entering G1 phase (Chen et al., 2007). Because repeated cell divisions are required to deplete 5mC levels in *Dnmt1* deleted cells, our model of *Dnmt1* deletion targets fetal urethral and prostate cells that divide rapidly during organogenesis.

We used two different strategies to delete *Dnmt1* in urethral epithelium (Figure 3.8). The *Shhcre* allele confers complete recombination and widespread *Dnmt1* deletion in urethral epithelium, leading to a drastic reduction in prostate bud number due to cell cycle arrest and apoptosis of urethral and prostate epithelial cells. In contrast, the tamoxifen inducible $Shh^{creErt2}$ allele confers mosaic inactivation of *Dnmt1*, resulting in DNMT1+ and DNMT1- cell occupation of the same tissue. Mosaic inactivation of *Dnmt1* using the $Shh^{creErt2}$ allele does not affect prostate bud number indicating that sufficient cells escaped Cre recombination and constituted prostate buds. Within mosaic i*Dnmt1*LOF mutants, DNMT1+ cells accumulate in the rapidly proliferating Keratin 14+ basal layer and in prostatic buds, suggesting a competitive advantage over the replication impeded DNMT1- cells and highlighting a requirement for DNMT1 in prostate bud formation.

We used gamma tubulin immunostaining to evaluate whether prostatic bud epithelial cell division occurs in an oriented manner. We found that mitotic spindles are largely parallel and perpendicular to the long axes of prostatic buds, supporting a role of oriented cell division in prostatic bud elongation and widening. We used i*Dnmt1*LOF mice to examine whether cell division is required across all prostatic bud epithelial cells. Replication competent (DNMT1+) cells accumulate in margins and tips of i*Dnmt1*LOF prostatic buds but replication impeded (DNMT1-) cells accumulate in prostatic bud cores. It is unlikely DNMT1- cells incorporate into buds by cell division because they are replication impeded.

Their presence in buds therefore challenges the existing paradigm that prostatic buds form and elongate exclusively by a proliferation dependent mechanism and suggests that prostatic bud core cells may arise from a different mechanism. We then asked, what is the origin of prostatic bud core cells and by which mechanisms do they integrate into prostatic buds? One possible origin is urethral intermediate or superficial epithelium (Abler et al., 2011a). The intermediate and superficial urethral epithelial layers (Keratin 14-) in i*Dnmt1*LOF mutants accumulate 5mC- cells similar to the core of prostatic buds. Intermediate and superficial epithelial cells could stream into prostatic bud cores while margin cells are extending prostatic bud axes by oriented cell division. Existence of two distinct cell lineages within prostatic buds opens several new lines of investigation. Do characteristics and behaviors of these cells remain different into adulthood? Do both cell lineages possess or retain progenitor capacities and can they generate all prostatic epithelial cell types? Further studies are required to follow these separate lineages into adulthood to determine how they contribute to the composition of the adult prostate.

In conclusion, we have established a requirement for urethral epithelial DNMT1 for prostatic bud formation and survival of early prostatic bud epithelial cells. Using *Dnmt1* ablation as a novel tool, we have identified that prostatic buds are elongated in part by oriented cell division, but that a unique cell lineage in prostatic bud cores arises by a proliferation independent mechanism.

3.5. Figures and Tables

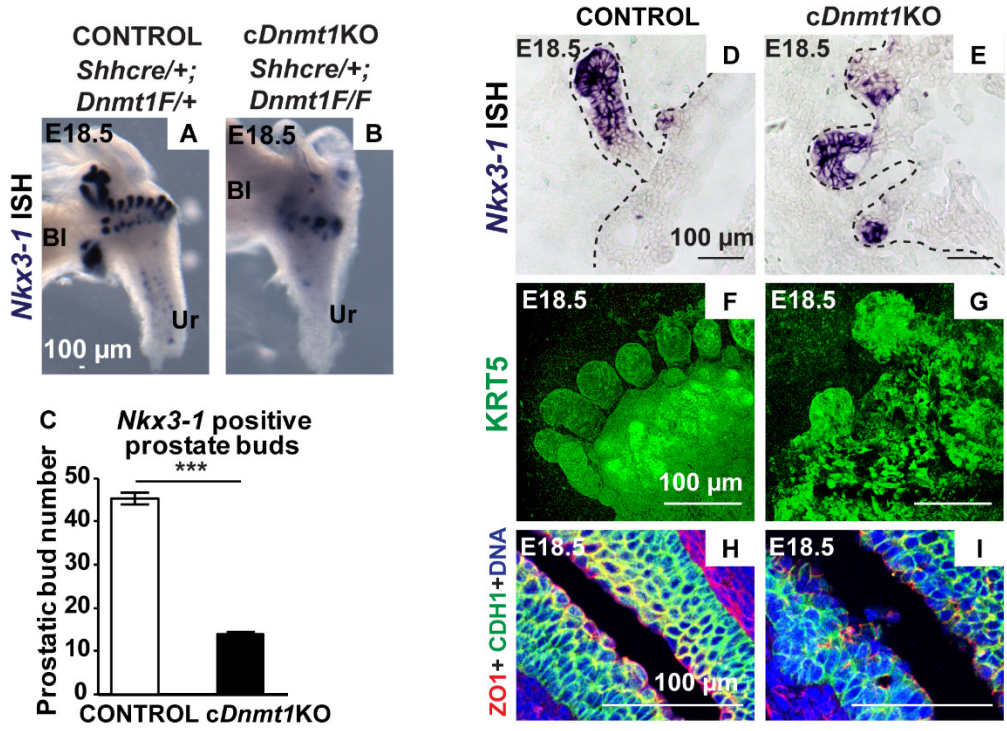

Figure 3.1 DNMT1 is required for prostate bud formation and maintains epithelial organization in the urethra

E18.5 control and c*Dnmt1*KO urethras were (A-B) labeled with an *Nkx3-1* riboprobe to visualize prostatic buds (purple) and (C) buds were quantified. (D-E) 10-micron frozen sections from E18.5 control and c*Dnmt1*KO urethras were labeled with an *Nkx3-1* riboprobe (purple) to visualize the cellular organization of prostatic buds. Black dashed lines indicate the epithelial-mesenchymal interface. (F-G) E18.5 control and c*Dnmt1*KO male urethras were stained in whole-mount with an antibody against KRT5 (in green) to visualize the basal epithelial surface of the urethra and prostatic buds. (H-I) E18.5 urethral sections were labeled with antibodies against ZO-1 (in red, labels tight junctions) and CDH1 (in green, labels epithelium). The white arrow indicates an acellular hole with apical

ZO-1 staining in c*Dnmt1*KO urethra. DAPI staining is shown in blue. Scale bar is 100 microns. Graphical results are the mean ± SEM of at least three mice per group. p-values indicate significant differences (*** p<0.001) between groups based on Student's t-test.

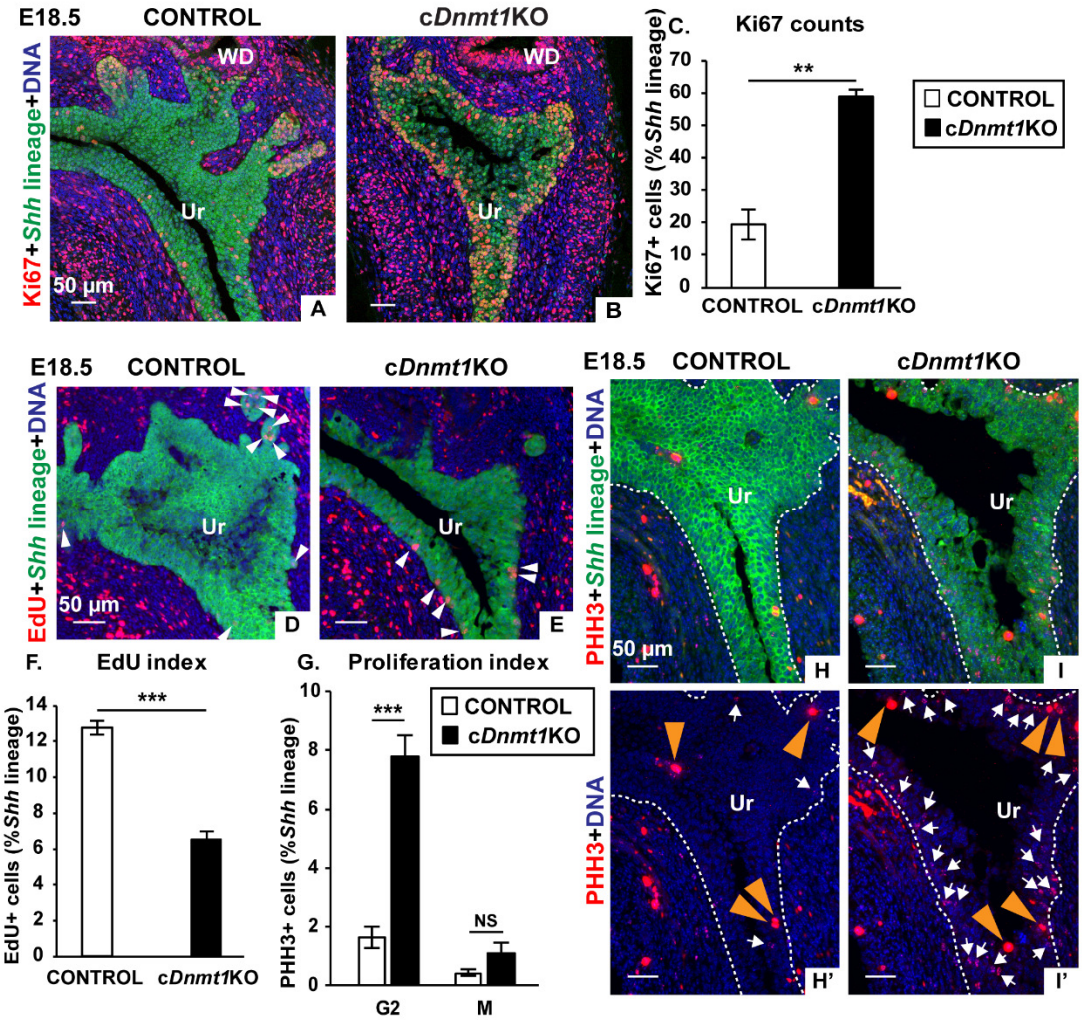

Figure 3.2 DNMT1 is required for normal cell cycle progression in urethral and prostatic epithelial cells

(A-B) E18.5 urethra sections were labeled with antibodies against Ki67 (red, labels proliferating cells) and EYFP (green, labels *Shh* lineage epithelium). (C) Ki67 positive cells as a percentage of total urethral *Shh* lineage cells was determined. (D-E) E18.5

urethra sections were labeled for EdU (in red, labels S-phase cells) and EYFP (in green, labels *Shh* lineage epithelium). White arrowheads indicate EdU positive cells. (F) EdU positive cells as a percentage of total urethral *Shh* lineage cells was determined. (G) G2 and M phase cells as a percentage of total urethral *Shh* lineage cells was determined (H-I) E18.5 urethra sections were labeled with antibodies against Phospho-histone H3 Ser10 (PHH3 in red, labels cells in the G2 and M phase) and EYFP (in green, labels *Shh* lineage epithelium). (H') and (I') show (H) and (I) with the green channel excluded. G2 phase cells have speckled nuclear staining of PHH3 and are indicated by white arrows. M phase cells have bright, uniform nuclear staining for PHH3 and are indicated by orange arrowheads. White dashed lines indicate the epithelial-mesenchymal interface. DAPI staining is shown in blue. Scale bar is 50 microns. Graphical results are the mean $\pm$ SEM of at least three mice per group. p-values indicate significant differences (** $p<0.01$, *** $p<0.001$) between groups based on Student's unpaired t-test. NS: Not significant $p>0.05$. Abbreviations are WD: Wolffian duct, Ur: Urethra.

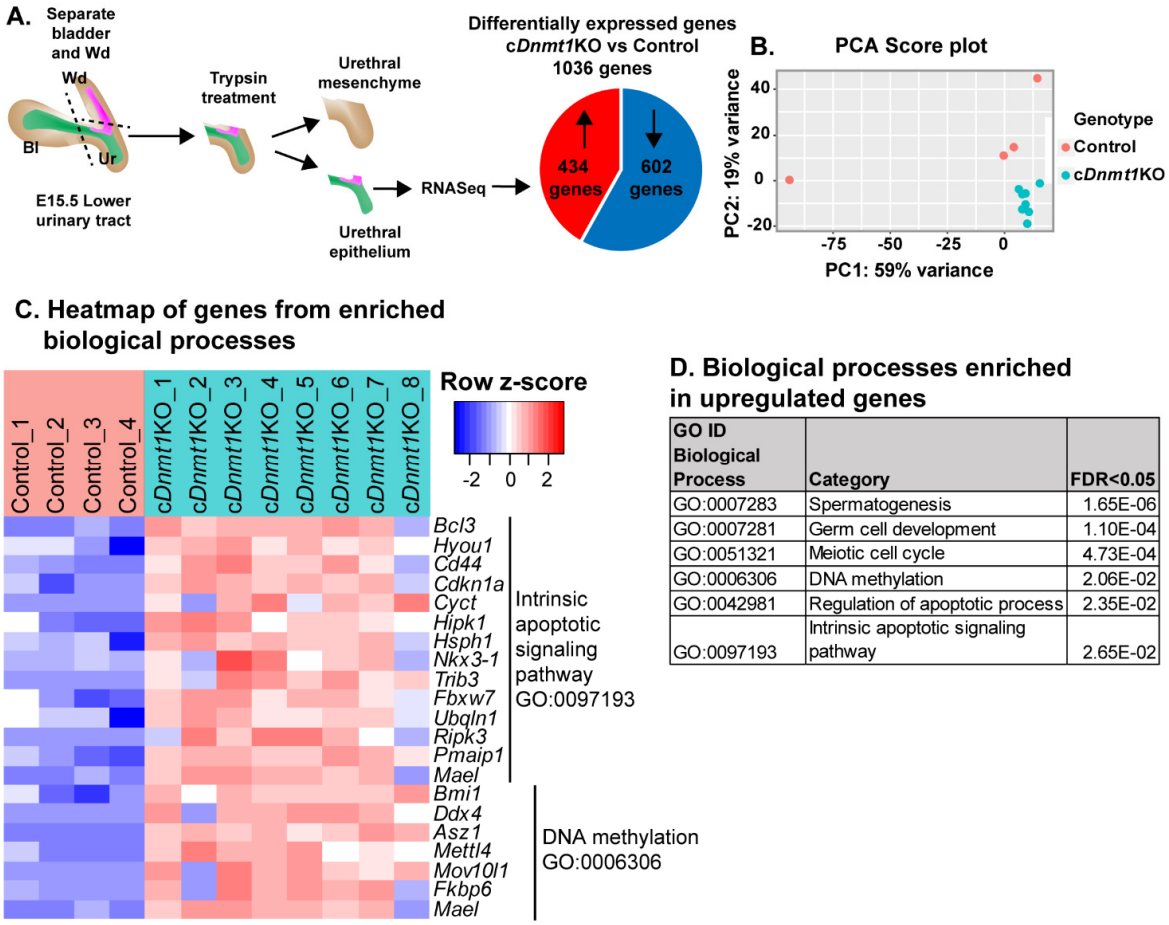

D. Biological processes enriched in upregulated genes

GO ID Biological Process	Category	FDR<0.05
GO:0007283	Spermatogenesis	1.65E-06
GO:0007281	Germ cell development	1.10E-04
GO:0051321	Meiotic cell cycle	4.73E-04
GO:0006306	DNA methylation	2.06E-02
GO:0042981	Regulation of apoptotic process	2.35E-02
GO:0097193	Intrinsic apoptotic signaling pathway	2.65E-02

Figure 3.3 RNA-Seq analysis shows upregulation of p53 target genes in E15.5 c*Dnmt1*KO urethral epithelium compared to control urethral epithelium.

(A) Experimental design for isolation and RNA-seq analysis of E15.5 control (n=4 samples) and c*Dnmt1*KO urethral epithelium (n=8 samples). (B) Principal components analysis (C) Heatmap of differentially expressed genes from enriched biological processes (D) Biological processes enriched in upregulated genes from c*Dnmt1*KO urethral epithelium.

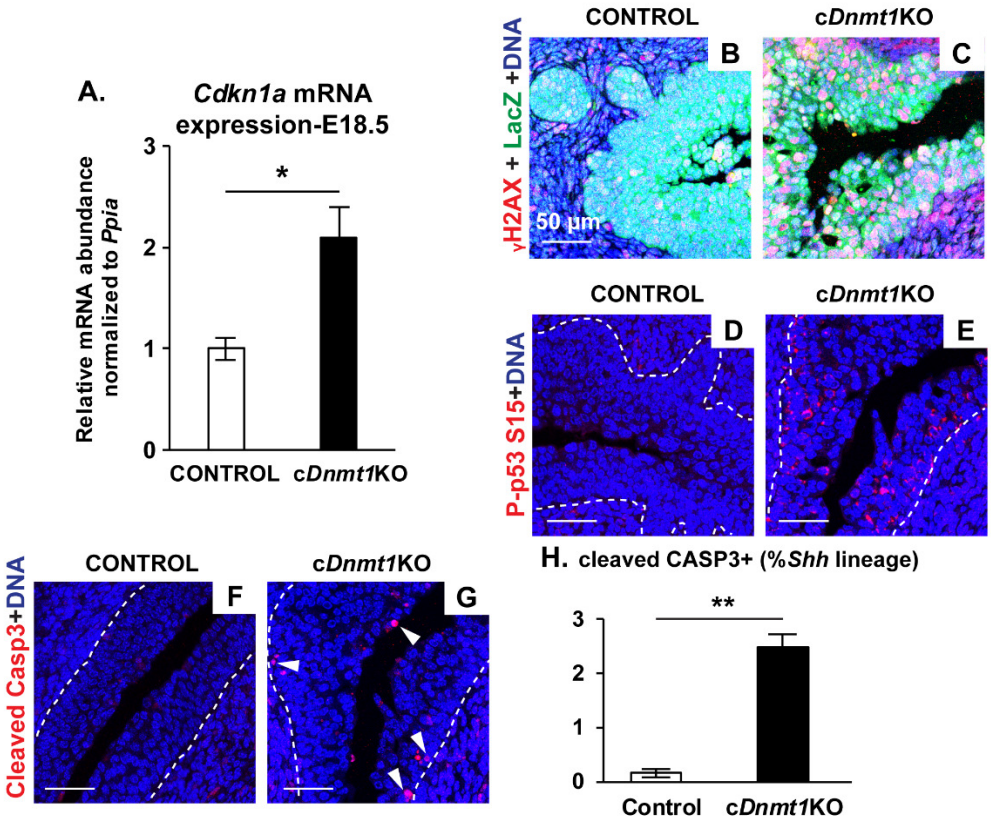

Figure 3.4 DNMT1 suppresses DNA damage, p53 activation and apoptosis in the developing urethral epithelium

(A) RT-PCR for *Cdkn1a* mRNA in E18.5 control and c*Dnmt1*KO urethras. (B-C) E18.5 urethra sections were labeled with antibodies against Gamma-H2AX (in red, DNA damage marker) and LacZ (in green, labels *Shh* lineage epithelium). (D-E) E18.5 urethra sections were labeled with antibodies against Phospho-p53 Ser15 (in red, marks active p53). (F-G) E18.5 urethra sections were labeled with antibodies against Cleaved caspase 3 (in red, marks apoptotic cells) and EYFP (in green, labels *Shh* lineage epithelium). Green channel is excluded for ease of visualization. (H) Percentage of cleaved Caspase 3 labeled cells in the *Shh* lineage urethral epithelium. White arrowheads indicated cleaved Caspase 3 positive apoptotic cells. White dotted lines indicate epithelial-mesenchymal

interface. DAPI staining is shown in blue. Scale bar is 50 microns. Graphical results are the mean ± SEM of at least three mice per group. p-values indicate significant differences (* $p<0.05$, ** $p<0.01$) between groups based on Student's unpaired t-test.

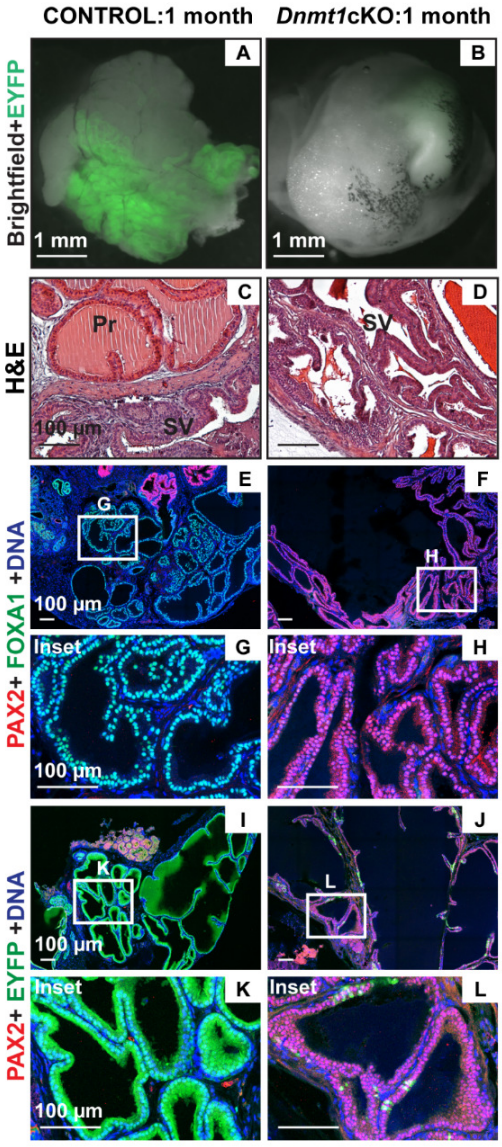

Figure 3.5 DNMT1 is required for prostate gland genesis and maturation in renal grafts

(A-B) Brightfield images of renal grafts overlaid with EYFP (in green, labels *Shh* lineage epithelium). Scale bar is 1 mm. (C-D) Hematoxylin and eosin labeling of sections from renal grafts. (E-F) Sections from renal grafts were labeled with antibodies against PAX2 (in red, marks seminal vesicle epithelium) and FOXA1 (in green, marks prostate epithelium). (G) and (H) show magnified regions from (E) and (F). (I-J) Sections from renal grafts were labeled with antibodies against PAX2 and EYFP. (K) and (L) show magnified regions from (I) and (J). DAPI staining is shown in blue. Scale bar is 100 microns. Images are representative of at least three mice per group. Abbreviations are Pr: Prostate, SV: Seminal Vesicle.

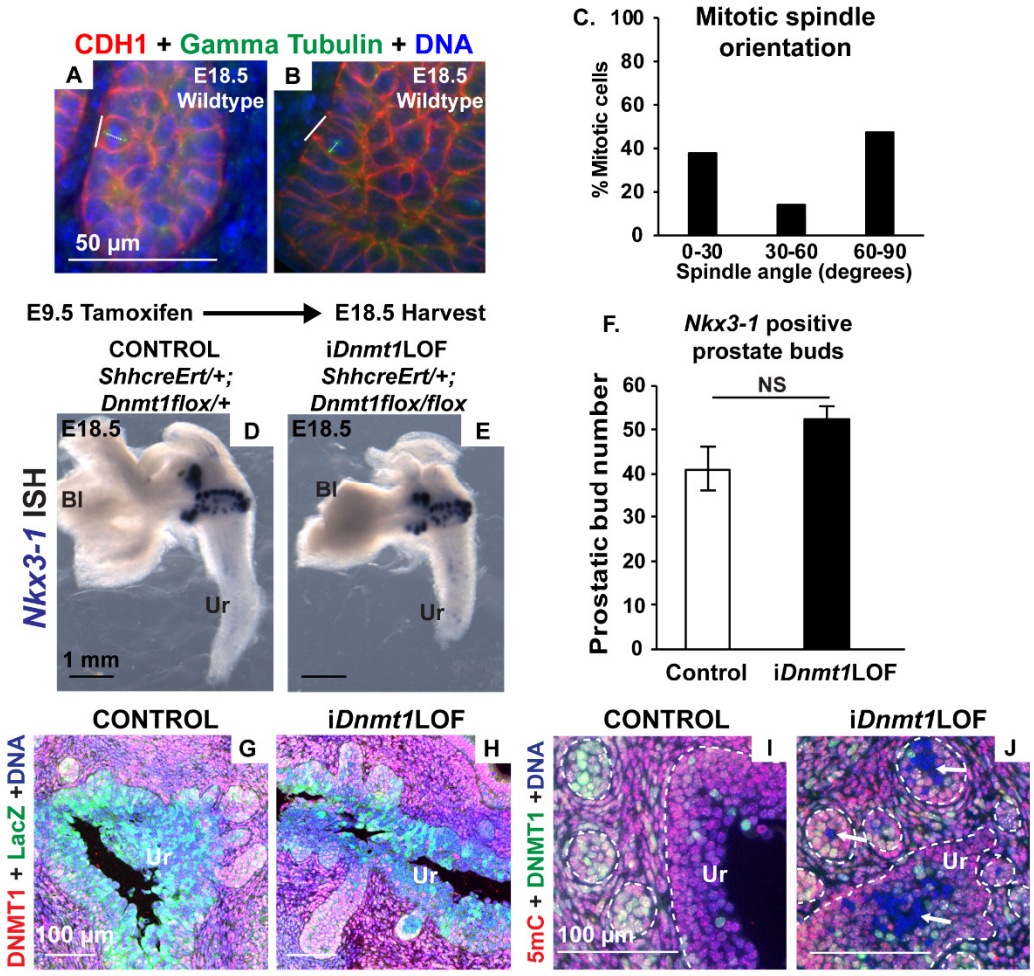

Figure 3.6 Prostatic buds extend by oriented cell division but mosaic inactivation of *Dnmt1* does not affect bud formation

(A-B) Wildtype E18.5 prostatic bud sections were labeled with antibodies to Gamma tubulin (in green, labels the mitotic spindle) and CDH1 (in red, labels epithelium). The mitotic spindle axis is indicated by the white dashed line. Mitotic spindle angles are computed with respect to a tangent drawn to the nearest prostatic bud edge indicated by solid white lines. (C) Graph showing the percentage of mitotic cells (n=21) with mitotic spindle angles that fall into the bins 0-30 degrees (parallel), 30-60 degrees (random) and 60-90 degrees (perpendicular). (D-E) E18.5 control and i*Dnmt1*LOF urethras were

labeled with an *Nkx3-1* riboprobe to label prostatic buds (in purple, scale bar is 500 microns) and (F) buds were quantified. Graphical results are the mean ± SEM of at least three mice per group. There were no differences between groups based on Student's unpaired t-test test. Not significant NS $p>0.05$ (G-H) E18.5 urethra sections were labeled with antibodies against DNMT1 (in red) and LacZ (in green, labels *Shh* lineage epithelium). (I-J) E18.5 urethra sections were labeled with antibodies against 5mC (in red) and DNMT1 (in green). White arrows indicate DNMT1-, 5mC- regions. White dotted lines indicate the epithelial-mesenchymal interface. Scale bar is 100 microns. Images are representative of three mice per group. DAPI staining is shown in blue. Abbreviations are Bl: Bladder, Ur: Urethra.

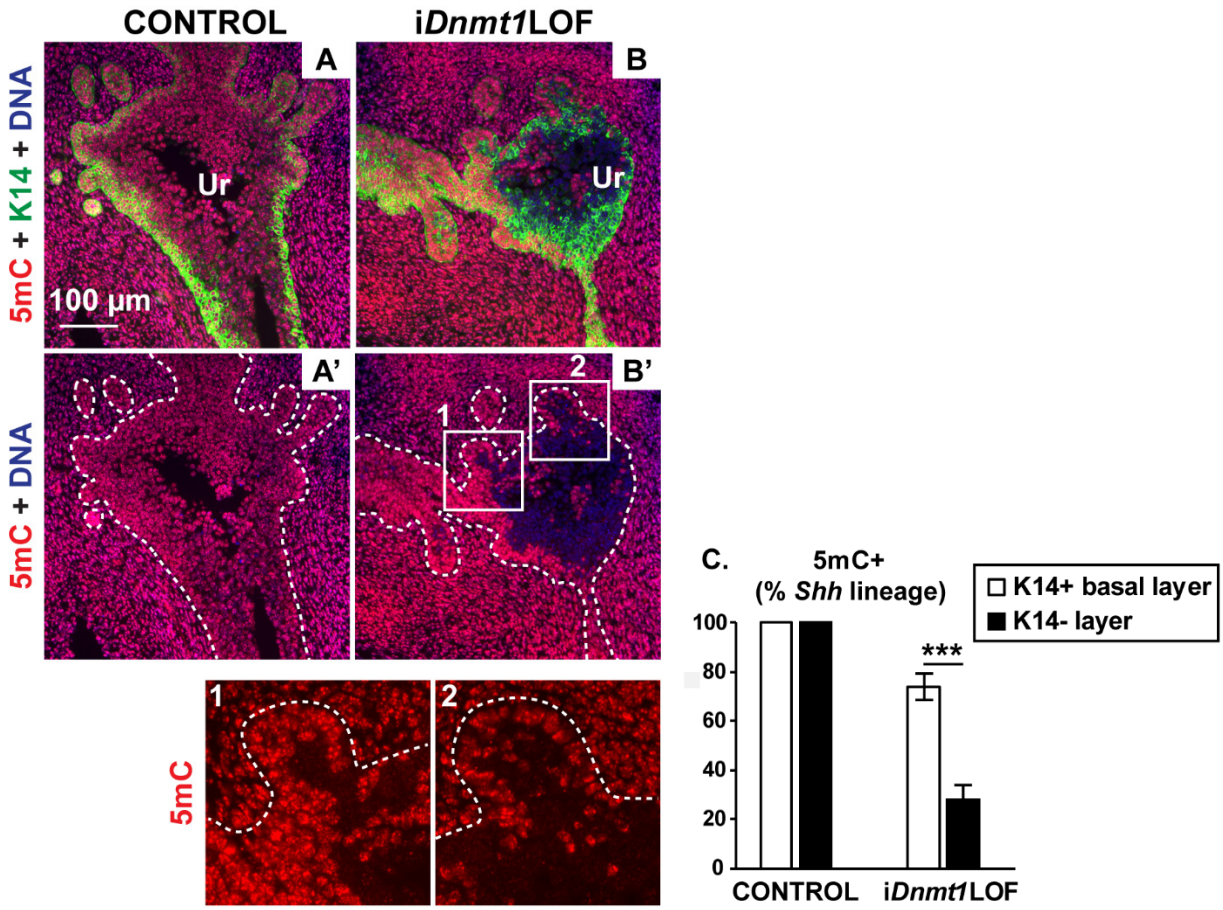

Figure 3.7 Replication competent DNMT1+ cells preferentially localize to prostatic bud margins while replication impeded DNMT1- cells accumulate in prostatic bud cores

(A-B) E18.5 urethra sections were labeled with antibodies against 5mC (in red) and Keratin 14 (in green). (A') and (B') show (A) and (B) with green channel excluded. Magnified regions from (A') and (B') with blue channel excluded are shown in insets 1 and 2. (C) The percentage of 5mC positive cells was determined as a function of all epithelial cells in either the K14+ or K14- cell layers. Graphical results are the mean ± SEM of six mice per group. p-values indicate significant differences (*** $p<0.001$) between groups based on Student's unpaired t-test. White dashed lines indicate the epithelial-

mesenchymal interface. Scale bar is 100 microns. DAPI staining is shown in blue. Abbreviation Ur: Urethra.

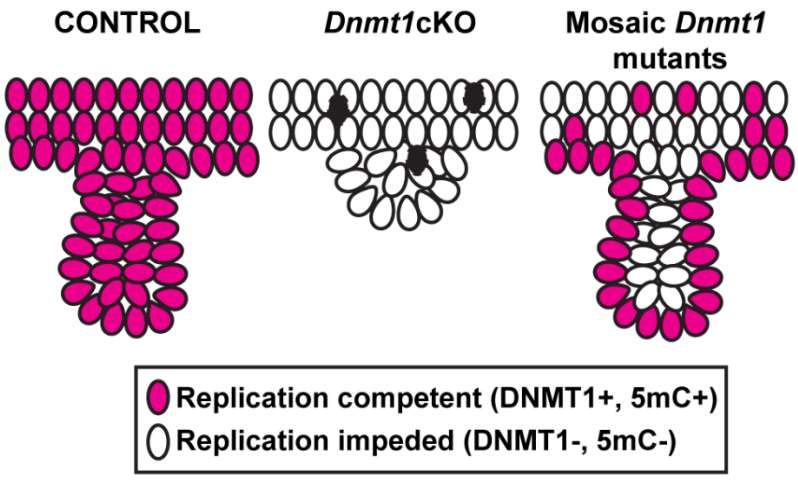

Figure 3.8 Model of the role of DNMT1 in prostatic bud formation

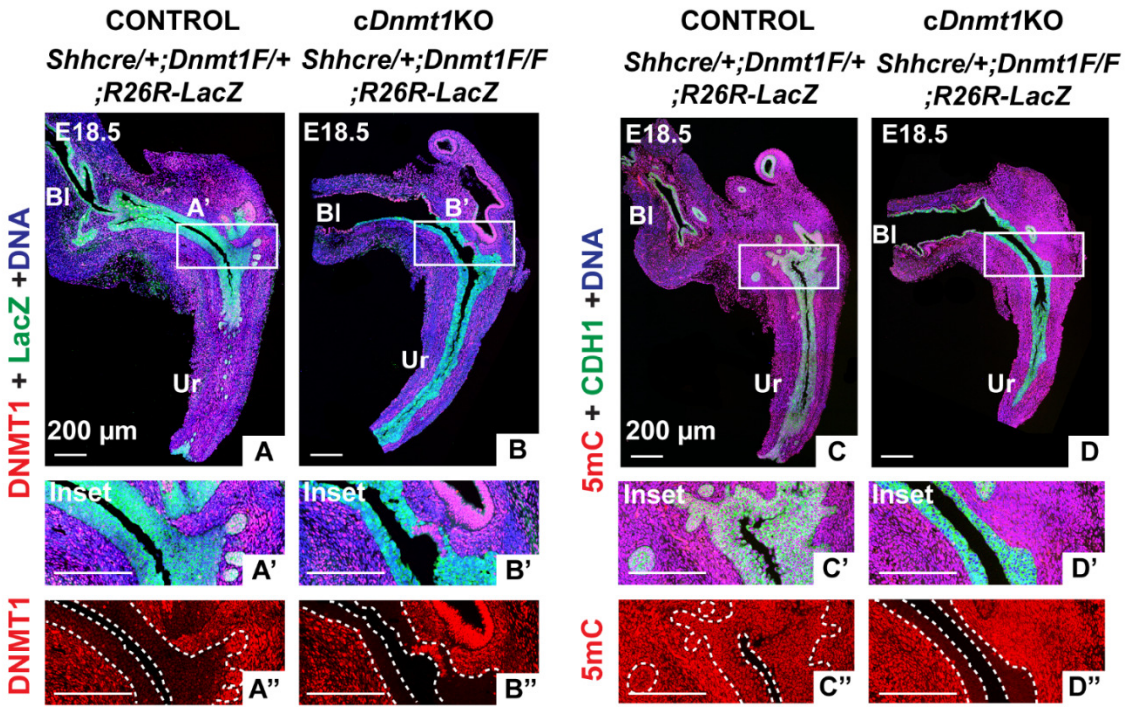

Figure S 3.1 c*Dnmt1*KO mutants have loss of DNMT1 protein and 5-methylcytosine in *Shh* lineage urethral epithelium

(A-B) E18.5 urethra sections were labeled with antibodies against DNMT1 (in red) and LacZ (in green, labels *Shh* lineage epithelium). (A') and (B') show magnified regions from (A) and (B). (A'') and (B'') show (A') and (B') with green channel excluded. (C-D) E18.5 urethra sections were labeled with antibodies against 5mC (red) and CDH1 (green, labels epithelium). (C') and (D') show magnified regions from (C) and (D). (C'') and (D'') show (C') and (D') with green channel excluded. White dotted lines enclose the urethral epithelium. DAPI staining is shown in blue. Scale bar is 200 microns. Images are representative of three mice per group. Abbreviations are Bl: Bladder, Ur: Urethra.

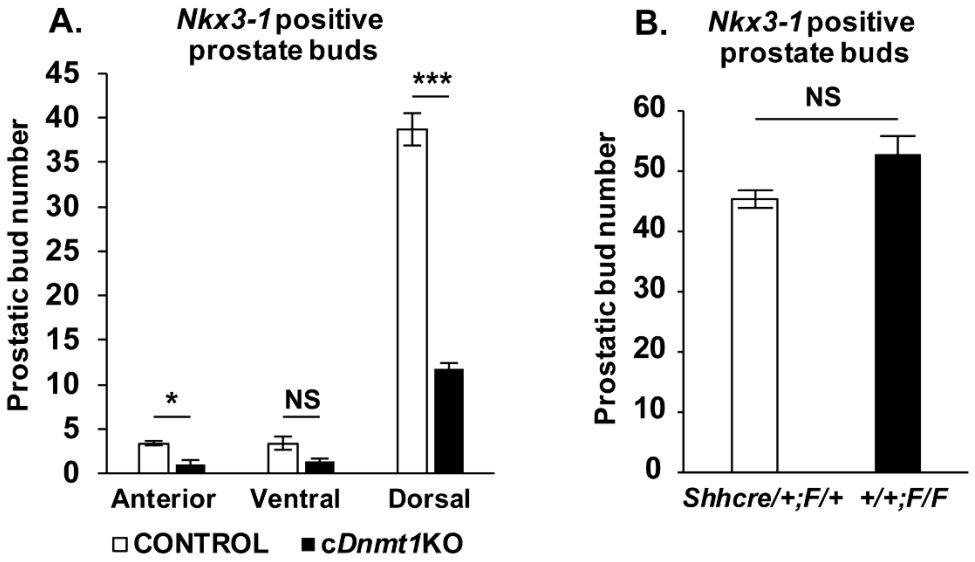

Figure S 3.2 Anterior, ventral and dorsal bud counts in c*Dnmt1*KO mutants; Number of prostatic buds in control tissues do not differ from *cre* negative animals

(A) Anterior, ventral and dorsal prostate bud counts from control and c*Dnmt1*KO mutants. (B) Prostate bud counts from E18.5 control (*Shhcre/+; Dnmt1flox/+*) and *cre* negative (*+/+; Dnmt1flox/+*) embryos. Graphical results are the mean ± SEM of three mice per group. p-values indicate significant differences (** $p<0.01$, *** $p<0.001$) between groups based on Student's unpaired t-test. NS: Not significant $p>0.05$.

Table 3.1 Reagents and resources

REAGENT or RESOURCE	SOURCE	IDENTIFIER
Antibodies		
Mouse monoclonal anti-5 methylcytosine	Abcam	Cat#ab10805; RRID:AB_442823
Chicken polyclonal anti-LacZ	Abcam	Cat# ab9361, RRID:AB_307210
Chicken polyclonal anti-GFP	Abcam	Cat#ab13970; RRID:AB_300798
Rabbit polyclonal anti-Ki67	Abcam	Cat#ab15580; RRID:AB_443209
Rabbit polyclonal anti-Gamma Tubulin	Abcam	Cat# ab11317; RRID:AB_297921

Rabbit polyclonal anti-PAX2	Covance	Cat#PRB-276P-200; RRID:AB_291611
Mouse monoclonal anti-FOXA1	Millipore	Cat#05-1466; RRID:AB_1977191
Chicken polyclonal anti-KRT5	Biolegend	Cat#905901; RRID: AB_2565054
Rabbit monoclonal anti-5 methylcytosine	Cell Signaling	Cat#28692
Rabbit monoclonal anti-DNMT1	Cell Signaling	Cat#D63A6; RRID:AB_10828695
Rabbit monoclonal anti-CDH1	Cell Signaling	Cat#3195S
Rabbit polyclonal anti-Histone H2AX (phospho Ser139)	Cell Signaling	Cat#2577; RRID:AB_2118011
Mouse monoclonal anti-p53 (phospho Ser15) 16G8	Cell Signaling	Cat#9286; RRID:AB_331741
Rabbit monoclonal anti-Cleaved Casp3 (Asp 175)	Cell Signaling	Cat#9664; RRID:AB_2070042
Rabbit polyclonal anti-Phospho-Histone H3 (Ser10)	Cell Signaling	Cat#9701; RRID:AB_331535
Mouse monoclonal anti-CDH1	BD Transduction Labs	Cat#610181; RRID:AB_397580
Mouse monoclonal anti-ZO1	Thermo Fisher Scientific	Cat#33-9100; RRID:AB_2533147
Mouse monoclonal anti-KRT14	Thermo Fisher Scientific	Cat# MS-115-P0, RRID:AB_63786
Goat polyclonal anti-Chicken Alexa488 conjugated	Jackson Immunoresearch	Cat#103-545-155; RRID:AB_2337390
Goat polyclonal anti-Mouse Alexa488 conjugated	Jackson Immunoresearch	Cat# 115-547-003; RRID:AB_2338869
Goat polyclonal anti-Rabbit Alexa488 conjugated	Jackson Immunoresearch	Cat# 111-547-003; RRID:AB_2338058
Goat polyclonal anti-Mouse Alexa594 conjugated	Jackson Immunoresearch	Cat# 115-585-062; RRID:AB_2338876
Goat polyclonal anti-Rabbit Alexa594 conjugated	Jackson Immunoresearch	Cat# 111-586-045; RRID:AB_2338067
Sheep polyclonal anti-Digoxygenin Alkaline phosphatase conjugated	Roche	Cat#11093274910; RRID:AB_514497
Chemicals, Peptides, and Recombinant Proteins		
Tamoxifen, free base	Sigma Aldrich	T5648; CAS: 10540-29-1
5-ethynyl-2'-deoxyuridine (EdU)	Thermo Fisher	A10044
Critical Commercial Assays		
Click-iT® EdU Alexa Fluor® 488 Imaging Kit	Thermo Fisher	C10337
Deposited Data		
RNA-Seq data	This paper	GEO: GSE121086
Experimental Models: Organisms/Strains		
Mouse: B6.129S4-*Dnmt1*$^{tm2Jae/Mmucd}$	MMRRC, UC Davis	Stock#014114-UCD; RRID:MMRRC_014114-UCD
Mouse: B6. Cg*Shh*$^{tm1(EGFP/cre)Cjt/J}$	Jackson Laboratory	Stock#005622; RRID:IMSR_JAX:005622

Mouse: B6.129S4-*Gt(ROSA)26*$^{Sortm1Sor/J}$	Jackson Laboratory	Stock#003309; RRID:IMSR_JAX:003309
Mouse: B6.129X1-*Gt(ROSA)26*$^{Sortm1(EYFP)Cos/J}$	Jackson Laboratory	Stock#006148; RRID:IMSR_JAX:006148
Mouse: B6.129S6-*Shh*$^{tm2(cre/ERT2)Cjt}$/J	Jackson Laboratory	Stock#005623; RRID:IMSR_JAX:005623
Mouse: CD-1 IGS mouse (wildtype)	Charles Rives	Stock#022
Mouse: C57BL/6	Jackson Laboratory	Stock#000664, RRID:IMSR_JAX:000664
Mouse: Athymic nude nu/nu	Jackson Laboratory	Stock#002019
Oligonucleotides		
Primer: *Cdkn1a* Forward 5'-ATACCGTGGGTGTCAAAGCAC-3'	This paper	N/A
Primer: *Cdkn1a* Reverse 5'-ACAGGGAGGGAGCCACAATAC-3'	This paper	N/A
Primer: *Ppia* Forward 5'-TCTCTCCGTAGATGGACCTG-3'	This paper	(Keil et al., 2014a)
Primer: *Ppia* Reverse 5'-ATCACGGCCGATGACGAGCC-3'	This paper	(Keil et al., 2014a)
Mouse *Nkx3-1* ISH probe Forward primer 5'-CAGTGGCTGATGTCAAGG-3'	This paper	(Abler et al., 2011a)
Mouse *Nkx3-1* ISH probe Reverse primer 5'-CGATGTTAATACGACTCACTATAGGGCTAAGCAGGAAGGGCAGGAG-3' (T7 binding site underlined)	This paper	(Abler et al., 2011a)
Nkx3-1 ISH probe binding site NM_010921.3	This paper	(Abler et al., 2011a)
Software and Algorithms		
ImageJ	imagej.nih.gov	Version 1.51k
R for Windows	cran.r-project.org	Version 3.3.1
Adobe Illustrator	adobe.com	CC2017
Adobe Photoshop	adobe.com	CC2017
DESeq2 package	bioconductor.org	(Love et al., 2014)

3.6. References

Abler, L.L., Keil, K.P., Mehta, V., Joshi, P.S., Schmitz, C.T., Vezina, C.M., 2011a. A high-resolution molecular atlas of the fetal mouse lower urogenital tract. Dev. Dyn. 240, 2364-2377.

Abler, L.L., Mehta, V., Keil, K.P., Joshi, P.S., Flucus, C.L., Hardin, H.A., Schmitz, C.T., Vezina, C.M., 2011b. A high throughput in situ hybridization method to characterize mRNA expression patterns in the fetal mouse lower urogenital tract. J Vis Exp.

Agarwal, M.L., Agarwal, A., Taylor, W.R., Stark, G.R., 1995. p53 controls both the G2/M and the G1 cell cycle checkpoints and mediates reversible growth arrest in human fibroblasts. Proc. Natl. Acad. Sci. U. S. A. 92, 8493-8497.

Banin, S., Moyal, L., Shieh, S., Taya, Y., Anderson, C.W., Chessa, L., Smorodinsky, N.I., Prives, C., Reiss, Y., Shiloh, Y., Ziv, Y., 1998. Enhanced phosphorylation of p53 by ATM in response to DNA damage. Science 281, 1674-1677.

Bulut, H.E., Ozdemir, O., Basimoglu-Koca, Y., Korkmaz, M., Atalay, A., 1999. Effects of a DNA demethylating agent--5-azacytidine--on testicular morphology during mouse embryo development. Okajimas Folia Anat. Jpn. 76, 47-53.

Chen, T., Hevi, S., Gay, F., Tsujimoto, N., He, T., Zhang, B., Ueda, Y., Li, E., 2007. Complete inactivation of DNMT1 leads to mitotic catastrophe in human cancer cells. Nat. Genet. 39, 391-396.

Choi, J.-Y., Lee, S., Hwang, S., Jo, S.A., Kim, M., Kim, Y.J., Pang, M.-G., Jo, I., 2013. Histone H3 lysine 27 and 9 hypermethylation within the Bad promoter region mediates 5-Aza-2′-deoxycytidine-induced Leydig cell apoptosis: implications of 5-Aza-2′-deoxycytidine toxicity to male reproduction. Apoptosis 18, 99-109.

Cisneros, F.J., Branch, S., 2003. 5-AZA-2′-deoxycytidine (5-AZA-CdR): a demethylating agent affecting development and reproductive capacity. J. Appl. Toxicol. 23, 115-120.

Cunha, G.R., Baskin, L., 2016. Mesenchymal-epithelial interaction techniques. Differentiation 91, 20-27.

Elliott, E.N., Sheaffer, K.L., Schug, J., Stappenbeck, T.S., Kaestner, K.H., 2015. Dnmt1 is essential to maintain progenitors in the perinatal intestinal epithelium. Development 142, 2163-2172.

Feng, Y., Sentani, K., Wiese, A., Sands, E., Green, M., Bommer, G.T., Cho, K.R., Fearon, E.R., 2013. Sox9 induction, ectopic Paneth cells, and mitotic spindle axis defects in mouse colon adenomatous epithelium arising from conditional biallelic Apc inactivation. Am. J. Pathol. 183, 493-503.

Fischer, M., 2017. Census and evaluation of p53 target genes. Oncogene 36, 3943-3956.

Georgia, S., Kanji, M., Bhushan, A., 2013. DNMT1 represses p53 to maintain progenitor cell survival during pancreatic organogenesis. Genes Dev. 27, 372-377.

Grant, C.M., Kyprianou, N., 2013. Epithelial mesenchymal transition (EMT) in prostate growth and tumor progression. Translational andrology and urology 2, 202-211.

Harfe, B.D., Scherz, P.J., Nissim, S., Tian, H., McMahon, A.P., Tabin, C.J., 2004. Evidence for an expansion-based temporal Shh gradient in specifying vertebrate digit identities. Cell 118, 517-528.

Hou, J., Charters, A.M., Lee, S.C., Zhao, Y., Wu, M.K., Jones, S.J., Marra, M.A., Hoodless, P.A., 2007. A systematic screen for genes expressed in definitive endoderm by Serial Analysis of Gene Expression (SAGE). BMC Dev. Biol. 7, 92.

Hou, Z., Jiang, P., Swanson, S.A., Elwell, A.L., Nguyen, B.K., Bolin, J.M., Stewart, R., Thomson, J.A., 2015. A cost-effective RNA sequencing protocol for large-scale gene expression studies. Sci. Rep. 5, 9570.

Jackson-Grusby, L., Beard, C., Possemato, R., Tudor, M., Fambrough, D., Csankovszki, G., Dausman, J., Lee, P., Wilson, C., Lander, E., Jaenisch, R., 2001. Loss of genomic methylation causes p53-dependent apoptosis and epigenetic deregulation. Nat. Genet. 27, 31-39.

Joseph, D.B., Chandrashekar, A.S., Abler, L.L., Chu, L.-F., Thomson, J.A., Mendelsohn, C., Vezina, C.M., 2018. In vivo replacement of damaged bladder urothelium by Wolffian duct epithelial cells. Proceedings of the National Academy of Sciences 115, 8394-8399.

Keil, K.P., Abler, L.L., Laporta, J., Altmann, H.M., Yang, B., Jarrard, D.F., Hernandez, L.L., Vezina, C.M., 2014a. Androgen receptor DNA methylation regulates the timing and androgen sensitivity of mouse prostate ductal development. Dev. Biol. 396, 237-245.

Keil, K.P., Abler, L.L., Mehta, V., Altmann, H.M., Laporta, J., Plisch, E.H., Suresh, M., Hernandez, L.L., Vezina, C.M., 2014b. DNA methylation of E-cadherin is a priming mechanism for prostate development. Dev. Biol. 387, 142-153.

Keil, K.P., Altmann, H.M., Mehta, V., Abler, L.L., Elton, E.A., Vezina, C.M., 2013. Catalog of mRNA expression patterns for DNA methylating and demethylating genes in developing mouse lower urinary tract. Gene Expr Patterns 13, 413-424.

Keil, K.P., Mehta, V., Abler, L.L., Joshi, P.S., Schmitz, C.T., Vezina, C.M., 2012a. Visualization and quantification of mouse prostate development by in situ hybridization. Differentiation 84, 232-239.

Keil, K.P., Mehta, V., Branam, A.M., Abler, L.L., Buresh-Stiemke, R.A., Joshi, P.S., Schmitz, C.T., Marker, P.C., Vezina, C.M., 2012b. Wnt inhibitory factor 1 (Wif1) is regulated by androgens and enhances androgen-dependent prostate development. Endocrinology 153, 6091-6103.

Kurita, T., Medina, R.T., Mills, A.A., Cunha, G.R., 2004. Role of p63 and basal cells in the prostate. Development 131, 4955-4964.

Langmead, B., Trapnell, C., Pop, M., Salzberg, S.L., 2009. Ultrafast and memory-efficient alignment of short DNA sequences to the human genome. Genome Biol. 10, R25.

Li, B., Dewey, C.N., 2011. RSEM: accurate transcript quantification from RNA-Seq data with or without a reference genome. BMC Bioinformatics 12, 323.

Li, E., Bestor, T.H., Jaenisch, R., 1992. Targeted mutation of the DNA methyltransferase gene results in embryonic lethality. Cell 69, 915-926.

Love, M.I., Huber, W., Anders, S., 2014. Moderated estimation of fold change and dispersion for RNA-seq data with DESeq2. Genome Biol. 15, 550.

Mehta, V., Abler, L.L., Keil, K.P., Schmitz, C.T., Joshi, P.S., Vezina, C.M., 2011. Atlas of Wnt and R-spondin gene expression in the developing male mouse lower urogenital tract. Dev. Dyn. 240, 2548-2560.

Mehta, V., Schmitz, C.T., Keil, K.P., Joshi, P.S., Abler, L.L., Lin, T.M., Taketo, M.M., Sun, X., Vezina, C.M., 2013. Beta-catenin (CTNNB1) induces Bmp expression in urogenital sinus epithelium and participates in prostatic bud initiation and patterning. Dev. Biol. 376, 125-135.

Monk, M., Boubelik, M., Lehnert, S., 1987. Temporal and regional changes in DNA methylation in the embryonic, extraembryonic and germ cell lineages during mouse embryo development. Development 99, 371-382.

Nasonkin, I.O., Merbs, S.L., Lazo, K., Oliver, V.F., Brooks, M., Patel, K., Enke, R.A., Nellissery, J., Jamrich, M., Le, Y.Z., Bharti, K., Fariss, R.N., Rachel, R.A., Zack, D.J., Rodriguez-Boulan, E.J., Swaroop, A., 2013. Conditional knockdown of DNA methyltransferase 1 reveals a key role of retinal pigment epithelium integrity in photoreceptor outer segment morphogenesis. Development 140, 1330-1341.

Niculescu, A.B., 3rd, Chen, X., Smeets, M., Hengst, L., Prives, C., Reed, S.I., 1998. Effects of p21(Cip1/Waf1) at both the G1/S and the G2/M cell cycle transitions: pRb is a critical determinant in blocking DNA replication and in preventing endoreduplication. Mol. Cell. Biol. 18, 629-643.

Ozawa, K., 2008. Reduction of phosphorylated histone H3 serine 10 and serine 28 cell cycle marker intensities after DNA damage. Cytometry. Part A : the journal of the International Society for Analytical Cytology 73, 517-527.

Palii, S.S., Van Emburgh, B.O., Sankpal, U.T., Brown, K.D., Robertson, K.D., 2008. DNA methylation inhibitor 5-Aza-2'-deoxycytidine induces reversible genome-wide DNA damage that is distinctly influenced by DNA methyltransferases 1 and 3B. Mol. Cell. Biol. 28, 752-771.

Quick, C.M., Gokden, N., Sangoi, A.R., Brooks, J.D., McKenney, J.K., 2010. The distribution of PAX-2 immunoreactivity in the prostate gland, seminal vesicle, and ejaculatory duct: comparison with prostatic adenocarcinoma and discussion of prostatic zonal embryogenesis. Hum. Pathol. 41, 1145-1149.

Reik, W., Dean, W., Walter, J., 2001. Epigenetic reprogramming in mammalian development. Science 293, 1089-1093.

Seifert, A.W., Harfe, B.D., Cohn, M.J., 2008. Cell lineage analysis demonstrates an endodermal origin of the distal urethra and perineum. Dev. Biol. 318, 143-152.

Signoretti, S., Loda, M., 2006. Defining cell lineages in the prostate epithelium. Cell cycle (Georgetown, Tex.) 5, 138-141.

Signoretti, S., Pires, M.M., Lindauer, M., Horner, J.W., Grisanzio, C., Dhar, S., Majumder, P., McKeon, F., Kantoff, P.W., Sellers, W.R., Loda, M., 2005. p63 regulates commitment to the prostate cell lineage. Proc. Natl. Acad. Sci. U. S. A. 102, 11355-11360.

Soriano, P., 1999. Generalized lacZ expression with the ROSA26 Cre reporter strain. Nat. Genet. 21, 70-71.

Srinivas, S., Watanabe, T., Lin, C.S., William, C.M., Tanabe, Y., Jessell, T.M., Costantini, F., 2001. Cre reporter strains produced by targeted insertion of EYFP and ECFP into the ROSA26 locus. BMC Dev. Biol. 1, 4.

Taube, J.H., Allton, K., Duncan, S.A., Shen, L., Barton, M.C., 2010. Foxa1 functions as a pioneer transcription factor at transposable elements to activate Afp during differentiation of embryonic stem cells. J. Biol. Chem. 285, 16135-16144.

Wang, J., Vasaikar, S., Shi, Z., Greer, M., Zhang, B., 2017. WebGestalt 2017: a more comprehensive, powerful, flexible and interactive gene set enrichment analysis toolkit. Nucleic Acids Res. 45, W130-W137.

Wozniak, R.J., Klimecki, W.T., Lau, S.S., Feinstein, Y., Futscher, B.W., 2007. 5-Aza-2'-deoxycytidine-mediated reductions in G9A histone methyltransferase and histone H3 K9 di-methylation levels are linked to tumor suppressor gene reactivation. Oncogene 26, 77-90.

Yuan, J.S., Reed, A., Chen, F., Stewart, C.N., 2006. Statistical analysis of real-time PCR data. BMC Bioinformatics 7, 85.

CHAPTER 4. A FOLIC ACID-ENRICHED DIET ATTENUATES PROSTATE INVOLUTION IN RESPONSE TO ANDROGEN DEPRIVATION

Adapted from **Diya B Joseph**, Anoop S Chandrashekar, Li-Fang Chu, James A Thomson and Chad M Vezina

A folic acid-enriched diet attenuates prostate involution in response to androgen deprivation. The Prostate (2018) ;1–12. https://doi.org/10.1002/pros.23723

4.1. Introduction

The prostate is susceptible to aging related hyperplastic growth, which contributes to urethral obstruction and urinary dysfunction (McVary, 2006; Rosen et al., 2005). Diet is a potential risk modifier for prostate-related urinary disorders. For example, excessive caloric intake is associated with obesity and diabetes, which in turn increases risk of benign prostatic hyperplasia (BPH) and associated Lower Urinary Tract symptoms (LUTS) (Breyer and Sarma, 2014; Parikesit et al., 2016; Parsons et al., 2013; Sarma and Kellogg Parsons, 2009). On the other hand, dietary modifications and supplements are increasingly used alone or in combination with pharmacological and surgical interventions in attempt to control BPH symptoms (Espinosa, 2013). Environmental factors, including diet, have also been linked to prostate cancer incidence. Dietary modifications are gaining popularity as inexpensive and minimally invasive strategies for reducing prostate cancer risk, slowing its progression and preventing advanced disease (Ma and Chapman, 2009; Stacewicz-Sapuntzakis et al., 2008).

Folates are water soluble vitamins involved in numerous biochemical processes including one-carbon transfer, DNA synthesis, cell growth, hematopoiesis, metabolism and DNA methylation. Folates are the naturally occurring form of Vitamin B9 and are particularly concentrated in green leafy vegetables (Crider et al., 2012). Folic acid is the synthetic form in fortified food stuffs and most multi-vitamin supplements, the use of which is prevalent across all age groups, and particularly in older men (Bailey et al., 2010a; Bailey et al., 2011; Bailey et al., 2010b). Folic acid consumption by pregnant women is so effective in reducing the incidence of neural tube defects in offspring (Honein et al., 2001; MRC, 1991) that the United States mandated folic acid fortification of cereal grains

beginning in 1998 (Jagerstad, 2012). This action has affected many individuals, not just pregnant women. In fact, 34% of American men over 60 years of age have serum biomarkers consistent with folic acid excess (Bailey et al., 2010c).

Despite the overwhelming positive effects of folic acid in preventing neural tube defects, the consequences of folate supplementation at various stages of life and during disease processes are not fully understood. The complex roles of folates in the body could yield protective or deleterious effects depending on the context. Unmetabolized folic acid reduces natural killer cell function in post-menopausal women (Troen et al., 2006a). Maternal and post-weaning folic acid supplementation increases mammary cancer risk in rats (Ly et al., 2011) and induces anxiety-like behavior in mice (Barua et al., 2014a). Folic acid supplementation changes DNA methylation at several gene loci in mice and humans with unknown consequences (Barua et al., 2016a, b; Barua et al., 2014b; Sie et al., 2011; Steegers-Theunissen et al., 2009). Folates are also involved in the synthesis of polyamines (Bistulfi et al., 2009; Sun et al., 2002), depletion of which has been proposed as a prostate cancer therapy (Devens et al., 2000). We reported previously that a folic acid (FA) enriched diet given from conception through adulthood diminishes urinary symptom severity in male mice with hormone induced urinary obstruction (Keil et al., 2015). However, the impact of folic acid supplementation on adult prostate homeostasis has not been specifically investigated.

Here we examine how exposure to a FA enriched diet during the *in utero* period and continuing into adulthood affects the mouse prostate and its response to androgen deprivation by castration. Though intact mouse prostate weight weights are unaffected by diet, mice exposed to the FA enriched diet have significantly higher prostate wet weights

compared to mice on a control diet after castration. The FA enriched diet also leads to taller prostate luminal epithelial cells and more abundant secretory protein-encoding mRNAs compared to control diet mice after castration. Together, our results indicate that dietary folic acid attenuates the prostate response to androgen deprivation. This has important implications for androgen deprivation therapies that are commonly used to treat prostate cancer and benign prostatic hyperplasia (McConnell, 1990; Nicholson and Ricke, 2011; Perlmutter and Lepor, 2007). Elevated folate levels could diminish the efficacy of these therapies.

4.2. Materials and Methods

Mice

C57BL/6J (000664, The Jackson laboratory) nulliparous females were housed as previously described (Keil et al., 2015). At sexual maturity, females were placed on a base diet (control diet, Envigo 2019, Harlan Teklad, Madison, WI) containing 4 mg folic acid / kg feed or the same base diet containing 24 mg folic acid / kg feed (FA enriched diet, Envigo 120256, Harlan Teklad, Madison, WI) for 2 weeks prior to mating. The manufacturer of the diet estimates 4 mg folic acid/kg feed in the Control diet. This estimate includes folates derived from cereal grains and yeast extract. The folic acid enriched diet is prepared by adding 20 mg folic acid/kg feed to the Control diet. While absolute values of folic acid may differ seasonally, the magnitude of difference is consistently the same: 20 mg folic acid / kg feed. The control diet (4 mg folic acid/kg feed) provides twice the daily folic acid requirement for mice (2 mg folic acid/kg feed) (Meadows et al., 2015). The FA enriched diet provides approximately 12 times the daily folic acid requirement for mice (Meadows, 2015) which is comparable to the 10x higher dose consumed by pregnant

women at risk for neural tube defects (0.4 mg/day vs 4 mg/day) (CDC, 1991). The 2-week loading period has been shown to raise maternal serum folic acid concentrations (Oh et al., 2009).

Dams were placed on the diets throughout pregnancy and lactation and resulting offspring were also maintained on the same diet throughout the experiment. At 7 weeks of age, male mice were euthanized by CO_2 asphyxiation for tissue collection (Intact) or subject to bilateral orchiectomy (castration) under isoflurane anesthesia and given 5 mg/kg ketoprofen for analgesia. Castrated mice were euthanized 3, 10 or 14 days post-castration. Body weights were recorded at time of necropsy and prostate, seminal vesicles and serum were collected. Prostate and seminal vesicle absolute wet weights were measured using an analytical balance and divided by mouse whole body weights to obtain relative weights. All procedures involving mice were approved by the University of Wisconsin Animal Care and Use Committee and conducted in accordance with the National Institutes of Health Guide for the Care and Use of Laboratory Animals.

Fluorescent Immunohistochemistry

Fluorescent immunohistochemistry was performed as described previously (Abler et al., 2011). Dissected tissues were fixed overnight in 4% paraformaldehyde solution and embedded in paraffin for sectioning. 5 μm paraffin sections were deparaffinized in xylene and hydrated through a series of ethanol washes. Heat mediated antigen retrieval was performed by boiling slides in 10 mM sodium citrate (pH 6.0) for 20 mins in a conventional microwave oven. Tissues were washed with a solution containing 25 mM Tris-HCl, pH 7.5, 140 mM NaCl, 2.7 mM KCl, and 0.1% Tween-20 (TBSTw) and non-specific binding sites were blocked for 1 hr in TBSTw containing 1% Blocking Reagent (Roche

Diagnostics, Indianapolis, IN), 5% normal goat sera, and 1% bovine serum albumin fraction 5 (RGBTw). Tissues were incubated overnight at 4^0C with primary antibodies diluted in RGBTw. Primary antibody sources and dilutions are: Ki67 (ab15580, 1:400 dilution) from Abcam, Cambridge, MA, USA. CDH1 (610181, 1:500 dilution) from BD Biosciences, San Jose, CA, USA. Cleaved Caspase 3 Asp175 (9664, 1:200 dilution) from Cell Signaling Technology, Beverly, MA, USA. Androgen Receptor (sc-816, 1:200 dilution) from Santa Cruz Biotechnology, Dallas, TX, USA. Tissues were washed several times in TBSTw and incubated with secondary antibodies diluted in RGBTw for 1 hour at room temperature. The secondary antibodies and dilutions are: goat anti-Mouse AlexaFluor488 (115-547-003, 1:500 dilution), goat anti-Rabbit AlexaFluor594 (111-586-045, 1:500 dilution), goat anti-Mouse AlexaFluor594 (115-585-062, 1:500 dilution), goat anti-Rabbit AlexaFluor488 (111-487-003, 1:500 dilution) from Jackson ImmunoResearch, West Grove, PA, USA. Following several washes with TBSTw, tissues sections were incubated with 4',6-diamidino-2-phenylindole, dilactate (DAPI) to visualize cell nuclei and mounted in phosphate buffered saline containing 80% glycerol and 0.2% n-propyl gallate. Images were captured using a Leica SP8 Confocal Microscope fitted with a 20X oil immersion objective (HC PL Apo CS2 NA = 0.75) (Leica, Wetzlar, Germany) or a Nikon Eclipse E600 compound microscope fitted with 10X (Plan Fluor NA = 0.30) and 20X (Plan Fluor NA = 0.50) objectives (Nikon Instruments Inc., Tokyo, Japan). Tissue sections from both diet groups were imaged using the same exposure settings.

Prostate luminal cell height measurements

Fluorescent immunohistochemistry for the epithelial marker E-cadherin (CDH1) was performed as described above on 5 μm paraffin sections of ventral prostate tissue.

Images were obtained using a 20x objective on a Nikon Eclipse E600 compound microscope. Prostate luminal cells were identified by their characteristic tall, columnar morphology. Cell heights were measured using the *Straight-line* tool and *Analyze>Measure* function in ImageJ. Measurements were taken from 7 individual cells separated by > 5 cells in each field. Ventral prostate tissue sections from at least three mice per diet group were used for analyses.

Proliferative and apoptotic index measurements

Fluorescent immunohistochemistry for Ki67 and cleaved Caspase 3 was performed as described above on 5 μm paraffin sections of ventral prostate tissue. Slides were counterstained with DAPI to visualize nuclei. Images were obtained using a 20x objective on a Nikon Eclipse E600 compound microscope. DAPI stained nuclei in the field were counted using the *Analyze Particles* function in ImageJ. Ki67 and cleaved Caspase 3 positive cells were manually counted using the *Cell counter* plugin for ImageJ. Proliferative index is defined as Ki67 positive cells as a percent of total cells and the apoptotic index is defined as cleaved Caspase 3 positive cells as a percent of total cells. Ventral prostate tissue sections from at least three mice per diet group were used for analyses.

Real time quantitative PCR

Quantitative PCR was carried out as previously described (Keil et al., 2012) on ventral prostate tissue using gene-specific primers. Primer sequences are provided in Table 4.1. Relative mRNA abundance was determined using the ΔCt method (Yuan et al., 2006) and normalized to the abundance of beta-2-microglobulin (*B2m*). Ventral prostate tissue from at least three mice per diet group were used for analyses.

Serum Testosterone measurements

Mice were euthanized by CO_2 asphyxiation and blood was collected by cardiac puncture, clotted for 45 mins and centrifuged at 6000g for 10 mins to clear the serum. Serum testosterone measurements were carried out using a testosterone ELISA kit (#55-TESMS-E01, ALPCO, Salem, NH, USA) following the manufacturer's instructions. Sera from at least three mice per diet group were used for the analysis.

RNA-Seq

RNA was isolated from the ventral prostates of mice belonging to six experimental groups: Control diet-Intact (N=4), FA diet-Intact (N=4), Control diet-3d post-castration (N=3), FA diet-3d post-castration (N=4), Control diet-10d post-castration (N=4) and FA diet-10d post-castration (N=4) using the Illustra RNAspin Mini kit (#25-0500-72, GE Healthcare, Chicago, Illinois, USA). Approximately 100 ng of total RNA from each diet group was used to construct the RNA-Seq library according to the LM-seq protocol (Hou et al., 2015). The reads generated from the Illumina HiSeq 3000 (78 cycles of insert read and 10 cycles of index read) were processed with CASAVA-1.8.2 basecalling software (Illumina). The demultiplexing step allotted approximately 253 million total reads across all the samples, ranging from ~6.5 million to ~15.8 million reads assigned per sample. Reads were mapped to *Mus musculus* reference mm10 assembly with an average of ~82.4% mapping rate using Bowtie (Langmead et al., 2009), and gene expression estimates were obtained using RSEM (Li and Dewey, 2011). Differentially expressed genes were identified using the *EBSeq* package (Leng et al., 2013). Gene Ontology enrichment analysis for biological processes was conducted using WebGestalt (Wang et al., 2017). RNA-seq data are available in Gene Expression Omnibus under GSE116299.

Statistics

Statistical analyses were conducted with *R* version 3.2.4. Homogeneity of variance was determined using Bartlett's test or Levene's test packages for *R*. Student's t-test was performed on parametric data with two groups. P values less than 0.05 were considered statistically significant. Results are presented as mean ± standard error of the mean (SEM). NS: Not significant, * $p<0.05$, ** $p<0.01$, *** $p<0.001$.

4.3. Results

FA enriched diet blunts castration-mediated mouse prostate gland involution

Reducing androgen synthesis is a therapeutic strategy for prostate-related growth diseases including BPH and prostate cancer. Our primary goal was to determine if continuous dietary FA supplementation modifies the prostate involution response to castration. Folate levels have risen across all age groups in the US, including women of child bearing age, children and older adults, since cereal grain fortification was mandated in 1998 (CDC, 2007; Pfeiffer et al., 2012; Pfeiffer et al., 2007). Our study design parallels this historical change by continuously exposing male mice to high levels of folic acid across all life stages. C57Bl6/J female mice were loaded on a control or FA enriched diet 2 weeks before mating and through pregnancy and lactation. Male offspring were continued on a matched diet through study completion (Figure 4.1 A).

The first objective was to test whether the FA enriched diet affects prostate homeostatic regulation by changing prostate wet weight. We did not find significant diet group differences in body weight (Figure 4.1 B), relative prostate weight (all prostate lobes combined) (Figure 4.2 A) or relative seminal vesicle weight in intact mice (Figure 4.2 E).

We next tested whether a FA enriched diet interferes with castration-induced prostate involution. 7-week old sexually mature mice were castrated and tissues weighed at 3, 10 and 14 days post- castration. The relevance of these time points is that prostate apoptosis peaks approximately 3 days post-castration and prostate involution is complete by 14 days post-castration (Lee, 1981; Wang et al., 2007). Body weights did not differ between diet groups for each treatment (Figure 4.1 B). Relative prostate and seminal vesicle weights were reduced by castration in both diet groups as expected. However, castration-mediated prostate gland involution was unexpectedly incomplete in FA enriched diet fed mice, as evidenced by significantly greater relative prostate weights than castrated control diet fed mice at 3, 10 and 14 days post-castration (Figure 4.2 B-D). Similarly, FA enriched diet fed mice had significantly greater relative seminal vesicle weights than castrated control diet fed mice at 3 and 10 days post-castration (Figure 4.2 F-H).

FA enriched diet prostates retain greater luminal epithelial secretory gene expression and luminal cell heights after castration

Castration causes prostate luminal epithelial cells to undergo apoptosis (English et al., 1987; Isaacs et al., 1994; Lee, 1981; Wang et al., 2007). Dietary modulation of prostatic apoptosis could underlie differences in the castration response. We tested whether there were also diet-mediated changes to prostatic cell proliferation for the same reason. Indices of Ki67 labeling (proliferation) and Cleaved Caspase 3 labeling (apoptosis) were very low in intact mouse ventral prostates and unaffected by diet. Likewise, ventral prostate Ki67 and Cleaved caspase 3 labeling indices did not differ significantly between control and FA enriched diet fed castrated mice (Figure 4.3 A-N).

Because prostate cell cycling was unaffected by diet, we evaluated changes to prostate secretory protein synthesis as an alternative explanation for why prostates of FA enriched diet fed castrated mice are larger than those of control diet fed castrated mice. Androgen dependent secretory proteins are stored in apically localized granules within prostate luminal epithelial cells (Cohen et al., 1998). Castration reduces secretory granule number and luminal epithelial cell height (Kawamura et al., 1993). Ventral prostate luminal epithelial cell height is progressively reduced by castration in both diet groups as expected. However, the FA enriched diet confers partial resistance and is associated with taller luminal epithelial cells at 3 and 10 days post-castration compared to control diet fed mice (Figure 4.3 O-U).

Castration reduces androgen dependent prostatic secretory gene transcription and secretory protein content, which is a major component of prostate weight (Isaacs et al., 1994; Mills et al., 1987; Wang et al., 1997). We focused on the ventral prostate and quantified mRNA abundance of spermine binding protein (*Sbp*), a ventral prostate-specific secretory protein (Mills et al., 1987). Castration reduces *Sbp* mRNA abundance but *Sbp* mRNA was significantly more abundant in castrated FA diet fed mice compared to control diet fed mice at 10 days and 14 days post-castration (Figure 4.4 A). We further quantified abundance of another mRNA encoding a ventral prostate specific androgen dependent secreted protein, Serine protease inhibitor Kazal-type 1 (*Spink1*) (Berquin et al., 2005). Similar to *Sbp*, Castration reduces *Spink1* mRNA expression but *Spink1* mRNA was significantly more abundant in castrated FA diet fed mice compared to control diet fed mice at 10 days and 14 days post-castration (Figure 4.4 B). Taken together, our

results suggest that the increased prostate weights in castrated FA diet mice are a result of increased secretory activity and not increased proliferation or decreased apoptosis.

FA enriched diet does not change circulating androgens or Androgen receptor expression

We hypothesized that the FA diet might impair testosterone metabolism, thereby prolonging its half-life in castrated mouse serum and slowing the rate of prostate gland involution. Such a mechanism would explain the taller luminal cells and more abundant secretory gene mRNA expression in FA enriched diet mice compared to control diet fed castrated mice. Serum testosterone concentrations were measured by ELISA. As expected, testosterone concentrations were reduced at 3 and 10 days post-castration compared to intact mice in both diet groups. Surprisingly, there were no diet group differences in serum testosterone concentrations among intact or castrated mice (Figure 4.5 A).

We tested whether the FA diet changed ventral prostate Androgen receptor (*Ar*) mRNA abundance as an alternative mechanism to blunt glandular involution following castration. Relative *Ar* mRNA abundance was increased in both diet groups after castration, consistent with the previous observation that AR signaling negatively regulates *Ar* transcription (Banerjee et al., 2001). However, *Ar* mRNA abundance in castrated mice did not differ between control and FA enriched diet mice (Figure 4.5 B). Nuclear localization of AR, an indicator of active androgen signaling, is detected in luminal epithelial cells and a subset of stromal cells in intact prostates from both diet groups. However, nuclear AR is undetectable at 3, 10 and 14 days post castration in both diet groups (Figure 4.5 C-J).

FA enriched diet changes the mouse ventral prostate gene expression signature, affecting genes involved in nucleotide metabolism and DNA repair

To identify global changes in gene expression in FA enriched diet mice, RNA-Seq analysis was performed on RNA from intact, 3 and 10 days post-castration ventral prostates from both diet groups. Comparing Intact mice from both diet groups, we observed upregulation of 123 genes and downregulation of 193 genes in the FA enriched diet prostates (Table 4.2). Gene Ontology analysis revealed that genes upregulated in the FA enriched diet prostates were enriched for biological processes involved in DNA repair and cellular response to DNA damage stimulus. Downregulated genes in the FA enriched diet prostates were enriched for biological processes involved in muscle contraction and endoplasmic reticulum stress (Table 4.3). These results indicate that the FA enriched diet changes the gene expression program in ventral prostates from intact mice.

Comparing mice from both diet groups at 3 days post-castration, we observed upregulation of 113 genes and downregulation of 131 genes in the FA enriched diet prostates (Table 4.2). Downregulated genes in the FA enriched diet prostates at 3 days post-castration were enriched for biological processes regulating cell motility and migration (Table 4.3). Comparing mice from both diet groups at 10 days post-castration, we observed upregulation of 38 genes and downregulation of 84 genes in the FA enriched diet prostates (Table 4.2). The lower number of differentially expressed genes at 10 days post-castration compared to intact mice could be due to the overall reduction in transcriptional activity in the prostate following androgen deprivation. Upregulated genes in the FA enriched diet prostates at 10 days post-castration were enriched for biological

processes mediating purine nucleotide metabolism (Table 4.3). Significant upregulation of differentially expressed genes associated with the purine ribonucleoside diphosphate metabolic process (*Ampd3*, *Dlg2* and *P2rx7*) were confirmed by quantitative PCR (Figure 4.6). In summary, the FA enriched diet changes the baseline transcriptional program of the intact mouse ventral prostate. The ventral prostate gene expression pattern of mice consuming a FA enriched diet was different than that of control diet fed mice at 3 and 10 days post-castration.

4.4. Discussion

We showed that dietary folic acid supplementation changes mouse prostatic gene expression and blunts castration-mediated prostate involution. Mice fed a diet supplemented with folic acid at 12 times the daily requirement for mice, and examined 3, 10 and 14 days after castration had larger prostates, taller prostatic luminal epithelial cells and more abundant ventral prostate specific *Sbp* and *Spink1* secretory gene mRNA than treatment matched controls. In addition, the FA enriched diet changed the prostatic gene expression profile, specifically affecting genes involved in nucleotide biosynthesis and DNA repair. Because androgens are required for prostate and seminal vesicle maintenance, attenuated involution of both organs after castration suggests that the FA diet affects these organs by the same mechanism. Taller prostatic luminal epithelial cells and more abundant secretory mRNAs are consistent with glandular secretory activity enduring longer after castration in FA enriched diet fed mice than in controls.

Folic acid is a synthetic and oxidized form of dietary folates and is more stable and bioavailable. Excessive folic acid consumption causes un-metabolized folic acid to accumulate in circulation. Unmetabolized folic acid is detectable in serum of 40% of older

adults and is particularly abundant in folic acid supplement users (Bailey et al., 2010c). The consequences are not always beneficial (Caudill, 2010; Crider et al., 2011; Smith et al., 2008). For example, excessive unmetabolized folic acid has been linked to impaired immune function in post-menopausal women (Troen et al., 2006b). Folic acid, in the form of folate, also participates in several metabolic processes including nucleotide biosynthesis, polyamine synthesis and DNA methylation that influence cell proliferation and survival. Folic acid reduces efficacy of anti-proliferative cancer drugs *in vitro* (Xavier et al., 2016) and supports cancer stem cell-like properties of human colorectal cancer cells *in vitro* (Farias et al., 2015). In this model, we do not observe any effect of the FA enriched diet on prostate cell proliferation. The impact of the FA enriched diet on castration-mediated prostate involution could be a consequence of a systemic shift in metabolism that favors cell survival, a notion supported by the altered prostatic gene expression profile resulting from continuous exposure to the FA enriched diet.

The impact of folates on prostate cancer risk is currently inconclusive. A 5-year clinic trial involving folic acid supplementation found no correlation between folic acid supplementation and cancer risk (Vollset et al., 2013). However, in another study, men given folic acid supplements had an increased risk of prostate cancer compared to the placebo group although baseline folate levels in non-supplement users were inversely associated with prostate cancer risk (Figueiredo et al., 2009). Additional studies report that high serum folate levels modestly increase prostate cancer risk (Collin et al., 2010; de Vogel et al., 2013) and prostate cell proliferation in prostate cancer patients (Tomaszewski et al., 2011). Further research on the impact of folates on prostate biology is needed due to widespread fortification and supplement use.

Serum folate levels have risen in all age groups in the last few decades, with aging men experiencing a substantial increase (Pfeiffer et al., 2012). We found that a FA enriched diet attenuates the prostate involution response to castration. Because drugs that reduce or prevent androgen synthesis are widely used for treating BPH and prostate cancer, our study identifies a new need to address interactions between dietary folate and androgen-reducing therapy efficacy.

In conclusion, we identified an interaction between dietary folic acid supplementation and tissue involution in response to androgen deprivation. Dietary folic acid supplementation attenuated the involution of two androgen dependent organs, the prostate and seminal vesicle, after castration. In the prostate, this was accompanied by greater luminal epithelial cell secretory activity and secretory gene expression compared to castrated controls. Given the widespread use of folic acid in dietary supplements and fortified food stuffs, our conclusions warrant further research into the interaction between folic acid supplementation and anti-androgen therapies used to treat prostate disease.

4.5. Figures and Tables

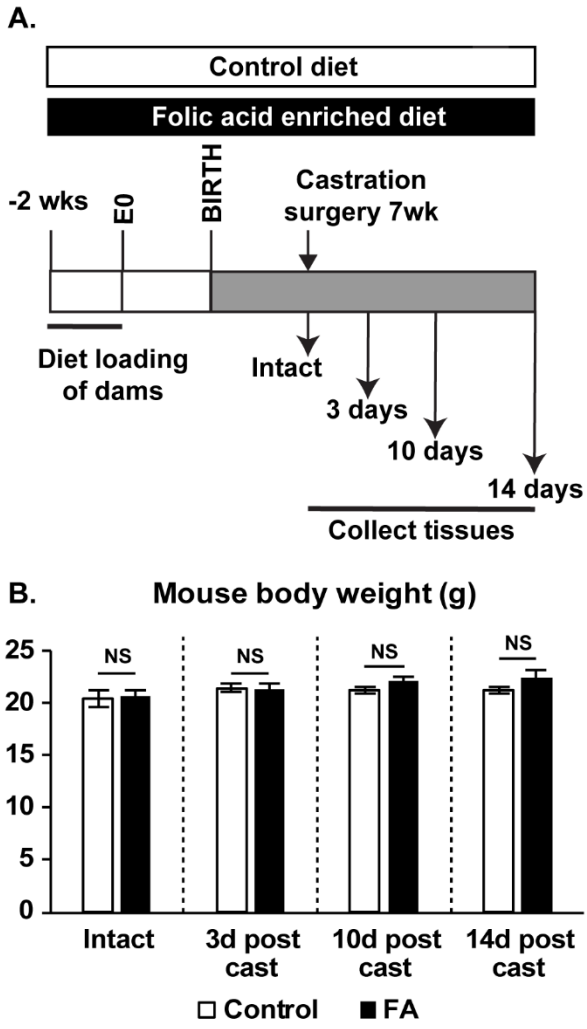

Figure 4.1 Study design

(A) Study design. (B) Mouse body weights do not change across diet or treatment groups. Number of mice per group: Control-Intact N=8, FA-Intact N=11, Control-3d post cast N=8, FA-3d post cast N=7, Control-10d post cast N=14, FA-10d post cast N=15, Control-14d post cast N=5, FA-14d post cast N=5. Results are presented as mean ± SEM. Homogeneity of variance was tested using Bartlett's test. p-values represent results from

unpaired Student's t-test between diet groups for each treatment. NS: Not significant p>0.05. Abbreviations FA: Folic Acid, d post cast: days post castration.

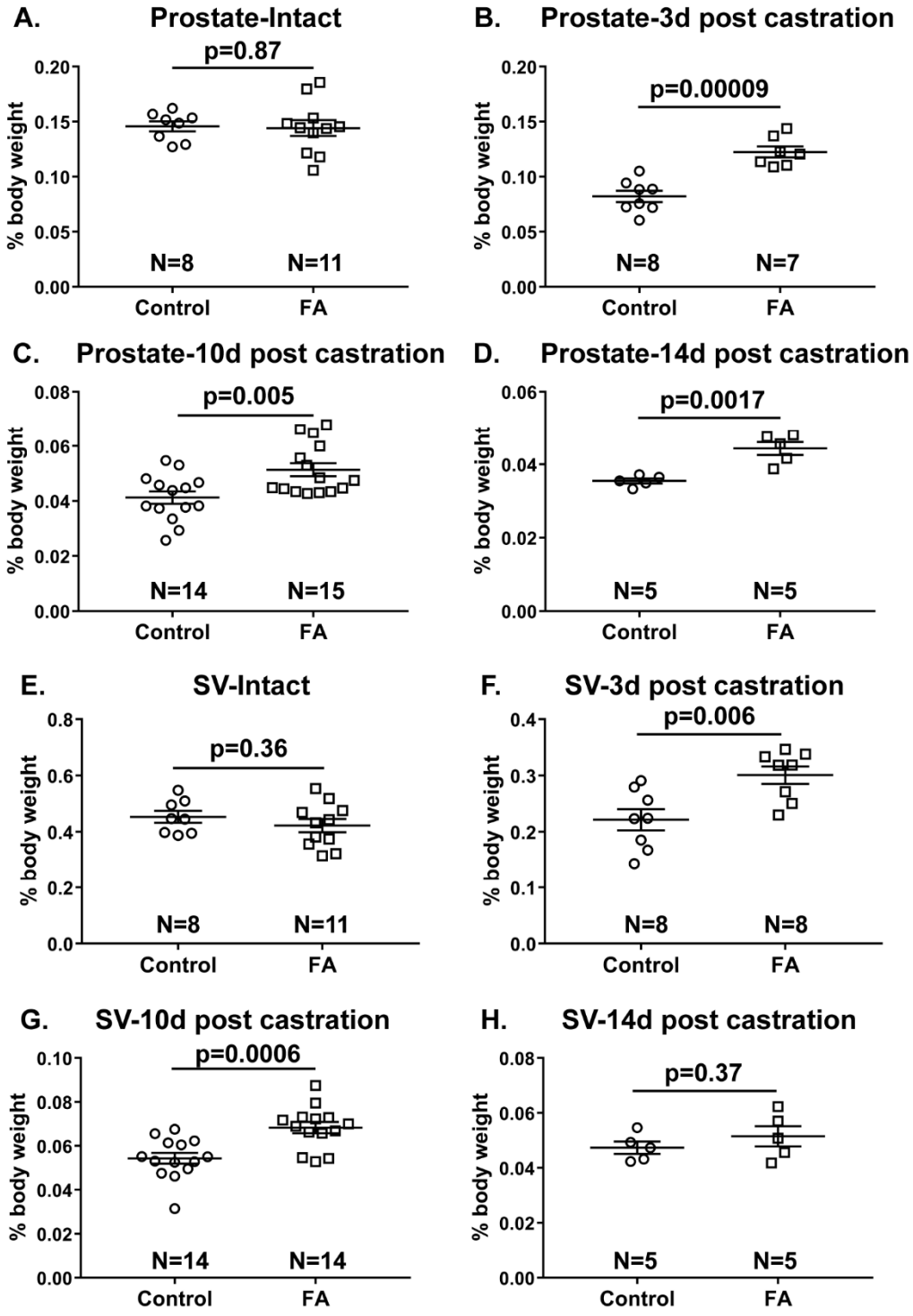

Figure 4.2 Mice fed a FA enriched diet and then castrated have greater prostate and seminal vesicle weights than mice fed a control diet and castrated.

Relative prostate and seminal vesicle (SV) wet weights were determined as percentage of mouse body weight for: (A, E) Intact mice or mice (B, F) 3 days (C, G) 10 days (D, H) or 14 days post castration. N value indicates number of mice/group. Results are presented as mean ± SEM. Homogeneity of variance was tested using Bartlett's test. p-values represent results from unpaired Student's t-test between diet groups for each treatment.

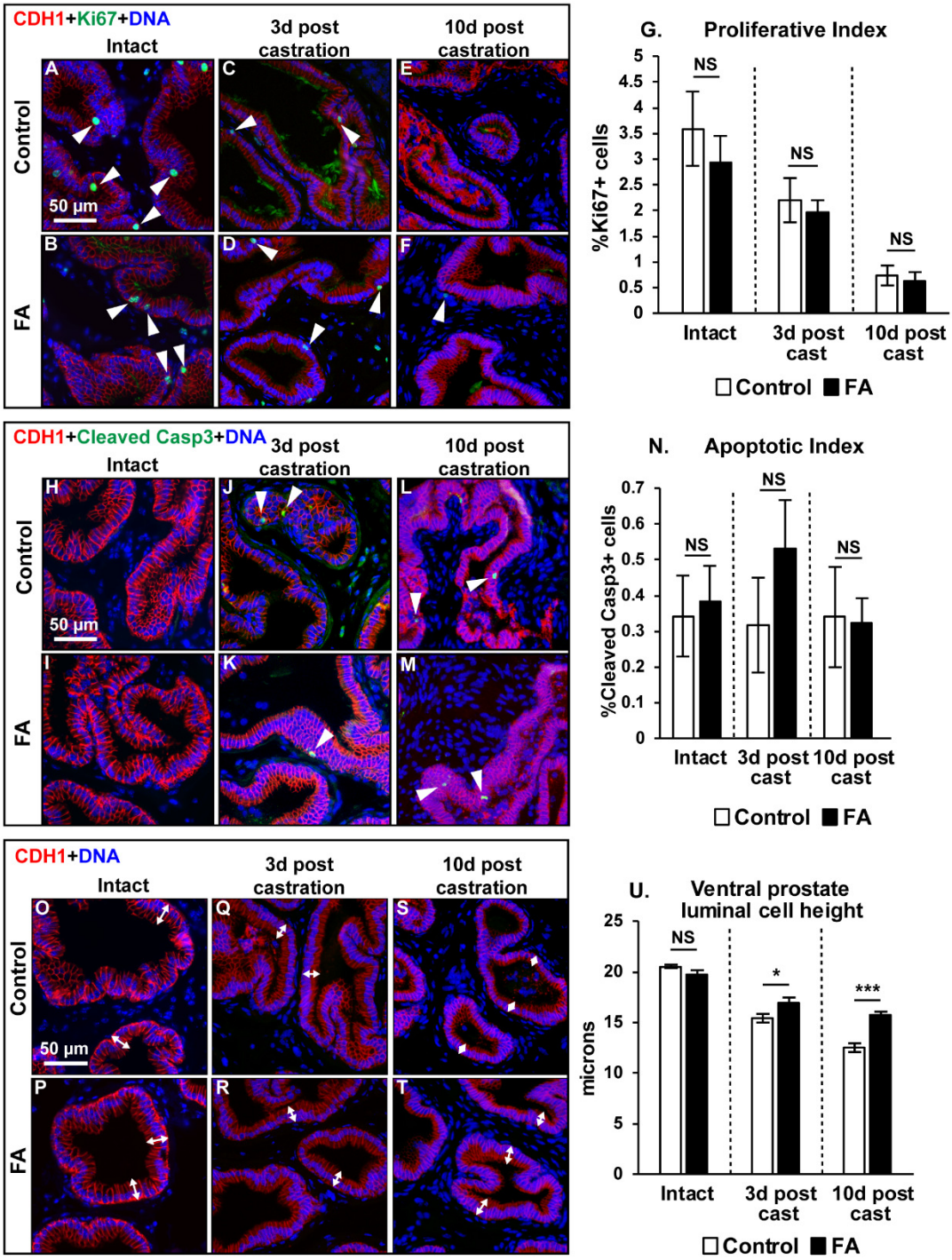

Figure 4.3 Greater luminal epithelial cell heights in castrated FA diet prostates compared to control diet mice but no differences in prostate cell proliferation and apoptosis between diet groups.

Mouse ventral prostate sections were labeled with antibodies to CDH1 (red) and Ki67 (green). Representative images are shown for (A-B) Intact mice or mice (C-D) 3 days (E-F) or 10 days post-castration. (G) Proliferation indices were compared between diet groups. Number of mice per group: Control-Intact N=7, FA-Intact N=8, Control-3d post cast N=7, FA-3d post cast N=7, Control-10d post cast N=6, FA-10d post cast N=5. Mouse ventral prostate sections were also labeled with antibodies to CDH1 (red) and Cleaved caspase 3 (green). Representative images are shown for (H-I) Intact mice or mice (J-K) at 3 days (L-M) or 10 days post-castration. (N) Apoptotic indices were compared between diet groups. Number of mice per group: Control-Intact N=8, FA-Intact N=10, Control-3d post cast N=8, FA-3d post cast N=6, Control-10d post cast N=6, FA-10d post cast N=4. Ventral prostate sections from both diet groups were labeled with antibodies to CDH1 (red). Representative images are shown for (O-P) Intact mice, (Q-R) mice at 3 days post-castration (S-T) and 10 days post castration. (U) Prostate luminal epithelial cell heights were compared between diet groups. N values for groups are as follows: Control-Intact N=4, FA-Intact N=5, Control-3d post cast N=4, FA-3d post cast N=3, Control-10d post cast N=6, FA-10d post cast N=5. DAPI staining is show in blue. Scale bar is 50 μm. White arrowheads indicate Ki67 or cleaved caspase 3 labeled cells. White double headed arrows depict cell height of selected luminal epithelial cells. Graphical results are presented as mean $\pm$ SEM. Homogeneity of variance was tested using Bartlett's test. p-values represent results from unpaired Student's t-test test between diet groups for each treatment. * $p<0.05$, ** $p<0.01$, ***$p<0.001$, NS: Not significant $p>0.05$.

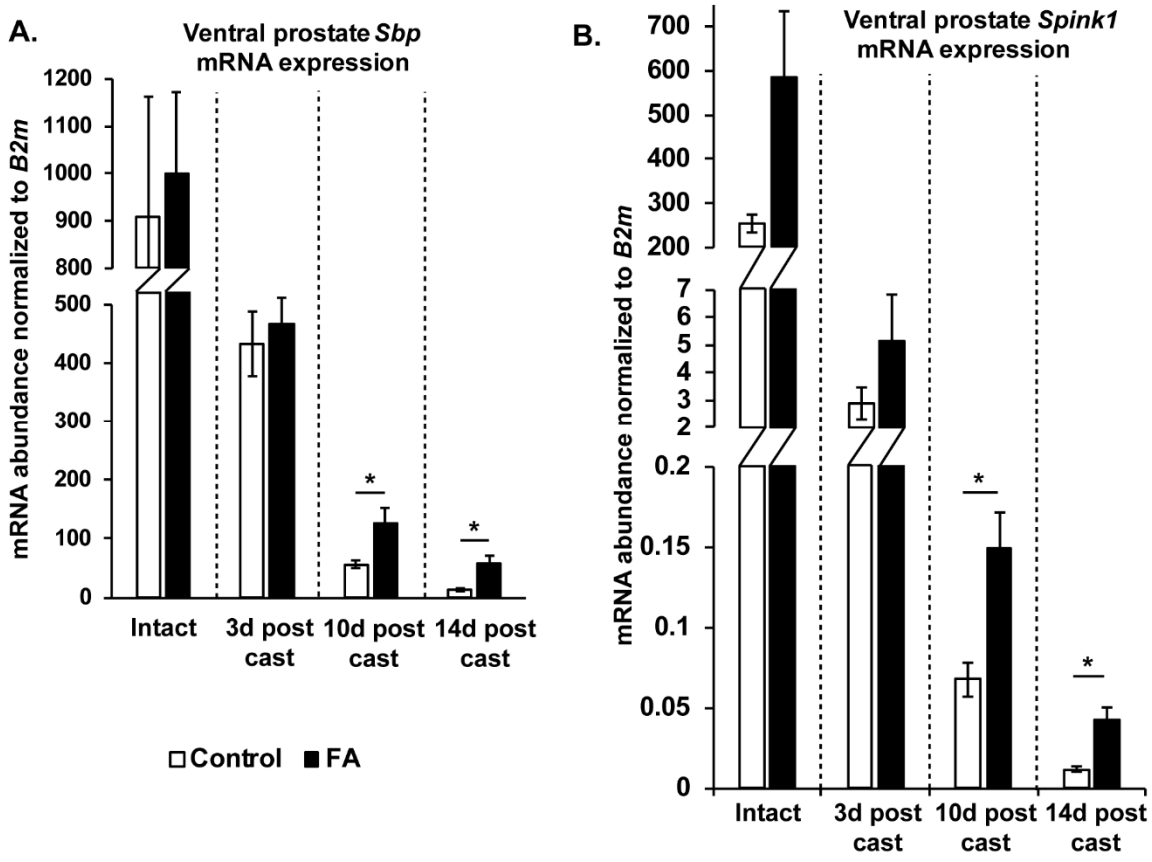

Figure 4.4 Mice fed a FA enriched diet and then castrated have relatively more ventral prostate specific secretory mRNAs *Sbp* and *Spink1*, than controls.

(A) mRNA abundance of *Sbp* was measured in Intact, 3 days, 10 days and 14 days post-castration ventral prostates from FA enriched diet or control diet fed mice. The abundance of *Sbp* was normalized to that of *B2m*. N values for groups are as follows: Control-Intact N=4, FA-Intact N=4, Control-3d post cast N=3, FA-3d post cast N=4, Control-10d post cast N=4, FA-10d post cast N=3, Control-14d post cast N=3, FA-14d post cast N=3. (B) mRNA abundance of *Spink1* was measured in Intact, 3 days, 10 days and 14 days post-castration ventral prostates from FA enriched diet or control diet fed mice. The abundance of *Spink1* was normalized to that of *B2m*. N values for groups are as follows: Control-

Intact N=4, FA-Intact N=4, Control-3d post cast N=3, FA-3d post cast N=4, Control-10d post cast N=3, FA-10d post cast N=3, Control-14d post cast N=3, FA-14d post cast N=3. Graphical results are presented as mean ± SEM of mRNA abundance. p-values represent results from unpaired Student's t-test between diet groups for each treatment, * $p<0.05$. Comparisons that did not produce significant p-values (>0.05) are not indicated.

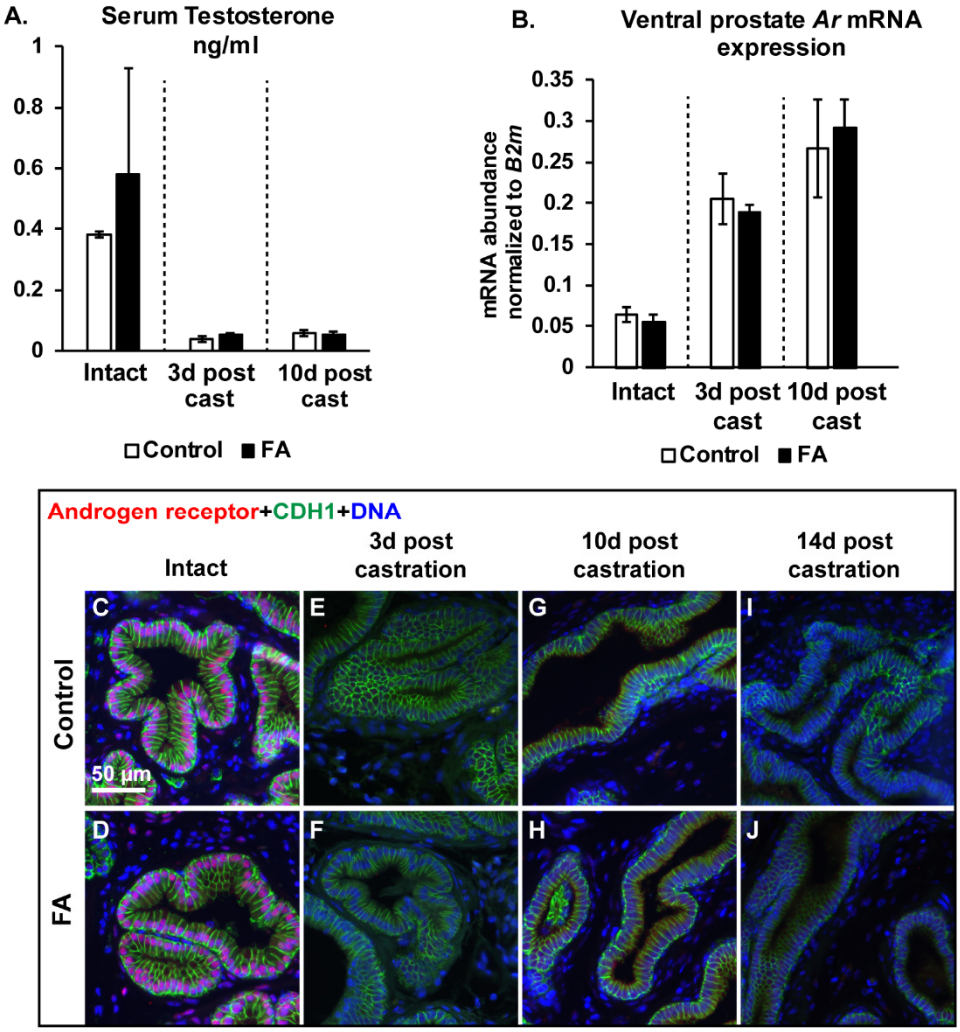

Figure 4.5 The FA enriched diet does not change circulating androgens or prostatic Androgen receptor (*Ar*) abundance compared to controls

(A) Serum testosterone concentrations were determined by ELISA. Serum from N=3 mice/group was used for analysis. (B) Ventral prostate *Ar* mRNA abundance normalized to *B2m*. N values for groups are as follows: Control-Intact N=4, FA-Intact N=4, Control-3d post cast N=3, FA-3d post cast N=4, Control-10d post cast N=4, FA-10d post cast N=4. Graphical results are presented as mean ± SEM. p-values represent results from unpaired Student's t-test between diet groups for each treatment. Comparisons that did not produce significant p-values (>0.05) are not indicated. Mouse ventral prostate sections were also labeled with antibodies to Androgen receptor (AR, red) and CDH1 (green). Representative images are shown for (C-D) Intact mice or mice (E-F) at 3 days (G-H) or 10 days post-castration or (I-J) or 14 days post-castration. DAPI staining is show in blue. Scale bar is 50 μm.

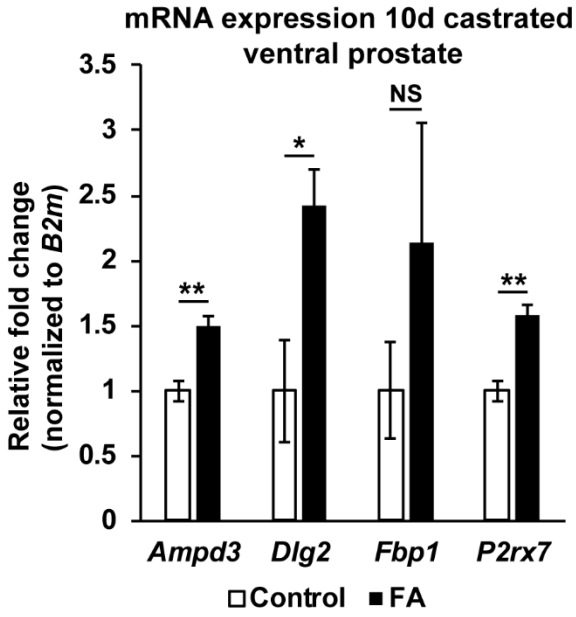

Figure 4.6 Increased expression of genes involved in purine ribonucleoside metabolism in FA enriched diet prostates after castration.

mRNA abundance of *Ampd3* (N=4 mice/diet group), *Dlg2* (N=4 mice/diet group), *Fbp1* (N=3 mice/diet group) and *P2rx7* (N=3 mice/diet group) were measured in 10 days post-castration ventral prostates from FA enriched diet or control diet fed mice. mRNA abundance was normalized to that of *B2m* and expressed as relative fold change to control diet samples. Graphical results are presented as mean ± SEM. p-values represent results from unpaired Student's t-test between diet groups for each treatment. * $p<0.05$, ** $p<0.01$, NS: Not significant $p>0.05$.

Table 4.1 Quantitative RT-PCR primer sequences

Gene name	Genbank entry	Forward 5'-3'	Reverse 5'-3'
B2m	NM_009735.3	GTGACCCTGGTCTTTCTGGTG	TATGTTCGGCTTCCCATTCTC
Sbp	NM_011321.2	AGAGCCCAGAATGTCCTGGG	TTATCACGTGCTCTCCGTCC
Spink1	NM_009258.5	GAAACGCATAGAGCCTGTCCTC	AACGAACCCACTTGCCAAAC
Ar	NM_013476.3	GATGGTATTTGCCATGGGTTG	GGCTGTACATCCGAGACTTGTG
Ampd3	NM_001276301.1	TGACTGGGTTTGACAGTGTGG	ACTATAGGGCGGGTTCTGCTC
Dlg2	NM_001243046.1	ACATCCCGCTCCTAAGTTTCC	CTTTGCTTTCTGGGCTGAGTG
Fbp1	NM_019395.3	GGATTGTGGTGTCAACTGCTTC	ATTGATGGCAGGGTCAAAGTC
P2rx7	NM_001038839.2	GCCAACTATGAACGGCTCTTG	CCATGATTCCTCCCTGAACTG

Table 4.2 Summary of differential gene expression determined by RNA-Seq

Comparison	Differentially expressed genes (FDR cutoff 0.05)	Upregulated in FA diet	Downregulated in FA diet
Intact: FA vs Control diet	n= 316	n= 123	n= 193
3d castration: FA vs Control diet	n= 244	n= 113	n= 131
10d castration: FA vs Control diet	n= 122	n= 38	n= 84

Table 4.3 Enriched GO terms in differentially expressed gene sets

Treatment	Differentially expressed gene list analyzed	GO ID Biological Process	Category	p-value	FDR (cutoff 0.05)	#genes	Genes
Intact	upregulated in FA	GO: 0006974	cellular response to DNA damage stimulus	2.85E-06	2.01E-02	14	*Bcl3,Gadd45a,Ei24,Mc1r,Rad23a, Morf4l1,Tdp2,Uchl5,Rec8,Dmap1, Ube2t,Nsmce4a,Ap5s1,Parp9*
Intact	upregulated in FA	GO:0006281	DNA repair	4.82E-06	2.01E-02	11	*Mc1r,Rad23a,Morf4l1,Tdp2,Uchl5, Rec8,Dmap1,Ube2t,Nsmce4a,Ap 5s1,Parp9*
Intact	downregulated in FA	GO:0003012	muscle system process	5.37E-09	4.47E-05	16	*Mybpc1,Actc1,Atp2a1,Casq1,Mef2 a,Myh4,Myh8,Myl3,Myl,Tcap,Tead1 ,Tnni2,Tnnt3,Mybpc2,Pgam2,Trdn*
Intact	downregulated in FA	GO:0006936	muscle contraction	1.50E-08	6.25E-05	14	*Mybpc1, Actc1, Atp2a1,Casq1,Myh4, Myh8, Myl3, Myl1, Tcap, Tnni2, Tnnt3, Mybpc2, Pgam2, Trdn*
Intact	downregulated in FA	GO:0034976	response to endoplasmic reticulum stress	1.41E-07	2.93E-04	12	*Dnajc3,Txndc5,Atp2a1,Pdia4,Pdia 3,Sel1l,Creb3l2,Erlin1,Dnajb9,Ed em3,Derl3,Syvn1*
3d castration	downregulated in FA	GO:0030334	regulation of cell migration	7.96E-07	4.31E-03	16	*Sema3d,Cygb,Capn7,Ecm1,Lam a4,Mmp9,Cxcl2,Cxcl5,Sphk1,Stat5 a,Tac1,Ndrg4,Pla2g7,Cxcl3,Nsmf, Rtn4*
3d castration	downregulated in FA	GO:2000145	regulation of cell motility	1.69E-06	4.69E-03	16	*Sema3d,Cygb,Capn7,Ecm1,Lam a4,Mmp9,Cxcl2,Cxcl5,Sphk1,Stat5 a,Tac1,Ndrg4,Pla2g7,Cxcl3, Nsmf,Rtn4*
3d castration	downregulated in FA	GO:0016477	cell migration	4.16E-06	6.71E-03	20	*Sema3d,Cygb,Artn,Capn7,Ecm1, Lama4,Mmp9,Pstpip2,Cxcl2,Cxcl5 ,Sphk1,Stat5a,Stat5b,Tac1,Ndrg4, Pla2g7,Cxcl3,Nsmf,Vav3,Rtn4*
10d castration	upregulated in FA	GO:0009135	purine nucleoside diphosphate metabolic process	9.84E-06	3.31E-02	4	*Ampd3,Fbp1,P2rx7,Dlg2*
10d castration	upregulated in FA	GO:0009179	purine ribonucleoside diphosphate metabolic process	9.84E-06	3.31E-02	4	*Ampd3,Fbp1,P2rx7,Dlg2*
10d castration	upregulated in FA	GO:0009167	purine ribonucleoside monophosphate metabolic process	3.15E-05	4.47E-02	5	*Ampd3,Fbp1,Myh8,P2rx7,Dlg2*

4.6. References

Abler, L.L., Keil, K.P., Mehta, V., Joshi, P.S., Schmitz, C.T., Vezina, C.M., 2011. A high-resolution molecular atlas of the fetal mouse lower urogenital tract. Dev. Dyn. 240, 2364-2377.

Bailey, R.L., Dodd, K.W., Gahche, J.J., Dwyer, J.T., McDowell, M.A., Yetley, E.A., Sempos, C.A., Burt, V.L., Radimer, K.L., Picciano, M.F., 2010a. Total folate and folic acid intake from foods and dietary supplements in the United States: 2003-2006. Am. J. Clin. Nutr. 91, 231-237.

Bailey, R.L., Gahche, J.J., Lentino, C.V., Dwyer, J.T., Engel, J.S., Thomas, P.R., Betz, J.M., Sempos, C.T., Picciano, M.F., 2011. Dietary supplement use in the United States, 2003-2006. J. Nutr. 141, 261-266.

Bailey, R.L., McDowell, M.A., Dodd, K.W., Gahche, J.J., Dwyer, J.T., Picciano, M.F., 2010b. Total folate and folic acid intakes from foods and dietary supplements of US children aged 1-13 y. Am. J. Clin. Nutr. 92, 353-358.

Bailey, R.L., Mills, J.L., Yetley, E.A., Gahche, J.J., Pfeiffer, C.M., Dwyer, J.T., Dodd, K.W., Sempos, C.T., Betz, J.M., Picciano, M.F., 2010c. Unmetabolized serum folic acid and its relation to folic acid intake from diet and supplements in a nationally representative sample of adults aged > or =60 y in the United States. Am. J. Clin. Nutr. 92, 383-389.

Banerjee, P.P., Banerjee, S., Brown, T.R., 2001. Increased Androgen Receptor Expression Correlates with Development of Age-Dependent, Lobe-Specific Spontaneous Hyperplasia of the Brown Norway Rat Prostate. Endocrinology 142, 4066-4075.

Barua, S., Chadman, K.K., Kuizon, S., Buenaventura, D., Stapley, N.W., Ruocco, F., Begum, U., Guariglia, S.R., Brown, W.T., Junaid, M.A., 2014a. Increasing maternal or post-weaning folic acid alters gene expression and moderately changes behavior in the offspring. PLoS One 9, e101674.

Barua, S., Kuizon, S., Brown, W.T., Junaid, M.A., 2016a. DNA Methylation Profiling at Single-Base Resolution Reveals Gestational Folic Acid Supplementation Influences the Epigenome of Mouse Offspring Cerebellum. Front. Neurosci. 10, 168.

Barua, S., Kuizon, S., Brown, W.T., Junaid, M.A., 2016b. High Gestational Folic Acid Supplementation Alters Expression of Imprinted and Candidate Autism Susceptibility Genes in a sex-Specific Manner in Mouse Offspring. J. Mol. Neurosci. 58, 277-286.

Barua, S., Kuizon, S., Chadman, K.K., Flory, M.J., Brown, W.T., Junaid, M.A., 2014b. Single-base resolution of mouse offspring brain methylome reveals epigenome modifications caused by gestational folic acid. Epigenetics Chromatin 7, 3.

Berquin, I.M., Min, Y., Wu, R., Wu, H., Chen, Y.Q., 2005. Expression signature of the mouse prostate. J. Biol. Chem. 280, 36442-36451.

Bistulfi, G., Diegelman, P., Foster, B.A., Kramer, D.L., Porter, C.W., Smiraglia, D.J., 2009. Polyamine biosynthesis impacts cellular folate requirements necessary to maintain S-adenosylmethionine and nucleotide pools. FASEB J. 23, 2888-2897.

Breyer, B.N., Sarma, A.V., 2014. Hyperglycemia and Insulin Resistance and the Risk of BPH/LUTS: an Update of Recent Literature. Current urology reports 15, 462.

Caudill, M.A., 2010. Folate bioavailability: implications for establishing dietary recommendations and optimizing status. Am. J. Clin. Nutr. 91, 1455s-1460s.

CDC, 1991. Use of folic acid for prevention of spina bifida and other neural tube defects--1983-1991. MMWR Morb. Mortal. Wkly. Rep. 40, 513-516.

CDC, 2007. Folate status in women of childbearing age, by race/ethnicity--United States, 1999-2000, 2001-2002, and 2003-2004. MMWR Morb. Mortal. Wkly. Rep. 55, 1377-1380.

Cohen, R.J., McNeal, J.E., Edgar, S.G., Robertson, T., Dawkins, H.J., 1998. Characterization of cytoplasmic secretory granules (PSG), in prostatic epithelium and their transformation-induced loss in dysplasia and adenocarcinoma. Hum. Pathol. 29, 1488-1494.

Collin, S.M., Metcalfe, C., Refsum, H., Lewis, S.J., Zuccolo, L., Smith, G.D., Chen, L., Harris, R., Davis, M., Marsden, G., Johnston, C., Lane, J.A., Ebbing, M., Bonaa, K.H., Nygard, O., Ueland, P.M., Grau, M.V., Baron, J.A., Donovan, J.L., Neal, D.E., Hamdy, F.C., Smith, A.D., Martin, R.M., 2010. Circulating folate, vitamin B12, homocysteine, vitamin B12 transport proteins, and risk of prostate cancer: a case-control study, systematic review, and meta-analysis. Cancer Epidemiol. Biomarkers Prev. 19, 1632-1642.

Crider, K.S., Bailey, L.B., Berry, R.J., 2011. Folic Acid Food Fortification—Its History, Effect, Concerns, and Future Directions. Nutrients 3, 370-384.

Crider, K.S., Yang, T.P., Berry, R.J., Bailey, L.B., 2012. Folate and DNA methylation: a review of molecular mechanisms and the evidence for folate's role. Adv. Nutr. 3, 21-38.

de Vogel, S., Meyer, K., Fredriksen, A., Ulvik, A., Ueland, P.M., Nygard, O., Vollset, S.E., Tell, G.S., Tretli, S., Bjorge, T., 2013. Serum folate and vitamin B12 concentrations in relation to prostate cancer risk--a Norwegian population-based nested case-control study of 3000 cases and 3000 controls within the JANUS cohort. Int. J. Epidemiol. 42, 201-210.

Devens, B.H., Weeks, R.S., Burns, M.R., Carlson, C.L., Brawer, M.K., 2000. Polyamine depletion therapy in prostate cancer. Prostate Cancer Prostatic Dis. 3, 275-279.

English, H.F., Santen, R.J., Isaacs, J.T., 1987. Response of glandular versus basal rat ventral prostatic epithelial cells to androgen withdrawal and replacement. Prostate 11, 229-242.

Espinosa, G., 2013. Nutrition and benign prostatic hyperplasia. Current opinion in urology 23, 38-41.

Farias, N., Ho, N., Butler, S., Delaney, L., Morrison, J., Shahrzad, S., Coomber, B.L., 2015. The effects of folic acid on global DNA methylation and colonosphere formation in colon cancer cell lines. J. Nutr. Biochem. 26, 818-826.

Figueiredo, J.C., Grau, M.V., Haile, R.W., Sandler, R.S., Summers, R.W., Bresalier, R.S., Burke, C.A., McKeown-Eyssen, G.E., Baron, J.A., 2009. Folic Acid and Risk of Prostate Cancer: Results From a Randomized Clinical Trial. J. Natl. Cancer Inst. 101, 432-435.

Honein, M.A., Paulozzi, L.J., Mathews, T.J., Erickson, J.D., Wong, L.Y., 2001. Impact of folic acid fortification of the US food supply on the occurrence of neural tube defects. JAMA 285, 2981-2986.

Hou, Z., Jiang, P., Swanson, S.A., Elwell, A.L., Nguyen, B.K., Bolin, J.M., Stewart, R., Thomson, J.A., 2015. A cost-effective RNA sequencing protocol for large-scale gene expression studies. Sci. Rep. 5, 9570.

Isaacs, J.T., Furuya, Y., Berges, R., 1994. The role of androgen in the regulation of programmed cell death/apoptosis in normal and malignant prostatic tissue. Semin. Cancer Biol. 5, 391-400.

Jagerstad, M., 2012. Folic acid fortification prevents neural tube defects and may also reduce cancer risks. Acta paediatrica 101, 1007-1012.

Kawamura, H., Kimura, M., Ichihara, I., 1993. The effect of androgen and estrogen on secretory epithelial cells and basal cells of the rat ventral prostate after long-term castration. Annals of anatomy = Anatomischer Anzeiger : official organ of the Anatomische Gesellschaft 175, 569-575.

Keil, K.P., Abler, L.L., Altmann, H.M., Wang, Z., Wang, P., Ricke, W.A., Bjorling, D.E., Vezina, C.M., 2015. Impact of a folic acid-enriched diet on urinary tract function in mice treated with testosterone and estradiol. Am. J. Physiol. Renal Physiol. 308, F1431-1443.

Keil, K.P., Mehta, V., Branam, A.M., Abler, L.L., Buresh-Stiemke, R.A., Joshi, P.S., Schmitz, C.T., Marker, P.C., Vezina, C.M., 2012. Wnt inhibitory factor 1 (Wif1) is regulated by androgens and enhances androgen-dependent prostate development. Endocrinology 153, 6091-6103.

Langmead, B., Trapnell, C., Pop, M., Salzberg, S.L., 2009. Ultrafast and memory-efficient alignment of short DNA sequences to the human genome. Genome Biol. 10, R25.

Lee, C., 1981. Physiology of castration-induced regression in rat prostate. Prog. Clin. Biol. Res. 75a, 145-159.

Leng, N., Dawson, J.A., Thomson, J.A., Ruotti, V., Rissman, A.I., Smits, B.M., Haag, J.D., Gould, M.N., Stewart, R.M., Kendziorski, C., 2013. EBSeq: an empirical Bayes hierarchical model for inference in RNA-seq experiments. Bioinformatics 29, 1035-1043.

Li, B., Dewey, C.N., 2011. RSEM: accurate transcript quantification from RNA-Seq data with or without a reference genome. BMC Bioinformatics 12, 323.

Ly, A., Lee, H., Chen, J., Sie, K.K., Renlund, R., Medline, A., Sohn, K.J., Croxford, R., Thompson, L.U., Kim, Y.I., 2011. Effect of maternal and postweaning folic acid supplementation on mammary tumor risk in the offspring. Cancer Res. 71, 988-997.

Ma, R.W., Chapman, K., 2009. A systematic review of the effect of diet in prostate cancer prevention and treatment. J. Hum. Nutr. Diet. 22, 187-199; quiz 200-182.

McConnell, J.D., 1990. Androgen ablation and blockade in the treatment of benign prostatic hyperplasia. Urol. Clin. North Am. 17, 661-670.

McVary, K.T., 2006. BPH: epidemiology and comorbidities. Am. J. Manag. Care 12, S122-128.

Meadows, D.N., 2015. High Dietary Folate in Mice Alters Immune Response and Reduces Survival after Malarial Infection. 10.

Meadows, D.N., Bahous, R.H., Best, A.F., Rozen, R., 2015. High Dietary Folate in Mice Alters Immune Response and Reduces Survival after Malarial Infection. PLoS One 10, e0143738.

Mills, J.S., Needham, M., Parker, M.G., 1987. Androgen regulated expression of a spermine binding protein gene in mouse ventral prostate. Nucleic Acids Res. 15, 7709-7724.

MRC, 1991. Prevention of neural tube defects: results of the Medical Research Council Vitamin Study. MRC Vitamin Study Research Group. Lancet 338, 131-137.

Nicholson, T.M., Ricke, W.A., 2011. Androgens and estrogens in benign prostatic hyperplasia: past, present and future. Differentiation 82, 184-199.

Oh, K.H., Lee, J.H., Kim, K.N., Chang, N., 2009. Effects of folic acid intake on plasma folate, vitamin B12 and homocysteine levels, hepatic SAM/SAH ratio and the expression of cerebral myelin basic protein in pregnant and lactating rats. The FASEB Journal 23, 904.905-904.905.

Parikesit, D., Mochtar, C.A., Umbas, R., Hamid, A., 2016. The impact of obesity towards prostate diseases. Prostate International 4, 1-6.

Parsons, J.K., Sarma, A.V., McVary, K., Wei, J.T., 2013. Obesity and benign prostatic hyperplasia: clinical connections, emerging etiological paradigms and future directions. J. Urol. 189, S102-106.

Perlmutter, M.A., Lepor, H., 2007. Androgen Deprivation Therapy in the Treatment of Advanced Prostate Cancer. Reviews in Urology 9, S3-8.

Pfeiffer, C.M., Hughes, J.P., Lacher, D.A., Bailey, R.L., Berry, R.J., Zhang, M., Yetley, E.A., Rader, J.I., Sempos, C.T., Johnson, C.L., 2012. Estimation of Trends in Serum and RBC Folate in the U.S. Population from Pre- to Postfortification Using Assay-Adjusted Data from the NHANES 1988–2010. J. Nutr. 142, 886-893.

Pfeiffer, C.M., Johnson, C.L., Jain, R.B., Yetley, E.A., Picciano, M.F., Rader, J.I., Fisher, K.D., Mulinare, J., Osterloh, J.D., 2007. Trends in blood folate and vitamin B-12 concentrations in the United States, 1988 2004. Am. J. Clin. Nutr. 86, 718-727.

Rosen, R.C., Giuliano, F., Carson, C.C., 2005. Sexual dysfunction and lower urinary tract symptoms (LUTS) associated with benign prostatic hyperplasia (BPH). Eur. Urol. 47, 824-837.

Sarma, A.V., Kellogg Parsons, J., 2009. Diabetes and benign prostatic hyperplasia: emerging clinical connections. Current urology reports 10, 267-275.

Sie, K.K., Medline, A., van Weel, J., Sohn, K.J., Choi, S.W., Croxford, R., Kim, Y.I., 2011. Effect of maternal and postweaning folic acid supplementation on colorectal cancer risk in the offspring. Gut 60, 1687-1694.

Smith, A.D., Kim, Y.I., Refsum, H., 2008. Is folic acid good for everyone? Am. J. Clin. Nutr. 87, 517-533.

Stacewicz-Sapuntzakis, M., Borthakur, G., Burns, J.L., Bowen, P.E., 2008. Correlations of dietary patterns with prostate health. Mol. Nutr. Food Res. 52, 114-130.

Steegers-Theunissen, R.P., Obermann-Borst, S.A., Kremer, D., Lindemans, J., Siebel, C., Steegers, E.A., Slagboom, P.E., Heijmans, B.T., 2009. Periconceptional maternal folic acid use of 400 microg per day is related to increased methylation of the IGF2 gene in the very young child. PLoS One 4, e7845.

Sun, D., Wollin, A., Stephen, A.M., 2002. Moderate folate deficiency influences polyamine synthesis in rats. J. Nutr. 132, 2632-2637.

Tomaszewski, J.J., Cummings, J.L., Parwani, A.V., Dhir, R., Mason, J.B., Nelson, J.B., Bacich, D.J., O'Keefe, D.S., 2011. Increased cancer cell proliferation in prostate cancer patients with high levels of serum folate. Prostate 71, 1287-1293.

Troen, A.M., Mitchell, B., Sorensen, B., Wener, M.H., Johnston, A., Wood, B., Selhub, J., McTiernan, A., Yasui, Y., Oral, E., Potter, J.D., Ulrich, C.M., 2006a. Unmetabolized folic acid in plasma is associated with reduced natural killer cell cytotoxicity among postmenopausal women. J. Nutr. 136, 189-194.

Troen, A.M., Mitchell, B., Sorensen, B., Wener, M.H., Johnston, A., Wood, B., Selhub, J., McTiernan, A., Yasui, Y., Oral, E., Potter, J.D., Ulrich, C.M., 2006b. Unmetabolized Folic Acid in Plasma Is Associated with Reduced Natural Killer Cell Cytotoxicity among Postmenopausal Women. The Journal of Nutrition 136, 189-194.

Vollset, S.E., Clarke, R., Lewington, S., Ebbing, M., Halsey, J., Lonn, E., Armitage, J., Manson, J.A.E., Hankey, G.J., Spence, J.D., Galan, P., Bønaa, K.H., Jamison, R., Gaziano, J.M., Guarino, P., Baron, J.A., Logan, R.F.A., Giovannucci, E.L., den Heijer, M., Ueland, P.M., Bennett, D., Collins, R., Peto, R., 2013. Effects of folic acid on overall and site-specific cancer incidence during the randomised trials: meta-analyses of data on 50 000 individuals. Lancet 381.

Wang, J., Vasaikar, S., Shi, Z., Greer, M., Zhang, B., 2017. WebGestalt 2017: a more comprehensive, powerful, flexible and interactive gene set enrichment analysis toolkit. Nucleic Acids Res. 45, W130-W137.

Wang, X.D., Wang, B.E., Soriano, R., Zha, J., Zhang, Z., Modrusan, Z., Cunha, G.R., Gao, W.Q., 2007. Expression profiling of the mouse prostate after castration and hormone replacement: implication of H-cadherin in prostate tumorigenesis. Differentiation 75, 219-234.

Wang, Z., Tufts, R., Haleem, R., Cai, X., 1997. Genes regulated by androgen in the rat ventral prostate. Proc. Natl. Acad. Sci. U. S. A. 94, 12999-13004.

Xavier, M.A., de Oliveira, M.T., Baranoski, A., Mantovani, M.S., 2016. Effects of folic acid on the antiproliferative efficiency of doxorubicin, camptothecin and methyl methanesulfonate in MCF-7 cells by mRNA endpoints. Saudi J. Biol. Sci.

Yuan, J.S., Reed, A., Chen, F., Stewart, C.N., 2006. Statistical analysis of real-time PCR data. BMC Bioinformatics 7, 85.

CHAPTER 5. CONCLUSIONS AND FUTURE RESEARCH OPPORTUNITIES

5.1. Further investigation into maintenance mechanisms of the Wolffian duct-urethra junction

Epithelial junctions are essential for organogenesis and cell specialization. Junctions formed by epithelial fusion, cell segregation or patterning gradients define sequential tissue compartments and confer them with specialized functions needed for complex physiological processes such as respiration, digestion and excretion. Following the establishment of these junctions, they need to be constantly maintained to prevent intermingling of epithelial populations. The Wolffian duct-urethra junction, along with cloacal and oropharyngeal membranes, comprise a rare junctional subtype between epithelia from two different germ layers. The Wolffian duct-urethra junction is established during embryonic development when mesoderm-derived Wolffian ducts (also called nephric or mesonephric ducts) fuse with the endoderm-derived cloaca at embryonic day (E)9.5 in mice. The Wolffian duct-urethra junction is one of the few junctions formed by fusion of epithelial structures, the other being the ureter-bladder junction. The junction is transitory in females (Wolffian ducts degenerate by E16.5 in females but are maintained throughout life in males) (Welsh et al., 2006; Welsh et al., 2009; Zhao et al., 2017). The two epithelial populations separated by the Wolffian duct-urethra junction possess and maintain unique identities throughout urogenital tract growth and differentiation. The distinct molecular and histological characteristics of the Wolffian duct and urethral epithelium are maintained by the unique inductive mesenchyme surrounding each epithelial structure. The findings described in Chapter 2 demonstrate that the Wolffian duct-urethral junction keeps the epithelium of the Wolffian duct and urethra distinct, preventing them from being reprogrammed by heterotypic mesenchyme.

My work (described in Chapter 2) reveals an unexpected role for *Dnmt1* in maintaining the Wolffian duct-urethral junction. Here, I define junction maintenance as the separation of the two epithelial populations without intermixing. In the absence of urethral *Dnmt1* expression, Wolffian duct epithelial cells crossed the Wolffian duct-urethra junction and were found intermixing with urethral and bladder epithelium. I found that the urogenital sinus (UGS) ridge formed normally in *Dnmt1* mutant mice but then receded in response to urethral epithelial cell death and impaired differentiation, allowing Wolffian duct epithelial cells to cross the Wolffian duct-urethra junction. Based on our observations, the UGS ridge is lost because of endodermal depletion which creates a permissive environment for Wolffian duct cell invasion. These findings raise the possibility that the UGS ridge actively maintains the Wolffian duct-urethra junction. In our study, endodermal depletion and loss of the UGS ridge was caused by apoptosis associated with *Dnmt1* ablation. These results also suggest that damage to endodermal cell populations through mechanisms other than apoptosis may function more broadly as a trigger for Wolffian duct epithelial cell movement into the urethra and bladder. Further studies are required to identify the types of tissue damage that can trigger breakdown of the Wolffian duct-urethra junction.

These results provide crucial insights into how the Wolffian duct-urethra junction is maintained, but the entire mechanism has not been elucidated yet. The Wolffian duct-urethra junction is a lineage junction (or lineage boundary) between two cell populations derived from distinct progenitors. Epithelial junctions elsewhere in the body are generally maintained by two major mechanisms. The first is a cohesive mechanism which restricts cell movement through transmembrane spanning anchors such as the cadherins

(Dahmann et al., 2011; Halbleib and Nelson, 2006). The second is a repulsive mechanism mediated by signaling molecules such as Eph receptors and ephrins (Batlle and Wilkinson, 2012; Cayuso et al., 2015). Epithelial disorganization and loss of apico-basal polarity (reduced ZO-1 staining in the *Dnmt1* mutant urethra) indicates that cell-cell adhesion is impaired in *Dnmt1* ablated endodermal epithelium. This raises the question of whether reduced cell-cell adhesion in the urethral epithelium but not in the Wolffian duct epithelium is sufficient for the invasion of Wolffian duct epithelial cells. The appearance of individual invading cells suggests that invading Wolffian duct cells are not adhered to each other and do not migrate as epithelial sheets. Invading cells appear to break cell-cell adhesions with the Wolffian duct epithelium to move into the urethral epithelium. These results indicate that the Wolffian duct epithelium is not restricted by adhesive forces, although Wolffian duct cell-cell adhesions might be sufficient to prevent reciprocal movement of urethral epithelial cells into the Wolffian duct epithelium. Other mechanisms like cell-cell repulsion might be involved in junction maintenance. Our results are consistent with the hypothesis that urethral epithelial cells actively repulse Wolffian duct epithelial cells to maintain the junction. This repulsive force could be maintained by cell autonomous or non-autonomous factors that are yet to be determined. When urethra and bladder epithelial cells are depleted, the repulsive force is lost, and the junction breaks down. The fact that I did not observe reciprocal invasion into the Wolffian duct by urethral epithelial cells is evidence that Wolffian duct epithelium possesses its own repulsive force against the urethral epithelium. By deleting *Dnmt1* in the Wolffian duct epithelium using the *Hoxb7*-cre (Yu et al., 2002) , I can test whether epithelial damage to the Wolffian duct permits urethral epithelium to invade across the Wolffian duct-urethra

junction. Further studies are required to identify the exact signaling pathways controlling maintenance of the Wolffian duct-urethra junction.

5.2. Probing the role of DNMT3A, DNMT3B and demethylases in lower urinary tract and prostate development

The results described in Chapter 3 demonstrate the requirement for epithelial DNMT1 expression for prostate bud formation. Epithelial *Dnmt1* deletion leads to widespread hypomethylation, DNA damage, P53-activation, cell cycle arrest and apoptosis. DNMT1 expression is required for normal cell cycle progression and survival of early prostate progenitors. Further, I demonstrated that cells at the tips and margins of prostate buds have a greater requirement for DNMT1 expression than cells in the core of prostate buds.

By identifying the role of DNMT1 in lower urinary tract development, I have just made a start in understanding the wider role of the DNA methylation machinery in this process. Previous studies have shown that temporal changes in expression of the DNA methylation machinery occur during prostate development. There is a shift in *Dnmt* expression from the urethral mesenchymal to the urethral epithelium and prostate buds as development proceeds. As the expression of the *Dnmts* are coupled with the cell cycle, this shift could be a consequence of increased epithelial proliferation and reduced mesenchymal proliferation during prostate bud outgrowth. However, it is interesting that the shift in expression does not occur equally for the all the *Dnmts. Dnmt1* mRNA expression is strongly localized to prostate buds by E18.5. At this stage *Dnmt3a* appears to be widespread in both the epithelial and mesenchymal compartments while *Dnmt3b* appears to be mostly in the developing prostate buds and mesenchymal compartment. (Keil et al., 2013). Immunohistochemistry for DNMT3A protein levels at E18.5 confirms

that DNMT3A is expression is widespread in the epithelium and mesenchyme. At this stage, DNMT3B protein can be detected in the nuclei of cells at the tips of prostate buds (Figure 5.1). The disparate expression patterns of DNMT3A and DNMT3B during prostate budding suggests that they play different roles during this process. Further studies are required to test this by conditionally depleting *Dnmt3a* and *Dnmt3b* in the urethral epithelium during prostate budding. This would involve the use of *Shhcre* alleles and existing floxed alleles for *Dnmt3a* (Kaneda et al., 2004) and *Dnmt3b* (Dodge et al., 2005). To account for redundancies in *de novo* methylation functions, double knockouts of *Dnmt3a* and *Dnmt3b* can be generated.

Conditional epithelial *Dnmt1* ablation and widespread demethylation results in a reduction in prostate bud number. The labile nature of DNA methylation marks allows rapid transcriptional remodeling and makes it an important regulatory process in prostate development. The shift of DNMT1 expression from the mesenchyme to epithelium turns on stromal Androgen receptors and regulates the onset of prostate bud formation (Keil et al., 2014a). Reduction of *Dnmt1* expression can lead to passive DNA demethylation over several cell divisions. Rapid demethylation can be carried out by the demethylases *Tet1*, *Tet2* and *Tet3* which are expressed in the urethra during prostate development (Keil et al., 2013). The consequences of sustained DNA methylation can be studied using epithelium or mesenchymal *cre* drivers and floxed alleles for the *Tet* genes (Kang et al., 2015; Zhang et al., 2013; Zhao et al., 2015).

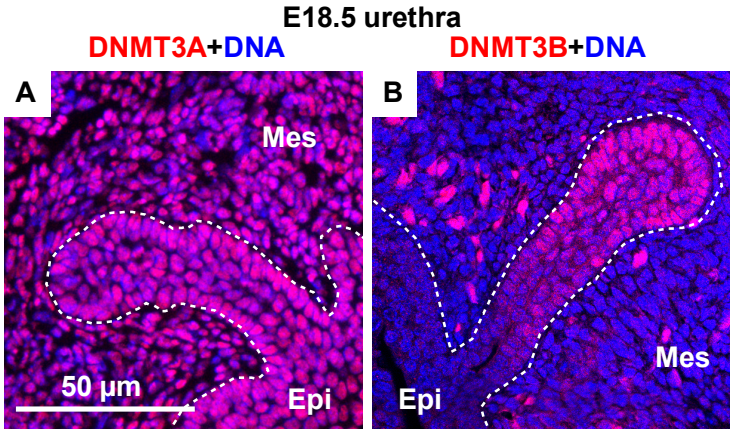

Figure 5.1 DNMT3A and DNMT3B expression in developing prostate buds

Urethral sections from male embryos were labeled with antibodies to (A) DNMT3A (Santa Cruz Biotechnology # sc-20703) and (B) DNMT3B (Novus Biologicals # NB100-56514). DAPI staining is shown in blue. White dotted line represents the epithelial-mesenchymal interface. Scale bar is 50 microns. Epi: Epithelium, Mes: Mesenchyme.

5.3. Transcriptional regulation by DNA Methylation in the lower urinary tract

Comparison of the transcriptomes of *Dnmt1* mutant and control urethral epithelia at E15.5 yielded several insights into the role of DNA methylation during this crucial period of development (Chapter 3). At E15.5, the urethral mesenchyme is at the cusp of signaling to the urethral epithelium to initiate prostate bud formation. DNMT1 protein expression reduces in the mesenchyme and concentrates in the developing prostate buds. In developing buds, methylation of the E-cadherin (*Cdh1*) gene promoter has been shown to promote budding. Inhibition of DNMT1 expression by the pharmacological DNA methylation inhibitor, 5'-aza-deoxycytidine, blocked prostate bud elongation by de-repressing E-cadherin expression (Keil et al., 2014b).

RNA-Seq analysis of *Dnmt1* mutant urethral epithelium at E15.5 revealed several candidate genes that were significantly upregulated by the loss of *Dnmt1.* Out of these, some upregulated genes were P53 target genes and genes involved in the cell cycle or apoptosis. These genes were expressed in the control urethral epithelium, but their expression was increased several-fold in *Dnmt1* deleted urethral epithelium. I identified another group of differentially expressed genes whose expression increased from barely detected in the controls to highly expressed in the *Dnmt1* mutant urethral epithelium. Several genes in the category participate in spermatogenesis and germ cell development (*Taf7l*, *Dazl, Stra8* etc.) (Anderson et al., 2008; VanGompel and Xu, 2011; Zhou et al., 2013) but other genes like *Wnt10b*, *Krt13* and *Krt17* exhibited similar de-repression of expression (Table 5.1). This RNA-Seq dataset provides a starting point for identifying DNA methylation regulated genes in the epithelium of the developing prostate. Further confirmatory studies using methylation-specific PCR are required to confirm the methylation status of promoters associated with these genes. Changes in DNMT1 expression caused by endocrine disrupting environmental chemicals could fundamentally alter the transcriptional program of the developing prostate by modifying expression of DNA methylation regulated genes.

5.4. Differentiation of Wolffian duct derivatives by bladder mesenchyme: Implications for bladder regenerative therapies

During development, epithelial-mesenchymal interactions play an important role in the differentiation of bladder urothelium and stroma (Baskin et al., 1997). The remarkable inductive capacity of the embryonic bladder mesenchyme has been demonstrated in several experimental models. Primary cultures of adult rodent bladder epithelial cells organize into urothelium when artificially recombined with embryonic bladder

mesenchyme even after several passages (Oottamasathien et al., 2006). Going a step further, it was demonstrated that bladder mesenchyme can direct differentiation of embryonic stem cells into endodermal urothelium (Oottamasathien et al., 2007). The inductive capacity of embryonic bladder mesenchyme was also demonstrated to direct the differentiation of non-embryonic mesenchymal stem cells into bladder urothelium (Anumanthan et al., 2008).

As described in Chapter 2, cells from the embryonic Wolffian duct can be reprogrammed by bladder mesenchyme to create cells that resemble basal, intermediate and uroplakin expressing superficial bladder urothelium. Another observation was that the Wolffian duct cells only acquire expression of Keratin 5, P63 and Uroplakins in the bladder and not in the urethra. This suggests that the bladder mesenchyme expresses additional signals that can direct cells to form bladder urothelium. Comparing the transcriptomes of bladder mesenchyme to urethral mesenchyme can provide a list of genes that are differentially expressed in the bladder mesenchyme compared to the urethral mesenchyme. These genes products could be the mediators of the inductive capacity of embryonic bladder mesenchyme to induce urothelial differentiation.

When a patient suffers from interstitial cystitis or bladder cancer, autologous cells cannot be used for bladder regeneration. Currently, bladder replacement is performed by removing the diseased bladder and replacing it with a segment of intestine which serves as a urine reservoir. However, the specialized functions of the intestine often lead to complications including metabolic changes, increased mucous production, urinary tract infection and stone formation when the intestinal epithelial is in prolonged contact with urine (Vasdev et al., 2013). In several cases, the portion of the bladder that is diseased

is removed and the bladder is augmented by a segment of intestine. In such cases, reprogramming of the adjacent bladder urothelium due to the proximity to the intestinal stroma is a serious concern that has been experimentally demonstrated in rodents (Li et al., 2000). Other cell sources are being sought out as alternatives to the intestinal epithelium.

Based on the results described in Chapter 2, the Wolffian duct epithelium could be an alternate source of epithelium to regenerate the bladder. Directed differentiation of Wolffian duct epithelium into Uroplakin positive urothelium and seeding onto biomatrices can be done to form artificial bladders. For this, the signals emanating from the bladder mesenchyme that direct urothelial differentiation must be completely elucidated. In addition, the capacity of adult Wolffian duct epithelium to be reprogrammed to form urothelium must be tested. The ureters are also a potential source of cells for bladder regeneration as these Wolffian duct derivatives already express Uroplakins.

5.5. Exploring folic acid interaction with prostate disease and androgen reduction therapies

In Chapter 4, I describe the interaction between a folic acid enriched diet and the prostate response to androgen deprivation. In this study, mice were exposed to a folic acid enriched diet throughout gestation and until reaching sexual maturity at 7 weeks of age. When these mice were castrated, their prostates were consistently larger than the prostates of castrated control diet mice. In addition, we observed that the castrated folic acid diet prostates had greater luminal cell heights (indicating increased secretory activity) and increased expression of the prostate specific secretory genes *Sbp1* and *Spink1*. Folic

acid supplementation also results in transcriptional changes in the prostate with increased expression of genes involved in the purine nucleotide metabolism pathway.

The diet regimen used in this study mimics the lifetime of folic acid consumption that people are exposed to. Folic acid is consumed in the form of prenatal vitamins, from fortified foods and in the form of multi-vitamin supplements. In this study, I only examined one method of androgen deprivation namely surgical castration. Finasteride, a 5-alpha-reductase inhibitor, blocks the conversion of testosterone to the more potent Dihydrotestosterone and is used to shrink prostate size in patients with Benign Prostatic Hyperplasia (BPH). The impact of folic acid supplementation on finasteride mediated androgen deprivation is a clinically relevant avenue to pursue.

Androgen deprivation therapies are used as treatments for prostate cancer and Benign prostatic hyperplasia (BPH) which are prevalent in aging men. This same population consumes large amounts of folic acid in the form of vitamin supplements (Bailey et al., 2011; Bailey et al., 2010). The study described in Chapter 4 suggests that the folic acid diet could interfere with the prostate response to androgen deprivation therapies used to treated prostate cancer and BPH in older men. Further studies are required to confirm the interaction of folic acid supplementation with androgen responsiveness in the aging and diseased prostate.

Clinical studies have tenuously linked folic acid consumption with prostate cancer risk (Collin et al., 2010; de Vogel et al., 2013; Figueiredo et al., 2009; Tomaszewski et al., 2011). The interaction between folic acid supplementation and prostate cancer progression can be tested in experimental rodent models of prostate cancer.

Table 5.1 Selected differentially expressed genes upregulated in *Dnmt1*cKO urethral epithelium compared to Control urethral epithelium

Gene	Gene name	TPM-Control	TPM-*Dnmt1*cKO	Log2 Fold change *Dnmt1*cKO over Control	p-adj
Taf7l	TATA-Box Binding Protein Associated Factor 7 Like	0.25	336.48	9.74	2.10E-27
Sycp1	Synaptonemal Complex Protein 1	0	53.47	9.23	1.03E-14
Dazl	Deleted in Azoospermia Like	1.48	155.70	6.21	5.75E-13
Syce1	Synaptonemal Complex Central Element Protein 1	0	96.82	8.98	1.77E-12
Wnt10b	Wingless-type MMTV integration site family 10b	1.45	54.74	4.47	2.29E-06
Stra8	Stimulated by Retinoic Acid 8	0	18.34	6.50	0.00013
Krt13	Keratin 13	3.85	137.08	4.59	0.00029
Hoxd13	homeobox D13	44.28	257.89	1.77	0.00524
Krt17	Keratin 17	66.44	387.04	2.09	0.02641

TPM: Transcripts per million, p-adj: Adjusted p-value; $p < 0.05$ indicates differential expression

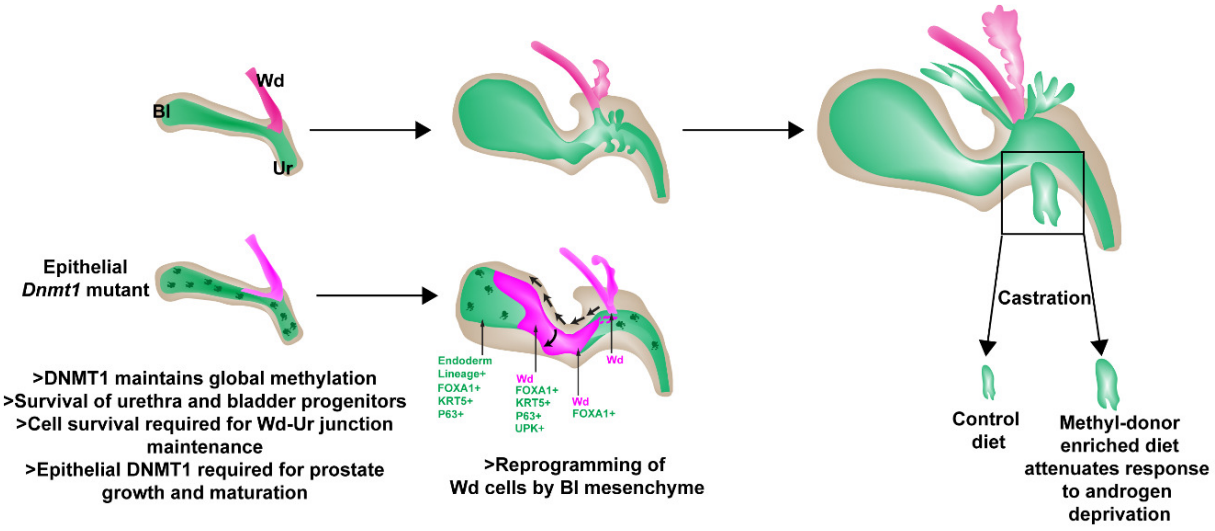

Figure 5.2 Proposed role of DNA methylation in lower urinary tract development and prostate homeostasis

5.6. References

Anderson, E.L., Baltus, A.E., Roepers-Gajadien, H.L., Hassold, T.J., de Rooij, D.G., van Pelt, A.M.M., Page, D.C., 2008. Stra8 and its inducer, retinoic acid, regulate meiotic initiation in both spermatogenesis and oogenesis in mice. Proceedings of the National Academy of Sciences 105, 14976-14980.

Anumanthan, G., Makari, J.H., Honea, L., Thomas, J.C., Wills, M.L., Bhowmick, N.A., Adams, M.C., Hayward, S.W., Matusik, R.J., Brock, J.W., Pope, J.C., 2008. Directed Differentiation of Bone Marrow Derived Mesenchymal Stem Cells Into Bladder Urothelium. J. Urol. 180, 1778-1783.

Bailey, R.L., Gahche, J.J., Lentino, C.V., Dwyer, J.T., Engel, J.S., Thomas, P.R., Betz, J.M., Sempos, C.T., Picciano, M.F., 2011. Dietary supplement use in the United States, 2003-2006. J. Nutr. 141, 261-266.

Bailey, R.L., McDowell, M.A., Dodd, K.W., Gahche, J.J., Dwyer, J.T., Picciano, M.F., 2010. Total folate and folic acid intakes from foods and dietary supplements of US children aged 1-13 y. Am. J. Clin. Nutr. 92, 353-358.

Baskin, L.S., Hayward, S.W., Sutherland, R.A., DiSandro, M.S., Thomson, A.A., Cunha, G.R., 1997. Cellular signaling in the bladder. Front. Biosci. 2, d592-595.

Batlle, E., Wilkinson, D.G., 2012. Molecular mechanisms of cell segregation and boundary formation in development and tumorigenesis. Cold Spring Harb. Perspect. Biol. 4, a008227.

Cayuso, J., Xu, Q., Wilkinson, D.G., 2015. Mechanisms of boundary formation by Eph receptor and ephrin signaling. Dev. Biol. 401, 122-131.

Collin, S.M., Metcalfe, C., Refsum, H., Lewis, S.J., Zuccolo, L., Smith, G.D., Chen, L., Harris, R., Davis, M., Marsden, G., Johnston, C., Lane, J.A., Ebbing, M., Bonaa, K.H., Nygard, O., Ueland, P.M., Grau, M.V., Baron, J.A., Donovan, J.L., Neal, D.E., Hamdy, F.C., Smith, A.D., Martin, R.M., 2010. Circulating folate, vitamin B12, homocysteine, vitamin B12 transport proteins, and risk of prostate cancer: a case-control study, systematic review, and meta-analysis. Cancer Epidemiol. Biomarkers Prev. 19, 1632-1642.

Dahmann, C., Oates, A.C., Brand, M., 2011. Boundary formation and maintenance in tissue development. Nat. Rev. Genet. 12, 43-55.

de Vogel, S., Meyer, K., Fredriksen, A., Ulvik, A., Ueland, P.M., Nygard, O., Vollset, S.E., Tell, G.S., Tretli, S., Bjorge, T., 2013. Serum folate and vitamin B12 concentrations in relation to prostate cancer risk--a Norwegian population-based nested case-control study of 3000 cases and 3000 controls within the JANUS cohort. Int. J. Epidemiol. 42, 201-210.

Dodge, J.E., Okano, M., Dick, F., Tsujimoto, N., Chen, T., Wang, S., Ueda, Y., Dyson, N., Li, E., 2005. Inactivation of Dnmt3b in mouse embryonic fibroblasts results in DNA hypomethylation, chromosomal instability, and spontaneous immortalization. J. Biol. Chem. 280, 17986-17991.

Figueiredo, J.C., Grau, M.V., Haile, R.W., Sandler, R.S., Summers, R.W., Bresalier, R.S., Burke, C.A., McKeown-Eyssen, G.E., Baron, J.A., 2009. Folic Acid and Risk of Prostate Cancer: Results From a Randomized Clinical Trial. J. Natl. Cancer Inst. 101, 432-435.

Halbleib, J.M., Nelson, W.J., 2006. Cadherins in development: cell adhesion, sorting, and tissue morphogenesis. Genes Dev. 20, 3199-3214.

Kaneda, M., Okano, M., Hata, K., Sado, T., Tsujimoto, N., Li, E., Sasaki, H., 2004. Essential role for de novo DNA methyltransferase Dnmt3a in paternal and maternal imprinting. Nature 429, 900.

Kang, J., Lienhard, M., Pastor, W.A., Chawla, A., Novotny, M., Tsagaratou, A., Lasken, R.S., Thompson, E.C., Surani, M.A., Koralov, S.B., Kalantry, S., Chavez, L., Rao, A., 2015. Simultaneous deletion of the methylcytosine oxidases Tet1 and Tet3 increases transcriptome variability in early embryogenesis. Proc. Natl. Acad. Sci. U. S. A. 112, E4236-4245.

Keil, K.P., Abler, L.L., Laporta, J., Altmann, H.M., Yang, B., Jarrard, D.F., Hernandez, L.L., Vezina, C.M., 2014a. Androgen receptor DNA methylation regulates the timing and androgen sensitivity of mouse prostate ductal development. Dev. Biol. 396, 237-245.

Keil, K.P., Abler, L.L., Mehta, V., Altmann, H.M., Laporta, J., Plisch, E.H., Suresh, M., Hernandez, L.L., Vezina, C.M., 2014b. DNA methylation of E-cadherin is a priming mechanism for prostate development. Dev. Biol. 387, 142-153.

Keil, K.P., Altmann, H.M., Mehta, V., Abler, L.L., Elton, E.A., Vezina, C.M., 2013. Catalog of mRNA expression patterns for DNA methylating and demethylating genes in developing mouse lower urinary tract. Gene Expr Patterns 13, 413-424.

Li, Y., Liu, W., Hayward, S.W., Cunha, G.R., Baskin, L.S., 2000. Plasticity of the urothelial phenotype: effects of gastro-intestinal mesenchyme/stroma and implications for urinary tract reconstruction. Differentiation 66, 126-135.

Oottamasathien, S., Wang, Y.Q., Williams, K., Franco, O.E., Wills, M.L., Thomas, J.C., Saba, K., Sharif-Afshar, A.R., Makari, J.H., Bhowmick, N.A., DeMarco, R.T., Hipkens, S., Magnuson, M., Brock, J.W., Hayward, S.W., Pope, J.C., Matusik, R.J., 2007. Directed differentiation of embryonic stem cells into bladder tissue. Dev. Biol. 304, 556-566.

Oottamasathien, S., Williams, K., Franco, O.E., Thomas, J.C., Saba, K., Bhowmick, N.A., Staack, A., Demarco, R.T., Brock, J.W., 3rd, Hayward, S.W., Pope, J.C.t., 2006. Bladder tissue formation from cultured bladder urothelium. Dev. Dyn. 235, 2795-2801.

Tomaszewski, J.J., Cummings, J.L., Parwani, A.V., Dhir, R., Mason, J.B., Nelson, J.B., Bacich, D.J., O'Keefe, D.S., 2011. Increased cancer cell proliferation in prostate cancer patients with high levels of serum folate. Prostate 71, 1287-1293.

VanGompel, M.J.W., Xu, E.Y., 2011. The roles of the DAZ family in spermatogenesis: More than just translation? Spermatogenesis 1, 36-46.

Vasdev, N., Moon, A., Thorpe, A.C., 2013. Metabolic complications of urinary intestinal diversion. Indian J. Urol. 29, 310-315.

Welsh, M., Saunders, P.T., Marchetti, N.I., Sharpe, R.M., 2006. Androgen-dependent mechanisms of Wolffian duct development and their perturbation by flutamide. Endocrinology 147, 4820-4830.

Welsh, M., Sharpe, R.M., Walker, M., Smith, L.B., Saunders, P.T., 2009. New insights into the role of androgens in wolffian duct stabilization in male and female rodents. Endocrinology 150, 2472-2480.

Yu, J., Carroll, T.J., McMahon, A.P., 2002. Sonic hedgehog regulates proliferation and differentiation of mesenchymal cells in the mouse metanephric kidney. Development 129, 5301-5312.

Zhang, R.R., Cui, Q.Y., Murai, K., Lim, Y.C., Smith, Z.D., Jin, S., Ye, P., Rosa, L., Lee, Y.K., Wu, H.P., Liu, W., Xu, Z.M., Yang, L., Ding, Y.Q., Tang, F., Meissner, A., Ding, C., Shi, Y., Xu, G.L., 2013. Tet1 Regulates Adult Hippocampal Neurogenesis and Cognition. Cell stem cell 13, 237-245.

Zhao, F., Franco, H.L., Rodriguez, K.F., Brown, P.R., Tsai, M.J., Tsai, S.Y., Yao, H.H., 2017. Elimination of the male reproductive tract in the female embryo is promoted by COUP-TFII in mice. Science 357, 717-720.

Zhao, Z., Chen, L., Dawlaty, Meelad M., Pan, F., Weeks, O., Zhou, Y., Cao, Z., Shi, H., Wang, J., Lin, L., Chen, S., Yuan, W., Qin, Z., Ni, H., Nimer, Stephen D., Yang, F.-C., Jaenisch, R., Jin, P., Xu, M., 2015. Combined Loss of Tet1 and Tet2 Promotes B Cell, but Not Myeloid Malignancies, in Mice. Cell reports 13, 1692-1704.

Zhou, H., Grubisic, I., Zheng, K., He, Y., Wang, P.J., Kaplan, T., Tjian, R., 2013. Taf7l cooperates with Trf2 to regulate spermiogenesis. Proc. Natl. Acad. Sci. U. S. A. 110, 16886-16891.

APPENDIX 1: DNMT1 DELETION IN LUMINAL EPITHELIUM DOES NOT AFFECT ADULT PROSTATE HOMEOSTASIS AND REGENERATION

A1.1 Introduction

The study described in Chapter 3 demonstrates the requirement for DNMT1 expression in the epithelium of the developing prostate. DNMT1 is closely linked to cell proliferation which occurs at rapid rates in the developing prostate epithelium. DNMT1 is required for ensuring proper cell cycle progression and maintaining cell survival in the developing prostate epithelium. I tested whether DNMT1 expression is similarly required for adult prostate homeostasis and regeneration. To test this, I used a PbCre-4 mouse line that carries the *cre* gene under the control of an engineered promoter containing sequences from the rat Probasin gene promoter. This allele causes Cre recombination in prostate luminal epithelial cells which can be identified as early as 1 week after birth (Wu et al., 2001). To test the requirement for *Dnmt1* in the adult prostate, I performed deletion of *Dnmt1* using *Dnmt1* floxed alleles (Jackson-Grusby et al., 2001) and the PbCre-4 allele.

A1.2 Materials and Methods

Generation of adult prostate specific *Dnmt1* mutants

Mice were housed as previously described (Mehta et al., 2011) in clear plastic cages containing corn cob bedding and maintained on a 12-hr light and dark cycle at 25+5^{o}C and 20–50% relative humidity. Feed (Diet 2019 for males and Diet 7002 for pregnant females, Harlan Teklad, Madison, WI) and water were available *ad libitum*. All procedures performed on mice were approved by the University of Wisconsin-Madison Animal Care

and Use Committee and were carried out in accordance with the Guide for the Care and Use of Laboratory Animals. Mice carrying the *Dnmt1Flox* allele (B6.129S4-*Dnmt1*$^{tm2Jae/Mmucd}$) were from the Mutant Mouse Research and Resource Centers at the University of California, Davis (MMRRC, 014114-UCD). Genotyping for the *Dnmt1Flox* allele was carried out as described previously (Jackson-Grusby et al., 2001). The PbCre-4 line and its genotyping have been described previously (Wu et al., 2001). Mice carrying the *R26R-EYFP* reporter allele (B6.129X1-*Gt(ROSA)26*$^{Sortm1(EYFP)Cos/J}$ (The Jackson Laboratory, 006148) were genotyped using the following primers: 5'-AAAGTCGCTCTGAGTTGTTAT -3' and 5'-AAGACCGCGAAGAGTTTGTC -3' (Srinivas et al., 2001). *Dnmt1Flox* mice were bred to mice carrying the *R26R-EYFP* alleles to obtain *Dnmt1Flox/Flox; R26R/R26R* females. These females were crossed with Pbcre-4/+*; Dnmt1Flox/+* males. Mice carrying one copy of the Pbcre-4 transgene and one copy of a *Dnmt1flox* allele (Control) served as experimental controls for mice carrying one copy of the Pbcre-4 allele and two copies of the *Dnmt1flox* allele (*Pbcre-4*; *Dnmt1*LOF).

Male mice were euthanized by CO2 asphyxiation at 7 weeks of age for tissue harvesting. A separate group of mice from each genotype were castrated at 7 weeks of age and implanted with a testosterone capsule after 2 weeks. The prostate regenerated for 7 days and the mice were euthanized for tissue harvesting. Tissue wet weights were obtained using an analytic balance and are presented as percentages of mouse body weights.

Fluorescent Immunohistochemistry

Fluorescent immunohistochemistry was performed as described previously (Abler et al., 2011). Primary antibody sources and dilutions are: 5mC (ab10805, 1:200 dilution) from Abcam, Cambridge, MA, USA and GFP (600-401-215, 1:200 dilution) from Rockland

Immunochemicals, Limerick, PA, USA). The secondary antibodies and dilutions are: goat anti-Mouse AlexaFluor594 (115-585-062, 1:500 dilution), goat anti-Rabbit AlexaFluor488 (111-487-003, 1:500 dilution) from Jackson ImmunoResearch, West Grove, PA, USA.

Statistics

Statistical analyses were conducted with *R* version 3.2.4. Homogeneity of variance was determined using Bartlett's test packages for *R*. Student's t-test was performed on parametric data with two groups. P values less than 0.05 were considered statistically significant. Results are presented as mean ± standard error of the mean (SEM). NS: Not significant

A1.3 Results

To test whether *Dnmt1* deletion in luminal epithelial cells impacted postnatal and adult prostate growth, tissues from 7-week old mice from each genotype were harvested and the prostate weights compared. Intact prostate weights did not differ significantly between the Control and PbCre-4*; Dnmt1*LOF groups. I then tested whether *Dnmt1* deletion would affect the ability of the prostate to regenerate to full size after castration and testosterone supplementation. 7-week old male mice from both genotypes were subjected to one round of castration and regeneration. Following this, the mice were euthanized, and the tissues were harvested for prostate weight comparisons. Regenerated prostate weights did not differ significantly between the Control and PbCre-4*; Dnmt1*LOF groups. Immunohistochemical analysis showed patchy Cre recombination with no change in DNA methylation (measured by 5mC) in the intact and regenerated prostates from each group.

A1.4 Figures

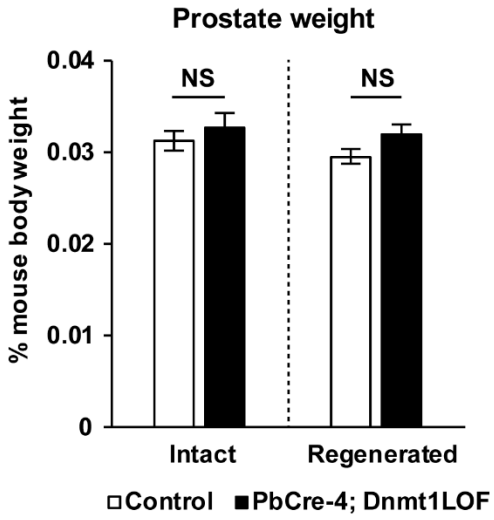

Figure A1. 1 No change in prostate weight after *Dnmt1* deletion in adult luminal epithelium

Relative prostate wet weights were determined as a percentage of mouse body weight for Intact mice (n=7/genotype) and mice that had undergone castration and regeneration (n=3/genotype). Results are presented as mean ± SEM. p-values represent results from unpaired Student's t-test. NS: Not significant P>0.05.

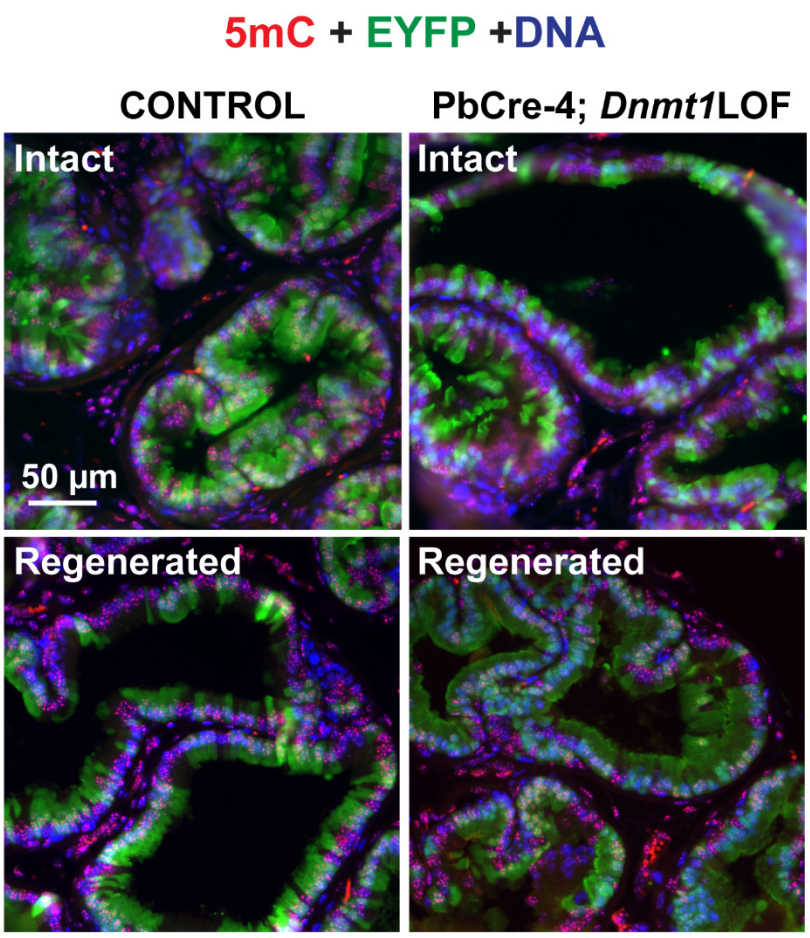

Figure A1. 2 *Dnmt1* deletion did not affect DNA methylation in the adult ventral prostate

Mouse ventral prostate sections were labeled with antibodies to 5mC (red) and EYFP (green). Representative images are shown for intact and regenerated prostates from the Control and PbCre-4; *Dnmt1*LOF groups. Scale bar is 50 microns. DAPI staining is shown in blue.

A1.5 Discussion

Dnmt1 deletion in the adult prostate luminal epithelium did not cause significant loss of DNA methylation. As shown in Chapter 2 and 3, *Dnmt1* deletion severely impacts

progenitor cells that are dividing and differentiating. The intact prostate has a low rate of cell proliferation. The regenerating prostate has a lot of cell proliferation, but it is likely that the basal cells proliferate to give rise to the new luminal epithelial cells. The luminal epithelial cells themselves are terminally differentiated and do not undergo multiple rounds of cell division. As multiple rounds of cell division are required to deplete DNMT1 and 5mC levels, these cells are unaffected by *Dnmt1* deletion. Keratin 5 or Keratin 14 *cre* drivers could be used to test the requirement for DNMT1 in prostate basal epithelial cells.

A1.6 References

Abler, L.L., Keil, K.P., Mehta, V., Joshi, P.S., Schmitz, C.T., Vezina, C.M., 2011. A high-resolution molecular atlas of the fetal mouse lower urogenital tract. Dev. Dyn. 240, 2364-2377.

Jackson-Grusby, L., Beard, C., Possemato, R., Tudor, M., Fambrough, D., Csankovszki, G., Dausman, J., Lee, P., Wilson, C., Lander, E., Jaenisch, R., 2001. Loss of genomic methylation causes p53-dependent apoptosis and epigenetic deregulation. Nat. Genet. 27, 31-39.

Mehta, V., Abler, L.L., Keil, K.P., Schmitz, C.T., Joshi, P.S., Vezina, C.M., 2011. Atlas of Wnt and R-spondin gene expression in the developing male mouse lower urogenital tract. Dev. Dyn. 240, 2548-2560.

Srinivas, S., Watanabe, T., Lin, C.-S., William, C.M., Tanabe, Y., Jessell, T.M., Costantini, F., 2001. Cre reporter strains produced by targeted insertion of EYFP and ECFP into the ROSA26 locus. BMC Dev. Biol. 1, 4-4.

Wu, X., Wu, J., Huang, J., Powell, W.C., Zhang, J., Matusik, R.J., Sangiorgi, F.O., Maxson, R.E., Sucov, H.M., Roy-Burman, P., 2001. Generation of a prostate epithelial cell-specific Cre transgenic mouse model for tissue-specific gene ablation. Mech. Dev. 101, 61-69.

APPENDIX 2: IMMUNOHISTOCHEMICAL COMPARISON OF NOVEL EPITHELIAL AND STROMAL SUBTYPES IN THE HUMAN AND MOUSE PROSTATE

- Staining and imaging of adult human prostates shown in Appendix 2 was carried out by Diya Binoy Joseph and adapted from:

  Gervaise H. Henry, Alicia Malewska, **Diya B. Joseph**, Venkat S. Malladi, Jeon Lee, Jose Torrealba, Ryan J. Mauck, Jeffrey C. Gahan, Claus G. Roehrborn, Gary C. Hon, Jeffrey C. Reese, Ryan C. Hutchinson, Chad M. Vezina, Douglas W. Strand

  A Cellular Anatomy of the normal Human Prostate

  Cell Reports (2018), in press
- Staining and imaging of young human and mouse prostate tissues was carried out by Simran K Sandhu under the supervision of Diya Binoy Joseph.

A2.1 Introduction

The mouse and human prostate differ considerably in anatomy. While the human prostate is a walnut shaped organ with ducts confined within a capsule, the mouse prostate consists of multiple lobes similar to leaves on a tree branch. Despite the striking anatomical differences, the mouse prostate is a widely used model for studying human prostate diseases including prostate cancer, Benign prostatic hyperplasia (BPH) and prostatitis. The mouse prostate contains the basic epithelial cell types found in the human prostate which are the basal, luminal and neuroendocrine cells. Within these epithelial sub-types, further stem cell sub-populations and castration resistant luminal epithelial

cells have been identified (Collins et al., 2005; Wang et al., 2009). The identification of these sub-populations suggests that the basal, luminal and neuroendocrine cell populations are more complex and heterogenous than previously thought. However, the heterogeneity of the basal, luminal and neuroendocrine cell populations has not been fully characterized. To address this, a group at the UT Southwestern Medical Center (Gervaise et al, Cell Reports, in press) performed single cell RNA-sequencing on healthy prostate tissue from human donors. The single cell RNA-sequencing study provides a snapshot of all the cell types in the normal human prostate. This technique was used to identify novel basal and luminal epithelial sub-populations in the prostate. The immunohistochemical markers used in this study have been informed by this single cell RNA-sequencing study. Compared to the epithelium, the prostate stroma is relatively underexplored. The single cell RNA-sequencing dataset divides prostate stromal cells into paracrine fibroblasts and prostate smooth muscle cells. The distribution of stromal cell populations in the prostate have been assessed by immunohistochemistry.

The aims of this study are the following:

1. To verify the novel sub-types identified by single RNA-sequencing using immunohistochemistry.
2. To test whether the novel epithelial and stromal sub-populations identified in human prostates are also found in the mouse prostate. This is a relevant line of investigation as the mouse is a widely used model for studying human prostate disease.
3. To test whether the novel epithelial and stromal sub-populations are specified in the developing prostate. Tissues from the branching stage of the prostate (17-22 weeks in humans and postnatal day (P) 9 in mice) were used to test whether the novel cell

populations can be detected at early stages of prostate development and whether their abundance increases or decreases in the adult tissue.

A2.2 Materials and Methods

Generation of mouse tissues

Mice were housed as previously described (Mehta et al., 2011) in clear plastic cages containing corn cob bedding and maintained on a 12-hr light and dark cycle at 25+5ºC and 20–50% relative humidity. Feed (Diet 2019 for males and Diet 7002 for pregnant females, Harlan Teklad, Madison, WI) and water were available *ad libitum*. All procedures performed on mice were approved by the University of Wisconsin-Madison Animal Care and Use Committee and were carried out in accordance with the Guide for the Care and Use of Laboratory Animals. For adult mouse tissues, C57Bl6/J mice (Jackson Laboratories #000664) between 7-12 weeks of age were euthanized by CO_2 and the lower urinary tract was harvested. The anterior prostate lobes, bladder and seminal vesicle were removed. The urethra with the ventral, lateral and dorsal prostate lobes attached was fixed in 4% paraformaldehyde overnight before embedding in paraffin. For young mouse tissues, postnatal day 9 male mouse pups were euthanized and the lower urinary tract (urethra, bladder and prostate) was harvested.

Human tissues

Paraffin embedded adult human prostate tissues sections from organ donors were obtained from the Southwest Transplant alliance and the UT Southwestern Medical Center courtesy of Dr. Douglas Strand in the Department of Urology. Young human prostates were obtained from the University of Pittsburgh.

Fluorescent Immunohistochemistry

Fluorescent immunohistochemistry was performed as described previously (Abler et al., 2011). Images were obtained using the Keyence BZ-X710 All-in-one fluorescence microscope. Antibody sources and dilutions are listed in Table A2.1.

A2.3 Results

Immunohistochemical detection of a novel basal epithelial sub-populations in the human prostate

Single cell RNA-sequencing in the adult human prostate identified a Keratin 13 (KRT13) expressing epithelial sub-population in the prostate. Immunohistochemistry on adult human prostates confirmed the existence of this KRT13+ population. KRT13+ cells appeared to be a sub-population of the Keratin 5+ basal epithelial population. The basal sub-population expressing Keratin 14 (KRT14) does not overlap with the KRT13 expressing cell population. In the adult human prostate, KRT13+ cells were enriched in the urethra and the urethra-proximal prostate ducts while the KRT14+ cells were found further away from the urethra.

I then looked at young human samples to determine when the KRT13+ and KRT14+ populations emerge. KRT13+ cells are enriched in the urethra and prostate ducts of the young human prostates while no KRT14 expression is detected at this stage. Conversely, mouse prostates express KRT14 in the urethra and prostate while no KRT13 expression is detected at the young and adult stages (Figure A2. 1).

Distribution of prostate stromal cell types is conserved across mouse and human

Human single cell RNA-sequencing confirmed that two major types of stromal cells exist in the prostate: paracrine fibroblasts (Decorin, DCN+) and prostate smooth muscle cells (Myosin heavy chain 11, MYH11+ or Smooth muscle actin, ACTA2+). The distribution of these cell types was conserved between the adult human and mouse. DCN expressing fibroblasts are concentrated in the urethral and proximal prostate region. The smooth muscle cells are distributed throughout the prostate organ. This same distribution is observed in the young human prostate. In the young mouse prostate, DCN expressing fibroblasts are mostly absent. The organization of smooth muscle cells differ between the mouse and human. In the mouse, smooth muscle cells are organized into thick bands around prostate ducts. In humans, smooth muscle cells form small bundles distributed throughout the prostate organ (Figure A2. 2).

A novel KRT13+ epithelial sub-population is enriched in the urethra and proximal prostate region

The distribution of KRT13+ cells followed a striking pattern in the young and adult human prostate. KRT13 expression was highest in the urethra and the prostate ducts closes to the urethra (proximal). KRT13 expression gradually reduces with distance from the urethra and is mostly absent in the distal prostate ducts (Figure A2. 3).

Immunohistochemical detection of a novel luminal epithelial sub-population expressing Dehydrogenase/Reductase 7 (DHRS7)

Single cell RNA-sequencing in the adult human prostate identified a DHRS7 expressing luminal epithelial sub-population in the prostate which overlapped with Keratin 8/18 expression. Immunohistochemistry on adult human prostates confirmed the existence of

this DHRS7+ population. DHRS7+ cells are present in the urethra and prostate ducts of young humans. DHRS7 expression is absent in the adult urethra but is present in prostate ducts (Figure A2. 4).

A novel SCGB1A1+ epithelial sub-population is enriched in the urethra and proximal prostate region

Single cell RNA-sequencing identified prostate epithelial cells expressing Secretoglobin Family 1A member 1 (SCGB1A1). SCGB1A1 is highly expressed in lung club cells. Club cells participate in immunomodulation through the secretion of proteins that activate the immune response. The existence of SCGB1A1+ cells in the prostate suggests that these cells could perform similar functions as the lung club cells. SCGB1A1+ cells are abundant in the young human prostate and are present in the urethra and proximal ducts but absent in the distal ducts. A similar pattern is observed in the adult human prostate. SCGB1A1+ cells are abundant in the adult human urethra and are detectable in the proximal prostate ducts near the urethra. Distal ducts are completely devoid of SCGB1A1+ cells (Figure A2. 5).

Immunohistochemical detection of a novel neuroendocrine sub-population expressing Secrotogranin II (SCG2)

Single cell RNA-sequencing in the adult human prostate identified a SCG2 expressing neuroendocrine cell population in the prostate which overlapped with the established neuroendocrine marker Chromogranin A (CHGA). Immunohistochemistry on young and adult human prostates confirmed the existence of CHGA+ neuroendocrine cells

expressing SCG2. Neuroendocrine cells were enriched in the urethra and prostate ducts proximal to the urethra (Figure A2. 6).

A2.4 Figures and Tables

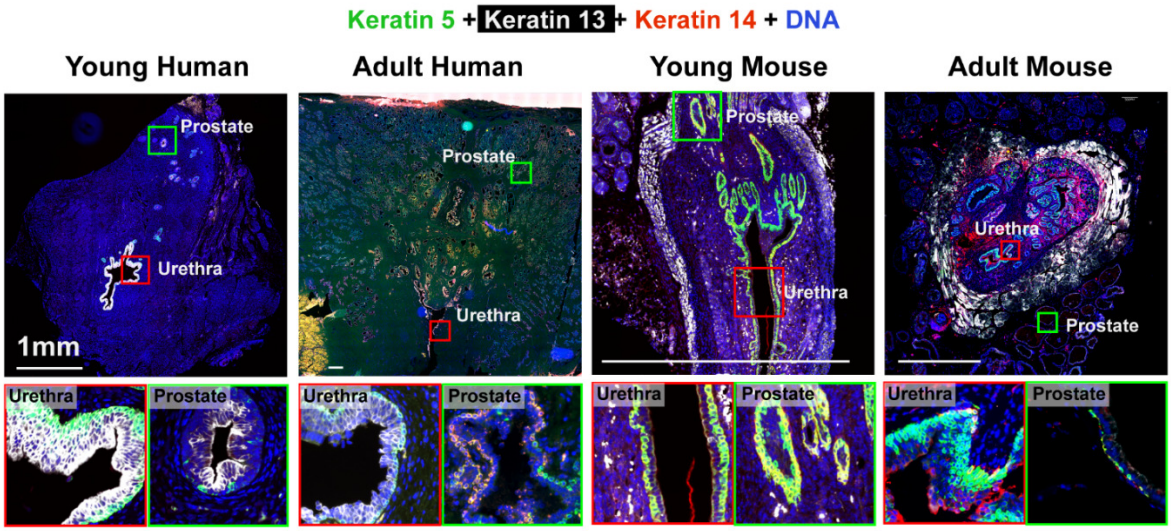

Figure A2. 1 Comparison of novel prostate basal epithelial subtypes (Keratin 13+ and Keratin 14+) in the human and mouse prostate

Sections containing prostate tissue from young human, adult human, young mouse and adult mouse were stained with antibodies to Keratin 5 (green), Keratin 13 (white) and Keratin 14 (red). Magnified regions of interest from the prostate and urethra are shown below the image of the whole-mount tissue. DAPI staining is shown in blue. Scale bar is 1 mm.

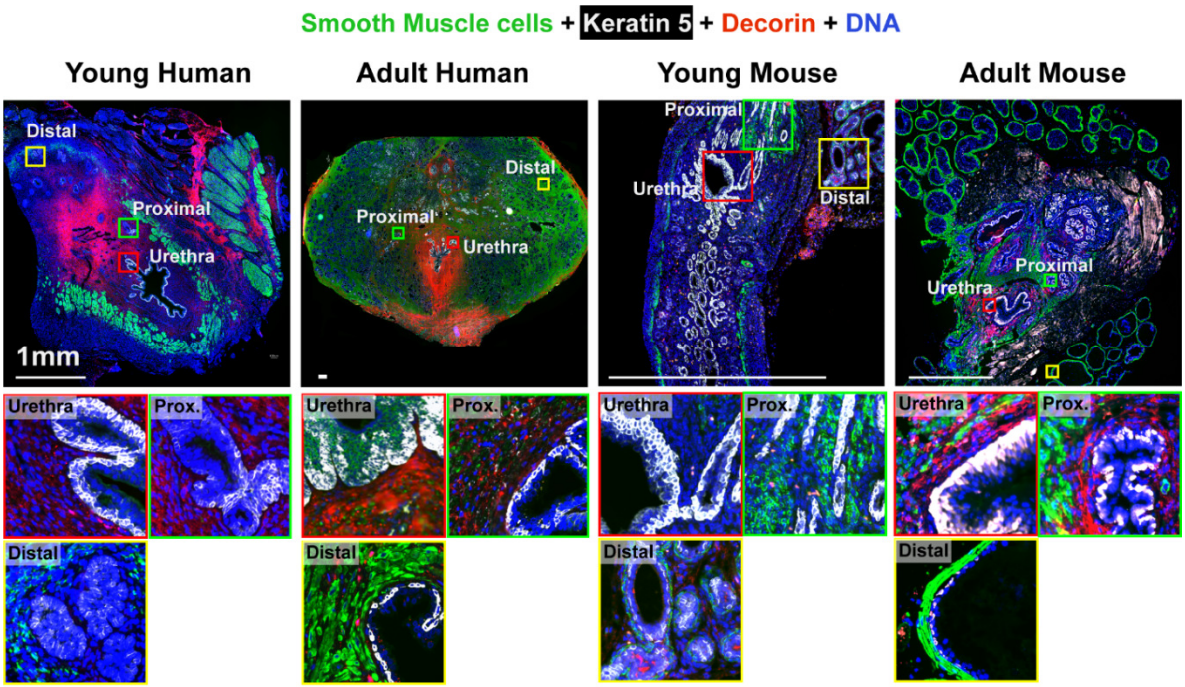

Figure A2. 2 Comparison of prostate stroma cell subtypes (Decorin+ paracrine fibroblast and MYH11 or ACTA2+ prostate smooth muscle cells) in the human and mouse prostate

Sections containing prostate tissue from young human, adult human, young mouse and adult mouse were stained with antibodies to MYH11 for human tissue and ACTA2 for mouse tissue (green), Keratin 5 (white) and Decorin (red). Magnified regions of interest from the proximal prostate, distal prostate and urethra are shown below the image of the whole-mount tissue. DAPI staining is shown in blue. Scale bar is 1 mm.

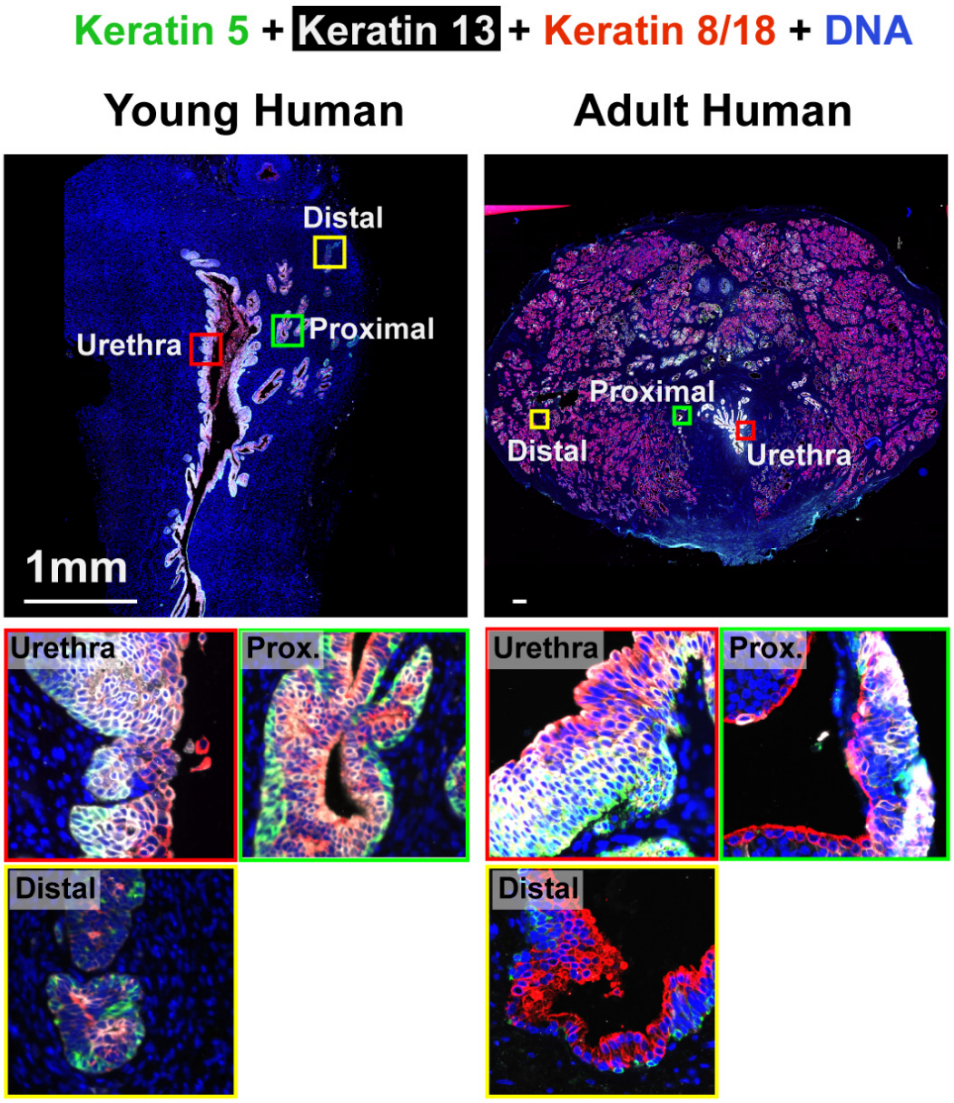

Figure A2. 3 The Keratin 13+ epithelial cell population is enriched in the urethra and proximal region of the developing and adult human prostate

Sections containing prostate tissue from young human and adult human were stained with antibodies to Keratin 5 (green), Keratin 13 (white) and Keratin 8/18 (red). Magnified regions of interest from the proximal prostate, distal prostate and urethra are shown below the image of the whole-mount tissue. DAPI staining is shown in blue. Scale bar is 1 mm.

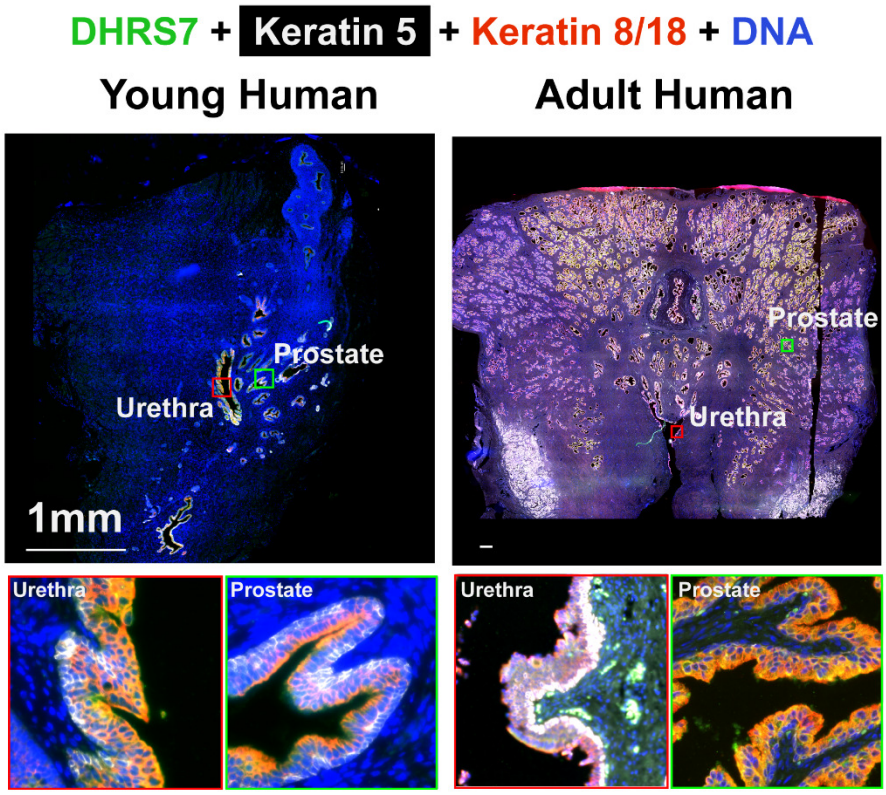

Figure A2. 4 The DHRS7+ luminal epithelial cell population is present in prostate ducts from young human and adult human prostate.

Sections containing prostate tissue from young human and adult human were stained with antibodies to Keratin 5 (white), DHRS7 (green) and Keratin 8/18 (red). Magnified regions of interest from the proximal prostate, distal prostate and urethra are shown below the image of the whole-mount tissue. DAPI staining is shown in blue. Scale bar is 1 mm.

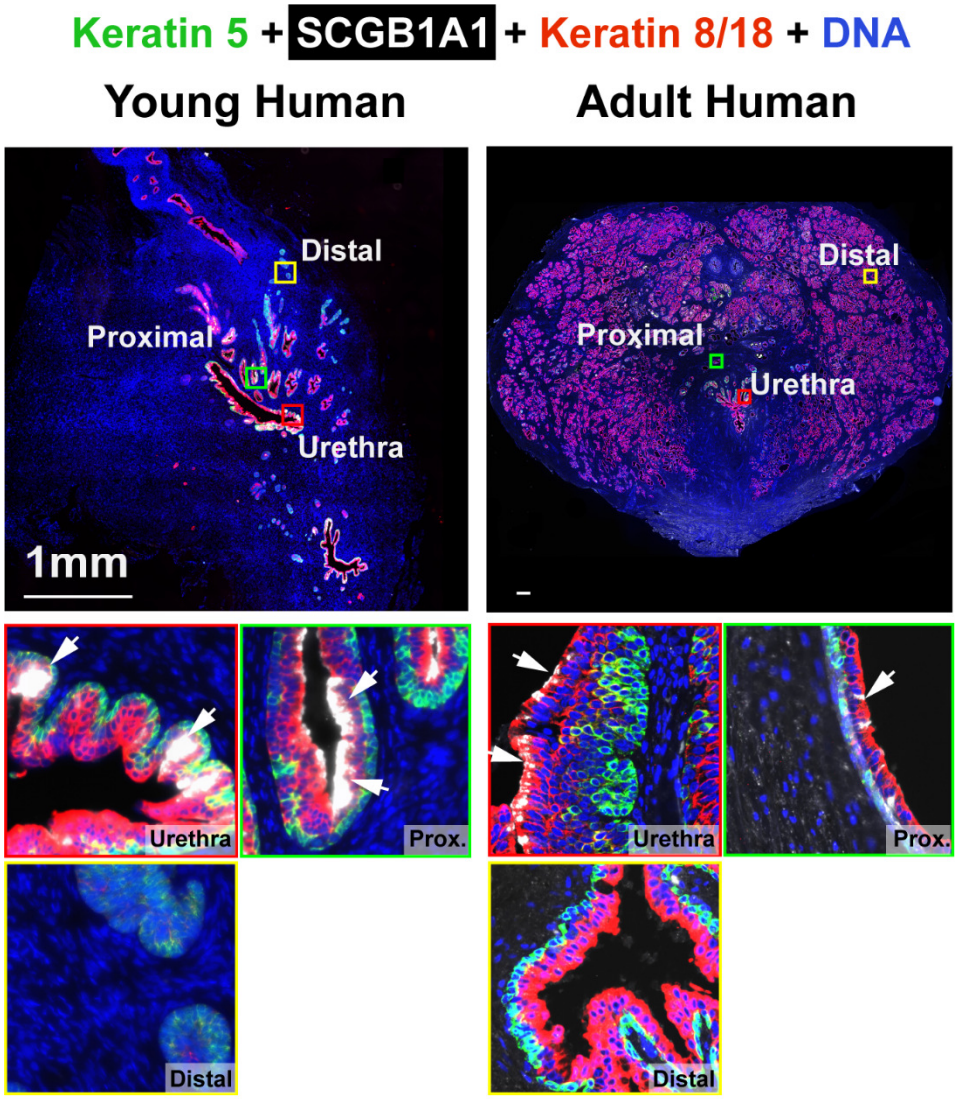

Figure A2. 5 The SCGB1A1+ epithelial cell population is enriched in the urethra and proximal region of the young human and adult human.

Sections containing prostate tissue from young human and adult human were stained with antibodies to Keratin 5 (green), SCGB1A1 (white) and Keratin 8/18 (red). Magnified regions of interest from the proximal prostate, distal prostate and urethra are shown below the image of the whole-mount tissue. DAPI staining is shown in blue. Scale bar is 1 mm.

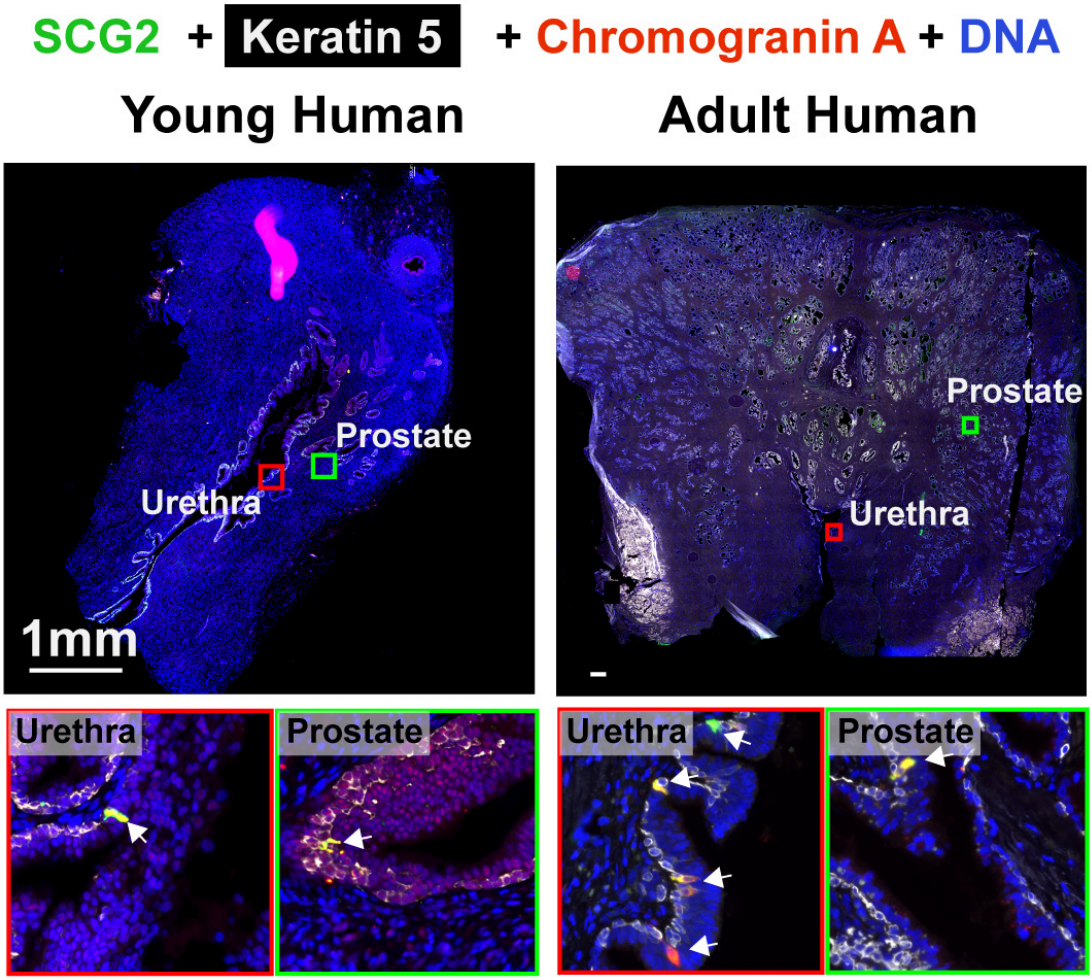

Figure A2. 6 SCG2+ neuroendocrine cells are enriched in the urethra and proximal region of the young human and adult human.

Sections containing prostate tissue from young human and adult human were stained with antibodies to Keratin 5 (white), SCG2 (green) and Chromogranin A (red). Magnified regions of interest from the proximal prostate, distal prostate and urethra are shown below the image of the whole-mount tissue. DAPI staining is shown in blue. Scale bar is 1 mm.

Table A2. 1 Antibodies used for immunohistochemical comparison between human and mouse prostate

Antibody	Clone	Dilution	Supplier	Conjugate	RRID
KRT5	chicken polyclonal	1:400	Biolegend #905901	n/a	AB_2565054
MYH11	MYH11/923	1:200	LS Bio #LS-C390741-100	n/a	AB_2728109
Decorin	Rabbit polyclonal	1:100	Sigma HPA003315	n/a	AB_1078639
DHRS7	rabbit polyclonal	1:200	Sigma Aldrich #HPA031121	n/a	AB_10600803
KRT8/18	guinea pig polyclonal	1:1000	Fitzgerald #20R-CP004	n/a	AB_1284055
KRT14	LL002	1:100	Thermo Scientific #ms-115-p0	n/a	AB_63786
KRT13	EPR3671	1:200	Abcam #ab92551	n/a	AB_2134681
SCGB1A1	394324	1:200	Novus Biologicals MAB4218-SP	n/a	AB_2183286
CHGA	CHGA (419)	1:100	Sigma Aldrich #SAB4200728	n/a	AB_2728111
SCG2	rabbit polyclonal	1:100	Sigma Aldrich #HPA011893	n/a	AB_1856656
anti-chicken	goat polyclonal	1:500	Jackson Immunoresearch #103-545-155	Alexa488	AB_2337390
anti-mouse	goat polyclonal	1:500	Thermo Scientific #A11030	Alexa546	AB_2534089
anti-rabbit	goat polyclonal	1:500	Thermo Scientific #A21070	Alexa633	AB_2535731
anti-rabbit	goat polyclonal	1:500	Jackson Immunoresearch #111-516-045	Alexa594	AB_2728112
anti-guinea pig	goat polyclonal	1:500	Jackson Immunoresearch #106-605-003	Alexa647	AB_2337446

A2.5 Discussion

Although this study only used a limited set of markers, these results begin to highlight the immense complexity in the cell types of the prostate. Further studies are required to characterize the functions of the newly identified cell types. Of particular interest are the KRT13 and SCGB1A1 expressing cell populations. KRT13 expression has been detected

in prostate stem cells, where its knockdown reduced the self-renewal capacity of stem cells (Hu et al., 2017). KRT13+ cells reside in the urethra and proximal prostate which are thought to be where prostate stem cells reside. SCGB1A1 expressing club cells in the lung are well characterized cells that participate in immunomodulation (Rawlins et al., 2009). The knowledge in the lung field can be extended to study the function of these cells in the prostate. SCGB1A1 cells are located in the urethra and prostate ducts draining into the urethra. At this location, these cells are poised to sense the entry of microbes into the prostate. These cells could potentially coordinate immune responses to prostate infection resembling their role in the lung (Fehervari, 2016).

The novel cell types described in this study are specified at early stages in prostate development and are retained into adulthood. Conditional knockout of these cell types in mouse models can be used to investigate whether these populations are required during early prostate development. Further, it can be tested whether these cell types expand in number during prostate cancer or Benign prostatic hyperplasia.

Although the distribution of prostate stromal cells is conserved between mouse and human prostates, expression of other markers like KRT13 and KRT13 differ between the mouse and human prostate. The mouse being a widely used model for studying prostate disease, it is imperative to constantly compare the cellular anatomy of the mouse and human prostate based on new research.

A2.6 References

Abler, L.L., Keil, K.P., Mehta, V., Joshi, P.S., Schmitz, C.T., Vezina, C.M., 2011. A high-resolution molecular atlas of the fetal mouse lower urogenital tract. Dev. Dyn. 240, 2364-2377.

Collins, A.T., Berry, P.A., Hyde, C., Stower, M.J., Maitland, N.J., 2005. Prospective identification of tumorigenic prostate cancer stem cells. Cancer Res. 65, 10946-10951.

Fehervari, Z., 2016. Club cells to the rescue. Nat. Immunol. 17, 480.

Hu, W.Y., Hu, D.P., Xie, L., Li, Y., Majumdar, S., Nonn, L., Hu, H., Shioda, T., Prins, G.S., 2017. Isolation and functional interrogation of adult human prostate epithelial stem cells at single cell resolution. Stem cell research 23, 1-12.

Mehta, V., Abler, L.L., Keil, K.P., Schmitz, C.T., Joshi, P.S., Vezina, C.M., 2011. Atlas of Wnt and R-spondin gene expression in the developing male mouse lower urogenital tract. Dev. Dyn. 240, 2548-2560.

Rawlins, E.L., Okubo, T., Xue, Y., Brass, D.M., Auten, R.L., Hasegawa, H., Wang, F., Hogan, B.L.M., 2009. The role of Scgb1a1(+) Clara cells in the long-term maintenance and repair of lung airway, but not alveolar, epithelium. Cell stem cell 4, 525-534.

Wang, X., Kruithof-de Julio, M., Economides, K.D., Walker, D., Yu, H., Halili, M.V., Hu, Y.P., Price, S.M., Abate-Shen, C., Shen, M.M., 2009. A luminal epithelial stem cell that is a cell of origin for prostate cancer. Nature 461, 495-500.